



Université de Lille  
École Doctorale ED 104  
Sciences de la Matière, du Rayonnement et de l'Environnement  
Laboratoire d'Océanologie et de Géoscience  
UMR 8187, Université de Lille, ULCO, CNRS, IRD

**THE BIOENERGETIC MODELING OF  
SYMBIOTROPHIC BIVALVES**  
**LA MODÉLISATION BIOÉNERGÉTIQUE  
DE BIVALVES SYMBIOTROPHIQUES**

Thèse de doctorat préparée en vue de l'obtention du grade de

**DOCTEUR EN BIOLOGIE  
DE L'ENVIRONNEMENT, DES ORGANISMES,  
DES POPULATIONS, ÉCOLOGIE**

Par  
**MARINE VANDENBERGHE**

Soutenue publiquement le 27 mars 2024  
Devant le jury composé de

Directrice de thèse	Sylvie M. GAUDRON, Maître de conférences HDR à Sorbonne Université
Co-encadrant - Invité	Gonçalo J. M. MARQUES, Maître de conférences à l'Université de Lisbonne
Rapporteur	Sebastiaan A. L. M. KOOIJMAN, Professeur émérite à l'Université Vrije Universiteit d'Amsterdam
Rapporteur	François H. LALLIER, Professeur à Sorbonne Université
Examineur (Président du jury)	Sébastien LEFEBVRE, Professeur à l'Université de Lille
Examinatrice	Konstada LIKA, Professeure à l'Université de Crète
Invitée	Ann C. ANDERSEN, Maître de conférences à Sorbonne Université



“Biology is the study of complicated things  
that have the appearance of  
having been designed with a purpose.”

Richard Dawkins



*To my grandparents, Danielle and Jacky, Mauricette and Robert.*

## Foreword

I always have been eager to understand the world, from the largest to the smallest. “Why” and “how” does the world work? What is the purpose of life on earth? I believe that the level of consciousness of human mind is, and always will, insufficient to answer these questions. Because of our fascination for what we don’t understand, we try to find answers at our level of perception of our reality to satisfy an endless curiosity. As a biologist, I am interested in the forms taken by life and their subtleties. This thesis do its bit by addressing questions on the intriguing concept of symbiosis with a focus on bivalve mollusks, from a modeling perspective.

First, I would like to express how grateful I am to my PhD supervisor Sylvie for giving me the opportunity to work on such an interesting subject, even so modeling was not the core of my formation. Thank you for taking me to the 16<sup>th</sup> Deep-Sea Biology Symposium in Brest, to the 8<sup>th</sup> International Symposium on Dynamic Energy Budget for Metabolic Organization in Bâton-Rouge and to send me to Lisbon to work with Gonçalo. Thank you for your help during the intense weeks of lucinid bivalve sampling in Roscoff and for the long car rides between Wimereux and Roscoff. I also would like to thank you for your understanding of my choice to pursue my passion for kendo, the practice at high level and my frequent travels. It has not been an easy path to strike a right balance between the two.

I am also thankful to my co-supervisor Gonçalo for its unfailing patience, pedagogy and availability to explain me the dynamic energy budget theory and to help me to build the “abj-farming” model, from the conceptual ideas to the equations; for sure I would not have been able to accomplish such work without your help. I would like to thank you for hosting me and showing me around Lisbon. I will remember to have tested the best pasteis de nata. The days working in your office have been ones of my most productive days so far.

Thank you both Sylvie and Gonçalo for the time you spent reviewing my work and thank you for believing in me and in my work much more than I did.

I am indebted to all the people that helped me to process samples at some points of my thesis work: Gwendoline Duong for the elemental analyses and the preparation of the growth experiment; Amélie for her serious work during her internship; the Sclerochronology Center of Ifremer at Boulogne-sur-mer, especially Romain Elleboode and Antoine Dussuel for their time; Lucie Courcot for the scanning electron

microscopy; Valerie Lefebvre for the histology of lucinid bivalve gonads; and Alice Delagrangé for the Axio-zoom.

I also would like to thank all the people that helped me to go through the past 3 years.

Thank you Bernadette and Stéphane, you are my favorite people I met during my thesis years. I really enjoyed practicing kendo with you and your help in overcoming my difficult moments. I have never met anyone as much big-hearted as you.

Thank you Lyna for answering my questions about the law of the sea from the other side of the world. I'm lucky to have such a passionate and inspiring friend as you.

Thank you Jérôme helping me to reconcile my thesis and kendo, for your interest and suggestions on my work.

Thank you my kendo girl teammates (Adélie, Fanny, Ines, Kiyoko, Minh Ha, Saya) and my coach Natsuki from the french national team for their trust in me and support. You are all strong and amazing people. I feel extremely lucky to have you in my life.

Finally, I am thanking my parents Caroline and Olivier and my sisters Elise and Solène which have and will always be there for me, in any circumstances.

I hope that you will enjoy reading my thesis and that I will convey successfully the interest of my work to you.

This work has received financial support through the funding of the CNRS MITI 80|Prime project.



## **Abstract: Bioenergetic modeling of symbiotrophic bivalves**

Bivalves live along a broad depth range, from shallow to deep-sea waters. Some bivalves built a peculiar relationship with endosymbiotic chemosynthetic bacteria, able to oxidize sulfur. These symbionts use sulfur compounds, such as hydrogen sulfide, as an inorganic source of electrons to synthesize organic compounds from carbon dioxide in particular. Symbiotic bivalve species from shallow waters feed on the organic matter available in suspension around them, and also derive nutritional benefits from their bacterial symbionts, whereas in deep waters they depend mostly on their symbionts. In this thesis, the dynamic relationship between a deep-sea vesicomyid bivalve and its sulfur-oxidizing symbionts was studied using the dynamic energy budget (DEB) theory (Kooijman, 2010). To parameterize the model, life history traits (called zero-variate data) and data associating a dependent variable with an independent variable (called univariate data) were used. This is the first time that such a DEB model explicitly integrating symbionts has been built for a deep-sea species. Currently, there is only one DEB model for a deep-sea benthic invertebrate species and two DEB models on symbiosis, between symbiotic photosynthetic algae and cnidarians (coral and anemone). Experimental work to obtain data on a shallow-water symbiotic lucinid bivalve species (growth experiment; sulfur content of gills) and conceptual advances in the development of a bioenergetic model for this species are presented. The relevance of developing such models, their possible applications and further developments are also discussed.

**Keywords:** dynamic energy budget, symbiosis, bivalve, cold seep, seagrass bed, seagrass, sulfur-oxidizing bacteria

## **Résumé : La modélisation bioénergétique de bivalves symbiotrophiques**

Les bivalves vivent à des profondeurs très variables, des eaux peu profondes aux eaux profondes. Certains bivalves ont établi une relation particulière avec des bactéries chimiosynthétiques endosymbiotiques capables d'oxyder le soufre. Ces symbiotes utilisent des composés soufrés, tels que le sulfure d'hydrogène, comme source inorganique d'électrons pour synthétiser des composés organiques à partir du dioxyde de carbone notamment. Les espèces de bivalves symbiotiques des eaux peu profondes se nourrissent de la matière organique disponible en suspension autour d'elles et tirent également des avantages nutritionnels de leurs symbiotes bactériens, tandis qu'en eaux profondes, elles dépendent principalement de leurs symbiotes. Dans cette thèse, la relation dynamique entre un bivalve vésicomysidé d'eau profonde et ses symbiotes oxydant le soufre a été étudiée à l'aide de la théorie du budget énergétique dynamique (DEB) (Kooijman, 2010). Pour paramétrer le modèle, des traits d'histoire de vie (appelés données zérovariées) et des données associant une variable dépendante à une variable indépendante (appelées données univariées) ont été utilisés. C'est la première fois qu'un tel modèle DEB intégrant explicitement les symbiotes est construit pour une espèce d'eau profonde. Actuellement, il n'existe qu'un seul modèle DEB sur une espèce d'invertébré benthique d'eau profonde et deux modèles sur la symbiose, entre les algues photosynthétiques symbiotiques et des cnidaires (corail et anémone). Des travaux expérimentaux visant à obtenir des données sur une espèce symbiotique côtière de lucine (expérience de croissance ; teneur en soufre des branchies) et des avancées conceptuelles dans le développement d'un modèle bioénergétique pour cette espèce sont présentés. La pertinence du développement de tels modèles, leurs possibles applications et développements ultérieurs sont également discutés.

**Mots clés:** budget énergétique dynamique, symbiose, bivalve, suintement froid, herbier marin, bactéries sulfo-oxydantes



# Contents

<b>Contents</b>	<b>i</b>
<b>List of Figures</b>	<b>v</b>
<b>List of Tables</b>	<b>ix</b>
<b>Glossary</b>	<b>xi</b>
<b>Abbreviations</b>	<b>xvii</b>
<b>Symbols</b>	<b>xix</b>
<b>1 General introduction</b>	<b>1</b>
1.1 Bivalvia (Linnaeus, 1758) . . . . .	1
1.1.1 Morphological description . . . . .	1
1.1.2 Classification, evolution and phylogeny . . . . .	3
1.1.3 Life cycle of bivalves . . . . .	6
1.2 Chemosymbiosis . . . . .	7
1.2.1 Symbiosis definition . . . . .	7
1.2.2 Chemosynthetic symbionts . . . . .	7
1.2.3 Chemosymbiosis in marine invertebrates . . . . .	11
1.2.4 Bivalve families involved in chemosymbioses . . . . .	14
1.3 Ecosystems of chemo-symbiotic bivalves . . . . .	18
1.3.1 Known chemosynthetic ecosystems . . . . .	18
1.3.2 Focus on two chemosynthetic ecosystems . . . . .	20
1.4 Modeling bivalve symbiotic relationships . . . . .	26
1.4.1 Ecological metabolic theories . . . . .	26
1.4.2 The dynamic energy budget theory: standard model	27
1.4.3 Examples of ecological applications of DEB theory	34
1.5 Objectives of the thesis . . . . .	36

2	<b><i>Christineconcha regab</i>, a deep-sea symbiotrophic bivalve</b>	51
2.1	Introduction . . . . .	52
2.2	Methods . . . . .	57
2.2.1	Model description . . . . .	57
2.2.2	Forcing variables for parameter estimation: Functional response and temperature . . . . .	60
2.2.3	Estimation of primary parameters . . . . .	61
2.3	Results . . . . .	62
2.3.1	Models' predictions . . . . .	62
2.3.2	Estimated functional responses . . . . .	63
2.3.3	Estimated parameters of the abj and abj-farming models . . . . .	64
2.3.4	Symbiont dynamics with the abj-farming model . . . . .	64
2.3.5	Energy fluxes with the abj-farming model . . . . .	65
2.3.6	Chemical element fluxes with the abj-farming model . . . . .	66
2.4	Discussion . . . . .	67
2.4.1	Models of symbiotic species and DEB . . . . .	67
2.4.2	abj versus abj-farming . . . . .	70
2.4.3	Host-symbiont dynamics with the abj-farming model . . . . .	73
2.4.4	Further applications and developments of the abj-farming model . . . . .	76
2.5	Conclusion . . . . .	76
2.6	Supplementary Methods . . . . .	86
2.6.1	Data collection . . . . .	86
2.6.2	Symbiont sulfide consumption . . . . .	88
2.6.3	Estimation of gill volume occupation by symbionts based on 3D-FISH . . . . .	88
2.6.4	Host-Symbiont biomass ratio . . . . .	89
2.6.5	Symbiont macrochemical equations for assimilation, dissipation and growth . . . . .	89
2.6.6	Temperature correction . . . . .	89
2.6.7	Symbiont state variables computation . . . . .	90
2.6.8	Host and symbiont chemical fluxes prediction . . . . .	96
2.6.9	Bacterial density in gills (vbg) prediction . . . . .	97
2.7	Supplementary Figures and Tables . . . . .	99
2.8	Additional work: in research of <i>C.regab</i> larval size(s) . . . . .	109
2.8.1	Preliminary observation . . . . .	109
2.8.2	Scanning Electron Microscopy (SEM) . . . . .	113
2.8.3	Sclerochronology . . . . .	113
2.8.4	Binocular observation on well preserved shell . . . . .	116

<b>3</b>	<b><i>Loripes orbiculatus</i>, a mixotroph shallow-water bivalve</b>	<b>133</b>
3.1	About Lucinidae (J. Fleming, 1828)	133
3.1.1	The diversity of the Lucinidae	133
3.1.2	Notheworthy features of the Lucinidae	135
3.2	About <i>Loripes orbiculatus</i> (Poli, 1795)	137
3.2.1	Description of <i>Loripes orbiculatus</i>	137
3.2.2	Distribution and ecology of <i>Loripes orbiculatus</i>	140
3.2.3	<i>Loripes orbiculatus</i> symbionts	142
3.2.4	<i>Loripes orbiculatus</i> mixotrophy	145
3.2.5	Reproduction of <i>Loripes</i>	149
3.3	A DEB model for <i>Loripes orbiculatus</i>	150
3.3.1	Biological cycle vs. DEB cycle	150
3.3.2	DEB modeling scheme of <i>Loripes orbiculatus</i>	152
3.4	Zero and univariate data for <i>Loripes orbiculatus</i> DEB model	152
3.4.1	List of required data	152
3.4.2	Acquisition methods of required data	154
3.5	Experiments carried on <i>L. orbiculatus</i>	161
3.5.1	Sampling and identification of the collected specimens	161
3.5.2	First sampling period - May 2022 Roscoff	163
3.5.3	Second sampling period - March 2023 Roscoff	164
3.5.4	Experimental settling and sample analysis protocols	165
3.6	Results and discussion	171
3.6.1	Length-weight data	171
3.6.2	Length at birth and length at metamorphosis	172
3.6.3	Length at puberty and reproduction rate	172
3.6.4	Growth of <i>Loripes orbiculatus</i>	174
3.6.5	Elemental contents analyses from field sampling	175
3.6.6	Gill and sediment elemental content from growth experiment	185
3.6.7	Fluorescence <i>in-situ</i> hybridization on gill	187
<b>4</b>	<b>General discussion and perspectives</b>	<b>203</b>
4.1	<i>Christineconcha regab</i> abj-farming model	203
4.1.1	Parameter estimation	203
4.1.2	abj-farming model hypotheses and assumptions	204
4.1.3	Perspectives on <i>Christineconcha regab</i> traits	206
4.2	Perspectives of the abj-farming model	207
4.2.1	Lead for <i>Loripes orbiculatus</i> DEB model development	207
4.2.2	Bivalve functional traits, from shallow to deep sea	207
4.2.3	abj-farming model applicability to other chemosymbiotic species	208

4.3	DEB and chemosynthetic environment challenges . . . . .	209
4.3.1	Coastal challenges . . . . .	209
4.3.2	Deep-sea chemosynthetic ecosystems challenges .	209
4.4	Conclusions on scientific contribution . . . . .	212

# List of Figures

1.1	Bivalvia general morphology. . . . .	2
1.2	Bivalve ctenidium filaments (gills). . . . .	3
1.3	Hypothesized intraphyletic relationships and evolution- ary pathways of Conchifera. . . . .	4
1.4	Classification of symbiotic bivalve families. . . . .	5
1.5	General metabolic pathways of symbionts' chemosynthesis. . . . .	9
1.6	Carbon sources in symbionts' chemosynthesis. . . . .	10
1.7	Energy sources in symbionts' chemosynthesis. . . . .	11
1.8	Terminal electron acceptors in symbiont's chemosynthesis. . . . .	12
1.9	Deep-sea chemosymbiotic marine invertebrates species. . . . .	13
1.10	Classification of symbiotic bivalve families. . . . .	14
1.11	Chemosymbiotic bivalves. . . . .	15
1.12	Chemosynthetic ecosystems. . . . .	19
1.13	Cold seeps distribution. . . . .	21
1.14	Cold seeps formation. . . . .	22
1.15	Cold seep anoxic oxidation of methane. . . . .	23
1.16	Worldwide distribution of seagrasses. . . . .	24
1.17	Mutualistic interactions between seagrasses, lucinid bi- valves and lucinid sulfide-oxidizing symbionts. . . . .	25
1.18	Model of an organism as a thermodynamic system. . . . .	26
1.19	Standard DEB model life stages. . . . .	27
1.20	Standard DEB model modeling scheme. . . . .	28
1.21	Architecture of the AmP procedure. . . . .	33
1.22	Dynamic Energy Budget and ecological risk assessment. . . . .	36
2.2	The "real world" representation of the biological life cycle versus the "abstract world" of the dynamic energy budget (DEB) theory on the different life stages of <i>Christineconcha</i> <i>regab</i> and its sulfur-oxidizing symbionts. . . . .	80
2.3	Modeled <i>Christineconcha regab</i> host and sulfur-oxidizing symbionts variables since host metamorphosis for 10 years using <i>C. regab</i> abj-farming model. . . . .	81

2.4	Modeled ingestion fluxes with <i>Christineconcha regab</i> abj-farming model. . . . .	82
2.5	Pie charts of the energy distribution within <i>Christineconcha regab</i> and its sulfur-oxidizing symbiont population using the abj-farming model. . . . .	83
2.6	Host <i>Christineconcha regab</i> modeled chemical element (carbon, oxygen and nitrogen) fluxes with the abj-farming dynamic energy budget model. . . . .	84
2.7	<i>Christineconcha regab</i> symbionts modeled chemical element fluxes with abj-farming dynamic energy budget model of assimilation, dissipation and growth transformations . . .	85
2.8	Map of the Gulf of Guinea (Southeast Atlantic) showing <i>Christineconcha regab</i> sampling sites. . . . .	99
2.9	<i>Christineconcha regab</i> univariate data and abj Dynamic Energy Budget model predictions . . . . .	100
2.10	<i>Christineconcha regab</i> univariate data and abj-farming Dynamic Energy Budget model predictions. . . . .	101
2.11	Parameter sensitivity to host functional response $f_h$ . . . . .	102
2.12	Pie charts of the energy distribution within <i>Christineconcha regab</i> using abj Dynamic Energy Budget model . . . . .	102
2.13	<i>C. regab</i> modeled chemical fluxes with abj Dynamic Energy Budget model of Assimilation, Dissipation and Growth transformations in function of <i>C. regab</i> shell length and functional response. . . . .	103
2.14	<i>Christineconcha regab</i> ingestion flux in function of <i>C. regab</i> functional response and shell length modeled with <i>C. regab</i> abj DEB model. . . . .	104
2.15	Images of <i>Christineconcha regab</i> shell with binocular magnifier. . . . .	112
2.16	<i>Christineconcha regab</i> shell preparation for scanning electron microscopy. . . . .	114
2.17	SEM of deep sea bivalves species. . . . .	114
2.18	Scanning Electron Micrographs on <i>Christineconcha regab</i> shells. . . . .	115
2.19	Slicing scheme of a cockle shell for schlerochronology. . .	116
2.20	<i>Christineconcha regab</i> shell preparation for sclerochronology. . . . .	117
2.21	Images of <i>Christineconcha regab</i> shell slices. . . . .	118
2.22	Binocular magnifier observation of a well preserved <i>C. regab</i> shell. . . . .	118
3.1	Lucine in its environment. . . . .	135

3.2	<i>Loripes orbiculatus</i> general anatomy. . . . .	136
3.3	Fluorescence in situ hybridization of sulfur-oxidizing symbionts in two lucinid gill species. . . . .	136
3.4	Distribution of lucinid symbiont species. . . . .	138
3.5	Lucinid <i>Loripes orbiculatus</i> life cycle. . . . .	138
3.6	abj model versus lucinid biological cycle. . . . .	151
3.7	<i>Loripes orbiculatus</i> and its thiotrophic symbionts' chemical element fluxes and conceptual modeling scheme for dynamic energy budget model. . . . .	153
3.8	Lucinid species sampling site, Roscoff, France. . . . .	161
3.9	First input of $Na_2S$ into the sediments in <i>L. orbiculatus</i> growth experiment. . . . .	168
3.10	<i>Loripes orbiculatus</i> growth experiment set-up. . . . .	169
3.11	Weights and shell heights of lucines sampled in May 2022 in Roscoff, France. . . . .	171
3.12	Scanning electron microscopy micrograph of two lucinid species, <i>Loripes orbiculatus</i> and <i>Lucinoma borealis</i> , from Roscoff, France. . . . .	172
3.14	Calcein mark on <i>Loripes orbiculatus</i> shell observed by fluorescence. . . . .	174
3.15	Measured and modeled growth with von Bertalanffy growth function of <i>Loripes orbiculatus</i> for each treatments. . . . .	176
3.16	Modeled growth of <i>Loripes orbiculatus</i> . . . . .	176
3.17	Carbon, nitrogen and sulfide content of Roscoff lucines' gills from the field. . . . .	183
3.18	C/N, N/S and C/S ratio of Roscoff lucines' gills from the field. . . . .	184
3.19	Carbon, nitrogen and sulfur content of sediments from <i>Loripes orbiculatus</i> growth experiment per feeding treatments. . . . .	186
3.20	Carbon, nitrogen and sulfide content of <i>Loripes orbiculatus</i> ' gills per treatment at the end the growth experiment. . . . .	188
3.21	C/N, N/S and C/S ratio of <i>Loripes orbiculatus</i> ' gills per treatment at the end the growth experiment. . . . .	189
3.22	Gill sulfur content in function of gill dry weight and shell height of lucines <i>Loripes orbiculatus</i> and <i>Lucinoma borealis</i> sampled in May 2022 and March 2023 in Roscoff (France). . . . .	190
4.1	Deep-sea polymetallic nodules. . . . .	210
4.2	Exploration contracts in the Area in 2023. . . . .	211



# List of Tables

1.1	Standard dynamic energy budget model dynamic state variables. . . . .	29
1.2	Fluxes ( $\text{J d}^{-1}$ ) between states variables of the standard Dynamic Energy Budget model. . . . .	30
1.3	Primary parameters of a standard Dynamic Energy model.	30
2.2	abj Dynamic Energy Budget model state variables (reserve, structure, maturity and reproduction buffer) and fluxes ( $\dot{p}$ ).	105
2.3	Acceleration coefficient ( $s_M$ ). . . . .	106
2.4	Zero- and univariate data of <i>Christineconcha regab</i> abj and abj-farming Dynamic Energy Budget models. . . . .	107
2.5	Functional responses in <i>Christineconcha regab</i> abj and abj-farming dynamic energy budget (DEB) models related to the studied sites and data. . . . .	108
2.6	abj Dynamic Energy Budget model estimated parameters	109
2.7	Zerovariate predictions by <i>Christineconcha regab</i> abj and abj-farming Dynamic Energy Budget models. . . . .	110
2.8	Estimated parameters of <i>Christineconcha regab</i> with abj model and abj-farming model. . . . .	111
3.1	Predicted major metabolic functions of <i>Loripes orbiculatus</i> symbionts. . . . .	139
3.2	<i>Loripes orbiculatus</i> $\delta^{13}\text{C}$ isotopic signatures. . . . .	148
3.3	Classic univariate data for an abj Dynamic Energy Budget (DEB) model, intended for <i>Loripes orbiculatus</i> DEB model.	154
3.4	Classic zerovariate data for an abj Dynamic Energy Budget (DEB) model, intended for <i>Loripes orbiculatus</i> DEB model.	155
3.5	Novel intended zerovariate data for <i>Loripes orbiculatus</i> Dynamic Energy Budget (DEB) model. . . . .	155
3.6	Additional univariate data for <i>Loripes orbiculatus</i> Dynamic Energy Budget model. . . . .	155
3.7	Tides table. . . . .	162

3.8	Planned analyses on lucinid specimens sampled in Roscoff (Western English channel, France). . . . .	163
3.9	Estimated $H_{\infty}$ (cm) and k coefficient of von Bertalanffy growth function per <i>Loripes orbiculatus</i> treatment. . . . .	175
3.10	Biometry and gill chemical elements composition of <i>Loripes orbiculatus</i> from Roscoff (France) . . . . .	177
3.11	Biometry and gill chemical elements composition of <i>Lucinoma borealis</i> from Roscoff (France). . . . .	178
3.12	Measured growths and chemical elements composition of <i>Loripes orbiculatus</i> 'gills from growth experiment (1/2). . .	179
3.13	Measured growths and chemical elements composition of <i>Loripes orbiculatus</i> ' gills from growth experiment (2/2). . .	180
3.14	Statistics on <i>Loripes orbiculatus</i> gill elemental composition (carbon, nitrogen and sulfide) from Roscoff. . . . .	185
3.15	Statistics on <i>Loripes orbiculatus</i> gill carbon, nitrogen and sulfur content from the growth experiment. . . . .	187
3.16	Comparison of gills elemental composition of <i>Loripes orbiculatus</i> collected in March 2023 and <i>L. orbiculatus</i> at the end of the growth experiment. . . . .	190

# Glossary

**abj model** DEB model with a metabolic acceleration between birth ( $E_H^b$ ) and metamorphosis ( $E_H^j$ ).

**abj-farming model** DEB model based on the abj model where sulfur-oxidizing symbionts were added explicitly, and where host obtain food through the digestion of its symbionts.

**adult** DEB terminology. Life stage where the organism is able to feed on external food sources and is able to reproduce.

**assimilation** DEB terminology. Process by which intaken energy is fixed into reserve(s).

**bacteria** one of the three domains in biology with Archaea and Eukarya. Belongs to prokaryotes (i.e., single-cell organism without nucleus and without membrane-bound organelles).

**benthic** living at the lowest level of a body of water; opposed to pelagic.

**birth** 1. biology. Emergence of offspring. 2. DEB terminology. Metabolic switch occurring when the organisms start feeding (start of assimilation) at maturity level  $E_H^b$ . Does not necessarily concomit with biological birth.

**bivalve** animal belonging to the Bivalvia class of mollusks; laterally compressed, have two valve articulated around a hinge.

**chemosymbiosis** “nutritional partnerships between eukaryotic hosts and bacterial symbionts. The symbionts gain energy by oxidizing reduced chemical compounds, such as sulfide or methane, to fix CO<sub>2</sub> and other small carbon compounds into biomass, to provide themselves and their hosts with nutrition” (Sogin et al., 2020). Synonym: chemosynthetic symbiosis.

**chemosymbiotic** uses chemosymbiosis.

**connectivity** “links between network entities; population connectivity is the exchange of individuals among geographically separated sub-populations that comprise a metapopulation. Set in the context of benthic-oriented marine species, population connectivity encompasses the dispersal phase from reproduction to the completion of the settlement process (including habitat choice and metamorphosis)” (Cowen et al., 2007).

**deep-sea** area below 200 m depth of the surface of seas and oceans, not reached by sun light; opposed to shallow sea.

**dissipation** DEB terminology. Process by which reserve is used, not linked to net biomass production (= metabolic work). Dissipation include somatic and maturity maintenances, maturation and reproduction overhead.

**dynamical system** “time-evolving system defined completely by a set of state variables, their changes being describable with one or more differential equations” (Kearney et al., 2021).

**embryo** 1. biology. Early developmental stage of an animal, before birth. 2. DEB terminology. Life-stage where the organism does not feed and relies on its egg reserves.

**fan** “deposits of variable shapes and sizes in deep-marine environments. The principal elements of submarine fans are canyons, channels, and lobes.” (Shanmugam, 2019).

**farming** in chemosymbiosis, host feeding strategy in which “the host provides ideal growth conditions for its symbionts and then digests them” (Sogin et al., 2020).

**filter-feeding** feeding by filtering food suspended in the water.

**functional response** “The ingestion rate of an organism as a function of food density” (Kooijman, 2010).

**gill** respiratory organ of aquatic animals extracting dissolved oxygen from water; used for filter-feeding by some animal, such as bivalves.

**growth** DEB terminology. Process linked to the increase of structure.

**host** larger partner in a symbiotic relationship.

**inorganic** derived from non-living components, lacking carbon-energy bonds.

**juvenile** 1. biology. immature organism, have not reached adult size and form. 2. DEB terminology. Life stage where the organism is able to feed on external food sources but is not able to reproduce yet. In the abj model this life stage is divided into two stages: the early juvenile (which correspond to a larval stage) and the late juvenile stage.

**larva** biological stage in the development of an animal occurring after birth or hatching that is not mature and has a form different from the adult mature form.

**lecithotrophic** larva developing from egg rich in energy, non-feeding by definition.

**maturation** DEB terminology. Increase of the organism maturity level  $E_H$ .

**maturity** DEB terminology. Level of energy invested by the organism to reach puberty.

**maintenance** DEB terminology. “A rather vague term denoting the collection of energy-demanding processes that life seems to require to keep going, excluding all production processes.” (Kooijman, 2010).

**metamorphosis** 1. biology. rapid physical changes occurring after birth. 2. DEB terminology. Level of maturity ( $E_H^j$ ) marking the end of metabolic acceleration to reach the metamorphosis.

**milking** in chemosymbiosis, the host feed by “direct transfer of organic carbon from the symbiont” (Sogin et al., 2020).

**organic** derived or produced by living organisms, having carbon-hydrogen bonds.

**organism** “an open thermodynamic system using energy to maintain and increase its ordered state, and matter to grow and reproduce, under the instruction of internally referenced information (RNA, DNA).” (Kearney et al., 2021)

**parameter** “a quantity in a model that describes the behavior of state variables. It is usually assumed to be a constant and its value is typically estimated from data using explicit criteria.” (Kooijman, 2010).

**pelagic** live in the water column; opposed to benthic.

**phylogenetics** “study of the evolutionary history and relationships among individuals, groups of organisms (e.g., populations, species), or other biological entities with evolutionary histories (e.g., genes, biochemicals, or developmental mechanisms)” (plato.stanford.edu).

**planktonic** micro-organism carried by currents, floating more or less passively.

**planktotrophic** feed on plankton. Usually larva developing from egg poor in energy reserve.

**puberty** DEB terminology. Metabolic switch, occurring at maturity level  $E_H^p$  where energy previously allocated to increase maturity is then allocated to reproduction.

**reserve** DEB terminology. Buffer to fluctuation of external food density. Used by the organism for its metabolic needs (growth, maturation, reproduction and maintenance).

**shallow-sea** area above 200 m depth of the surface of seas and oceans; opposed to deep-sea.

**species** “groups of actually or potentially interbreeding natural populations which are reproductively isolated from other such groups” (Mayr, 1999).

**state variable** “a variable which determines, together with other state variables, the behaviour of a system. The crux of the concept is that the collection of state variables, together with the input, determines the behaviour of the system completely” (Kooijman, 2010).

**structure** DEB terminology. Proportional to the physically measurable length  $L$  of the organism by the shape factor  $\delta$ .

**symbiosis** “association between different species from which all participating organisms benefit” (Stachowicz, 2011).

**symbiont** smaller partner in a symbiotic relationship.

**trochophore** first free-swimming planktonic larval stage characterized by bands of cilia; occurs in mollusks and polychaete annelids.

**univariate data** DEB terminology. Sets of pairs of values for an independent variable and an associated dependent variable.

**veliger** free-swimming larval stage in molluscs occurring after the trocophore larva. Bivalve veliger larva has three stage of development: the D-veliger, the umbo-veliger and the pediveliger. The D-veliger corresponds to the early veliger stage, named after its “D” capital letter form; umbo-veliger loses its D-form as the umbo (see Fig. 1.1 in Chapter 1) develops. The foot appears at pediveliger stage.

**velum** organ with ciliated bands of the trocophore and veliger larva; used for swimming and can be also use to feed.

**zerovariate data** DEB terminology. Scalars that quantify a characteristic of the organism at a given time.



# Abbreviations

**C. c. canutus** *Calidris canutus canutus*

**C. nodosa** *Cymodocea nodosa* (Ucria) Ascherson

**C. regab** *Christineconcha regab*

**C. T. endoloripes** *Candidatus Thiodiazotropha endoloripes*

**C. T. lotti** *Candidatus Thiodiazotropha lotti*

**C. T. taylori** *Candidatus Thiodiazotropha taylori*

**C. T. weberae** *Candidatus Thiodiazotropha weberae*

**DEB** dynamic energy budget

**FISH** fluorescence *in-situ* hybridization

**L. borealis** *Lucinoma borealis*

**L. divaricata** *Lucinella divaricata*

**L. lacteus** *Loripes lacteus*

**L. lucinalis** *Loripes lucinalis*

**L. orbiculatus** *Loripes orbiculatus*

**P1** prodissoconch 1

**P2** prodissoconch 1

**PLD** pelagic larval duration

**RNA** ribonucleic acid

**SEM** scanning electron microscopy

**SSU** small subunit

**T. endolucinida** Thiodiazotropha endolucinida

**WACS** West Africa Cold Seeps

**Z. marina** *Zostera marina*

**Z. noltii** *Zostera noltii*

# Symbols

$d_E$  density of reserve ( $\text{g cm}^{-3}$ )

$d_V$  density of structure ( $\text{g cm}^{-3}$ )

$E$  energy in reserve (J)

$[E_G]$  volume-specific costs of structure ( $\text{J cm}^{-3}$ )

$[E_{Gh}]$  host volume-specific costs of structure ( $\text{J cm}^{-3}$ )

$[E_{Gs}]$  symbiont volume-specific costs of structure ( $\text{J cm}^{-3}$ )

$E_h$  host energy in reserve, non allocated (J)

$E_{Vs}$  symbiont potential energy of structure (J)

$[E_{Vs}]$  symbiont volume-specific potential energy of structure ( $\text{J cm}^{-3}$ )

$E_s$  symbiont energy in reserve, non allocated (J)

$[E_s]$  symbiont reserve density ( $\text{J cm}^{-3}$ )

$E_{Gh}$  host volume-specific costs of structure ( $\text{J cm}^{-3}$ )

$E_{Gs}$  symbiont volume-specific costs of structure ( $\text{J cm}^{-3}$ )

$E_H$  accumulated energy investment into maturation (J)

$E_{Hh}$  host accumulated energy investment into maturation (J)

$E_H^b$  maturity at birth (J)

$E_{Hh}^b$  host maturity at birth (J)

$E_H^h$  maturity at hatching (J)

$E_{Hh}^h$  host maturity at hatching (J)

$E_H^j$  maturity at metamorphosis (J)

$E_{Hh}^j$  host maturity at metamorphosis (J)

$E_H^p$  maturity at puberty (J)

$E_{Hh}^p$  host maturity at metamorphosis (J)

$E_R$  energy in the reproduction buffer (J)

$E_{Rh}$  host energy in the reproduction buffer (J)

$f$  scaled functional response (-)

$f_h$  host scaled functional response (-)

$\{\dot{F}_m\}$  specific searching (filtering) rate ( $\text{cm}^2 \text{cm}^{-3} \text{d}^{-1}$ )

$\{\dot{F}_{mh}\}$  host specific searching (filtering) rate ( $\text{cm}^2 \text{cm}^{-3} \text{d}^{-1}$ )

$\{\dot{F}_{ms}\}$  symbiont specific searching rate ( $\text{cm}^2 \text{cm}^{-3} \text{d}^{-1}$ )

$f_s$  symbiont scaled functional response (-)

$\ddot{h}_a$  Weibull aging acceleration

$\ddot{h}_{ah}$  host Weibull aging acceleration

**J** (unit) Joule, International System unit of energy measurement (base unit)

**K** 1. (unit) Kelvin, International System unit of temperature measurement (base unit). 2. dynamic energy budget half saturation coefficient ( $\text{d}^{-1}$ )

$\dot{k}_{Es}$  symbiont specific-energy conductance ( $\text{d}^{-1}$ )

$\dot{k}_j$  maturity maintenance rate coefficient ( $\text{d}^{-1}$ )

$\dot{k}_{jh}$  host maturity maintenance rate coefficient ( $\text{d}^{-1}$ )

$L$  structural length (cm)

$L_b$  length at birth (cm)

$L_j$  length at metamorphosis (cm)

$L_m$  maximum structural length (cm)

$L_m^{ref}$  reference structural length (=1cm) (?)

$\dot{p}_A$  assimilation rate ( $J d^{-1}$ )

$\dot{p}_{Ah}$  host assimilation rate ( $J d^{-1}$ )

$\dot{p}_{As}$  symbiont assimilation rate ( $J d^{-1}$ )

$\{\dot{p}_{Am}\}$  surface-area-specific maximum assimilation rate ( $J cm^{-2} d^{-1}$ )

$\{\dot{p}_{Amh}\}$  host surface-area-specific maximum assimilation rate ( $J cm^{-2} d^{-1}$ )

$\{\dot{p}_{Ams}\}$  symbiont volume-specific maximum assimilation rate ( $J cm^{-3} d^{-1}$ )

$\dot{p}_C$  reserve mobilization rate ( $J d^{-1}$ )

$\dot{p}_{Ch}$  host reserve mobilization rate ( $J d^{-1}$ )

$\dot{p}_{Cs}$  symbiont reserve mobilization rate ( $J d^{-1}$ )

$\dot{p}_G$  growth rate ( $J d^{-1}$ )

$\dot{p}_{Gh}$  host growth rate ( $J d^{-1}$ )

$\dot{p}_{Gs}$  symbiont growth rate ( $J d^{-1}$ )

$\dot{p}_j$  maturity maintenance ( $J d^{-1}$ )

$\{\dot{p}_M\}$  volume-linked somatic maintenance rate ( $J cm^{-3} d^{-1}$ )

$\{\dot{p}_{Mh}\}$  host specific volume-linked somatic maintenance rate ( $J cm^{-3} d^{-1}$ )

$\{\dot{p}_{Ms}\}$  symbiont specific volume-linked somatic maintenance rate ( $J cm^{-3} d^{-1}$ )

$\dot{p}_S$  volume-specific somatic maintenance rate ( $J cm^{-3} d^{-1}$ )

$\dot{p}_{Sh}$  host volume-specific somatic maintenance rate ( $J cm^{-3} d^{-1}$ )

$\dot{p}_R$  maturation/reproduction rate ( $J cm^{-3} d^{-1}$ )

$\dot{p}_{Ss}$  symbiont volume-specific somatic maintenance rate ( $J cm^{-3} d^{-1}$ )

$\{\dot{p}_T\}$  specific surface area-linked somatic maintenance rate ( $J cm^{-2} d^{-1}$ )

$\dot{p}_X$  feeding rate ( $J d^{-1}$ )

$\dot{p}_{Xh}$  host feeding rate ( $J d^{-1}$ )

$\dot{p}_{XEh}$  host feeding rate from symbiont reserve ( $J d^{-1}$ )

$\dot{p}_{XhV}$  host feeding rate from symbiont structure ( $\text{J d}^{-1}$ )  
 $\{\dot{p}_{Xm}\}$  maximum feeding rate ( $\text{J d}^{-1}$ )  
 $\{\dot{p}_{Xmh}\}$  host maximum specific feeding rate ( $\text{J cm}^{-2} \text{d}^{-1}$ )  
 $\{\dot{p}_{Xms}\}$  symbiont maximum specific feeding rate ( $\text{J cm}^{-3} \text{d}^{-1}$ )  
 $\dot{p}_{Xs}$  symbiont feeding rate ( $\text{J d}^{-1}$ )  
 $\dot{r}_B$  von Bertalanffy growth rate ( $\text{d}^{-1}$  or  $\text{yr}^{-1}$ )  
 $s_G$  Gompertz stress coefficient (-)  
 $s_{Gh}$  host Gompertz stress coefficient (-)  
 $s_M$  acceleration factor (-)  
 $T$  temperature ( $^{\circ}\text{C}$ )  
 $T_A$  Arrhenius temperature ( $^{\circ}\text{C}$ )  
 $T_{ref}$  reference temperature ( $^{\circ}\text{C}$ )  
 $V$  structural volume ( $\text{cm}^3$ )  
 $V_h$  host structural volume ( $\text{cm}^3$ )  
 $V_s$  symbiont structural volume ( $\text{cm}^3$ )  
 $\dot{v}$  energy conductance ( $\text{cm d}^{-1}$ )  
 $\dot{v}_h$  host energy conductance ( $\text{cm d}^{-1}$ )  
 $v_{Ks}$  host half saturation coefficient, value of food ( $V_s + E_s$ ) density where ingestion ( $\dot{p}_{XEh} + \dot{p}_{XhV}$ ) is half of its maximum (-)  
 $z$  zoom factor (-)  
 $\delta_M$  shape coefficient (-)  
 $\delta_{Me}$  shape coefficient of larva (-)  
 $\delta_{Meh}$  host shape coefficient of larva (-)  
 $\delta_{Mh}$  host shape coefficient (-)  
 $\delta_{MV_s}$  symbiont structure shape coefficient (-)  
 $\kappa$  fraction of mobilised reserve allocated to soma (-)

- $\kappa_h$  host fraction of mobilised reserve allocated to soma (-)
- $\kappa_G$  growth efficiency, fraction of growth energy fixed in structure (-)
- $\kappa_{Gh}$  host growth efficiency, fraction of host growth energy fixed in structure (-)
- $\kappa_{Gs}$  symbiont growth efficiency, fraction of symbiont growth energy fixed in structure (-)
- $\kappa_P$  fraction of food energy fixed in non assimilated products (-)
- $\kappa_{Ph}$  host fraction of food energy fixed in non assimilated products (-)
- $\kappa_{Ps}$  fraction of food energy fixed in non assimilated products (-)
- $\kappa_R$  reproduction efficiency, fraction of reproduction energy fixed in eggs (-)
- $\kappa_{Rh}$  reproduction efficiency, Fraction of host reproduction energy fixed in eggs (-)
- $\kappa_X$  fraction of food energy fixed in reserve (-)
- $\kappa_{Xh}$  fraction of host food energy fixed in reserve (-)
- $\kappa_{Xs}$  fraction of symbiont food energy fixed in reserve (-)
- $\bar{\mu}_E$  chemical potential of reserve ( $\text{J mol}^{-1}$ )



# Chapter 1

## General introduction

### 1.1 Bivalvia (Linnaeus, 1758)

#### 1.1.1 Morphological description

Bivalves are mollusks sharing synapomorphic characters: an external shell compressed laterally composed of two valves articulated around a dorsal hinge and joined by a dorsal ligament, with one or two adductor muscles (Fig. 1.1) (Venkatesan & Mohamed, 2015). All of these morphological features allow the valves to be maintained together (Venkatesan & Mohamed, 2015). Bivalves do not have a radula (a kind of raspy tongue) which is present in other mollusk class (Venkatesan & Mohamed, 2015).

Bivalves live mainly in marine water, but also in fresh water. They live along a broad depth range, from shallow waters (> 200 m depth below surface water) to deep-sea waters (< 200 m depth below surface water from where sunlight decreases rapidly) (Venkatesan & Mohamed, 2015). Their lifestyles are greatly diversified. The ancestor of bivalves is thought to be vagile and epifaunal (i.e., living on the bottom sediments) and to have a flat sole as foot, which is present in the genus *Nucula* (Seilacher, 1985; Stanley, 1972). Infaunal bivalves (i.e., living within bottom sediments) burrow more or less close to the surface in various ways. Their shell structure is shaped in function of their environment, such as rocky, woody, soft and muddy substrates, and in

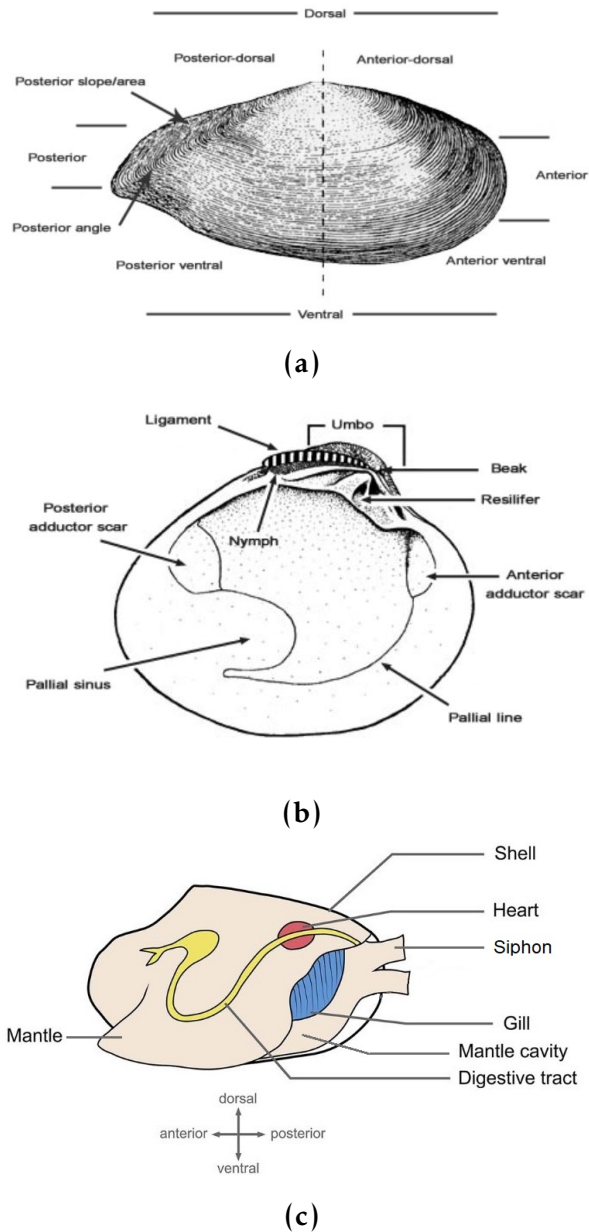


**Figure 1.1:** Bivalvia general morphology. (a) external shell (Figure from Oliver et al., 2016) ; (b) internal shell (Figure from Oliver et al., 2016); (c) internal general organization (Figure modified from Wada et al., 2020).

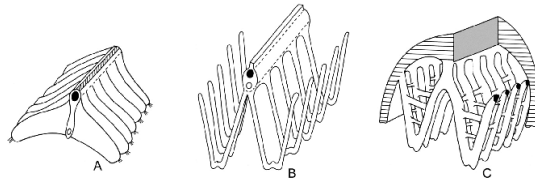


**Figure 1.2:** Bivalve ctenidium filaments (gills). A, protobranch ctenidium; B, filibranch ctenidium; C, eulamellibranch ctenidium (Figures from Coan and Valentich-Scott, 2006).

function of the depth they burrow (Seilacher, 1985). Bivalves that burrow deeper are more protected from environmental disturbances and predators (Seilacher, 1985). Epifaunal bivalves possess a byssus produced by a byssogen gland at the base of the foot to fix themselves to hard substrates and/or conspecifics (Stanley, 1972). Epifaunal species without byssogen gland are descendant of taxa that had it. Some bivalve species with a byssogen gland live buried in sediments (Stanley, 1972). Gills, also named ctenidia, are the respiratory and feeding organ. Bivalves are mainly filter-feeder that feed on suspended organic mater by filtering water with their gills. Primitive bivalves use palps to collect nutrients at the surface of sediments while others have advanced gill structure: gills of protobranch were improved to filibranch and then improved to eulamellibranch which have the most complex structure (Fig. 1.2) (Seilacher, 1985). Some species, such as photosymbiotic and chemosymbiotic ones, have a reduced digestive system and obtain their food through the symbiosis with photosynthetic algae or chemosynthetic bacteria, respectively (Seilacher, 1985).

### 1.1.2 Classification, evolution and phylogeny

Bivalves are thought to appear during early Cambrian time (Bieler & Mikkelsen, 2006; Wanninger & Wollesen, 2019) (Fig. 1.3). Bivalvia (Animalia, Mollusca) is the second class of the Mollusca phylum in term of species abundance, Gastropoda class being the first (Bieler & Mikkelsen, 2006; Bieler et al., 2013). The number of living bivalve species is estimated from 8 to 20 thousand species (Bieler et al., 2013). One of the

main scenario of the evolution of mollusks based on phylogenetic studies divides the Mollusca phylum into two paraphyletic sub-phylum, the Aculifera and the Conchifera. The Aculifera groups together vermiform aplacophorans and multi-shelled polyplacophorans whereas the Conchifera includes all the other mollusks (Fig. 1.3) (Wanninger & Wollesen, 2019). The Conchifera is monophyletic in major scenarios. However, opinions diverge on the relationships inside this sub-phylum (Wanninger & Wollesen, 2019). Conchiferans kept a single shell and a muscular seriality from their molluscan ancestor (Fig. 1.3) (Wanninger & Wollesen, 2019). In Bivalvia, a second shell valve appeared as well as two adductor muscles (Fig. 1.3) (Wanninger & Wollesen, 2019).

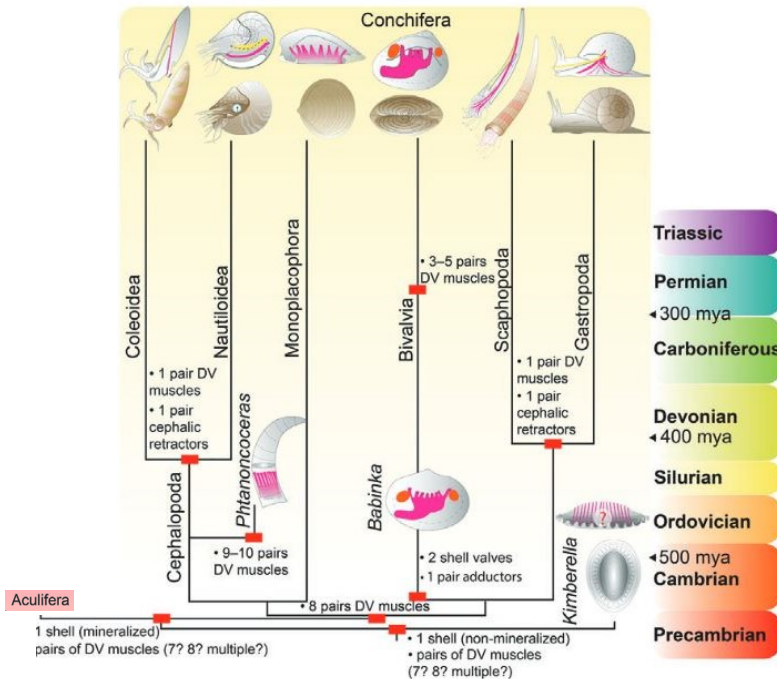


**Figure 1.3:** Hypothesized intraphyletic relationships and evolutionary pathways of Conchifera based on major exoskeletal and muscular subsets. DV, Dorso-ventral (muscles). Red square, change(s) in character(s) state. Colors on drawings: Magenta, dorso-ventral musculature; Orange, adductor muscles; Yellow, cephalic retractor muscles. (Figure from Wanninger and Wollesen, 2019).

Bivalvia classification was discussed a lot along history and still is. Old bivalve classifications since the end of the 18<sup>th</sup> century were solely

based on various hard and/or soft morphological features of bivalves, depending on taxonomists, such as valve forms, hinge-teeth, adductor muscles, the absence or the presence of byssogen gland, the fusion of mantle lobes, siphons, the shape of the foot, the absence or the presence of the pallial sinus, gills, the ligament and the stomach (Fig. 1.1) (Bieler & Mikkelsen, 2006; Cox, 1960). Different synonymous names to design bivalve class were advanced, such as Lamellibranchiata or Pelecypoda but they are not accepted in today's classification and Bivalvia name remained (Cox, 1960). Afterwards, many different hypotheses on Bivalvia classification were proposed based on phylogenetics, using method such as neighbor joining, maximum-likelihood and parsimony, which were not all congruent (Fig. 1.4) (Bieler & Mikkelsen, 2006; Giribet et al., 2002; Giribet & Wheeler, 2002). The classification of bivalves is rather confusing because of the richness of bivalve species and of the different division/sub-division made with various names depending on taxonomists (Bieler & Mikkelsen, 2006; Cox, 1960).

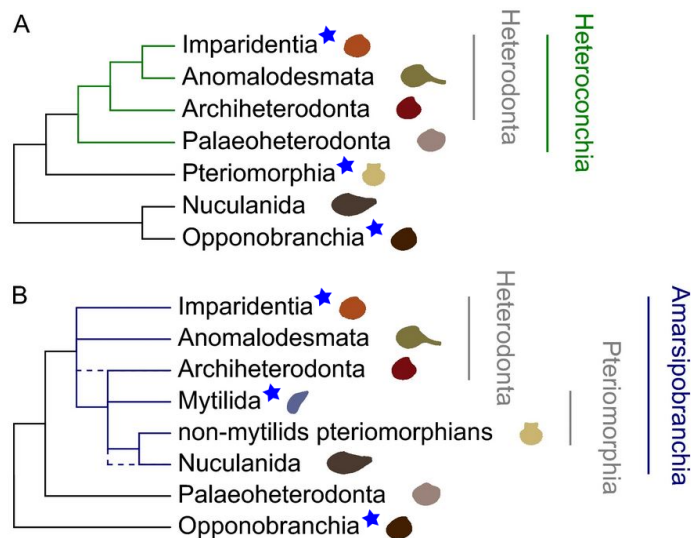


**Figure 1.4:** Two main recent Bivalvia (Linnaeus, 1758) classifications based on phylogenetics (modified from Formaggioni et al., 2022). A, Heteroconchia hypothesis; B, Amarsipobranchia hypothesis. Blue stars, presence of chemosymbiotic species.

### 1.1.3 Life cycle of bivalves

Bivalves have an indirect development (i.e., with a larval stage). Fertilization is most of the time external into the water column. Fertilized egg divides and becomes a trochophore larva, which then grows into a veliger larva (Venkatesan & Mohamed, 2015). Free-swimming larvae go through metamorphosis, leading to the bivalve definitive adult form and settling to a benthic lifestyle and (Joyce & Vogeler, 2018; Venkatesan & Mohamed, 2015). Most of species are gonochoric and others are hermaphrodite (Giribet & Wheeler, 2002). Hermaphroditism can occur simultaneously (having male and female reproductive features at the same time) or successively (as protandry, transforming from male to female or as protogyny (transforming from female to male), or alternatively (alternating between male and female) (Giribet & Wheeler, 2002).

There are by definition two types of larval development in bivalves, depending on how the larva feed, lecithotroph (i.e., “feeding on yolk”) and planktotroph (i.e., “feeding on plankton”). In lecithotroph development the larva rely on its egg maternal reserve whereas in planktotroph development, the larva feeds on phytoplankton and zooplankton (Allen & Pernet, 2007). Larger eggs with more energy reserve are attributed to a lecithotrophic development whereas smaller ones to a planktotrophic development (Allen & Pernet, 2007). Still, species with important egg reserve might be feeding at some stage of their larval development and be facultative planktotroph (Allen & Pernet, 2007).

The first shell secreted is formed at the onset of the veliger larval stage and named prodissoconch 1 (P1). Its secretion is homogeneous and smooth. In species with planktotrophic larva (i.e., feeding on plankton), a second prodissoconch (P2) is secreted by cells from mantle margin whereas in species with lecithotrophic larvae there is only P1. After settlement, the dissoconch which corresponds to the adult shell is formed (Taylor & Glover, 2021).

## 1.2 Chemosymbiosis

### 1.2.1 Symbiosis definition

Symbiosis is usually defined as an “association between different species from which all participating organisms benefit” (Stachowicz, 2011). However, symbiosis cover a large spectrum of interactions between partners, from mutualism to small parasitism, depending on the relationships between the host and its symbionts (Douglas, 2008; Douglas & Werren, 2016; Rosenberg & Zilber-Rosenberg, 2011). Symbiosis allows one of the partner to obtain novel metabolic capability (Douglas, 1994; Douglas, 2014). The concept of a superorganism, where host and its microbiome evolve together, require a fidelity between the symbiotic partners (Douglas & Werren, 2016). This is unlikely to happen to the whole host microbiome and such approach integrates features of both partners and excludes some interactions such as conflictual interactions (Douglas & Werren, 2016). Hologenome concept appears to be a restrictive assumption to study host-symbiont systems (Douglas & Werren, 2016).

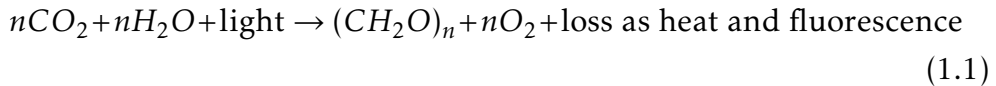
### 1.2.2 Chemosynthetic symbionts

#### 1.2.2.1 Symbionts, a carbon source for the host

Some organisms at the base of the food chain are able to produce their own food (e.g., sugars). Such processes require energy. Chemosynthesis and photosynthesis are the two known forms of primary production (Sogin et al., 2020). Photosynthetic organisms use light as an energy source to fix inorganic carbon while chemosynthetic organisms use alternative sources of energy (Sogin et al., 2020).

In 1796, Ingen-Housz was the first to use the terms “oxidation” and “respiration”, affirming also that “fixed air” by plants is composed of carbon and oxygen (carbon dioxide  $CO_2$ ) and that this process was dependant on light (Govindjee & Krogmann, 2004). In photosynthesis, the generation of organic molecules (e.g., glucose  $C_6H_{12}O_6$ ) is done by using inorganic carbon dioxide ( $CO_2$ ) and water ( $H_2O$ ), releasing dioxygen

( $O_2$ ) during the process (Eq. 1.1) (Govindjee & Krogmann, 2004; Stirbet et al., 2020). Plants (angiosperms, gymnosperms, pteridophytes, and bryophytes), green algae, multipigmented algae (e.g., red, brown and yellow algae, diatoms), and prokaryotes (cyanobacteria and prochlorophytes) do photosynthesis (Govindjee & Krogmann, 2004; Stirbet et al., 2020).



**Equation 1.1:** General equation of photosynthesis.  $CO_2$ , carbon dioxide;  $H_2O$ , water;  $CH_2O$ , sugar;  $O_2$ , dioxygen.

The first bacterial chemosynthesis was described more than one century later in 1906 by Söhngen. He observed that the bacterium *Bacillus methanicus* was able to oxidize methane ( $CH_4$ ) (Scheutz et al., 2009). Chemosynthesis has been observed in micro-organisms such as ammonium and nitrite oxidizers, sulfur reducers and oxidizers, iron and manganese oxidizers, methanogens (Archaea), methylotrophs and methanotrophs, hydrogen oxidizers and acetogens (Enrich-Prast et al., 2009). Most of chemosymbionts are part of the Proteobacteria and the Campylobacterota phyla (Sogin et al., 2020). A host can house more than one symbiont type which use different reduced compounds to fix carbon (Ansorge et al., 2019; Sogin et al., 2020). Sulfur-oxidizing bacteria are predominant in chemosymbioses, followed by methane-oxidizing bacteria.

Organisms that do chemosynthesis use energy released by chemical reactions to generate their own food (Sogin et al., 2021). Chemosynthetic bacteria are able to fix inorganic carbon (called autotrophy; e.g., carbon dioxide  $CO_2$ ) and/or C-1 organic carbon (called heterotrophy; e.g., methane  $CH_4$ ) (Figs. 1.5 and 1.6) (Sogin et al., 2021). The key enzymes fixing  $CO_2$  are the ribulose-1,5-bisphosphate carboxylase / oxygenase (RuBisCO), the adenosine triphosphate lyase (ACL), the carbon monoxide dehydrogenase (CODH) and the acetyl-CoenzymeA-synthase (ACS) whereas the key enzymes fixing  $CH_4$  are the serine-glyoxylate

aminotransferase (SagA), the methyl-CoA lyase (MclA) and the carboxylases (Fig. 1.6) (Sogin et al., 2021).

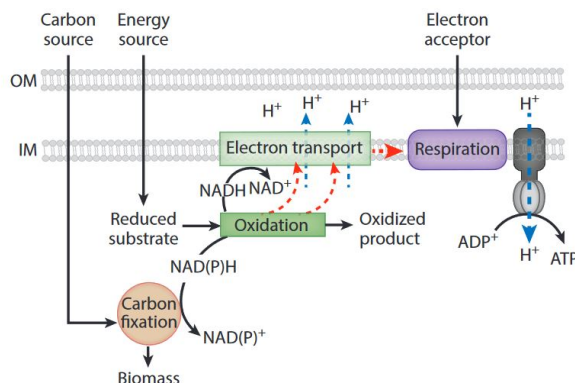


**Figure 1.5:** General metabolic pathways of symbionts' chemosynthesis. **Co-enzyme:**  $\text{NAD}^+$ , oxidize nicotinamide adenine dinucleotide;  $\text{NADH}$ , reduced nicotinamide adenine dinucleotide. **Nucleotide:**  $\text{ADP}$ , adenosine diphosphate;  $\text{ATP}$ , adenosine triphosphate. **Ion:**  $\text{H}^+$ , hydrogen; **Others:**  $\text{IN}$ , inner membrane;  $\text{OM}$ , outer membrane;  $\text{NAD(P)}^+$  oxidize nicotinamide adenine dinucleotide phosphate;  $\text{NAD(P)H}$ , reduced nicotinamide adenine dinucleotide phosphate (Figure from Sogin et al., 2021).

The energy sources used by chemosynthetic bacteria (instead of light in photosynthesis) can be from two origins, organic such as methane ( $\text{CH}_4$ ) or inorganic such as reduced inorganic sulfur compounds (hydrogen sulfide  $\text{H}_2\text{S}$  or thiosulfate  $\text{S}_2\text{O}_3^{2-}$ ), hydrogen ( $\text{H}_2$ ) or carbon monoxide ( $\text{CO}$ ) (Figs. 1.5 and 1.7) (Sogin et al., 2021). One kind of energy source or both can be used by chemosynthetic symbionts depending on their metabolism and available chemicals in their environment. Most of them use both (Sogin et al., 2021). Sulfur-oxidizing symbionts can use reduced sulfur compounds, carbon monoxide, and hydrogen while methanotrophic symbionts use methane as energy source (Fig. 1.7) (Sogin et al., 2020). In sulfur-oxidizing bacteria, key enzymes are sulfide quinone reductase (Sqr), flavocytochrome c (Fcc), sulfur oxidation enzyme complex (SOX), dissimilatory sulfite reductase (Dsr), Adenylyl-sulfate (APS) reductase, and adenosine triphosphate (ATP) sulfurylase (Fig. 1.7) (Sogin et al., 2021). The diversity of symbiont metabolic pathways within a bivalve species host may allow the symbionts to avoid competition for resources, to co-exist and to adapt to available nu-

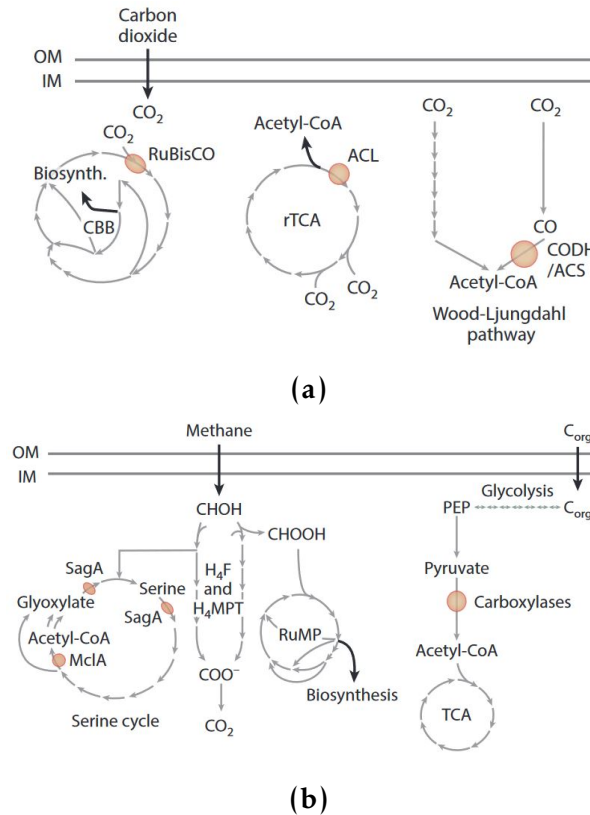


**Figure 1.6:** Carbon sources in symbionts' chemosynthesis with key enzymes involved in carbon assimilation. (a) Inorganic source (Carbon dioxide  $CO_2$ ); (b) Organic source (methane  $CH_4$ ). Brown, **key enzymes:** ACL, ATP-citrate lyase; RuBisCO, ribulose-1,5-bisphosphate carboxylase/oxygenase; ACS, acetyl-CoA-synthase; CO, carbon monoxide; CODH, carbon monoxide dehydrogenase; MclA, malyl-CoA lyase; SagA, serine-glyoxylate aminotransferase. **Coenzyme:**  $H_4F$ , tétrahydrofolate;  $H_4MPT$ , tétrahydromethanopterin; Series of chemical reactions: CBB, Calvin-Benson-Bassham cycle; rTCA, reductive tri-carboxylic acid pathway; RuMP, ribulose monophosphate pathway; TCA, tri-carboxylic acid cycle; **Molecules:** Acetyl-CoA, acetyl coenzyme A;  $CO_2$ , carbon dioxide; CHOH, formaldehyde (oxidized  $CH_4$ ); CHOOH, formate (oxidized CHOH); C<sub>org</sub>, organic carbon. **Others:** IM, inner membrane; OM, outer membrane; PEP, phosphoenolpyruvate (enzyme) (Figure from Sogin et al., 2021).

trients (Ansorge et al., 2019; Sogin et al., 2021). The cultivation of chemosynthetic symbionts have not been successful yet (Sogin et al., 2020).

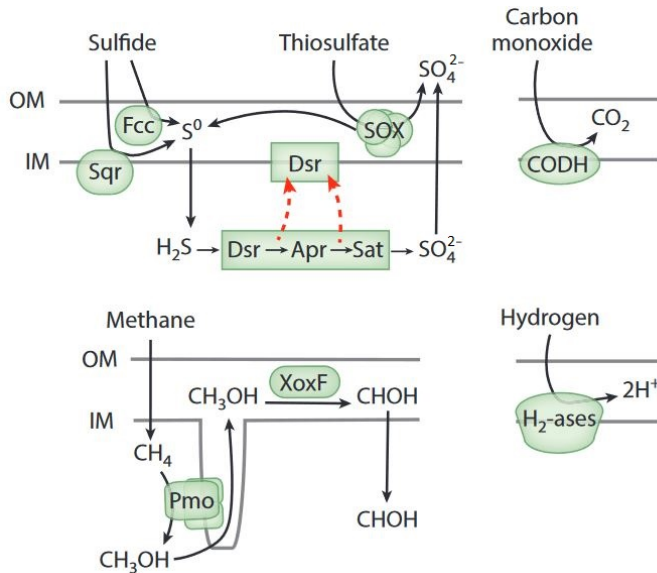


**Figure 1.7:** Energy sources in symbionts' chemosynthesis with key enzymes involved in the acquisition of energy. Green, **key enzyme:** Apr, Adenylyl-sulfate (APS) reductase; Dsr, dissimilatory sulfite reductase; H<sub>2</sub>-ase, hydrogenase; Fcc, flavocytochrome c; Pmo, particulate methane monooxygenase complex; Sat, ATP sulfurylase; SOX, sulfur oxidation enzyme complex; Sqr, sulfide:quinone oxidoreductase; XoxF, methanol dehydrogenase. **Molecule:** CH<sub>4</sub>, methane; CHOH, formaldehyde; CH<sub>3</sub>OH, methanol; H<sub>2</sub>S, hydrogen sulfide. **Ion:** H<sup>+</sup>, hydrogen cation; SO<sub>4</sub><sup>2-</sup>, sulfate anion; **Other:** IM, inner membrane; OM, outer membrane; S<sup>0</sup>, elemental sulfur; red arrow, flow of electron. (Figure modified from Sogin et al., 2021).

Some symbionts use oxygen as terminal electron acceptors, as their hosts, but some also use alternative terminal electron acceptors as nitrate, fumarate and dimethylsulfoxide that is believed to avoid competition with their hosts for oxygen (Figs. 1.5 and 1.8) (Sogin et al., 2021).

### 1.2.3 Chemosymbiosis in marine invertebrates

Chemosynthesis in marine invertebrates is believed to be a convergent evolution as it appeared at several times and independently (Sogin et al., 2020). Chemosymbiosis is present in marine Mollusca (bivalves and

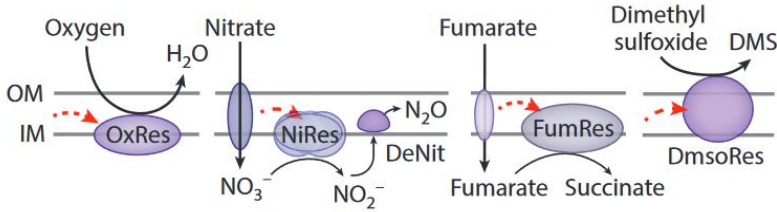


**Figure 1.8:** Terminal electron acceptors in symbiont's chemosynthesis. Purple, **key enzymes** involved in respiration: DeNit, denitrification; DmsRes, dimethyl sulfoxide respiration; FumRes, fumarate respiration; OxRes, oxygen respiration; NiRes, nitrate respiration. **Ion:**  $\text{NO}_3^-$ , nitrate anion;  $\text{NO}_2^-$ , nitrite anion. **Molecules:** DMS, dimethyl sulfide;  $\text{H}_2\text{O}$ , water;  $\text{N}_2\text{O}$ , nitrous oxide. **Others:** red arrows, flow of electrons (Figure modified from Sogin et al., 2021).

gastropods), Nematoda (nematodes), Platyhelminthes (flatworms), Annelida (polychaetes and clitellates), Arthropoda (shrimps and crabs) and Ciliophora (ciliates) phyla (Fig. 1.9) (Sogin et al., 2020).

The polychaete species *Riftia pachyptila* (Fig. 1.9a) from hydrothermal vent houses endosymbionts in a highly vascularised organ named trophosome (Sogin et al., 2020). Chemosymbiotic snails (Fig. 1.9b) have symbionts in their gills (Sogin et al., 2020). Chemosymbiotic clams and mussels from shallow water and from deep sea (e.g., Figs. 1.9c and d) have endosymbionts in their well developed gills (Sogin et al., 2020). Specialized cells containing bacteria within the gills are called bacteriocytes (Rosenberg & Zilber-Rosenberg, 2011). Deep-sea symbiotic shrimps (e.g., Fig. 1.9e) have chemosynthetic symbionts in their digestive system (Guéganton et al., 2022). In the phylum of Annelida, symbiotic oligochaete, such as the gutless *Olavius algarvensis* from shallow water, have endosymbionts (Dubilier et al., 2001; Sogin et al., 2021). Hydrothermal vent and cold-seep *Kiwa* crabs (Fig. 1.9f) have filamentous  $\epsilon$ - and  $\gamma$ - Proteobacteria epibionts on chelipeds setae which are able to fix inorganic carbon and oxidize sulfur (Goffredi et al., 2003; Goffredi et al., 2008; Thurber et al., 2011). Symbiotic marine nematods have specific epibionts (Sogin et al., 2020).

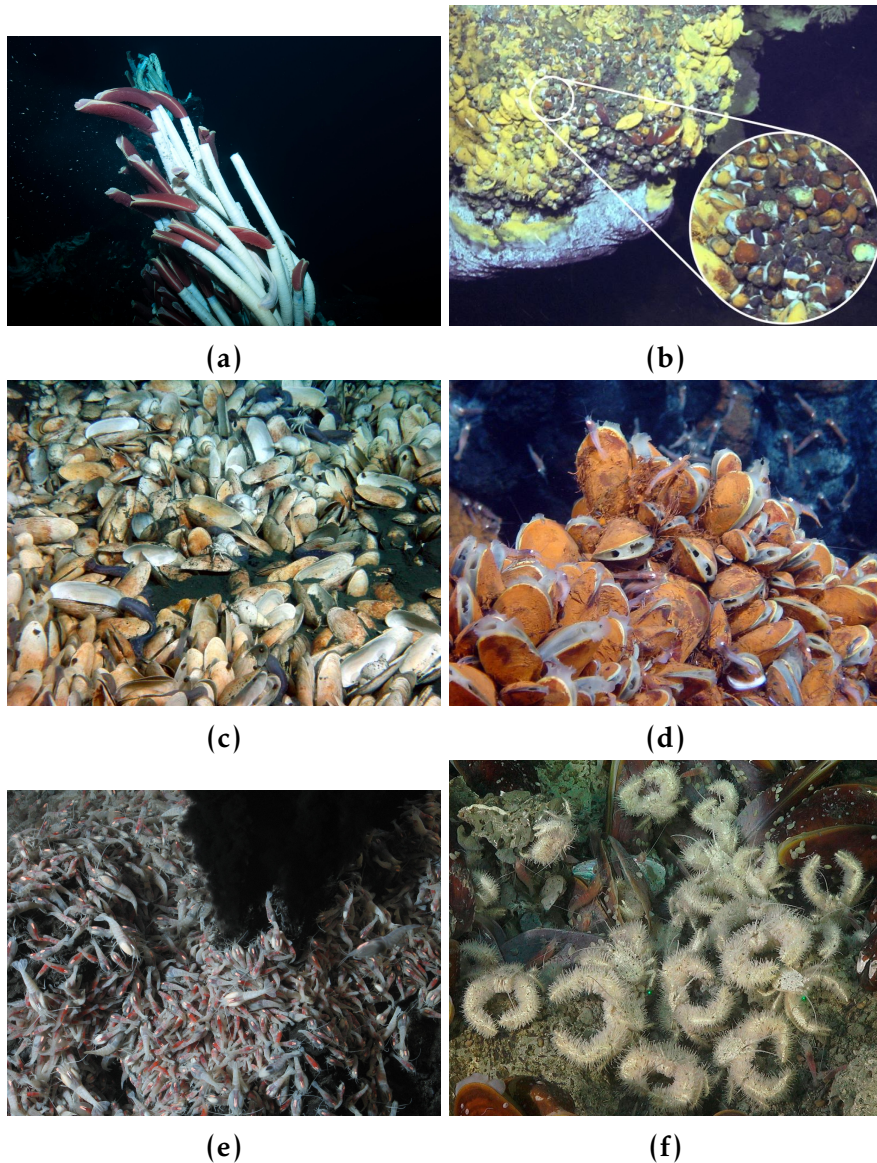


**Figure 1.9:** Deep-sea chemosymbiotic marine invertebrates species. (a) Giant tubeworms *Ryftia pachyptila* (Annelida, Polychaeta) (Ifremer (2010). <https://image.ifremer.fr/data/00568/67973/>); (b) Shrimp *Rimicaris exoculata* (Arthropoda, Crustacea) on hydrothermal vents. (Ifremer (2014). <https://image.ifremer.fr/data/00702/81445/>); (c) Vesicomyid clams (Mollusca, Bivalvia) (Ifremer (2001). Campagne BIOZAIRE2 <https://image.ifremer.fr/data/00574/68564/>); (d) *Bathymodiolus azoricus* mussels (Mollusca, Bivalvia) (Ifremer (2008). <https://image.ifremer.fr/data/00568/67992/>); (e) *Gigantopelta aegislan* snails (Mollusca, Gastropoda) (Image from Lan et al., 2021); (f) *Kiwa puravida* “yeti” crabs (Arthropoda, Crustacea) (Image from Azofeifa-Solano et al., 2022).

### 1.2.4 Bivalve families involved in chemosymbioses

Chemosymbiosis in bivalves is not restricted to a certain depth or climate, but rather a low oxygen level (Seilacher, 1990). The apparition of chemosymbiosis might have been favored by the sealed of sediments from above oxygenated water: by microbial mats during the Precambrian time and/or the colonization of shallow waters by angiosperms, as ealgrasses, during the late Cretaceous that also offered a protection against perturbations (Seilacher, 1990, 1999).

Chemosymbioses allow bivalve to live in various extreme reducing habitats such as hydrothermal vents and cold seeps. In the deep sea, some species rely only on their bacterial symbionts for food. Known living chemosymbiotic bivalves belong to nine bivalve families (Fig. 1.10).

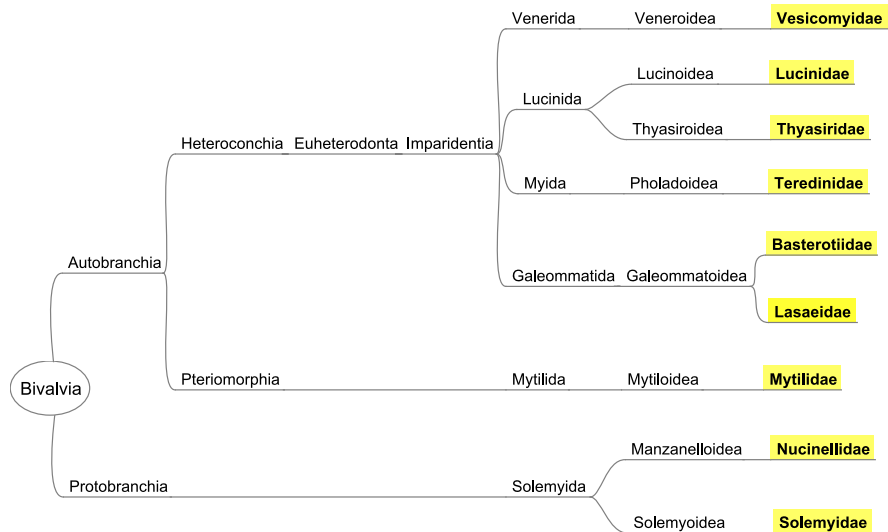


**Figure 1.10:** Classification of symbiotic bivalve families (according to World Register of Marine Species WoRMS). Note: Solemyida super-family is placed in the Opponobranchia clade in phylogenetic classifications presented in Chapter 1 Fig. 1.4.

**Basterotiidae (Cossmann, 1909)** In the Basterotiidae family, a symbiotic species has been discovered in the Saxicavellinae subfamily for

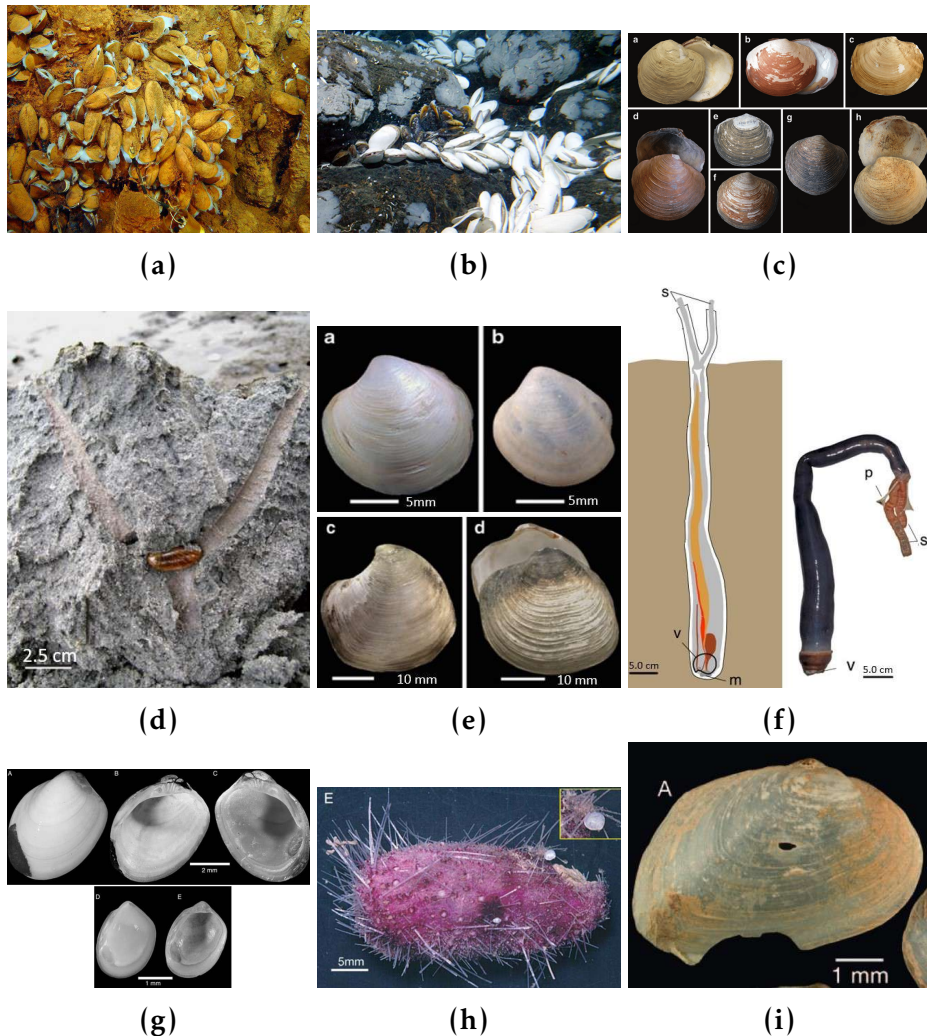


**Figure 1.11:** Chemosymbiotic bivalves. (a) *Bathymodiolus azoricus*, a mytilid of the Bathymodiolinae subfamily (Figure from IFREMER 2008). (b) Giant vesicomyid *Calyptogena magnifica* (in white) (Figure from Tim Shank (WHOI), noaa.gov). (c) Various Lucinid species (Figure 5.8 from Taylor and Glover, 2010). (d) *Solemya velum* of the Solemyidae family (Figure 1 from Roeselers and Newton, 2012). (e) Various thyasirids (Figure 5.6 A-D from Taylor 2010). (f) The giant shipworms *Kuphus polythalamia* of the Teredinidae family, burrowed in sediment (left) and removed from its calcaerous tube (right): m, mouth; s, siphon; v, valve (shell) (Figure 1.A and 1.C modified from Distel et al., 2017). (g) The only two confirmed symbiotic nucinellid species, *Nucinella owenensis* at the top and *Huxleyia habooba* at the bottom (Figure 8.A-E from Oliver and Taylor, 2012). (h) *Syssitomya pourtalesiana* of the Lasaeidae family attached on an echinoid *Pourtalesia miranda* (photo A.J. Southward, Figure 7.E from Oliver et al., 2013). (i) *Atopomya dolobrata* of the Basterotiidae family (Figure 1.A from Oliver, 2013).

the first time with the species *Atopomya dolobrata* in 2013 (Fig. 1.11i) (Oliver, 2013; Oliver et al., 2013).

**Lasaeidae (J. E. Gray, 1842)** Symbiosis in Montacutinae sub-family of Lasaeidae has been observed in *Syssitomya pourtalesiana*. This species is commensal on the deep-sea echinoid *Pourtalesia sp.* (Fig. 1.11h). *S.pourtalesiana* is suspected of mixotrophy as food particles were found in the stomach of the bivalve (Oliver et al., 2013).

**Lucinidae (J. Fleming, 1828)** Lucinids are burrowing bivalves in sulfide-rich sediments. They are the more diverse family of chemosymbiotic bivalves with over 400 living species (Roeselers and Newton, 2012; Taylor and Glover, 2006) (e.g., Fig. 1.11c). All known lucinids are symbiotic so far. They live in symbiosis with sulfur-oxidizing bacteria in gill bacteriocytes (Roeselers and Newton, 2012; Taylor and Glover, 2000, 2006). Their size is of the order of millimeters up to 150 mm (Roeselers and Newton, 2012).

**Mytilidae (Rafinesque, 1815)** Mytilids are commonly named mussels. Only mytilids of the Bathymodiolinae subfamily are symbiotics (e.g., Fig. 1.11a). Bathymodiolins use both filter feeding and their chemosynthetic symbionts as food sources. The symbionts are located in gill bacteriocytes. Bathymodiolin symbionts are thiotrophs and/or methanotrophs (Duperron et al., 2013; Roeselers and Newton, 2012). Bathymodiolin species live fixed to various type of hard substrates via their byssus, except for the species *Bathymodiolus boomerang*, which lives partially buried in the sediment (Duperron et al., 2013).

**Nucinellidae (H. E. Vokes, 1956)** Knowledge of nucinellids is scarce. Nucinellids were for a long time suspected of being symbiotic because of their reduced or absent gut (Taylor and Glover, 2010). Bacteria were observed in bacteriocytes in the large ctenidia of *Nucinella owenensis* and *Huxleyia habooba* species. Chemosynthesis in the Nucinellidae family was then confirmed for the first time (Fig. 1.11g) (Oliver and Taylor, 2012).

**Solemyidae (Gray, 1840)** Solemyidae are infaunal. They make U- or Y-shaped burrows in sediment (e.g., Fig. 1.11d). Solemyidae are able to filter feed but mostly rely on their symbiont for food (Duperron et al., 2013). Solemyidae family is composed of two genera: the shallow water genus *Solemya* and the deep-sea genus *Acharax* (Neulinger et al., 2006; Roeselers and Newton, 2012).

**Teredinidae (Rafinesque, 1815)** Teredinidae, also called shipworms, are wood-borer. Shipworms, usually possess cellulolytic symbionts that allow them to feed on wood. However it has been shown that the giant shipworm *Kuphus polythalamia*, which may reach 155 cm in length, possess thiotrophic bacteria instead of cellulolytic symbionts as well as a reduction of its digestive system and a loss of morphological features associated with wood digestion compared to other teredinid species. *Kuphus polythalamia* is the only described species of Teredinidae that do not only burrow in wood but also in marine sediments (Fig. 1.11f) (Distel et al., 2017).

**Thyasiridae (Dall, 1900 (1895))** Thyasirid clams are burrowers. Their size is about more or less 1 cm (Fig. 1.11e). Within the family, some species harbor symbiont whereas some do not. Symbiont of thyasirids are mostly extracellular (Dufour, 2005; Duperron et al., 2013). Thyasirids represent early stage of symbiosis evolution (Guo et al., 2023).

**Vesicomomyidae (Dall & C. T. Simpson, 1901)** Vesicomomyidae has two sub-families, the Pliocardiinae and Vesicomomyinae. Pliocardiinae have the particularities to have a reduced or absent gut and subfilamental tissue in gills whereas Vesicomomyinae do not. Pliocardiinae, composed of 15 genera, are found living in reduced environment with high density of thiotrophic bacteria in their hypertrophied gills (e.g., Fig. 1.11b). Pliocardiinae are medium to large in size (up to 30 cm in length) whereas Vesicomomyinae are smaller (often < 1cm). Vesicomomyinae sub-family is composed only of the genus *Vesicomomya* of which some species can be found living in non-sulfide-rich habitat (Krylova et al., 2010).

## 1.3 Ecosystems of chemo-symbiotic bivalves

### 1.3.1 Known chemosynthetic ecosystems

Chemosynthetic bivalves flourish in various chemosynthesis-based ecosystems where sulfide production is a shared characteristic.

**Hydrothermal vents** In 1977, an expedition of geologists searching for temperature anomalies at the Galapagos Ridge discovered the first hydrothermal vents (Corliss et al., 1979). Hydrothermal fluids, resulting from the meeting of seawater with magma and heated rocks, are emitted from spread centers (oceanic ridges) (Fisher et al., 2007). Hot emitted fluids are chemical-rich (sulfide and/or methane) and their color depends on their chemical composition. When those fluids reach seafloor, they are cooled down quickly and dissolved compounds precipitate forming black and white chimneys (Fisher et al., 2007). Temperature of black smoker emitted fluids are up to 400°C (Fouquet, 2011). White smoker fluids are cooler than black smokers, with a temperature between 260°C and 300°C, and are situated further away from the ridge than black smokers (Arndt, 2011).

**Cold seeps** In 1983, the first cold seep was discovered by chance during exploration of the lower Florida escarpment in the Gulf of Mexico, on a passive continental margin. The macrofauna is similar to those of hydrothermal vents but not necessarily the same species (Paull et al., 1984). Cold seeps are areas of the deep sea and shallow water from which fluids (rich in methane and/or sulfide) usually at ambient water temperature escape through cracks of the seabed (Suess, 2018). They are called cold as opposed to hydrothermal vents whose temperatures are much higher. Cold seeps originate from the transformation of hydrocarbon reservoir into methane, either by bacteria (biogenic) or by pressure and temperature (thermogenic). In the sediment, a part of emitted methane is used by a complex of archae/bacteria (methane oxidizing/sulfate

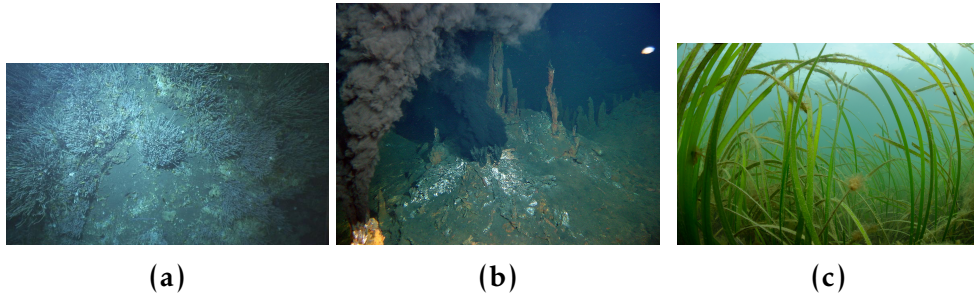


**Figure 1.12:** Chemosynthetic ecosystems. (a) Siboglinid tubeworm bushes at Regab pockmark (3200 m depth, Gulf of Guinea) (Ifremer (2011) <https://image.ifremer.fr/data/00558/67007/>); (b) Black smokers at Rainbow hydrothermal field (2300 m depth, Mid-Atlantic Ridge) (Ifremer (2008) <https://image.ifremer.fr/data/00568/67987/>); (c) *Zostera marina* seagrasses (Gulf of Morbihan, France) (Dugornay Olivier (2013) <https://image.ifremer.fr/data/00560/67187/>).

reducing bacteria), releasing reduced sulfur compounds (Laming, 2014). Cold seeps occur along active and passive continental margin (Sibuet and Roy, 2003).

**Organic fall** Organic fall are punctual input of important organic matter to the sea-floor such as dead carcasses (e.g. whale carcasses) and sunken wood. Sulfide is produced during their decomposition process. Organic falls might be "stepping stones" for bivalve species, in particular Mytilidae, to reach deep-sea cold seeps and hydrothermal vents (Distel et al., 2000). The bivalve families Mytilidae, Solemyidae, Thyasiridae, Vesicomidae and Nucinellidae may live on organic fall or around in close proximity in the sediments.

**Reduced sediments** Reduced sediments bearing chemo-symbiotic bivalves are found in coral reefs (Sogin et al., 2020), mangroves (Laurent et al., 2013), seagrass beds (Cavanaugh, 1983) and oxygen minimum zones (Levin, 2003).

**Other** The small symbiotic species *Syssitomya pourtalesiana* (Montacutiinae) is commensal to an abyssal echinoid species and lives attached to its anal spines (Oliver et al., 2013).

## 1.3.2 Focus on two chemosynthetic ecosystems

### 1.3.2.1 Cold seeps as an example of deep-water chemosynthetic ecosystem

Cold seep fluids originate from tens of meters to tens of km below the seafloor (Suess, 2014, 2018). Most of cold seeps occur at subduction zone and organic-rich passive margin and others at active margins with plate convergence and strike-slip faulting (Fig. 1.13) (Suess, 2014, 2018).

At passive margin (i.e., not active plate boundaries), expulsion of fluids is caused by sediment loading, differential compaction, over-pressure and facies (i.e., characteristics of a rock including its chemical, physical, and biological features) changes (Fig. 1.14a) (Suess, 2014, 2018). Various geologic settings such as pockmarks, carbonate chimneys, brine pool, asphalt seeps, and methane hydrate mounds are formed (Suess, 2014, 2018). Pockmarks are seafloor depression, from ten meters to one kilometer in diameter, caused by gas expulsion (Boetius & Wenzhöfer, 2013). The deposition of gas hydrates on the seafloor creates hydrate mounds (Boetius & Wenzhöfer, 2013). Carbonate slabs are formed by carbonate precipitation (Boetius & Wenzhöfer, 2013).

Where continental and oceanic plates converge, continental slope which is less dense than oceanic plate overrides oceanic plate, forming accretionary margins (formation of an accretionary prism) and erosive margins. Oceanic plate sediments are dewatered, letting fluids pass. Accretionary margin are formed by the off-scraping of sediments whereas erosive margins by the bypassing of oceanic sediments (Figs. 1.14b and c) (Sibuet & Olu, 1998; Suess, 2014, 2018). Geological formations such as mud volcanoes/mounds and seamounts occur (Sibuet & Olu, 1998; Suess, 2014, 2018). Mud volcanoes are from one to ten kilometers in diameter and characterized by an elevation of the seafloor formed by gas, pore fluids and mud eruptions (Boetius & Wenzhöfer, 2013). Features emerging from the seafloor higher than 100 m are seamounts (Staudigel et al., 2010).

In cold seeps, chemosynthetic life is fueled by chemical compounds from upward fluxes and rely mainly on anoxic oxidation of methane

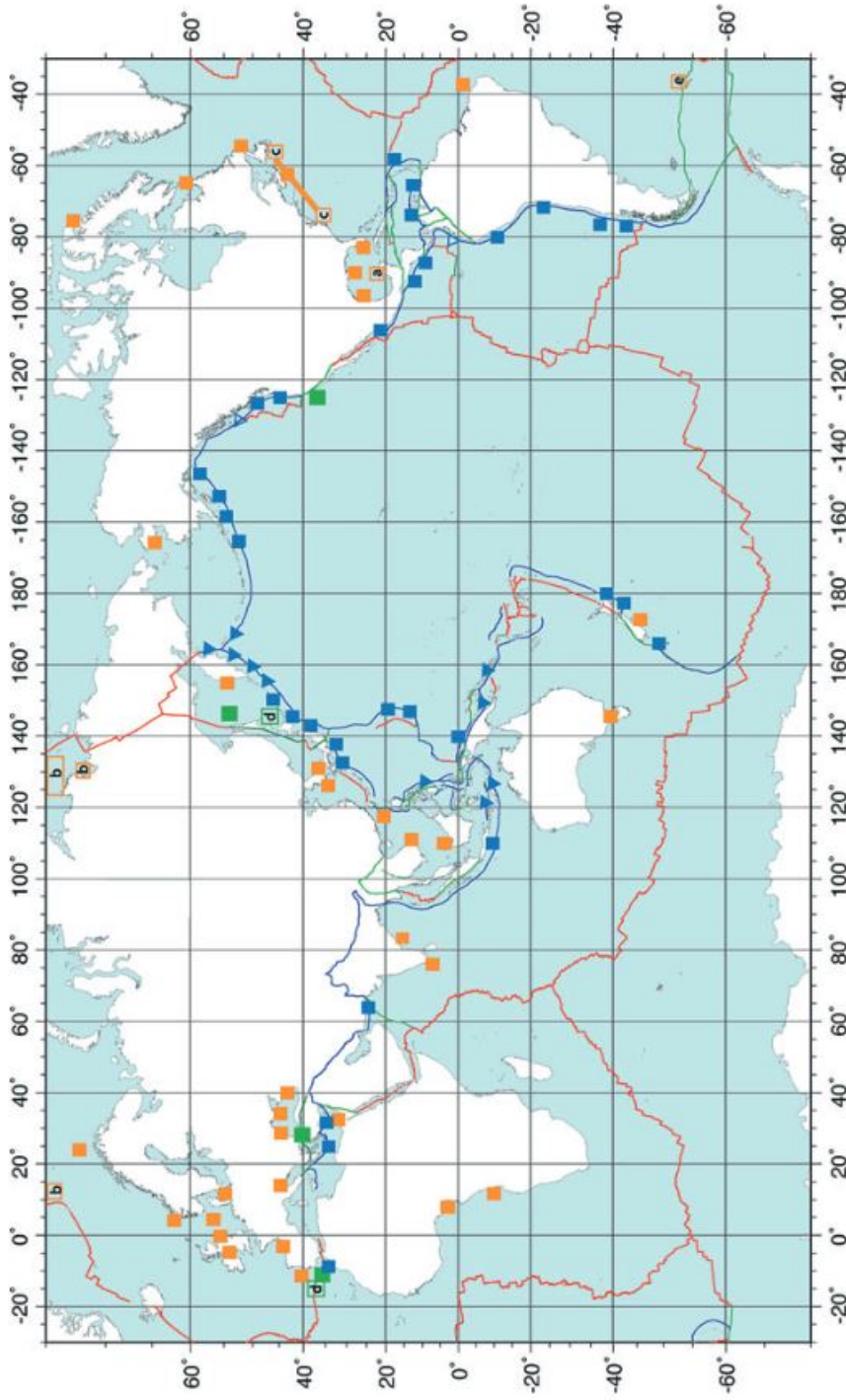


**Figure 1.13:** Cold seeps distribution. Red lines, plate boundaries, hydrocarbon-metazoan-microbe-carbonate (HMMC) associations at active margins; Orange squares, at passive margins incl. Groundwater seeps; Green squares, sites at transform and strike-slip faults. Data with complete site references in Campbell (2006) and Suess (2010, 2014). New sites (open squares, lettered): (a) asphalt seeps (Sahling et al. 2016); (b) East Siberian Shelf (Shakova et al. 2016) and Svalbard margin; (c) Atlantic margin (Skarke 2014); (d) Sakhalin strike-slip (Derkachev et al. 2015) and Africa-Eurasia strike-slip (Hensen et al. 2015); (e) South Georgia Island fjords (Römer et al. 2014) (Figure from Suess, 2018; *Reproduced with permission from Springer Nature*).

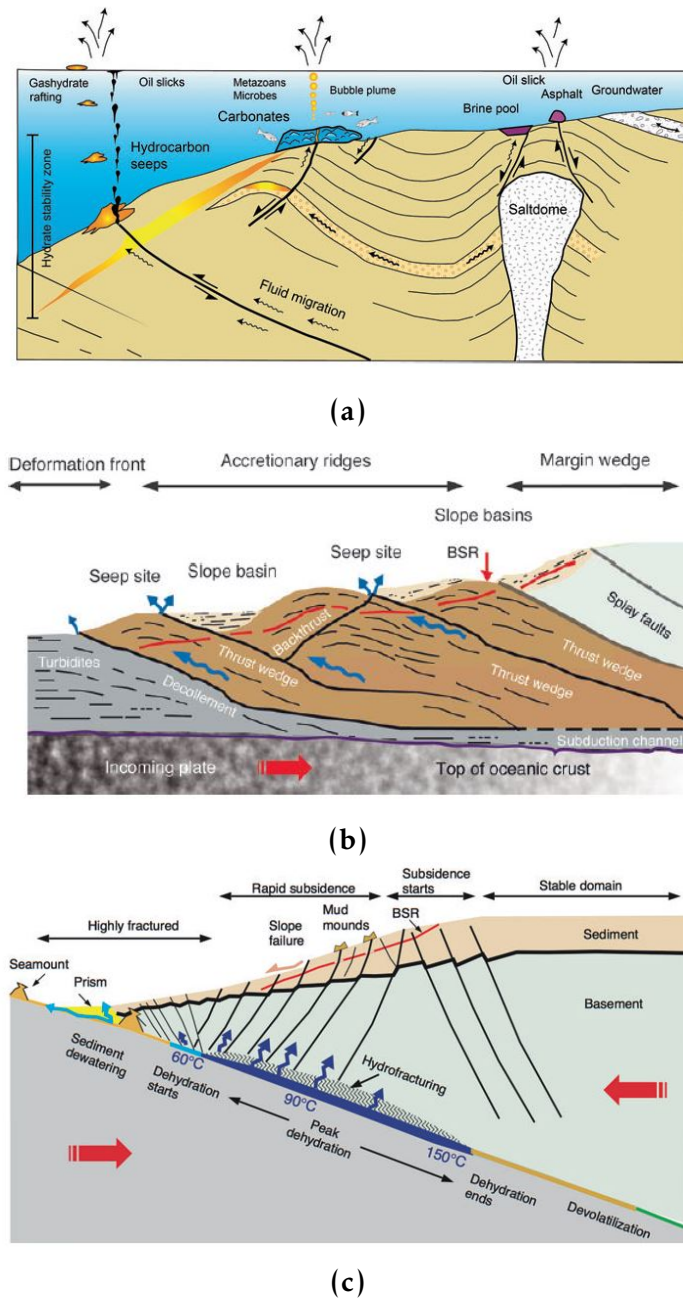


**Figure 1.14:** Cold seeps formation. (a) Passive margin; (b) Accretionary margin; (c) Erosive margin. BSR, bottom-simulating reflector. (Figures from Suess, 2018; *Reproduced with permission from Springer Nature*).

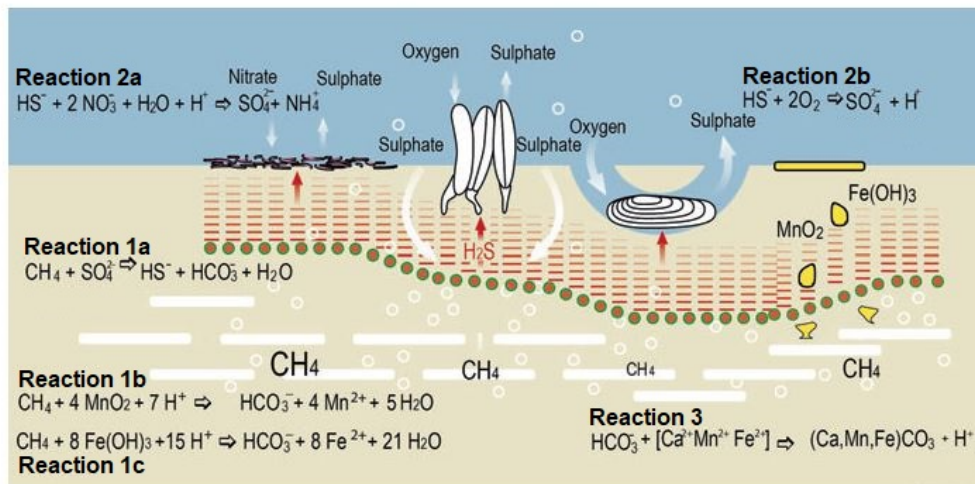


**Figure 1.15:** Cold seep anoxic oxidation of methane (AOM). Reactions: 1a, sulfate reduction by AOM-consortia; 1b, manganese dioxide reduction by AOM-consortia; 1c, iron hydroxide reduction; 2a, sulfide oxidation by microbial mat; 2b, sulfide oxidation by symbionts of macroorganisms; 3, precipitation of calcium carbonate. Red-green circles, AOM-consortia; White slabs, buried gas hydrates; Bubbles, free gas. (Figure from Suess, 2018; *Reproduced with permission from Springer Nature*).

(AOM) by Archaea (Suess, 2014, 2018). The AOM-consortia is composed of dense aggregates of Archaea surrounded by sulfate-reducing bacteria (Boetius et al., 2000). Using methane, the sulfate-AOM-consortia reduces sulfate from seawater into free sulfide that is then available for microbial mat and specialized symbiotic macrofauna to use. Bicarbonate ions are also released (Fig. 1.15) (Suess, 2018). In the presence of metal oxides (e.g., iron oxyhydroxide and manganese oxide), metal-AOM-consortia can reduce the metal oxides using methane and releases bicarbonates and metal ions such as ferric and manganese ions (Fig. 1.15) (Suess, 2018). Bicarbonate, together with calcium and metal ions, precipitate into mixed Ca-Mn-Fe-carbonate (Fig. 1.15) (Suess, 2018).

### 1.3.2.2 Seagrasses as an example of shallow-water chemosynthetic ecosystem

Seagrasses are distributed worldwide, from the arctic circle to temperate to tropical latitudes (Fig. 1.16) (Short et al., 2007). Seagrass mead-

ows are hot spot of biodiversity, and bioengineers of local environments (Maxwell et al., 2017; Unsworth et al., 2022). For example, they trap sediments improving water clarity and light penetration, uptake ammonium reducing sediments toxicity, oxygenate sediments reducing sulfate concentration, provide a shelter to mesograzers and juveniles, and attract megagrazers (Maxwell et al., 2017).

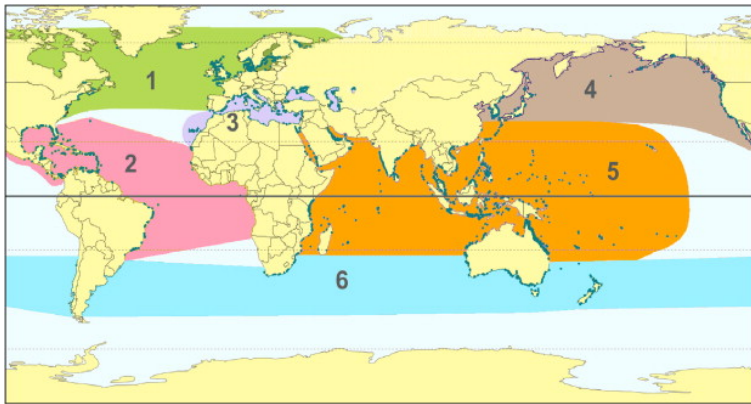


**Figure 1.16:** Worldwide distribution of seagrasses. Blue dots, seagrasses (data from 2005 UNEP-WCMC). Numbers, geographic bioregions: 1 (green), Temperate North Atlantic ; 2 (pink), Tropical Atlantic; 3 (purple), Mediterranean; 4 (brown), Temperate North Pacific; 5 (orange), Tropical Indo-Pacific; 6 (cyan), Temperate Southern Oceans (Figure from Short et al., 2007).

Beneficial interactions between lucinid clams and seagrasses have been extensively studied. As a result of its sulfur-oxidizing symbionts, Lucinids facilitate seagrass growth and favors an increase of seagrass biomass by mitigating sulfide stress (Fig. 1.17a) (Cardini et al., 2022; Chin et al., 2021; Lamers et al., 2013). Lucinid clams are under consideration for seagrass management, restoration and conservation (Cardini et al., 2022; Donaher et al., 2021). High organic matter level caused by an increase of seagrass mortality, break-down the fragile equilibrium of this mutualistic relationships (Fig. 1.17b) (de Fouw et al., 2016; Sanmartí et al., 2018).

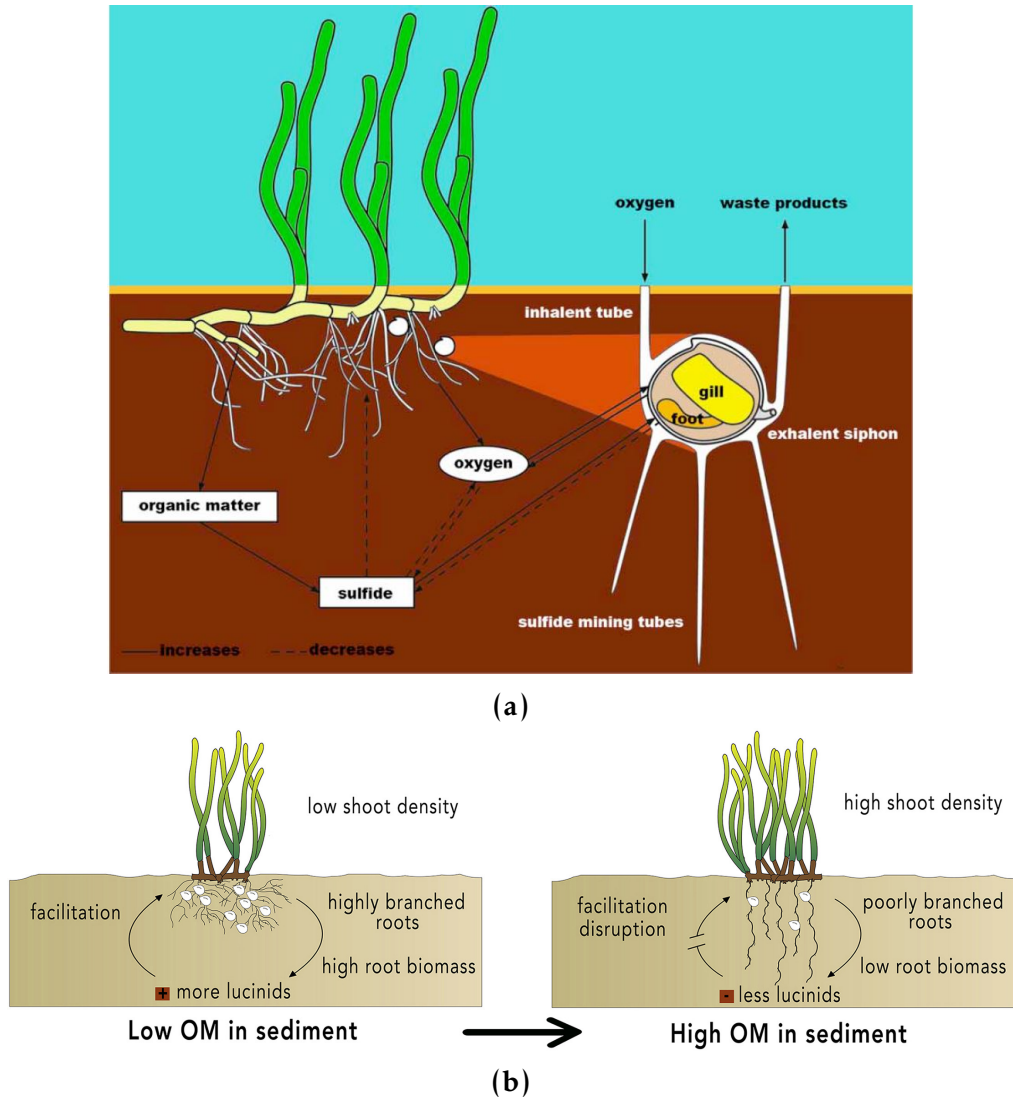


**Figure 1.17:** Mutualistic interactions between seagrasses, lucinid bivalves and lucinid sulfide-oxidizing symbionts. (a) Sulfide-driven coevolution: positive and negative feed-backs between the three parties (Figure from Lamers et al., 2013) (b) lucinid facilitation (Figure from Sanmartí et al., 2018).

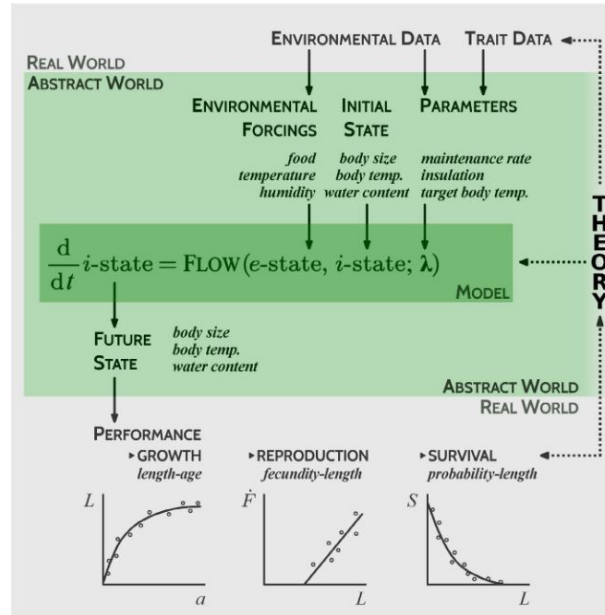


**Figure 1.18:** Model of an organism as a thermodynamic system (Figure from Kearney et al., 2021). Relationships between parameters, state variables of the individual (*i*-state), environmental variables (*e*-state) and traits in a dynamical systems model of organismal performance.

## 1.4 Modeling bivalve symbiotic relationships

### 1.4.1 Ecological metabolic theories

A definition of a metabolic theory is a “Theory governing the application of thermodynamic system principles to quantify the uptake and use of substrates by organisms for development, growth and reproduction, and the rate of ageing” (Kearney et al., 2021) (Fig. 1.18). Models based on metabolic theories were developed such as MTE (metabolic theory of ecology), EST (ecological system theory) and DEB (dynamic energy budget) (Allen & Gillooly, 2009; Kooijman, 2010; van der Meer, 2019). This thesis focus on the DEB theory. Comparing existing models based on metabolic theory is outside the scope of this study and will not be developed further.

### 1.4.2 The dynamic energy budget theory: standard model

The metabolism is all the biochemical reactions catalyzed by enzymes in a living organism to reproduce, developed and react to environmental stimuli. Biochemical reactions are governed by thermodynamic laws and organized themselves in metabolic pathways. Anabolism includes pathways of cellular component biosynthesis and catabolism includes pathways that degrade them.

DEB theory is based on the following assumptions:

- Pool homeostasis (strong homeostasis): for all organisms, pools or state variables with mass have a constant aggregated chemical composition and thermodynamic properties;
- Constant food homeostasis (weak homeostasis): organisms at constant food level tend to a constant chemical composition;
- Food independence: the mobilization of reserve is independent of food availability.

In a standard DEB model (Kooijman, 2010) life cycle begins with the fertilization of the egg and ends with the death of the organism. In this model, life cycle of the organism is divided in three stages according to the level of maturity ( $E_H$ ) of the organism : the embryo, the juvenile and the adult (Figure 1.19).



**Figure 1.19:** Standard DEB model life stages (Kooijman, 2010).

During the embryo stage starting from fertilization to birth, the organism does not feed. The organism starts feeding when birth (maturity  $E_H^b$ ) occurs. It then becomes a juvenile. At puberty (maturity  $E_H^p$ ), it begins to allocate energy to its reproduction buffer. The standard DEB model is defined by four state variables, the reserve ( $E$ ), structure ( $V$ ), maturity ( $E_h$ ) and the reproduction buffer (offspring) ( $E_R$ ) of the organism

(Fig. 1.20). From the mobilized energy of reserve ( $E$ ) a kappa ( $\kappa$ ) fraction is allocated to growth ( $\kappa_G$ ) and somatic maintenance ( $\dot{p}_S$ ), and a  $1-\kappa$  fraction to maturity maintenance ( $\dot{p}_j$ ) and maturation (before puberty) ( $E_h$ ) or reproduction (after puberty) ( $E_R$ ). That is called the "Kappa rule". The  $\kappa$  fraction of mobilized reserve that is allocated to growth and somatic maintenance is a constant which does not depend on the amount of reserve and structure. Somatic maintenance is the use of reserve for maintaining concentration gradients across membranes, heating in endotherms, osmotic work in fresh-water organisms, movement costs and energy dissipated into minerals needed for the turnover of the structure (e.g., the repair of proteins). Somatic maintenance is only proportional to structure ( $V$ ) and the volume-specific somatic maintenance cost ( $\{\dot{p}_M\}$ ). Endotherms and fresh water organisms have also a component of somatic maintenance that is proportional to surface area, the surface-specific somatic maintenance cost ( $\{\dot{p}_T\}$ ). A component of the maturity maintenance is the energy from the reserve dissipated into minerals used for the maintenance of regulation systems and defence work done by the immune system. Maturity maintenance is proportional to the maturity level ( $E_h$ ). Another rule, the priority rule, states that priority is always given to the maintenance branches (somatic and maturity maintenances). A lack of energy to somatic maintenance would lead to the death of the organism.

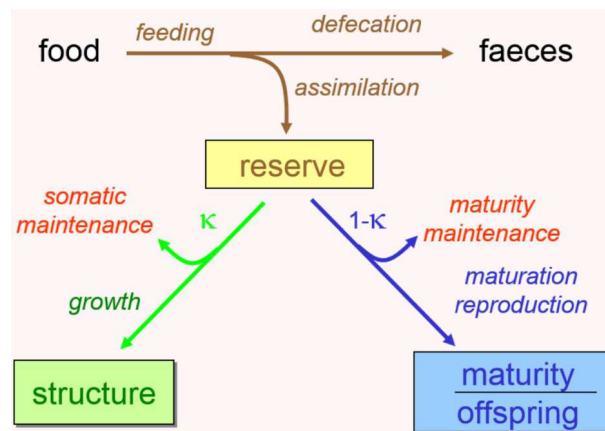


**Figure 1.20:** Standard DEB model modeling scheme (Marques et al., 2018). Boxes: state variables; Arrows: energy fluxes.

In the standard DEB model, the organism is considered as an isomorph, which means it grows proportionally in all three dimensions and maintains its shape as it grows. Its surface area is proportional to its volume raised to two third ( $S \propto V^{2/3}$ ). State variables (Table 1.1) and energy fluxes (Table 1.2) defining the model are expressed using primary parameters (Table 1.3).

Notation	Name (Unit)	Dynamic
$E$	reserve (J)	$\frac{dE}{dt} = \dot{p}_A - \dot{p}_C$
$V$	structure (cm <sup>3</sup> )	$\frac{dV}{dt} = \frac{\dot{p}_G}{[E_G]}$
$E_H$	maturity (J)	$\frac{dE_H}{dt} = \dot{p}_R$ if $E_H < E_H^p$ $\frac{dE_H}{dt} = 0$ otherwise
$E_R$	reproduction buffer (J)	$\frac{dE_R}{dt} = 0$ if $E_H < E_H^p$ $\frac{dE_R}{dt} = \kappa_R \dot{p}_R$ otherwise

**Table 1.1:** Standard dynamic energy budget model dynamic state variables.

The temperature (T) and the functional response (f) are the two forcing variables of a DEB model.  $f$  is an indicator of food availability. Its values are comprised between 0 (starvation) and 1 (fed *ad libitum*).  $f$  always increases to its maximum when the amount of available food increases. The functional response is defined as the Michaelis-Menten function (Eq. 1.2).

$$f = \frac{\frac{X}{K}}{1 + \frac{X}{K}} = \frac{x}{1 + x} \quad (1.2)$$

**Equation 1.2:** Functional response (f). X, food density; K, half saturation coefficient; x, scaled food density.

Temperature correction is applied to rates with a reference temperature  $T_{ref} = 293.15\text{K}$  (Eq. 1.3).

Notation	Name	Formula
$\dot{p}_X$	ingestion	$\{\dot{p}_{Xm}\} f V^{2/3}$ , when $E_H \geq E_H^b$
$\dot{p}_A$	assimilation	$\{\dot{p}_{Am}\} f V^{2/3}$
$\dot{p}_C$	mobilization	$E \frac{\dot{v}[E_G]V^{2/3} + \dot{p}_S}{\kappa E + [E_G]V}$
$\dot{p}_S$	somatic maintenance	$[\dot{p}_M] V + \{\dot{p}_T\} V^{2/3}$
$\dot{p}_G$	growth	$\kappa \dot{p}_C - \dot{p}_S$
$\dot{p}_J$	maturity maintenance cost	$\dot{k}_j E_H$
$\dot{p}_R$	maturation and reproduction	$(1 - \kappa) \dot{p}_C - \dot{p}_J$

**Table 1.2:** Fluxes ( $J d^{-1}$ ) between states variables of the standard Dynamic Energy Budget model.

Notation	Name (Unit)
$\{\dot{p}_{Am}\}$	maximum assimilation flux ( $J d^{-1} cm^{-2}$ )
$\{\dot{F}_m\}$	maximum surface area specific searching rate ( $cm d^{-1} m^{-2}$ )
$\kappa_X$	digestion efficiency of food to reserve (-)
$\kappa_P$	faecation efficiency of food to faeces (-)
$\dot{v}$	energy conductance ( $cm d^{-1}$ )
$\kappa$	allocation fraction to soma (-)
$\kappa_R$	reproduction efficiency (-)
$[\dot{p}_M]$	volume-specific somatic maintenance cost ( $J d^{-1} cm^3$ )
$\{\dot{p}_T\}$	surface-specific somatic maintenance cost ( $J d^{-1} cm^2$ )
$\dot{k}_j$	maturity maintenance rate coefficient ( $d^{-1}$ )
$[E_G]$	specific cost for structure ( $J cm^{-3}$ )
$E_H^b$	maturity at birth (J)
$E_H^p$	maturity at puberty (J)
$\dot{h}_a$	Weibull aging acceleration ( $d^{-2}$ )
$s_G$	Gonbertz stress coefficient (-)

**Table 1.3:** Primary parameters of a standard Dynamic Energy model.

$$\dot{k}(T) = \dot{k}_1 \exp\left(\frac{T_A}{T_{ref}} - \frac{T_A}{T}\right) \quad (1.3)$$

**Equation 1.3:** Temperature correction.  $\dot{k}$ , rate of interest at  $T$ ;  $\dot{k}_1$ , rate of interest at  $T_{ref}$ ;  $T_A$ , species-specific Arrhenius temperature (K);  $T$ , temperature (K)

The variation of the reserve  $E$  (Table 1.1) is the balance between the assimilation flux ( $\dot{p}_A$ ) and the mobilization flux  $\dot{p}_C$  (Table 1.2 for fluxes). The variation of the structure  $V$  (Table 1.1) depends on the energy allocated to growth  $\dot{p}_G$  (J) (Table 1.2) and the volume-specific costs of structure  $[E_G]$  ( $\text{Jcm}^{-3}$ ).  $[E_G]$  is the reserve energy that is required to synthesize a unit volume of structure. When maturity level  $E_H$  is below puberty level  $E_H^p$ , energy is used to increase maturity via  $\dot{p}_R$  flux (in J). When the organism reaches puberty level  $E_H^p$ , no more energy is allocated to maturation and energy is allocated to reproduction. The variation of the reproduction buffer depends on the energy flux allocated to it  $\dot{p}_R$  (J) and the coefficient of reproduction efficiency  $\kappa_R$ . What accumulates in the reproduction buffer is the fraction of energy fixed in eggs. The ingested flux  $\dot{p}_X$  (Table 1.2) depends on: the area responsible for the ingestion  $V^{2/3}$  (in  $\text{cm}^2$ ), the functional response  $f$  and the surface-area specific maximum ingestion rate  $\{\dot{p}_{Xm}\}$  meaning the maximum ingestion rate possible. A fraction of the ingested food is assimilated as reserve. Assimilation rate  $\dot{p}_A$  (Table 1.2) equals the surface-area specific maximum assimilation rate  $\{\dot{p}_{Am}\}$  times the functional response  $f$  times the structural area  $V^{2/3}$  (in  $\text{cm}^2$ ). Assimilation flux  $\dot{p}_A$  is also proportional to the feeding flux:  $\dot{p}_A = \kappa_X \dot{p}_X$ .  $\kappa_X$  is the assimilation efficiency of food, independent of the feeding rate.  $\kappa_X$  can depend on the type of food being assimilated. Different types of food can have different assimilation efficiency.

The Add-my-Pet (AmP) procedure (DEB-tool package, Matlab) (Marques et al., 2018) (Fig. 1.21) is used to estimate primary parameters (Table 1.3) from zero-variate and uni-variates data at given temperature and food level. Four matlab files constitute the architecture of the AmP procedure: the "mydata" file, the "predict" file, the "pars\_init" file and

the "run" file. Firstly, the user input data on its species (also called pet) into the "mydata" file. An initial set of parameters are in the "pars\_init" file. They can be free or fixed. Free parameters will be estimated again during the estimation procedure. Predictions are made from data and parameters with "predict" file using DEB model equations. The estimation procedure is launched by running the "run" file. The "run" file runs the three other files and re-estimate DEB model parameters using a loss-function to compare data and predictions, and a minimization method. The "run" file can be run many times until the loss function reach its minimum.

Primary parameters (Table 1.3) link state variables and compound parameters (Lika et al., 2011).  $z$  is the zoom factor, defined as  $z = L_m/L_m^{ref}$  where  $L_m = \frac{\kappa\{\dot{p}_{Am}\}}{[\dot{p}_M]}$  is the maximal structural length and  $L_m^{ref} = 1\text{cm}$  is a reference of structural length. The specific searching rate  $\{\dot{F}_m\}$  controls food intake if food is not abundant and has no effect at abundant food. In  $\{\dot{F}_m\}$  formulation, the cubed meters in the specific searching rate refer to the environment. Digestion efficiency of food to reserve  $\kappa_X$  is the fraction of ingested flux going to reserve and the faecation efficiency of food to faeces  $\kappa_P$  is the fraction of ingested flux going to faeces. An efficiency coefficient close to 1 means a high efficiency and if close to 0 a low efficiency. Energy conductance  $\dot{v}$  controls the reserve mobilization. A high  $\dot{v}$  gives a high growth rate, short development time to reach birth or maturity, a low maximum reserve density, a rapid occurrence of problems during starvation. The fraction  $\kappa$  is the fraction of mobilized reserve allocated to somatic maintenance and growth, and the reproduction efficiency  $\kappa_R$  is the fraction of mobilized reserve going to the reproduction buffer. Volume-specific somatic maintenance  $[\dot{p}_M]$  is the component of somatic maintenance ( $\dot{p}_S$ , see Table 1.2) that is only proportional to structure (fraction of biomass that is costly in maintenance needs). Surface-specific somatic maintenance cost  $\{\dot{p}_T\}$  is a component of somatic maintenance which is specific to endotherms and fresh water organisms for osmoregulation and heating. Specific cost for structure  $[E_G]$  is the reserve energy that is needed to synthesize a unit volume of structure. Weibull ageing acceleration  $\ddot{h}_a$  and Gompertz stress coeffi-

cient  $s_G$  refers to well-known models of ageing.

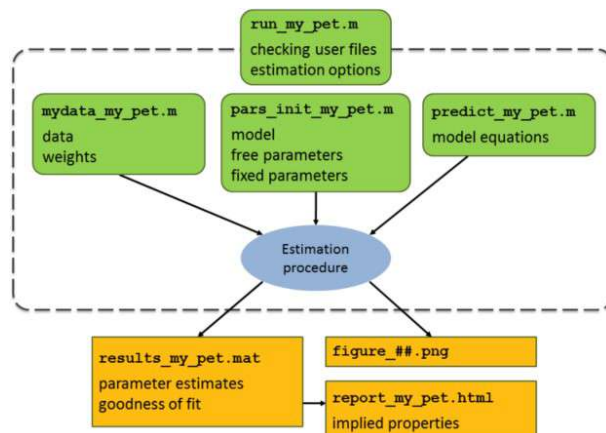


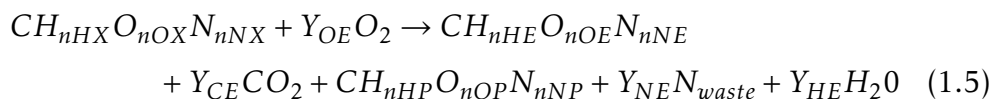
**Figure 1.21:** Architecture of the AmP procedure (Marques et al., 2018).

The standard macro-chemical equation for assimilation is defined in Eq.1.4.



**Equation 1.4:** Standard macro-chemical equation for assimilation (1).  $X$ , food;  $E$ : reserve;  $P$ , faeces;  $N_{waste}$ , nitrogenous waste. The composition depends on the species (e.g.  $NH_4^+$  for  $N_{waste}$  in aquatic environment).

The standard macro-chemical equation can also be written with explicit composition of food, reserve and faeces as in Eq. 1.5.



**Equation 1.5:** Standard macro-chemical equation for assimilation (2).  $E$ , reserve;  $P$ : faeces,  $Y$ , yield in mol/C-mol,  $n$ : chemical indices. By definition,  $n_C$  is equal to 1. For a standard pet the reserve composition is  $CH_{1.8}O_{0.5}N_{0.15}$  (Kooijman, 2010).

### 1.4.3 Examples of ecological applications of DEB theory

Models developed following the DEB theory have various ecological applications (Lavaud et al., 2021a).

#### 1.4.3.1 Inter-species and intra-species variations of functional traits

A functional trait is defined as "a property of a biological thermodynamic system (usually an individual) that functions in the quantification of the performance of that system in terms of survival, development, growth and reproduction." (Kearney et al., 2021). Examples of functional traits are lifespan, reproductive output, maximum body size, growth rate. Functional traits are inferred from estimated DEB parameters. Individual DEB model can be used to compare functional traits of individuals of the same species (i.e., intra-species genotypic and phenotypic variations) and individuals from different species (i.e., inter-species variations) (Augustine & Kooijman, 2019). As an example of inter-species comparison, two loggerhead population of turtles were studied; the Mediterranean population showed a higher maintenance and lower energy allocation to maturation compared to the population from the North Atlantic (Marn et al., 2019).

#### 1.4.3.2 Fluctuations of environmental variables

As forcing variables of DEB modeling are the temperature and the food, the model has been used to predict physiological responses of organisms to change in temperature and food-availability (Monaco & McQuaid, 2018). Dynamic energy budget theory focuses on the individual level (Kooijman, 2010). DEB has been coupled with Individual-Based Model (IBM), which is called DEB-IBM, to study population dynamics in function of environmental variables (Martin et al., 2012). DEB modeling has been used to improve aquaculture, to select the best locations and to study the impact of climate change on organisms' life-history traits such as growth, reproduction, and mortality (Lavaud et al., 2021b; Mangano et al., 2019). DEB-IBM was for example used to assess population dynamic of cultivated oyster populations in the Thau Lagoon (Mediter-

ranean, France) (Bacher & Gangnery, 2006). DEB models can be customized with additional variables, as it was done with salinity (Lavaud et al., 2021b).

### 1.4.3.3 Ecological niche modeling

A DEB model for ectotherm, NicheMapR, includes modeling of heat, water, energy and mass exchange between an ectothermic organism and its environment, and thermoregulatory behaviour (Kearney & Porter, 2020). NicheMapR was notably used to model a lizard growth and reproduction trajectory in function of simulated microclimatic conditions (Kearney & Porter, 2020).

### 1.4.3.4 Ecological risk assessment

Toxico-kinetics were coupled to individual DEB model, giving birth to the DEBtox and DEBKiss models (Baas et al., 2018). DEBtox (or DEB-TKTD) models include toxicokinetics and toxicodynamics parameters, such as the NEC (No Effect Concentration, time-independent threshold concentration below which no effects occurs),  $k_e$  (elimination rate of toxicant),  $k_r$  (killing rate for survival) and  $C_t$  (tolerance concentration for sub-lethal effects ( $\text{mol L}^{-1}$ )) which may affect the organism life traits (e.g., increasing maintenance costs and/or costs of growth and/or costs of reproduction, and/or decreasing the assimilation of food into reserve...) (Fig. 1.22) (Baas et al., 2018). DEBKiss (Jager et al., 2013) model is a simplification of the DEB theory which excludes the reserve dynamics and may also exclude maturity of the organism if not needed, resulting in less state variables (Baas et al., 2018; Jager et al., 2013). DEBKiss eases the study of complex toxicological effect such as the effect of mixtures (Baas et al., 2018; Jager, 2020; Jager et al., 2013). DEBtox is notably considered by the European Food Safety Authority for environmental risk assessment (ERA) of pesticides in Europe (Jager, 2020; Martin et al., 2024). As an example of ERA using DEB, the reproductive effects of a fungicide on a bird (*Colinus virginianus*) was modeled (Martin et al., 2024). Fungicide exposure in the eggs observed effects

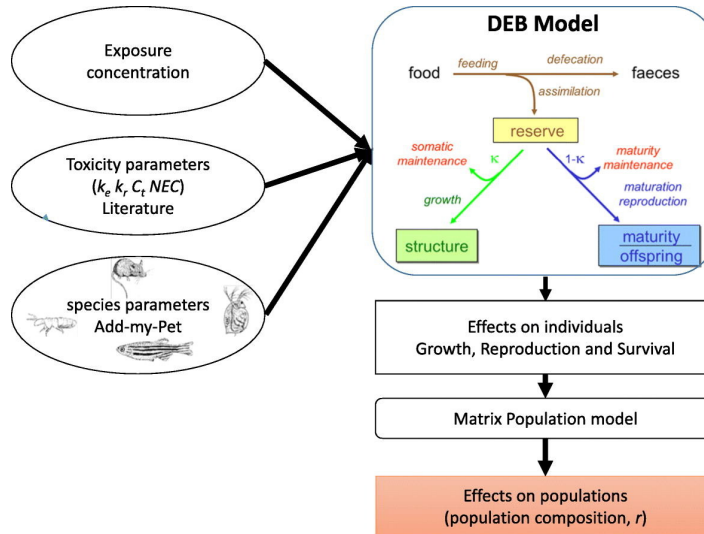


**Figure 1.22:** Dynamic Energy Budget and ecological risk assessment (Figure from Baas et al., 2018).

at hatching and post-hatching such as observed weight reductions were well predicted by the DEBtox model (Martin et al., 2024).

## 1.5 Objectives of the thesis

This thesis is a part of the BEVEGA project, initially the “Biology and ecology of deep-sea vesicomyid bivalves from the Guaymas Basin (Mexico, Pacific Ocean): engineer species of deep chemosynthetic ecosystems” (80 PRIME CNRS, PI Sylvie Gaudron, UMR8187 LOG). The project initially aimed at analyzing the ecology, the life traits, and the physiology of symbiotic vesicomyid species from the Guaymas Basin and the physico-chemical characterization of their habitats. As the oceanographic mission in the Guaymas Basin did not happen because of the COVID-19 crisis, the thesis focused on a deep-sea vesicomyid species from cold seeps of the Gulf of Guinea (eastern tropical Atlantic Ocean), for which lot of data were available, and on a symbiotic lucinid species from seagrasses in Roscoff, France (English channel) that can be easily sampled at low tide. Both deep-sea and shallow-water symbiotic species are endemic species and ecosystems engineer within their respective habitats. In the deep sea, the increasing anthropogenic pres-

sure such as the rapid expansion of mineral, oil and gas extraction is worrying (Cordes et al., 2016). Shallow-water chemosynthetic habitat such as seagrasses are under great anthropological pressure impacting the water quality, creating physical disturbance, and degrading the food webs (Unsworth et al., 2019). In addition, shallow-water chemosynthetic ecosystems are also subject to climate change (Chefaoui et al., 2018; Ward et al., 2016). The aim of the thesis was to develop dynamic energy budgets on these unique symbiotic species to later evaluate the impact of temperature and food availability changes on their life traits.

The Chapter 2 of this thesis focuses on the development of a dynamic energy budget model for the obligate deep-sea symbiotrophic bivalve species, *Christineconcha regab*, at the adult stage. The novel dynamic energetic model developed in this thesis incorporates the sulfur-oxidizing symbionts into the DEB model. There were no such DEB model developed yet. Results obtained are deciphered to understand both host and symbionts functional traits and dynamic relationship.

Then, the Chapter 3 of this thesis is about the conceptual ideas for the development of a DEB model for the shallow water lucinid species *Loripes orbiculatus* and its sulfur-oxidizing symbionts. Experimental data are collected to feed the model. The aim is to adapt the model developed in Chapter 2 (called abj-farming model) to a shallow water mixotrophic species, *Loripes orbiculatus*, which use both filter feeding of particulate organic mater and symbionts as food sources.

The last chapter discusses the Chapters 2 and 3 scientific contributions and perspectives, and the interest and relevance of the use of such models.

## References

- Allen, A. P., & Gillooly, J. F. (2009). Towards an integration of ecological stoichiometry and the metabolic theory of ecology to better understand nutrient cycling. *Ecology Letters*, 12(5), 369–384. <https://doi.org/10.1111/j.1461-0248.2009.01302.x>
- Allen, J. D., & Pernet, B. (2007). Intermediate modes of larval development: Bridging the gap between planktotrophy and lecithotrophy. *Evolution & Development*, 9(6), 643–653. <https://doi.org/10.1111/j.1525-142X.2007.00202.x>
- Ansorge, R., Romano, S., Sayavedra, L., Porras, M. Á. G., Kupczok, A., Tegetmeyer, H. E., Dubilier, N., & Petersen, J. (2019). Functional diversity enables multiple symbiont strains to coexist in deep-sea mussels. *Nature Microbiology*, 4(12), 2487–2497. <https://doi.org/10.1038/s41564-019-0572-9>
- Arndt, N. (2011). White Smoker. In M. Gargaud, R. Amils, J. C. Quintanilla, H. J. (Cleaves, W. M. Irvine, D. L. Pinti, & M. Viso (Eds.), *Encyclopedia of Astrobiology* (pp. 1779–1779). Springer. [https://doi.org/10.1007/978-3-642-11274-4\\_1691](https://doi.org/10.1007/978-3-642-11274-4_1691)
- Augustine, S., & Kooijman, S. A. L. M. (2019). A new phase in DEB research. *Journal of Sea Research*, 143, 1–7. <https://doi.org/10.1016/j.seares.2018.06.003>
- Azofeifa-Solano, J. C., Pereira, O. S., Cowell, E. J., Cordes, E. E., Levin, L. A., Goffredi, S. K., & Cortés, J. (2022). Sexual dimorphism in the methane seep-dwelling Costa Rican yeti crab *Kiwa puravida* (Decapoda: Anomura: Kiwaidae). *Frontiers in Marine Science*, 9. <https://www.frontiersin.org/articles/10.3389/fmars.2022.1051590>
- Baas, J., Augustine, S., Marques, G. M., & Dorne, J.-L. (2018). Dynamic energy budget models in ecological risk assessment: From principles to applications. *Science of The Total Environment*, 628–629, 249–260. <https://doi.org/10.1016/j.scitotenv.2018.02.058>
- Bacher, C., & Gangnery, A. (2006). Use of dynamic energy budget and individual based models to simulate the dynamics of cultivated

- oyster populations. *Journal of Sea Research*, 56(2), 140–155. <https://doi.org/10.1016/j.seares.2006.03.004>
- Bieler, R., & Mikkelsen, P. M. (2006). Bivalvia – a look at the Branches. *Zoological Journal of the Linnean Society*, 148(3), 223–235. <https://doi.org/10.1111/j.1096-3642.2006.00255.x>
- Bieler, R., Mikkelsen, P. M., & Giribet, G. (2013). Bivalvia—A Discussion of Known Unknowns\*. *American Malacological Bulletin*, 31(1), 123–133. <https://doi.org/10.4003/006.031.0105>
- Boetius, A., Ravensschlag, K., Schubert, C. J., Rickert, D., Widdel, F., Gieseke, A., Amann, R., Jørgensen, B. B., Witte, U., & Pfannkuche, O. (2000). A marine microbial consortium apparently mediating anaerobic oxidation of methane. *Nature*, 407(6804), 623–626. <https://doi.org/10.1038/35036572>
- Boetius, A., & Wenzhöfer, F. (2013). Seafloor oxygen consumption fuelled by methane from cold seeps. *Nature Geoscience*, 6(9), 725–734. <https://doi.org/10.1038/ngeo1926>
- Cardini, U., Marín-Guirao, L., Montilla, L. M., Marzocchi, U., Chiavarini, S., Rimauro, J., Quero, G. M., Petersen, J. M., & Procaccini, G. (2022). Nested interactions between chemosynthetic lucinid bivalves and seagrass promote ecosystem functioning in contaminated sediments. *Frontiers in Plant Science*, 13, 918675. <https://doi.org/10.3389/fpls.2022.918675>
- Cavanaugh, C. M. (1983). Symbiotic chemoautotrophic bacteria in marine invertebrates from sulphide-rich habitats. *Nature*, 302(5903), 58–61. <https://doi.org/10.1038/302058a0>
- Bandiera\_abtest: a  
Cg\_type: Nature Research Journals  
Primary\_atype: Research
- Chefaoui, R. M., Duarte, C. M., & Serrão, E. A. (2018). Dramatic loss of seagrass habitat under projected climate change in the Mediterranean Sea. *Global Change Biology*, 24(10), 4919–4928. <https://doi.org/10.1111/gcb.14401>
- Chin, D. W., de Fouw, J., van der Heide, T., Cahill, B. V., Katcher, K., Paul, V. J., Campbell, J. E., & Peterson, B. J. (2021). Facilitation

- of a tropical seagrass by a chemosymbiotic bivalve increases with environmental stress. *Journal of Ecology*, 109(1), 204–217. <https://doi.org/10.1111/1365-2745.13462>
- Coan, E., & Valentich-Scott, P. (2006, January 1). Chapter 27. Marine bivalves, in: *The mollusks: A guide to their study, collection, and preservation*.
- Cordes, E. E., Jones, D. O. B., Schlacher, T. A., Amon, D. J., Bernardino, A. F., Brooke, S., Carney, R., DeLeo, D. M., Dunlop, K. M., Escobar-Briones, E. G., Gates, A. R., Génio, L., Gobin, J., Henry, L.-A., Herrera, S., Hoyt, S., Joye, M., Kark, S., Mestre, N. C., ... Witte, U. (2016). Environmental Impacts of the Deep-Water Oil and Gas Industry: A Review to Guide Management Strategies. *Frontiers in Environmental Science*, 4. <https://www.frontiersin.org/articles/10.3389/fenvs.2016.00058>
- Corliss, J. B., Dymond, J., Gordon, L. I., Edmond, J. M., Herzen, R. P. von, Ballard, R. D., Green, K., Williams, D., Bainbridge, A., Crane, K., & Andel, T. H. van. (1979). Submarine Thermal Springs on the Galápagos Rift. *Science*, 203(4385), 1073–1083. <https://doi.org/10.1126/science.203.4385.1073>
- Cox, L. R. (1960). THOUGHTS ON THE CLASSIFICATION OF THE BIVALVIA. *Journal of Molluscan Studies*, 34(2), 60–88. <https://doi.org/10.1093/oxfordjournals.mollus.a064847>
- de Fouw, J., Govers, L. L., van de Koppel, J., van Belzen, J., Dorigo, W., Sidi Cheikh, M. A., Christianen, M. J. A., van der Reijden, K. J., van der Geest, M., Piersma, T., Smolders, A. J. P., Olf, H., Lamers, L. P. M., van Gils, J. A., & van der Heide, T. (2016). Drought, Mutualism Breakdown, and Landscape-Scale Degradation of Seagrass Beds. *Current Biology*, 26(8), 1051–1056. <https://doi.org/10.1016/j.cub.2016.02.023>
- Distel, D. L., Altamia, M. A., Lin, Z., Shipway, J. R., Han, A., Forteza, I., Antemano, R., Limbaco, M. G. J. P., Tebo, A. G., Dechavez, R., Albano, J., Rosenberg, G., Concepcion, G. P., Schmidt, E. W., & Haygood, M. G. (2017). Discovery of chemoautotrophic symbiosis in the giant shipworm *Kuphus polythalamia* (Bivalvia: Teredinidae)

- extends wooden-steps theory. *Proceedings of the National Academy of Sciences*, 114(18), E3652–E3658. <https://doi.org/10.1073/pnas.1620470114>
- Distel, D. L., Baco, A. R., Chuang, E., Morrill, W., Cavanaugh, C., & Smith, C. R. (2000). Do mussels take wooden steps to deep-sea vents? *Nature*, 403(6771), 725–726. <https://doi.org/10.1038/35001667>
- Donaher, S. E., Baillie, C. J., Smith, C. S., Zhang, Y. S., Albright, A., Trackenberg, S. N., Wellman, E. H., Woodard, N., & Gittman, R. K. (2021). Bivalve facilitation mediates seagrass recovery from physical disturbance in a temperate estuary. *Ecosphere*, 12(11), e03804. <https://doi.org/10.1002/ecs2.3804>
- Douglas, A. E. (1994, January 20). *Symbiotic Interactions*. Oxford University Press. <https://doi.org/10.1093/oso/9780198542865.001.0001>
- Douglas, A. E. (2008). Conflict, cheats and the persistence of symbioses. *New Phytologist*, 177(4), 849–858. <https://doi.org/10.1111/j.1469-8137.2007.02326.x>
- Douglas, A. E. (2014). Symbiosis as a General Principle in Eukaryotic Evolution. *Cold Spring Harbor Perspectives in Biology*, 6(2), a016113. <https://doi.org/10.1101/cshperspect.a016113>
- Douglas, A. E., & Werren, J. H. (2016). Holes in the Hologenome: Why Host-Microbe Symbioses Are Not Holobionts. *mBio*, 7(2), 10.1128/mbio.02099–15. <https://doi.org/10.1128/mbio.02099-15>
- Dubilier, N., Mülders, C., Ferdelman, T., de Beer, D., Pernthaler, A., Klein, M., Wagner, M., Erséus, C., Thiermann, F., Krieger, J., Giere, O., & Amann, R. (2001). Endosymbiotic sulphate-reducing and sulphide-oxidizing bacteria in an oligochaete worm. *Nature*, 411(6835), 298–302. <https://doi.org/10.1038/35077067>
- Dufour, S. C. (2005). Gill anatomy and the evolution of symbiosis in the bivalve family Thyasiridae. *The Biological Bulletin*, 208(3), 200–212. <https://doi.org/10.2307/3593152>
- Duperron, S., Gaudron, S. M., Rodrigues, C. F., Cunha, M. R., Decker, C., & Olu, K. (2013). An overview of chemosynthetic symbioses

- in bivalves from the North Atlantic and Mediterranean Sea. *Bio-geosciences*, 10(5), 3241–3267. <https://doi.org/10.5194/bg-10-3241-2013>
- Enrich-Prast, A., Bastviken, D., & Crill, P. M. (2009). Chemosynthesis. Elsevier. <https://urn.kb.se/resolve?urn=urn:nbn:se:liu:diva-28244>
- Fisher, C. R., Takai, K., & Le Bris, N. (2007). Hydrothermal Vent Ecosystems. *Oceanography*, 20(1), 14–23. <http://www.jstor.org/stable/24859970>
- Formaggioni, A., Plazzi, F., & Passamonti, M. (2022). Mito-nuclear co-evolution and phylogenetic artifacts: The case of bivalve mollusks. *Scientific Reports*, 12(1), 11040. <https://doi.org/10.1038/s41598-022-15076-y>
- Fouquet, Y. (2011). Black Smoker. In M. Gargaud, R. Amils, J. C. Quintanilla, H. J. (Cleaves, W. M. Irvine, D. L. Pinti, & M. Viso (Eds.), *Encyclopedia of Astrobiology* (pp. 213–213). Springer. [https://doi.org/10.1007/978-3-642-11274-4\\_201](https://doi.org/10.1007/978-3-642-11274-4_201)
- Giribet, G., DeSalle, R., & Wheeler, W. C. (2002). ‘Pluralism’ and the aims of phylogenetic research. In R. DeSalle, W. Wheeler, & G. Giribet (Eds.), *Molecular Systematics and Evolution: Theory and Practice* (pp. 141–146). Birkhäuser. [https://doi.org/10.1007/978-3-0348-8114-2\\_10](https://doi.org/10.1007/978-3-0348-8114-2_10)
- Giribet, G., & Wheeler, W. (2002). On bivalve phylogeny: A high-level analysis of the Bivalvia (Mollusca) based on combined morphology and DNA sequence data. *Invertebrate Biology*, 121(4), 271–324. <https://doi.org/10.1111/j.1744-7410.2002.tb00132.x>
- Goffredi, S. K., Hurtado, L., Hallam, S., & Vrijenhoek, R. (2003). Evolutionary relationships of deep-sea vent and cold seep clams (Mollusca: Vesicomidae) of the " pacifica/lepta " species complex. *Marine Biology*, 142(2), 311–320. <https://doi.org/10.1007/s00227-002-0941-3>
- Goffredi, S. K., Jones, W. J., Erhlich, H., Springer, A., & Vrijenhoek, R. C. (2008). Epibiotic bacteria associated with the recently discovered

- Yeti crab, *Kiwa hirsuta*. *Environmental Microbiology*, 10(10), 2623–2634. <https://doi.org/10.1111/j.1462-2920.2008.01684.x>
- Govindjee, & Krogmann, D. (2004). Discoveries in Oxygenic Photosynthesis (1727-2003): A Perspective - ProQuest. *Photosynthesis Research*, 80, 15–27. <https://doi.org/10.1023/B:PRES.0000030443.63979.e6>
- Guéganton, M., Rouxel, O., Durand, L., Cueff-Gauchard, V., Gayet, N., Pradillon, F., & Cambon-Bonavita, M.-A. (2022). Anatomy and Symbiosis of the Digestive System of the Vent Shrimp *Rimicaris Exoculata* and *Rimicaris Chacei* Revealed Through Imaging Approaches. *Frontiers in Marine Science*, 9. <https://www.frontiersin.org/articles/10.3389/fmars.2022.903748>
- Guo, Y., Meng, L., Wang, M., Zhong, Z., Li, D., Zhang, Y., Li, H., Zhang, H., Seim, I., Li, Y., Jiang, A., Ji, Q., Su, X., Chen, J., Fan, G., Li, C., & Liu, S. (2023). Hologenome analysis reveals independent evolution to chemosymbiosis by deep-sea bivalves. *BMC Biology*, 21(1), 51. <https://doi.org/10.1186/s12915-023-01551-z>
- Jager, T. (2020). Revisiting simplified DEBtox models for analysing ecotoxicity data. *Ecological Modelling*, 416, 108904. <https://doi.org/10.1016/j.ecolmodel.2019.108904>
- Jager, T., Martin, B. T., & Zimmer, E. I. (2013). DEBkiss or the quest for the simplest generic model of animal life history. *Journal of Theoretical Biology*, 328, 9–18. <https://doi.org/10.1016/j.jtbi.2013.03.011>
- Joyce, A., & Vogeler, S. (2018). Molluscan bivalve settlement and metamorphosis: Neuroendocrine inducers and morphogenetic responses. *Aquaculture*, 487, 64–82. <https://doi.org/10.1016/j.aquaculture.2018.01.002>
- Kearney, M. R., Jusup, M., McGeoch, M. A., Kooijman, S. A. L. M., & Chown, S. L. (2021). Where do functional traits come from? The role of theory and models. *Functional Ecology*, 35(7), 1385–1396. <https://doi.org/10.1111/1365-2435.13829>
- Kearney, M. R., & Porter, W. P. (2020). NicheMapR – an R package for biophysical modelling: The ectotherm and Dynamic Energy Bud-

- get models. *Ecography*, 43(1), 85–96. <https://doi.org/10.1111/ecog.04680>
- Kooijman, S. A. L. M. (2010). *Dynamic Energy Budget Theory for Metabolic Organisation*. Cambridge University Press.
- Krylova, E. M., Sahling, H., & Janssen, R. (2010). Abyssogena: A new genus of the family Vesicomidae (Bivalvia) from deep-water vents and seeps. *Journal of Molluscan Studies*, 76(2), 107–132. <https://doi.org/10.1093/mollus/eyp052>
- Lamers, L., Govers, L., Janssen, I., Geurts, J., Van der Welle, M., Van Katwijk, M., Van der Heide, T., Roelofs, J., & Smolders, A. (2013). Sulfide as a soil phytotoxin—a review. *Frontiers in Plant Science*, 4. <https://www.frontiersin.org/articles/10.3389/fpls.2013.00268>
- Laming, S. (2014, September 24). *Patterns in adaptive developmental biology and symbioses of small-sized deep-sea chemosymbiotic mussels (Bathymodiolinae)* (These de doctorat). Paris 6. <http://www.theses.fr/fr/2014PA066265>
- Lan, Y., Sun, J., Chen, C., Sun, Y., Zhou, Y., Yang, Y., Zhang, W., Li, R., Zhou, K., Wong, W. C., Kwan, Y. H., Cheng, A., Bougouffa, S., Van Dover, C. L., Qiu, J.-W., & Qian, P.-Y. (2021). Hologenome analysis reveals dual symbiosis in the deep-sea hydrothermal vent snail *Gigantopelta aegis*. *Nature Communications*, 12(1), 1165. <https://doi.org/10.1038/s41467-021-21450-7>
- Laurent, M. C. Z., Le Bris, N., Gaill, F., & Gros, O. (2013). Dynamics of wood fall colonization in relation to sulfide concentration in a mangrove swamp. *Marine Environmental Research*, 87–88, 85–95. <https://doi.org/10.1016/j.marenvres.2013.03.007>
- Lavaud, R., Filgueira, R., & Augustine, S. (2021a). The role of Dynamic Energy Budgets in conservation physiology. *Conservation Physiology*, 9(1), coab083. <https://doi.org/10.1093/conphys/coab083>
- Lavaud, R., La Peyre, M. K., Justic, D., & La Peyre, J. F. (2021b). Dynamic Energy Budget modelling to predict eastern oyster growth, reproduction, and mortality under river management and cli-

- mate change scenarios. *Estuarine, Coastal and Shelf Science*, 251, 107188. <https://doi.org/10.1016/j.ecss.2021.107188>
- Levin, L. (2003). Oxygen minimum zone benthos: Adaptation and community response to hypoxia. *Oceanography and Marine Biology: An Annual Review*, 41, 1–45.
- Lika, K., Kearney, M. R., & Kooijman, S. A. L. M. (2011). The “covariation method” for estimating the parameters of the standard Dynamic Energy Budget model II: Properties and preliminary patterns. *Journal of Sea Research*, 66(4), 278–288. <https://doi.org/10.1016/j.seares.2011.09.004>
- Mangano, M. C., Giacoletti, A., & Sarà, G. (2019). Dynamic Energy Budget provides mechanistic derived quantities to implement the ecosystem based management approach. *Journal of Sea Research*, 143, 272–279. <https://doi.org/10.1016/j.seares.2018.05.009>
- Marn, N., Jusup, M., Catteau, S., Kooijman, S. A. L. M., & Klanjšček, T. (2019). Comparative physiological energetics of Mediterranean and North Atlantic loggerhead turtles. *Journal of Sea Research*, 143, 100–118. <https://doi.org/10.1016/j.seares.2018.06.010>
- Marques, G. M., Augustine, S., Lika, K., Pecquerie, L., Domingos, T., & Kooijman, S. A. L. M. (2018). The AmP project: Comparing species on the basis of dynamic energy budget parameters. *PLOS Computational Biology*, 14(5), e1006100. <https://doi.org/10.1371/journal.pcbi.1006100>
- Martin, B. T., Zimmer, E. I., Grimm, V., & Jager, T. (2012). Dynamic Energy Budget theory meets individual-based modelling: A generic and accessible implementation. *Methods in Ecology and Evolution*, 3(2), 445–449. <https://doi.org/10.1111/j.2041-210X.2011.00168.x>
- Martin, T., Bauer, B., Baier, V., Paini, A., Schaller, S., Hubbard, P., Ebeling, M., Heckmann, D., & Gergs, A. (2024). Reproductive toxicity in birds predicted by physiologically-based kinetics and bioenergetics modelling. *Science of The Total Environment*, 912, 169096. <https://doi.org/10.1016/j.scitotenv.2023.169096>

- Maxwell, P. S., Eklöf, J. S., van Katwijk, M. M., O'Brien, K. R., de la Torre-Castro, M., Boström, C., Bouma, T. J., Krause-Jensen, D., Unsworth, R. K. F., van Tussenbroek, B. I., & van der Heide, T. (2017). The fundamental role of ecological feedback mechanisms for the adaptive management of seagrass ecosystems – a review. *Biological Reviews*, 92(3), 1521–1538. <https://doi.org/10.1111/brv.12294>
- Monaco, C. J., & McQuaid, C. D. (2018). Applicability of Dynamic Energy Budget (DEB) models across steep environmental gradients. *Scientific Reports*, 8(1), 16384. <https://doi.org/10.1038/s41598-018-34786-w>
- Neulinger, S. C., Sahling, H., Süling, J., & Imhoff, J. F. (2006). Presence of two phylogenetically distinct groups in the deep-sea mussel *Acharax* (Mollusca: Bivalvia: Solemyidae). *Marine Ecology Progress Series*, 312, 161–168. <https://doi.org/10.3354/meps312161>
- Oliver, P. G. (2013). Description of *Atopomya dolobrata* gen. et sp. nov.: First record of bacterial symbiosis in the Saxicavellinae (Bivalvia). *Journal of Conchology*, 41, 359–367.
- Oliver, P. G., Holmes, A. M., Killeen, I. J., & Turner, J. A. (2016). *Marine Bivalve Shells of the British Isles*. Amgueddfa Cymru - National Museum Wales. <http://naturalhistory.museumwales.ac.uk/britishbivalves>
- Oliver, P. G., Southward, E. C., & Dando, P. R. (2013). Bacterial symbiosis in *Syssitomya pourtalesiana* Oliver, 2012 (Galeommatoidea: Montacutidae), a bivalve commensal with the deep-sea echinoid *Pourtalesia*. *Journal of Molluscan Studies*, 79(1), 30–41. <https://doi.org/10.1093/mollus/eyr031>
- Oliver, P. G., & Taylor, J. D. (2012). Bacterial symbiosis in the Nucinellidae (Bivalvia: Solemyida) with descriptions of two new species. *Journal of Molluscan Studies*, 78(1), 81–91. <https://doi.org/10.1093/mollus/eyr045>
- Paull, C. K., Hecker, B., Commeau, R., Freeman-Lynde, R. P., Neumann, C., Corso, W. P., Golubic, S., Hook, J. E., Sikes, E., & Curray, J. (1984). Biological Communities at the Florida Escarpment Re-

- semble Hydrothermal Vent Taxa. *Science*, 226(4677), 965–967. <https://doi.org/10.1126/science.226.4677.965>
- Roeselers, G., & Newton, I. L. G. (2012). On the evolutionary ecology of symbioses between chemosynthetic bacteria and bivalves. *Applied Microbiology and Biotechnology*, 94(1), 1–10. <https://doi.org/10.1007/s00253-011-3819-9>
- Rosenberg, E., & Zilber-Rosenberg, I. (2011). Symbiosis and development: The hologenome concept. *Birth Defects Research Part C: Embryo Today: Reviews*, 93(1), 56–66. <https://doi.org/10.1002/bdrc.20196>
- Sanmartí, N., Solé, L., Romero, J., & Pérez, M. (2018). Seagrass-bivalve facilitative interactions: Trait-mediated effects along an environmental gradient. *Marine Environmental Research*, 133, 99–104. <https://doi.org/10.1016/j.marenvres.2017.12.002>
- Scheutz, C., Kjeldsen, P., Bogner, J., De Visscher, A., Gebert, J., Hilger, H., Huber-Humer, M., & Spokas, K. (2009). Microbial Methane Oxidation Processes and Technologies for Mitigation of Landfill gas Emissions. *Waste management & research : the journal of the International Solid Wastes and Public Cleansing Association, ISWA*, 27, 409–55. <https://doi.org/10.1177/0734242X09339325>
- Seilacher, A. (1985). Bivalve Morphology and Function. *Series in Geology, Notes for Short Course*, 13, 88–101. <https://doi.org/10.1017/S0271164800001111>
- Seilacher, A. (1990). Aberrations in bivalve evolution related to photo- and chemosymbiosis. *Historical Biology*, 3(4), 289–311. <https://doi.org/10.1080/08912969009386528>
- Seilacher, A. (1999). Biomat-Related Lifestyles in the Precambrian. *PALAIOS*, 14(1), 86–93. <https://doi.org/10.2307/3515363>
- Short, F., Carruthers, T., Dennison, W., & Waycott, M. (2007). Global seagrass distribution and diversity: A bioregional model. *Journal of Experimental Marine Biology and Ecology*, 350(1), 3–20. <https://doi.org/10.1016/j.jembe.2007.06.012>
- Sibuet, M., & Roy, K. O.-L. (2003). Cold Seep Communities on Continental Margins: Structure and Quantitative Distribution Relative

- to Geological and Fluid Venting Patterns. In G. Wefer, D. Billett, D. Hebbeln, B. B. Jørgensen, M. Schlüter, & T. C. E. van Weering (Eds.), *Ocean Margin Systems* (pp. 235–251). Springer. [https://doi.org/10.1007/978-3-662-05127-6\\_15](https://doi.org/10.1007/978-3-662-05127-6_15)
- Sibuet, M., & Olu, K. (1998). Biogeography, biodiversity and fluid dependence of deep-sea cold-seep communities at active and passive margins. *Deep Sea Research Part II: Topical Studies in Oceanography*, 45(1), 517–567. [https://doi.org/10.1016/S0967-0645\(97\)00074-X](https://doi.org/10.1016/S0967-0645(97)00074-X)
- Sogin, E. M., Kleiner, M., Borowski, C., Gruber-Vodicka, H. R., & Dubilier, N. (2021). Life in the Dark: Phylogenetic and Physiological Diversity of Chemosynthetic Symbioses. *Annual Review of Microbiology*, 75(1), 695–718. <https://doi.org/10.1146/annurev-micro-051021-123130>
- Sogin, E. M., Leisch, N., & Dubilier, N. (2020). Chemosynthetic symbioses. *Current Biology*, 30(19), R1137–R1142. <https://doi.org/10.1016/j.cub.2020.07.050>
- Stachowicz, J. J. (2011). Symbiosis. *BioScience*, 61(4), 326–327. <https://doi.org/10.1525/bio.2011.61.4.16>
- Stanley, S. M. (1972). Functional Morphology and Evolution of Byssally Attached Bivalve Mollusks. *Journal of Paleontology*, 46(2), 165–212. <https://www.jstor.org/stable/1302843>
- Staudigel, H., Koppers, A., Lavelle, J. W., Pitcher, T., & Shank, T. (2010). Defining the Word "Seamount". *Oceanography*, 23(01), 20–21. <https://doi.org/10.5670/oceanog.2010.85>
- Stirbet, A., Lazar, D., Guo, Y., & Govindjee, G. (2020). Photosynthesis: Basics, history and modelling. *Annals of Botany*, 126(4), 511–537. <https://doi.org/10.1093/aob/mcz171>
- Suess, E. (2014). Marine cold seeps and their manifestations: Geological control, biogeochemical criteria and environmental conditions. *International Journal of Earth Sciences*, 103(7), 1889–1916. <https://doi.org/10.1007/s00531-014-1010-0>
- Suess, E. (2018). Marine Cold Seeps: Background and Recent Advances. In H. Wilkes (Ed.), *Hydrocarbons, Oils and Lipids: Diversity, Origin,*

- Chemistry and Fate* (pp. 1–21). Springer International Publishing. [https://doi.org/10.1007/978-3-319-54529-5\\_27-1](https://doi.org/10.1007/978-3-319-54529-5_27-1)
- Taylor, J. D., & Glover, E. (2000). Functional anatomy, chemosymbiosis and evolution of the Lucinidae. *Geological Society, London, Special Publications*, 177(1), 207–225. <https://doi.org/10.1144/GSL.SP.2000.177.01.12>
- Taylor, J. D., & Glover, E. (2006). Lucinidae (Bivalvia)–the most diverse group of chemosymbiotic molluscs. *Zoological Journal of the Linnean Society*, 148(3), 421–438. <https://doi.org/10.1111/j.1096-3642.2006.00261.x>
- Taylor, J. D., & Glover, E. (2010). Chemosymbiotic Bivalves. In S. Kiel (Ed.), *The Vent and Seep Biota: Aspects from Microbes to Ecosystems* (pp. 107–135). Springer Netherlands. [https://doi.org/10.1007/978-90-481-9572-5\\_5](https://doi.org/10.1007/978-90-481-9572-5_5)
- Taylor, J. D., & Glover, E. (2021, January 14). *Biology, evolution and generic review of the chemosymbiotic bivalve family Lucinidae*.
- Thurber, A. R., Jones, W. J., & Schnabel, K. (2011). Dancing for Food in the Deep Sea: Bacterial Farming by a New Species of Yeti Crab. *PLOS ONE*, 6(11), e26243. <https://doi.org/10.1371/journal.pone.0026243>
- Unsworth, R. K. F., Cullen-Unsworth, L. C., Jones, B. L. H., & Lilley, R. J. (2022). The planetary role of seagrass conservation. *Science*, 377(6606), 609–613. <https://doi.org/10.1126/science.abq6923>
- Unsworth, R. K. F., McKenzie, L. J., Collier, C. J., Cullen-Unsworth, L. C., Duarte, C. M., Eklöf, J. S., Jarvis, J. C., Jones, B. L., & Nordlund, L. M. (2019). Global challenges for seagrass conservation. *Ambio*, 48(8), 801–815. <https://doi.org/10.1007/s13280-018-1115-y>
- van der Meer, J. (2019, January 1). Metabolic Theories in Ecology: The Dynamic Energy Budget Theory and the Metabolic Theory of Ecology. In B. Fath (Ed.), *Encyclopedia of Ecology (Second Edition)* (pp. 463–471). Elsevier. <https://doi.org/10.1016/B978-0-12-409548-9.10568-8>
- Venkatesan, V., & Mohamed, K. S. (2015). *Bivalve classification and taxonomy*. <http://eprints.cmfri.org.in/10413/>

- Wada, H., Phuangphong, S., Hashimoto, N., & Nagai, K. (2020). Establishment of the novel bivalve body plan through modification of early developmental events in mollusks. *Evolution & Development*, 22(6), e12334. <https://doi.org/10.1111/ede.12334>
- Wanninger, A., & Wollesen, T. (2019). The evolution of molluscs. *Biological Reviews*, 94(1), 102–115. <https://doi.org/10.1111/brv.12439>
- Ward, R. D., Friess, D. A., Day, R. H., & Mackenzie, R. A. (2016). Impacts of climate change on mangrove ecosystems: A region by region overview. *Ecosystem Health and Sustainability*, 2(4), e01211. <https://doi.org/10.1002/ehs2.1211>

## Chapter 2

# *Christineconcha regab*, a deep-sea symbiotrophic bivalve

Trade-off strategy hypothesis between a deep-sea clam and its sulfur-oxidizing symbiont deciphered by a bioenergetic model

M. Vandenberghe<sup>1\*</sup>, G. M. Marques<sup>2</sup>, A. C. Andersen<sup>3</sup>, C. Decker<sup>4</sup>, K. Olu<sup>4</sup>, S. Duperron<sup>5</sup>, S. M. Gaudron<sup>1,6</sup>

1 UMR 8187 Laboratoire d'Océanologie et de Géosciences (LOG), Université de Lille, ULCO, CNRS, IRD, F-59000 Lille, France

2 Marine, Environment & Technology Center (MARETEC), LARSyS, Instituto Superior Técnico, University of Lisboa, Portugal

3 Sorbonne Université-CNRS UMR 7144 Adaptation et Diversité des Organismes Marins, Station Biologique de Roscoff, France

4 IFREMER, Laboratoire Environnement Profond (REM - EEP - LEP), 29280 Plouzané, France

5 UMR7245 Molécules de Communication et Adaptation des Microorganismes, Muséum national d'Histoire naturelle, Paris, France

6 Sorbonne Université, UFR 927, F-75005 Paris, France

## Abstract

Symbiotic nutrition is widespread in macro-invertebrates in deep-sea chemosynthetic ecosystems. A novel Dynamic Energy Budget (DEB) model was developed for a symbiotic deep-sea bivalve species (*Christineconcha regab*, Mollusca, Bivalvia, Vesicomidae). The digestion of sulfur-oxidizing bacterial symbionts for host nutrition, called “farming”, was included within the bioenergetic model, named here after “abj-farming model”. The model was parameterized with available data on the biology, physiology and ecology of the host clam and of its symbionts and original unpublished data (symbiont sulfide consumption and volume of the bacterial symbionts within the gill). Unexpected results were obtained with the abj-farming model regarding the dynamics of the host and its symbionts: The host appears to forgo a maximal ingestion for a lower and stable one as a kind of homeostasis. Also the total oxygen consumption of the symbionts was predicted to be higher than that of its host. The abj-farming DEB model was compared with a classical typified abj-DEB model, which did not have explicit data and parameters related to the symbionts. Both models’ predictions fit the data well; however, only the abj-farming model provided new insights into the *C. regab* host-symbiont relationship and the symbiont dynamics. Additionally, the abj-model predicted a faster growth rate for the host, 4-fold faster than the abj-farming model that provided a growth rate closer to what is expected for such species. The abj-farming DEB model could be applied to other symbiotrophic species (bivalves, gastropods and polychaetes) and be used as a basis to model more complex host-symbiont relationships.

## 2.1 Introduction

Deep-sea chemosynthesis-based ecosystems (> 200 m depth) derive their energy from chemical compounds than from sunlight. Examples are hydrothermal vents, cold seeps, and organic falls in which dense communities of specialized symbiotic animals such as clams, tubeworms and

mussels occur. These species are nutritionally dependent on symbiotic relationships with chemosynthetic bacteria that use available reduced chemical compounds, such as hydrogen sulfide or/and methane, as energy sources to fix inorganic carbon and synthesize organic molecules (Dubilier et al., 2008; Sibuet & Olu, 1998; Sogin et al., 2021; Sogin et al., 2020).

Vesicomidae (Mollusca, Bivalvia) are typical bivalves inhabiting various reduced habitats from the continental shelf to hadal depths worldwide (Johnson et al., 2017; Krylova & Sahling, 2010). The Pliorcardiinae subfamily (Mollusca, Bivalvia, Vesicomidae) includes symbiotic species (Johnson et al., 2017; Krylova & Sahling, 2010). These clams have several unique features to thrive in extreme and nutrient-poor environments, in particular their enlarged gills (compared to other bivalves of a similar size) hosting high density of sulfur-oxidizing autotrophic bacteria (Decker, 2011; Decker et al., 2013; Krylova & Sahling, 2010) and providing an important surface area for extracting oxygen and exchanging compounds with surrounding waters. These symbiotic bacteria are located in specialized gill epithelial cells called bacteriocytes. An additional distinctive characteristic of the Pliorcardiinae is a reduced gut (Krylova & Sahling, 2010). In most symbiotic vesicomid species, a single bacterial strain belonging to the Gammaproteobacteria class is highly dominant and is host species specific. Symbionts have reduced genomes compared to free-living relatives (Cruaud et al., 2019; Decker et al., 2013; Ip et al., 2020; Newton et al., 2008; Perez et al., 2022; Stewart & Cavanaugh, 2009). Bacterial symbionts were also observed in vesicomid eggs (Ikuta et al., 2016; Newton et al., 2008; Szafranski et al., 2014) and around primary oocytes (Cary & Giovannoni, 1993) suggesting vertical, mother-to-offspring transmission. Nonetheless, some lateral transmission of symbionts from nearby hosts may occur (Decker et al., 2013; Newton et al., 2008; Ozawa et al., 2017; Stewart et al., 2008). The previous elements indicate a coevolution between symbiotic vesicomid and their major symbionts (Cruaud et al., 2019; Ip et al., 2020; Peek et al., 1998).

The species *Christineconcha regab* (Mollusca, Bivalvia, Vesicomidae,

Pliocardiinae) was discovered at the Regab pockmark, a cold seep situated in the Gulf of Guinea (southeast Atlantic) (Ondréas et al., 2005; von Cosel & Olu, 2009). Since 1964, the Gulf of Guinea has been extensively explored by oil and gas companies, and deep-sea scientists (Bayer et al., 1966; Bridges et al., 2023; Savoye et al., 2009; Savoye et al., 2000). Two oceanographic campaigns, ZaiAngo (Savoye et al., 1998) and Biozaire (Vangriesheim, 2001), were carried out jointly by french institute Ifremer and the former Elf petroleum compagny. The ZaiAngo campaign (1998–2000) consisted in a geological exploration of a large area of the Gabon-Congo-Angola margin, near the Congo (formerly Zaire) deep-sea fan. The aim was to map the Congo deep-sea fan and study the deep margin structure, the slope stability and the related gas hydrates (Ondréas et al., 2005). Between 2001 and 2003, the Biozaire campaigns focused on the understanding of deep-sea ecosystems on the continental margin and near the Congo channel (Ondréas et al., 2005). Three oceanographic campaigns were led solely by Ifremer: Guineco (Boetius, 2008), WACS (West Africa Cold Seeps) (Olu, 2011) and Congolobe (Rabouille, 2011). The Gabon-Congo-Angola margin was formed during the break-up of South America and Africa about 140 Ma ago during the early Cretaceous, which was associated with the opening of the South Atlantic Ocean (Ondréas et al., 2005). During Aptian-Eocene period, long and continuous post-rift thermal subsidence occurred with sedimentation as aggradation of siliceous and clastic deposits, followed by another sedimentary episode as silty-sand turbiditic sediment progradation from Miocene period to now (Ondréas et al., 2005). The turbidite system of the Congo River develops in an east-west direction, perpendicular to the Congo-Angola margin (Savoye et al., 2000). The Congo deep-sea fan consists in a huge detrital sedimentary system with stacked buried channel-levee systems, the end of this system being called terminal Lobes (Rabouille et al., 2019). Pockmarks which may have been formed from the explosive release of overpressurized interstitial fluids and where fluids escape have been spotted (Ondréas et al., 2005). The giant pockmark Regab (800 m width, 15–20 m depth) was the first observed in 1998 during the ZaiAngo cruise 1

(Ondréas et al., 2005). At Regab pockmark, methane was the major chemical component of the emitted fluids (fluid composition with Raman spectroscopy: methane 99.1%, carbone dioxide 0.83%, methane 0.043%, propane, butane, pentane and hydrogen sulfide 0.02%). At 1–2 m above seafloor, highest methane concentration measured was at the center of the pockmark (129  $\mu\text{L/L}$ ) and the lowest at the periphery ( $< 1 \mu\text{L/L}$ ) (Charlou et al., 2004).  $\delta^{13}\text{C}$  signature of fluids showed that methane originated from microbial activity (Charlou et al., 2004). In the Gulf of Guinea, *C. regab* was observed at -2820 m depth near cold seeps (von Cosel & Olu, 2009) to -5070 m depth at the Lobes of the Congo fan (Khripounoff et al., 2017). *C. regab* was also encountered on the Bonjardim mud volcano in the Gulf of Cadiz (-3060 m depth) (Olive et al., 2011; Rodrigues et al., 2013) and in reduced sediments in the Bay of Biscay in the Gulf of Gascony in the Northeast Atlantic (-4125 m depth) (Krylova et al., 2010).

*C. regab* was observed living in aggregates, about two-third of its shell buried in sediments (Decker, 2011). Its foot was highly vascularized and was thought to be used to move and dig into the sediment for sulfide to sustain their sulfur-oxidizing symbionts (Taxonomy ID: NCBI:txid1365817) and overall contribute to bioturbation (Decker, 2011). Bioturbation favors oxygen and sulfate supply in surface sediments enhancing sulfate reduction and anaerobic oxidation of methane (AOM) (Bertics et al., 2007; Boetius et al., 2000; Boetius & Wenzhöfer, 2013; Menot et al., 2010; Pruski et al., 2017). Symbionts may acquired carbon dioxide, nitrate and dioxygen at the clam gill/seawater interface (Fig. 2.1a) (Childress & Girguis, 2011). Approximately two-thirds of *C. regab* gill volume was filled with these bacteria (Decker, 2011).

*C. regab* mantle and gills showed depleted carbon isotopic signatures ( $\delta^{13}\text{C}$  approximately -38.9 and -38.2 ‰ for mantle and gills, respectively), which were congruent with clam symbiotic nutrition (Pruski et al., 2017). The “farming” feeding strategy, (i.e., the host provides its symbionts with carbon, reduced compounds, and oxygen and then digests them to get organic matter) seems to exist in most of chemosymbioses (Sogin et al., 2020). Symbiotic vesicomids are very likely using

this farming strategy, as it was suggested by the observation of lysosomes in vesicomylid bacteriocytes by transmission electron microscopy and further supported by a high expression of lysozyme genes in vesicomylid species gills (Fiala-Medioni & Le Pennec, 1987; Lan et al., 2019). Degradation stages of symbionts were also observed in vesicomylid bacteriocytes (Newton et al., 2007). Vesicomylids may use an additional feeding strategy called “milking” (i.e., transfer of carbon from the symbionts to the host via organic molecules and/or via the symbiont production of outer membrane vesicles) (Sogin et al., 2021). High transcription of substrate-specific transporters by symbionts and expanded transport genes in vesicomylid species indicated that milking may occur (Ip et al., 2020; Newton et al., 2007).

Energy transfer between the host clam and its sulfur-oxidizing symbionts is not straightforward and is hardly measurable. Using the dynamic energy budget (DEB) theory (Kooijman, 2010), the aim was to understand the dynamics between the host vesicomylid clam *C. regab* and its obligate sulfur-oxidizing symbionts given the preliminary hypothesis that the host feeds using only “farming”. The DEB theory is a bioenergetic individual-based framework encompassing the whole life cycle of an organism. Processes, such as ingestion, assimilation, growth, reproduction and respiration, are quantified in terms of energy fluxes forced by environmental parameters (e.g., food level and temperature). Sulfur-oxidizing symbionts have been explicitly incorporated within the developed farming DEB model for *C. regab*. Currently, there are only a few DEB models on symbiotic relationships from shallow marine habitats that explicitly incorporate symbionts, such as coral-Symbiodinium (Muller et al., 2009) and anemone-*Symbiodinium* (Kaare-Rasmussen et al., 2023) symbioses. Additionally, only one DEB model was developed for deep-sea benthic invertebrates, namely, the obligate wood-feeder bivalve *Xylonora atlantica* (Gaudron et al., 2021). The objectives were as follows:

1. To develop a DEB model for *C. regab* based on existing DEB models;

2. To develop a novel DEB model for *C. regab* with the “farming” hypothesis, including sulfur-oxidizing symbionts within the previously developed model;
3. To compare predicted functional responses (i.e., food levels) for *C. regab* and its sulfur-oxidizing symbionts at sampling sites with both models;
4. To compare *C. regab* life traits and energy allocation obtained with the two models for different sizes of host and food levels at a typical cold-seep temperature;
5. To observe symbiont energy allocation for different sizes of hosts and food levels at a typical cold-seep temperature;
6. To compare the chemical fluxes of carbon, oxygen and nitrogen within the vesicomid clam and its sulfur-oxidizing symbionts for different host sizes and food levels at a typical cold-seep temperature.

## 2.2 Methods

### 2.2.1 Model description

#### 2.2.1.1 The abj model

DEB theory has been widely applied to bivalve species (> 140 species). The abj-DEB model (abj: metabolic acceleration (a) between “birth” (b) and “metamorphosis” (j)) is the most applied to bivalves (“Add-My-Pet Species List”, 2024). For bivalves, metamorphosis corresponds to a metabolic switch resulting in the transition from planktonic to benthic life with morphological changes (loss of the velum of the umbo-veliger larva and development of the foot of the pediveliger larva) (Fig. 2.2). The abj model has four life stages: embryo, juvenile I, juvenile II and adult. The transitions from each life stage to the next one (birth  $E_H^b$ , metamorphosis  $E_H^j$  and puberty  $E_H^p$ ) occurs when a specific level of maturity  $E_H$

is reached through the investment of energy into it (Fig. 2.2). During the embryo stage, the organism does not feed and relies on its egg reserves. After birth  $E_H^b$ , as a juvenile, the organism can feed on external food sources but cannot reproduce yet. When puberty  $E_H^p$  is reached, the organism no longer needs to allocate energy to increase its maturity and instead starts allocating energy to a reproduction buffer (Fig. 2.2) (Kooijman, 2010; Marques et al., 2018).

During the juvenile I phase, a metabolic acceleration occurs to reach metamorphosis. This acceleration is modeled by the increase of food assimilation into reserve  $\dot{p}_A$  and energy reserve mobilization  $\dot{p}_C$ . Two parameters, the maximum assimilation flux  $\{\dot{p}_{Am}\}$  and the energy conductance  $\dot{v}$ , increase in tandem to model these effects (Fig. 2.1, Tables 2.2 and 2.3). The surface area responsible for assimilation is proportional to its structural volume  $V$ . The organism changes its shape as it grows (V1-morphy) and the growth is exponential for juvenile I. In all other life stages, the growth follows Von Bertalanffy curve and the organism grows proportionally in all three dimensions, maintaining its shape as it grows (isomorphy), with the surface area responsible for assimilation proportional to its structural area  $V^{2/3}$ .

The abj model includes four state variables (i.e., variables describing the current state of the organism): the reserve  $E$  (J), the structure  $V$  ( $\text{cm}^3$ ), the maturity level  $E_H$  (J) and the reproduction buffer  $E_R$  (J) (Fig. 2.1a, Table 2.2). The structure is an abstract DEB notion, linked to the physically measurable length  $L$  (cm) of the organism by a shape factor  $\delta$  ( $\delta_M$  for adult,  $\delta_{Me}$  for larva, Table 2.6), such as  $V^{1/3} = L \delta$ .

The *C. regab* abj model has eighteen parameters (Table 2.6).

### 2.2.1.2 The abj-farming model

The novel abj-farming model was built from the *C. regab* abj-DEB model by adding eleven parameters related to the symbionts (Table 2.1). This model was based on the “farming” feeding strategy of the host and was named abj-farming to distinguish from the abj-DEB model. The model was built by integrating the sulfur-oxidizing bacteria into the abj model of the bivalve host (Fig. 2.1). Symbionts macrochemical equations for

assimilation, dissipation and growth transformations were written for one C-mol of symbiont reserve, using a standard reserve composition  $CH_{1.8}O_{0.5}N_{0.15}$  (Kooijman, 2010) (Eq. 2.5a, b and c for assimilation, dissipation and growth, respectively). As bacteria divide, they do not need to invest energy into a reproduction buffer as the bivalve host does. Therefore, the bacterial symbionts were modeled by a single juvenile stage (Fig. 2.2). No investment in maturation was needed for bacteria either. Consequently, two state variables were added for the symbionts: reserve  $E_s$  and structure  $V_s$  (Table 2.1). The symbiont population is modeled with the same dynamics as a single bacterium. Unicellular organisms that divide into two daughter cells are well modeled as V1-morphs (changing its shape as it grows) (Kooijman, 2010). Symbiont population has an ingestion rate proportional to its structure ( $V$ ) ( $\dot{p}_{X_s}$ , Table 2.1) (Kooijman, 2010). Symbiont fluxes describing ingestion, assimilation, mobilization, maintenance and growth were added (Fig. 2.1, Table 2.1). The bivalve host was modeled as in the abj-DEB model except for its ingestion flux  $\dot{p}_{X_h}$  (Fig. 2.1): In the abj-farming model, the ingestion flux came from the symbiont reserve and structure to model the host digestion of its symbionts whereas in the abj model, the host ingestion flux came from the environment (Fig. 2.1, Table 2.1).

### 2.2.1.3 Biological data for model parameterization

Several cruises were undertaken to explore the Congo submarine channel and cold seep ecosystems in the Gulf of Guinea (South–East Atlantic, Fig. 2.8), . Samples and experimental data acquired during these different cruises provided the data used to parameterize the models. Specimens came from two major areas: the end of the Congo submarine channel named the Lobe complex (Lobes A, B and C), and the Regab pockmark (center and southwest) (Fig. 2.8, Khripounoff et al., 2017).

## 2.2.2 Forcing variables for parameter estimation: Functional response and temperature

### 2.2.2.1 Functional response

**abj** The functional response ( $f$ ) is the Michaelis–Menten function, where  $X$  is the food density,  $K$  is the half saturation coefficient and  $x$  is the scaled food density (Kooijman, 2010):

$$f = \frac{\frac{X}{K}}{1 + \frac{X}{K}} = \frac{x}{1 + x} \quad (2.1)$$

In the *C. regab* abj-model, a functional response was estimated as a parameter for each sampling site, independently of the time/season of sampling: Regab Center, Regab Southwest, Lobe A, Lobe B and Lobe C (Fig. 2.8, Table 2.5). Regarding the Regab pockmark, it has been suggested that biogeochemical conditions have been relatively stable throughout time, at least between 2000 and 2008 (Pop Ristova et al., 2012). However the Lobes complex was characterized by high sediment accumulation and turbidity currents and appeared to be a less stable environment than Regab (Rabouille et al., 2017a; Sen et al., 2017). Nevertheless, for the parameter estimations, food (i.e., sulfide) was assumed to be more or less constant at each Lobe and Regab site throughout the years of sampling.

**abj-farming** In the abj-farming model, a functional response for symbionts ( $f_s$ ) was defined as  $f$  in the abj-model; one  $f_s$  was set to be estimated as a parameter for each sampling site.

The novelty was that the quantity of food available for the host was considered dependent on the ratio between symbiont structure ( $V_s$  and host structure  $V$ ); the idea behind this is that for the same volume of symbionts, a larger host will have less food available. A new parameter have been implemented, the half saturation coefficient  $v_{K_s}$ , where host ingestion is half of its maximum.

$$f_h = \frac{\frac{V_s}{V}}{\frac{V_s}{V} + v_{K_s}} \quad (2.2)$$

Host functional responses ( $f_h$ ) were predicted as a function of symbionts functional response parameters using the MATLAB "fzero" function to solve Eq. 2.3 where  $\dot{p}_X$  is the host ingestion flux ( $\text{Jd}^{-1}$ ),  $\{\dot{p}_{Xm}\}$  ( $\text{Jd}^{-1}$ ) is the maximum host ingestion flux ( $\text{Jd}^{-1} \text{cm}^{-2}$ ),  $s_M$  (-) is the host acceleration factor,  $V$  ( $\text{cm}^3$ ) is the host structure.

$$\frac{\dot{p}_X}{\{\dot{p}_{Xm}\} s_M V^{2/3}} - f_h = 0 \quad (2.3)$$

The parameter values impact on the estimation of  $f_h$  was represented in Fig. 2.11 (Supplementary Figures).

### 2.2.2.2 Temperatures

Body temperature impacts physiological rates therefore physiological rates of the host and symbiont were corrected to estimate parameters at a reference temperature  $T_{ref} = 293.15 \text{ K}$  ( $20^\circ\text{C}$ ) (Supplementary Methods 2.6.6) (Kooijman, 2010).

### 2.2.3 Estimation of primary parameters

The Add-my-Pet (AmP) procedure (DEB-tool package, MATLAB) (Lika et al., 2011; Marques et al., 2018) was used to estimate *C. regalis* abj and abj-farming parameters (Tables 2.6 and 2.1, respectively) from data (Table 2.4) at a given temperature and functional responses. Parameters were obtained using a minimization method of a loss function (function of data, predictions from parameters and data weight coefficients) (Marques et al., 2019). The accuracy of models fit was quantified with the mean relative error (MRE), the symmetric mean squared error (SMSE) and the standardized mean absolute error (SMAE). Constraints were added as customized filters for the symbionts to keep the estimation of parameters inside the biologically meaningful part of the parameter space during the minimization procedure. Additional codes for predictions (Supplementary Methods 2.6.7, 2.6.8, 2.6.9), compared to those available on the Add-My-Pet database, were developed in this study for new data types in the abj-farming model (CODE TO UPLOAD ONLINE).

## 2.3 Results

### 2.3.1 Models' predictions

The abj and abj-farming model predictions, compared to data, resulted in MRE (mean relative error) of 0.094 and 0.195 respectively, in SMAE (standardized mean absolute error) of 0.053 and 0.088 respectively, and finally with SMSE (symmetric mean squared error) of 0.029 and 0.049 respectively.

#### 2.3.1.1 Zerovariate data

Of the seven zerovariate data related to life history traits shared by the two models, length predictions at hatching, birth, metamorphosis and puberty, and life span were better predicted with the abj-farming model with a relative error (RE) less than 0.005, whereas the clam maximum reproduction rate and ultimate length were better predicted with the abj model (Table 2.7). Regarding chemical flux predictions, carbon flux predictions were more accurate (closer to data) with the abj-farming model whereas nitrogen fluxes predictions were better with the abj model (Table 2.7). For oxygen fluxes, no important differences between the models could be assessed (Table 2.7). The symbiont-related data could only be predicted with the abj-farming model, where the ratio of the bacteria-to-gill volume was well predicted ( $RE < 0.005$ ; Table 2.7). Fluxes of sulfur and yields were well predicted for sulfide and oxygen, but the yield for nitrogen was not well predicted ( $RE > 17$ ; Table 2.7). Bivalve biomass in  $g\ mol^{-1}$  was well predicted but less in terms of  $mol\ H_2S\ C\ mol^{-1}$  of biomass (Table 2.7).

#### 2.3.1.2 Univariate data

Univariate data (Table 2.8) were well predicted by both abj and abj-farming DEB models, for both the relationships between shell length and wet weight (L-Ww, Fig. 2.9a ( $RE = 0.08-0.21$ ), Fig. 2.10a ( $RE = 0.09-0.28$ ) respectively), between shell length and dry weight (L-Wd, Fig. 2.9b

(RE = 0.14–0.35)), Fig. 2.10b (RE = 0.13–0.41) ), between reproduction rate and shell length (R-L, Fig. 2.9c (RE = 0.60–7.50), Fig. 2.10c (RE = 0.58–7.57) respectively) and finally between reproduction rate and wet weight (R-Ww, Fig. 2.9d (RE = 0.62–6.46), Fig. 2.10d (RE = 0.58–5.63) respectively). With both models, univariate data sets related to the reproduction rate were less well predicted, with data sets R-L and R-Ww from site Regab southwest RE > 1. RE for time-length predictions with abj and abj-farming models were RE = 0.01 and RE = 0.03–0.02, respectively. The main difference between the two models lies in the estimated growth rate of the host (time-length curves, Fig. 2.9e for the abj-DEB model and Fig. 2.10e for the abj-farming model). In the abj-farming model, the von Bertalanffy growth coefficient ( $r_{TB}$ ) was estimated at  $2.3 \cdot 10^{-4} \text{ d}^{-1}$  while it was  $8.3 \cdot 10^{-4} \text{ d}^{-1}$  using the abj model (4-fold faster). The growth rate was similar for both the Regab Center and Southwest sites. With the estimated Bertalanffy growth coefficient, the *C. regab* growth rate could be estimated for Regab Center and Southwest, 1 day after metamorphosis ( $L_j$ ) to  $1 \text{ cm yr}^{-1}$  and to  $2.27 \text{ cm yr}^{-1}$  for abj-farming and abj models respectively, 5 years after  $L_j$  to  $0.72 \text{ cm yr}^{-1}$  and  $0.67 \text{ cm yr}^{-1}$  with abj-farming and abj models, respectively, and 12 years after  $L_j$  to  $0.4 \text{ cm yr}^{-1}$  and  $0.08 \text{ cm yr}^{-1}$  for abj-farming and abj models, respectively.

### 2.3.2 Estimated functional responses

With the abj model, the estimated functional responses ( $f$ ) were 0.68 and 0.65 for the Regab Center and Southwest sites, respectively, and 2.2, 0.8 and 5.90 for the Lobe A, B, and C sites, respectively. With the abj-farming model, the estimated host functional responses were very similar, with  $f_h = 0.176 \pm 0.002$  (mean  $\pm$  standard deviation) for all sites. The host's functional response to reach its maximum shell length was then set to 0.18. Symbiont functional responses were estimated at 0.57 and 0.54 for the Regab Center and Southwest sites, and 0.5 for the sites Lobe A and B sites, and 0.64 for Lobe C site. The symbiont functional response for the sulfide consumption experiment was set at 0.8.

### 2.3.3 Estimated parameters of the abj and abj-farming models

Somatic maintenance of the host [ $\dot{p}_M$ ] was estimated to be 30 times higher than symbionts' somatic maintenance [ $\dot{p}_{Ms}$ ] (Table 2.8). The symbionts' specific cost for their structure [ $E_{Gs}$ ] was high compared to the host's, i.e., three times higher (Table 2.8). The maximum assimilation rate of the symbionts [ $\dot{p}_{Ams}$ ] was not comparable to that of the host [ $\dot{p}_{Amh}$ ] because the first was given per unit of structural volume and the latter was per unit of structural area (Table 2.8). Comparing the abj and abj-farming model parameters, the estimated [ $\dot{p}_M$ ] was higher in the abj-farming model. The estimated energy conductance for *C. regab* was higher in the abj model. New parameters added for the abj-farming model could not be discussed much as they could not be compared to any value. *C. regab* maximum assimilation rate [ $\dot{p}_{Am}$ ] with the abj model was  $154.9 \text{ J d}^{-1} \text{ cm}^{-2}$  and the reserve capacity [ $E_m$ ] was  $199.6 \text{ J cm}^{-3}$ . With the abj-farming model, [ $\dot{p}_{Amh}$ ] was  $3005.1 \text{ J d}^{-1} \text{ cm}^{-2}$  and [ $E_m$ ]  $8.5 \cdot 10^5 \text{ J cm}^{-3}$ .

### 2.3.4 Symbiont dynamics with the abj-farming model

Modeled host shell length  $L_h$ , symbiont structure  $V_s$  and reserve  $E_s$ , and host and symbiont biomasses increased with time (Figs. 2.3a, b, c, d and e, respectively). When the symbiont functional response  $f_s$  was lower, the symbiont structure and biomass were predicted to be larger while the reserve energy was not impacted (Figs. 2.3b, c and e). Hence, the symbiont reserve density decreased with a lower  $f_s$ . The predicted symbiont structure increased dramatically when symbiont functional response was too low ( $f_s < 0.5$ ) and reached unreasonable sizes for symbionts compared to host. This indicated that the simplification of fast dynamics was no longer valid for such low values of functional responses. The symbiont biomass was predicted to be roughly one-sixteenth of the host biomass (Figs. 2.3d and e).

### 2.3.5 Energy fluxes with the abj-farming model

With the abj-farming model, the predicted ingestions of both symbionts and hosts remained more or less constant for different symbiont functional responses  $f_s$  and were higher with larger hosts (Fig. 2.4a, b). The bivalve ingestion dynamic was predicted differently with the abj model. Ingestion was higher for larger bivalve shell sizes and for higher functional responses  $f$  (Supplementary Material. Fig. 2.14).

In an adult host, a fraction of assimilated energy was used to increase its biomass (modeled as the variation in the host reserve plus host structure) and the other part was spent to cover maintenance costs (somatic and maturity maintenance), through transformation processes (assimilation and growth overheads) and through reproductive processes (reproduction overheads). Symbionts allocated energy to increase their biomass, and spent energy for assimilation and growth overheads, as observed for the host, but only to somatic maintenance, as there were no maturation/reproduction processes for the symbionts.

The variation in biomass and dissipated energy as maintenance and overheads were compared between an adult host and its symbionts for two different symbiont functional responses ( $f_s = 1$  and  $f_s = 0.5$ ) and two different sizes of adult bivalve hosts (0.8 times the maximal estimated shell length (= 10.5 cm) and 0.5 times the maximal estimated shell length (= 6.6 cm)) (Fig. 2.5).

The variation in symbiont biomass (i.e., variation in the symbionts' reserve plus variation in the symbionts' structure) could not be computed, as a fast dynamic of symbionts state variables was assumed in the abj-farming model; symbiont state variables adjust immediately to reach equilibrium in changing conditions (e.g., variation in symbiont functional response).

For a different symbiont functional response ( $f_s$ ), the host did not change the proportion of energy distribution between biomass and dissipation (Figs. 2.5a, c, d, f, g and i). The energy dissipated by the symbionts was negligible compared to that of the host (Figs. 2.5a, b and c).

A smaller host (Fig. 2.5b), compared to a larger host (Figs. 2.5a and c)

allocated a bigger fraction of its energy budget to increase its biomass. When the host was larger, the biomass was enhanced by an increase in the reproduction buffer (Fig. 2.5d), while for a smaller bivalve, the biomass was enhanced by an increase in the reserve and the structure (i.e., growth) (Fig. 2.5e).

The larger the host was, the higher the percentage of mobilized energy for somatic maintenance, and the smaller the host was, the lower the percentage of energy mobilized for somatic maintenance (Figs. 2.5g and h). Only a small percentage of energy was lost in reproduction overheads and maturity maintenance (Figs. 2.5g, h and i). A lower functional response increased the percentage of energy used for maintenance (Figs. 2.5g and i).

The size of the host did not impact the way symbionts allocated their energy (Figs. 2.5j and k): 3/4 of the symbionts dissipated energy as growth overhead, 1/4 as assimilation overhead and a small amount for somatic maintenance. Compared to the abj model, the increase in biomass due to the reproduction buffer was significantly higher in the abj-farming model (Supplementary Material Fig. 2.12).

### 2.3.6 Chemical element fluxes with the abj-farming model

With the abj-farming model, host chemical fluxes of oxygen (O), carbon (C) and nitrogen (N) for assimilation, dissipation and growth processes were independent of symbiont functional response ( $f_s$ ) (Fig. 2.6). Oxygen, carbon and nitrogen fluxes for assimilation and dissipation increased with host size (Assimilation Figs. 2.6 a, b, c and dissipation Figs. 2.6 d, e, f). For growth, chemical element (C, O, N) use first increased with host size and then decreased, which was congruent with a first acceleration phase of growth and then a slowing of growth when the host approached its maximum size. Most of the chemicals assimilated by the host (carbon Fig. 2.6a, oxygen Fig. 2.6b and nitrogen Fig. 2.6c) were lost to dissipation (carbon Fig. 2.6d, oxygen Fig. 2.6e and nitrogen Fig. 2.6f) and only a small fraction was mobilized for growth (carbon Fig. 2.6g, oxygen Fig. 2.6h and nitrogen Fig. 2.6i). Carbon, oxygen and

nitrogen assimilated by the symbionts (Figs. 2.7a, b and c, respectively) and carbon, oxygen and nitrogen used by the symbionts for growth (Figs. 2.7g, h and i, respectively) did not depend on the symbiont functional response ( $f_s$ ) and were constant for a given host size but increased with increasing host size whereas dissipated carbon, oxygen and nitrogen (Figs. 2.7d, e and f respectively) depended on the symbiont functional response ( $f_s$ ). Dissipated chemical fluxes increased with lower symbiont functional responses and larger hosts (Figs. 2.7d, e and f). Unlike the host, symbionts used more chemicals for growth (Figs. 2.7g, h and i) than the amount they dissipated (Figs. 2.7 d, e and f). Symbiont sulfur assimilation did not depend on the symbiont functional response ( $f_s$ ) but increased with host size (Fig. 2.7 j). abj model chemical fluxes are available in Supplementary Material Fig. 2.13.

## 2.4 Discussion

### 2.4.1 Models of symbiotic species and DEB

#### 2.4.1.1 Existing models for deep-sea symbiotic bivalves

Only two studies were carried out to model the metabolic rate of symbiotic bivalve species living in deep-sea reducing habitats. The models were developed on the mixotrophic mytilid *Bathymodiolus azoricus* from hydrothermal vents. Carbon consumption flux of the endosymbionts and host filtration of the particle organic matter were included (Husson et al., 2018; Martins et al., 2008). The first model included no effect of temperature in metabolic rates and no experimental data (Martins et al., 2008). The scale functional response of the endosymbionts were based on the concentration of either methane and sulfide based on a Michaelis–Menten function for the food level. The mass of their symbionts, which represented 4% of the gill wet weight, was used (Martins et al., 2008). The most recent model (Husson et al., 2018) was an improvement of the previous model (Martins et al., 2008) with more parameters controlling the input and uptake flows, symbiont biomass,

and the mussel assimilation with temperature correction for metabolic rates. However, both conceptual models did not include any ontogenic variations in carbon flux from embryo to adult stages as does the DEB model. These models also focused only on host growth, and did not include energy invested into the reproduction, maintenance and maturity/reproduction of the host, as DEB does.

#### 2.4.1.2 Existing DEB models for deep-sea/symbiotic species

The only DEB model developed for a deep sea species (available in the Add-My-Pet DEB database) was an abj model for a wood-boring bivalve, *Xylonora atlantica* (Bivalvia, Myida, Xylophagaidae) (MRE = 0.148; SMAE = 0.162; SMSE = 0.040) (Gaudron et al., 2021). An abj model was also developed for a symbiotic mixotroph bivalve species of the Thyasiridae, *Thyasira cf. gouldi* (Bivalvia, Lucinida, Thyasiridae) (MRE = 0.053; SMAE = 0.059; SMSE = 0.02) harboring intra- and extracellular sulfur-oxidizing bacteria (Mariño et al., 2019). Some *C. regab* abj parameters stand out compared to abj parameters of the deep-sea species *Xylonora atlantica* and the symbiotic species *Thyasira cf. gouldi*. The specific cost for structure [ $E_G$ ] ( $\text{J cm}^3$ ) and the volume-specific somatic maintenance [ $\dot{p}_M$ ] ( $\text{J d}^{-1} \text{ cm}^3$ ) were high for *C. regab* compared to the 2 other species. [ $E_G$ ] at 20°C was estimated at 6687  $\text{J cm}^3$  for *C. regab*, 2349  $\text{J cm}^3$  for *X. atlantica* and 2355  $\text{J cm}^3$  for *T. cf. gouldi*. [ $\dot{p}_M$ ] at 20°C was estimated at 568  $\text{J d}^{-1} \text{ cm}^3$  for *C. regab*, 29.22  $\text{J d}^{-1} \text{ cm}^3$  for *X. atlantica* and 15.78  $\text{J d}^{-1} \text{ cm}^3$  for *T. cf. gouldi*, respectively. [ $E_G$ ] and [ $\dot{p}_M$ ] are directly linked to the somatic maintenance rate coefficient ( $\dot{k}_M$ ,  $\text{d}^{-1}$ ). The somatic maintenance rate coefficient  $\dot{k}_M$  ( $\text{d}^{-1}$ ) is the volume-specific somatic maintenance [ $\dot{p}_M$ ] ( $\text{J d}^{-1} \text{ cm}^3$ ) divided by the specific cost for structure [ $E_G$ ] ( $\text{J cm}^3$ ). Somatic maintenance rate coefficient of *C. regab* (0.085  $\text{d}^{-1}$ ) was roughly seven times that of *X. atlantica* (0.012  $\text{d}^{-1}$ ), which was roughly twice that of *T. cf. gouldi* (0.007  $\text{d}^{-1}$ ). The somatic maintenance rate coefficient varies greatly between taxa, and *C. regab* is of the same order of magnitude as other bivalve species at 20°C (Kooijman, 2010).

Only two dynamic bioenergetic models have been developed to describe the symbiotic relationship between endosymbiotic photosynthetic

*Symbiodinium* algae with a shallow coral species (Cunning et al., 2017; Muller et al., 2009) and an anemone (Kaare-Rasmussen et al., 2023). Symbiotic anemones and corals can obtain nutrients from their environment and from their symbionts. In both symbiotic anemone and coral models, translocation of carbon from symbionts to host was modeled as a surplus flux, with symbionts using first the fixed photosynthetically carbon they need for themselves while the remaining becomes available to the host. In both models, priority access to nitrogen was given to host; however, symbiont access was modeled differently between the two models. In the anemone - *Symbiodinium* model, symbionts received nitrogen from host surplus flux while in the coral - *Symbiodinium*, they received nitrogen by "consuming" the host, as in a predator-prey relationship. Such translocation fluxes of nutrients from host to symbionts were not implemented in the *C. regab* abj-farming model although they could occur. These exchanges of nutrients remain poorly understood in deep-sea chemosymbiotic bivalves. In the abj-farming model, symbionts access to carbon and nitrogen first, and then the host can get obtain carbon and nitrogen by feeding on the symbiont. Countless symbiotic states happen in life (Kooijman et al., 2003), and these three models show different degrees of food dependency and equilibrium between host and symbionts. The *C. regab* abj-farming model with explicit symbionts is complex. The model could be simplified, as in anemone - *Symbiodinium* (2 state variables, symbionts and host biomasses) (Kaare-Rasmussen et al., 2023) and coral - *Symbiodinium* (3 state variables, symbionts and host biomasses and photooxidative synthesizing unit) (Cunning et al., 2017) models to answer specific scientific questions (i.e., symbiont cost and coral response photooxidative stress, respectively) and to prevent excessive model complexity. As there are fewer state variables (no reserve, no maturity, and no reproduction buffer) in these models, the number of parameters is reduced. The first published coral - *Symbiodinium* model (Muller et al., 2009) was much more complex than the second one (Cunning et al., 2017) which focused on the question of coral response to photooxidative stress. Complexifying the abj-farming model to add additional reserves (e.g., stored sulfur granules by

sulfur-oxidizing symbionts) and/or adding additional food sources for the host and its symbionts (e.g., nutrient translocation) might require some model simplification to keep the model usable (Pfab et al., 2022).

## 2.4.2 abj versus abj-farming

### 2.4.2.1 Model accuracy

In this study, the abj and abj-farming models provided good results as small errors were calculated (MRE, SMAE, SMSE) for predictions from the estimated set of parameters and data, collected from the field and lab experiments. The errors were greater for the abj-farming DEB model than for the abj DEB model. This to be expected as the former is a much more complex model, since it has eleven more parameters. Filters for prediction were added to lead the parameter estimation and maintain realistic values. More than half of the data (8 out of the 13 different types of data used in both models) were better predicted with the abj-farming model (e.g., growth rate of the host) than with the abj model. In addition, parameters related to the symbiont bioenergetics could be deciphered with this novel abj-farming model, highlighting the importance of integrating symbionts within the dynamic of the energy budget of a symbiotic model species to study host-symbiont relationship.

Time-length predictions (t-L) seem closer to what is expected with abj-farming model. For the abj model there was a need to use an anchor data point for the growth rate to have the estimation, set at  $1 \text{ cm yr}^{-1}$ . Without the anchor data point, the abj model growth was predicted too fast compared to the literature values. A rough growth rate was estimated to be  $0.8 \text{ cm yr}^{-1}$  for both Regab center and south-west sites with a cohort analysis on adult specimens (Decker, 2011). The anchor data point for the growth rate was not needed for the abj-farming model to obtain realistic growth rate values. Both abj and abj-farming models presented in this paper predicted growth-rates for small *C. regab* specimens at Regab sites southwest and center of the same order of magnitude as vesicomylid *Calypptogena kilmeri* (Barry et al., 2007). The growth rate of *C. kilmeri* from a cold seep off central California was estimated

by tag–recapture to 1 to 2  $\text{cm yr}^{-1}$  for small specimens (Barry et al., 2007). With radionuclide dating techniques on shells, the vesicomid species growth rate from the Galápagos Spreading Center hydrothermal field and 21°N East Pacific Rise hydrothermal area were estimated at 4  $\text{cm yr}^{-1}$  (Turekian & Cochran, 1981) and an average growth rate along the axis of maximum growth (10 cm) of 0.27  $\text{cm yr}^{-1}$  (Turekian et al., 1983), respectively. On-site calcein staining was tested deep-sea seep sites off Hatsushima Island (Western part of Sagami Bay, central Japan) on four vesicomid calyptogena clams, three identified as *C. soyoae* and one as *C. okutanii* at 1,174 m depth (Tada et al., 2010). The clams were exposed to calcein for 48 hours on site and then recovered ten days later; a well visible mark was visible (Tada et al., 2010).

#### 2.4.2.2 Functional responses and biogeochemical context of the sites

For Regab and Lobe sites, estimated functional responses with the abj model and symbiont functional responses with abj-farming model could be compared, as they are directly linked to environmental food density (and not host functional responses). The functional response was estimated to be the highest at the Lobe C site by both the abj-farming (for symbionts) and abj models (whole symbiotic association). The functional response for symbionts was estimated to be the lowest at Lobes A and B with the abj-farming model while with the abj model, the lowest estimated functional response was at southwest and center sites of the Regab pockmark.

In the Lobes, cold seep-like ecosystems are formed thanks to important deposits of organic material coming from the Congo River. Sites A and C were situated near the main channel, site A at the entrance and site C at the end, while site B was far from it (10 km). At Lobe C, which was estimated to have the highest symbiont functional response by both models, sedimentation rates were high compared to sites A and B, and dense and live vesicomid aggregates were dominated by *C. regab* with a few dead shells only (Olu et al., 2017; Rabouille et al., 2017b). Additionally, it was supposed that this site was the most recent deposition zone (Olu et al., 2017; Rabouille et al., 2017b).

At site Lobe A, vesicomids also formed dense beds dominated by *C. regab*. The Lobe B site had only small patches of reduced sediments, and few scattered vesicomid patches mainly consisting of dead shells were observed; moreover, *C. regab* was not the main vesicomid species (Rabouille et al., 2017b). Among the three Lobe sites, the Lobe C site biogeochemical context seemed to provide the best conditions for sulfide production and thus a higher food level for *C. regab* symbionts, which is congruent with the Lobe C site having the highest estimated functional response.

At the Regab site, a gradient of methane emission occurs along the pockmark radius from the center to the periphery (Ondréas et al., 2005; Pop Ristova et al., 2012). The highest sulfur content was measured in the sediment located in the center of the pockmark (Ondréas et al., 2005). Furthermore, a higher biomass and condition index on site was measured for specimens collected from the center than from the southwestern site (Decker, 2011). With both abj and abj-farming models, the functional response was estimated to be higher for the center of the Regab pockmark than for the southwestern site, which agrees with what was observed in the field.

Predictions of *C. regab* symbiont sulfur consumption rates were estimated to be higher for the Regab southwest site and the Regab center site than for the Lobe C site. The abj-farming model suggested that a higher symbiont consumption is linked to a lower symbiont functional response. Experimental data showed that the *C. regab* sulfur consumption rate of the gills from *C. regab* was higher for Regab's southwestern site, then Lobe C, and finally the Regab center (Decker unpublished). One explanation of these differences could be that for the sulfide experiment, the same functional response was set to be estimated for the specimens at the three different sites, as during the experiment, they were exposed to the same "food" density, since they were likely not in the field.

Symbiont functional responses are complex to explain, as symbionts' access to sulfide may be related not only to the concentration of sulfide in the near environment but also to how much/and how the host pro-

vides sulfide to its symbionts (host sulfide binding capacity and foraging capacity) and to sulfur“storage” by symbionts as granules and circulating sulfide inside the host (Cruaud et al., 2019).

The total elemental sulfur of *C. regab* specimens was analyzed, and a difference between Lobe C site specimens and Regab center site specimens was observed, with a mean percentage of elemental sulfur of 12.7% at the Lobe C site and 16% at the Regab center site (Khripounoff et al., 2017). Elemental sulfur granules were also found in other vesicomimid species gills, produced by sulfur-oxidizing symbionts and could constitute a "reserve" to buffer environmental fluctuations in sulfide availability (Cruaud et al., 2019). The gill sulfur contents in *Archivesica gigas* and *Phrageda soyoae* from the Guaymas Basin were 16.14% and 11.27% of gill dry weight on average, respectively (Cruaud et al., 2019). Adding an additional reserve for sulfur would be interesting to try to understand the dynamics of those granules, their formation and their use by the sulfur-oxidizing symbionts.

## 2.4.3 Host-symbiont dynamics with the abj-farming model

### 2.4.3.1 Host feeding strategy

Symbiotic associations rely on some kind of equilibrium between cost and benefits for the host and its symbionts. Symbionts can limit the fitness of the host but act as a buffer to stressors (Bénard et al., 2020). However symbiotic associations are more vulnerable to external stressors as having symbionts could shift from benefits to costs (Bénard et al., 2020). The abj-farming model, unlike the abj model, could study host-symbiont dynamics and proposed unexpected results. The simulations suggest that with this symbiosis the clam ensures itself a constant functional response that is independent of its sulfur-oxidizing symbiont functional response. This strategy might be a great way to prosper in fluctuating environments such as cold-seeps, where the flow of sulfide can cease for some time. In the abj-farming model, when less food was available for the symbionts (i.e., low functional response, low sulfide availability), symbionts might ingest more to cope with host constant

ingestion, acting as a buffer. The abj-farming model also suggests a high assimilation flux from the symbiont, in terms of energy, compared to the host. Symbionts have a reduced genome, where, for example, certain genes needed for multiplication are absent or controlled by the host (Perez et al., 2022).

This kind of homeostasis is a novel concept compared to what has been suggested thus far in the literature regarding deep-sea symbiotic species, where often the quantity of symbionts within the gills of bivalves is linked to the level of reduced compounds such as sulfide. In *Bathymodiolus azoricus* deep-sea mytilid, a pulse of sulfide induced an increase in sulfur-oxidizing bacteria (Halary et al., 2008). Host homeostasis and symbiont stoichiometric flexibility has been observed in a lucinid coastal species as the C:N ratio varied seasonally for the symbionts and not of the host (Cardini et al., 2019).

#### 2.4.3.2 Predicted biomasses

The maximum symbiont biomass estimated by the abj-farming model represented approximatively 5% of the maximal biomass of *C. regab* which is realistic value compared to other symbiotic bivalves such as *Bathymodiolus thermophilus* (Powell & Somero, 1986).

#### 2.4.3.3 Chemical element fluxes

The mean sulfide consumption by symbionts in *C. regab* gills used in this study to calibrate the abj-farming model was much lower than that in the vesicomid species *Calymene kilmeri* and *C. pacifica* from cold seep sites in Monterey Bay, U.S. state of California (Goffredi & Barry, 2002b). The mean gill consumption values were 0.13 and 0.96  $\mu\text{mol gill Ww g}^{-1} \text{min}^{-1}$  respectively while the *C. regab* gill consumption were 0.021, 0.036 and 0.052  $\mu\text{mol gill Ww g}^{-1} \text{min}^{-1}$  for the Regab Center, Regab Southwest and Lobe C sites, respectively (C.Decker unpublished). However, the symbiont explicit model predicted a consumption of sulfide 2-fold higher for *C. regab* than the real values used to calibrate the model getting closer to the values measured in situ in Monterey Bay on

other vesicomylid species.

In some symbioses, the oxygen consumption rates are so high that oxygen may be a limiting factor for host and symbiont metabolism. The high oxygen demand of chemosynthetic symbionts places a cost on their hosts that have evolved a range of adaptations to meet the aerobic demands of their symbionts (Sogin et al., 2021).

#### 2.4.3.4 Symbiont yields for macrochemical equations

Yields of mole of sulfate and of oxygen per yields of hydrogen sulfide assimilated by *C. regab* sulfur-oxidizing symbionts were predicted similar to *Thiobacillus denitrificans* yields (Sublette, 1987). Yields of moles of ammonium and biomass per yield were predicted with the model to be higher than data. There might be different explanations for this. First, the yields used as data to calibrate the models are not the yields of *C. regab* symbionts, but of another sulfur-oxidizing bacteria used as a proxy to estimate *C. regab* symbiont yields. Second, a standard DEB composition was used for symbionts' structure and reserve (the same as the host) and is not well adapted to *C. regab* bacterial symbionts. Third, something is missing linked to nitrogen metabolism in the macrochemical equation for *C. regab* symbionts assimilation.

#### 2.4.3.5 High energy allocation to maintenance of symbionts

The hypothesis of an important energy fraction allocated to maintenance, up to 30-50% of the total energy budget, was made for the vesicomylid species *Calyptogena kilmeri* and *C. magnifica* from cold seeps (Goffredi & Barry, 2002a). Symbiont sulfide oxidation produces proton and sulfate ions which could result in acidic conditions if they accumulate. To maintain ion homeostasis, the clam needs energy to eliminate protons (Goffredi & Barry, 2002a). The results of this paper suggested that the fraction of energy allocated to maintenance could be near 75% of the total energy budget for the largest specimens.

#### 2.4.4 Further applications and developments of the abj-farming model

This paper is the first DEB model developed for a symbiotic deep-sea bivalve species with symbionts integrated within the model. Thanks to this novel abj-farming DEB model, the dynamics of symbionts can be deciphered and predictions can be made for the symbionts' metabolism within their host and their interactions. Models with a similar structure can be developed for other symbiotic species that tend to be dominant in various types of chemosynthetic-based ecosystems (hydrothermal vents, cold seeps, wood fall and whale fall). As vesicomid species, various other chemosymbiotic metazoan species with endosymbiotic bacteria possess genes linked to lysosomal digestion in their genome and/or display lysis of symbionts, including siboglinid polychaetes (de Oliveira et al., 2022; Li et al., 2019), gastropod mollusks (Lan et al., 2021) and other bivalves, such as Lucinidae (König et al., 2015) and Mytilidae families (Zheng et al., 2017). Developing symbiotic DEB models might help to obtain new insights into host and symbiont dynamic relationships and highlight interspecies differences or similarities in functional traits.

## 2.5 Conclusion

A DEB model based on the farming nutritional relationships between the vesicomid *C. regab* and its sulfur-oxidizing symbionts has been successfully developed. This is a large step in modeling host-bacterial symbiont relationships using the DEB theory. The modeling approach is a way to derive valuable knowledge from data by making assumptions, to help answer scientific questions that are difficult, if not impossible to answer only by observation and experimentation given actual technological advancements. Developing such models may lead us to novel discoveries and enhance our understanding of key deep-sea symbiotic taxa, as the abj-farming model suggests a new kind of survival strategy such as homeostasis, for deep-sea species (i.e., low host functional response but but constant) feeding on symbiotic farmed bacteria to sur-

vive in a fluctuating environment. Data collection and modeling efforts of deep-sea species should continue in this direction to advance knowledge.

### *Acknowledgments*

Marine Vandenberghe was funded by a PhD fellowship provided by the CNRS through the 80-Prime Program. This work was financially supported by both the French National Program EC2CO and the CNRS through the 80-Prime Program.

**Table 2.1:** Additional symbiont related state variables, primary parameters and energy fluxes ( $\dot{p}_{\square s}$ ), and details of the modified bivalve host ingestion flux ( $\dot{p}_{Xh}$ ) of the abj-farming Dynamic Energy Budget model developed for *Christineconcha regab*. S.V., state variable; Param., parameter; h, host; sb, symbionts.

S.V.	Description	Unit	Formula	Param.	Description	Unit
$E_s$	sb. reserve	J	$\frac{dE_s}{dt} = \dot{p}_{As} - \dot{p}_{Cs} - \dot{p}_{XEH}$	$[\dot{p}_{Ams}]$	sb. maximum assimilation rate	J d <sup>-1</sup> cm <sup>-3</sup>
$V_s$	sb. structure	cm <sup>3</sup>	$\frac{dV_s}{dt} = \frac{\dot{p}_{Gs}}{[E_{Gs}]} - \frac{\dot{p}_{XV}}{[E_{Vs}]}$	$\{\dot{F}_{ms}\}$	sb. maximum specific searching rate	cm <sup>2</sup> d <sup>-1</sup> m <sup>-2</sup>
Flux	Description	Unit	Formula	$\kappa_{Xs}$	sb. digestion efficiency of food to reserve	-
$\dot{p}_{Xh}$	h. ingestion	J d <sup>-1</sup>	$\dot{p}_{XEH} + \dot{p}_{XVh}$ , when $E_H \geq E_h^b$	$\kappa_{Ps}$	sb. faecation efficiency of food to feces	-
$\dot{p}_{XEH}$	h. ingestion of sb. reserve $E_s$	J d <sup>-1</sup>	$\gamma \dot{p}_{XEH} = \frac{E_s}{E_{Vs}}$	$k_{Es}$	sb. specific-energy conductance	d <sup>-1</sup>
$\dot{p}_{XVh}$	h. ingestion of sb. structure $V_s$	J d <sup>-1</sup>	$(1 - \gamma) \dot{p}_{XVh} = \frac{E_s}{E_s} \dot{p}_{XEH}$	$[\dot{p}_{Ms}]$	sb. volume-specific somatic maintenance cost	J d <sup>-1</sup> cm <sup>-3</sup>
$\dot{p}_{Xs}$	sb. ingestion	J d <sup>-1</sup>	$[\dot{p}_{Xms}] f_s V_s$	$\delta_{MVs}$	sb. structure shape coefficient	-
$\dot{p}_{As}$	sb. assimilation	J d <sup>-1</sup>	$[\dot{p}_{Ams}] f_s V_s$	$vks$	h. half saturation coefficient, value of food ( $V_s + E_s$ ) density where ingestion ( $\dot{p}_{XE} + \dot{p}_{XV}$ ) is half of its maximum	-
$\dot{p}_{Cs}$	sb. mobilization	J d <sup>-1</sup>	$E_s \frac{k_{Ps} V_s [E_{Gs}] + \dot{p}_{Bs}}{E_s + [E_{Gs}] V_s}$	$\gamma_{SE}^{As}$	sb. H <sub>2</sub> S assimilation yield per C-mol of reserve	mol mol <sup>-1</sup>
$\dot{p}_{Ss}$	sb. somatic maintenance	J d <sup>-1</sup>	$[\dot{p}_{Ms}] V_s$	$\gamma_{HE}^{As}$	sb. H <sub>2</sub> O assimilation yield per C-mol of reserve	mol mol <sup>-1</sup>
$\dot{p}_{Gs}$	sb. growth	J d <sup>-1</sup>	$\dot{p}_{Cs} - \dot{p}_{Ss}$			

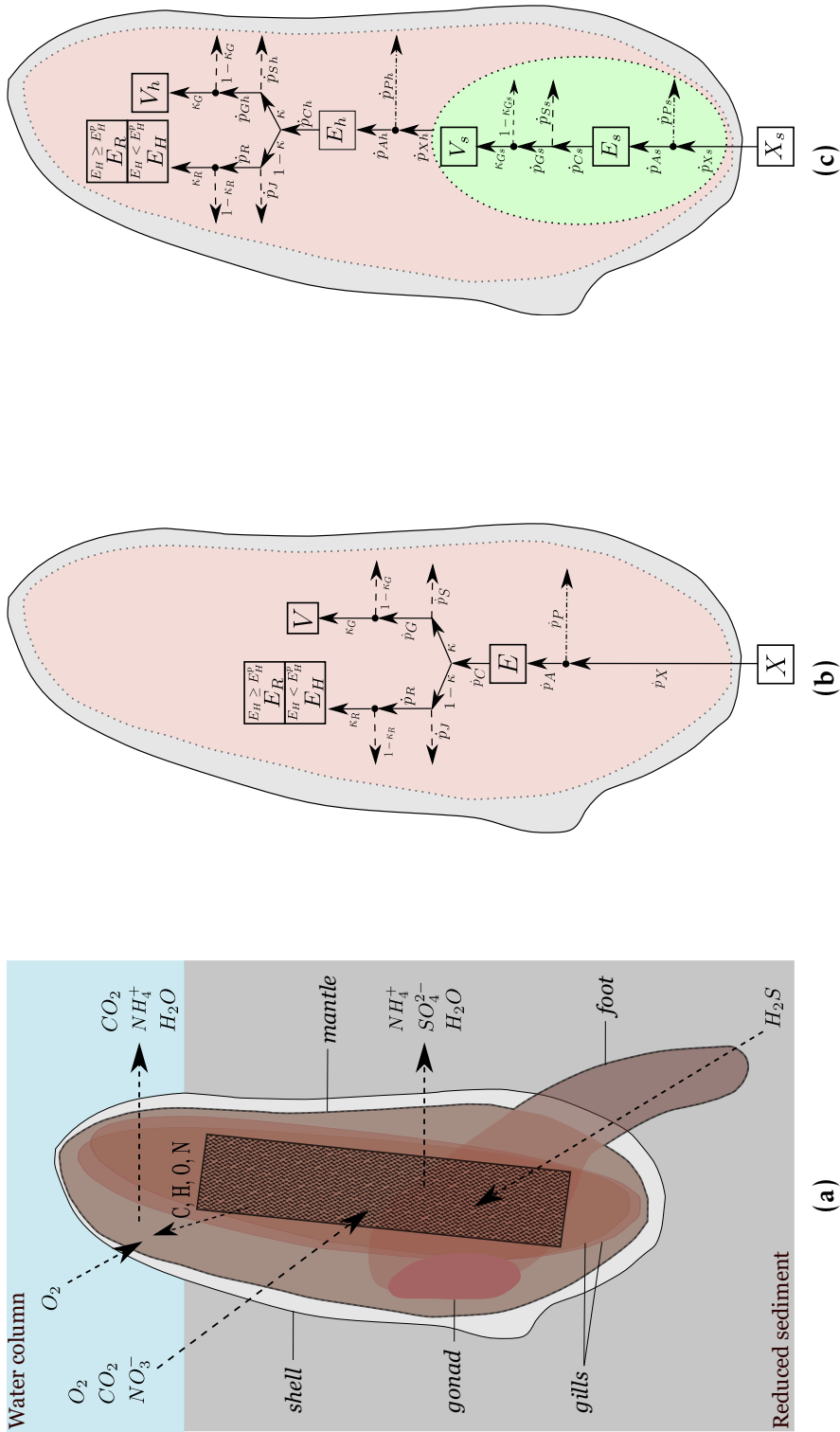


**Figure 2.1:** (a) Chemical fluxes between *Christineconcha regab* and its sulfur-oxidizing symbionts and their environment. *Christineconcha regab* Dynamic Energy Budget (DEB) modeling schemes: (b) abj model, (c) abj-farming model. (a) Black box: sulfur-oxidizing symbionts; dashed arrows: chemical fluxes; green background: sulfur-oxidizing symbionts; red background: bivalve host soft body; grey background: their environment. (b,c) Plain line text box: sulfur-oxidizing symbionts; red background: its sulfur-oxidizing symbionts and its sulfur-oxidizing symbionts and their environment.

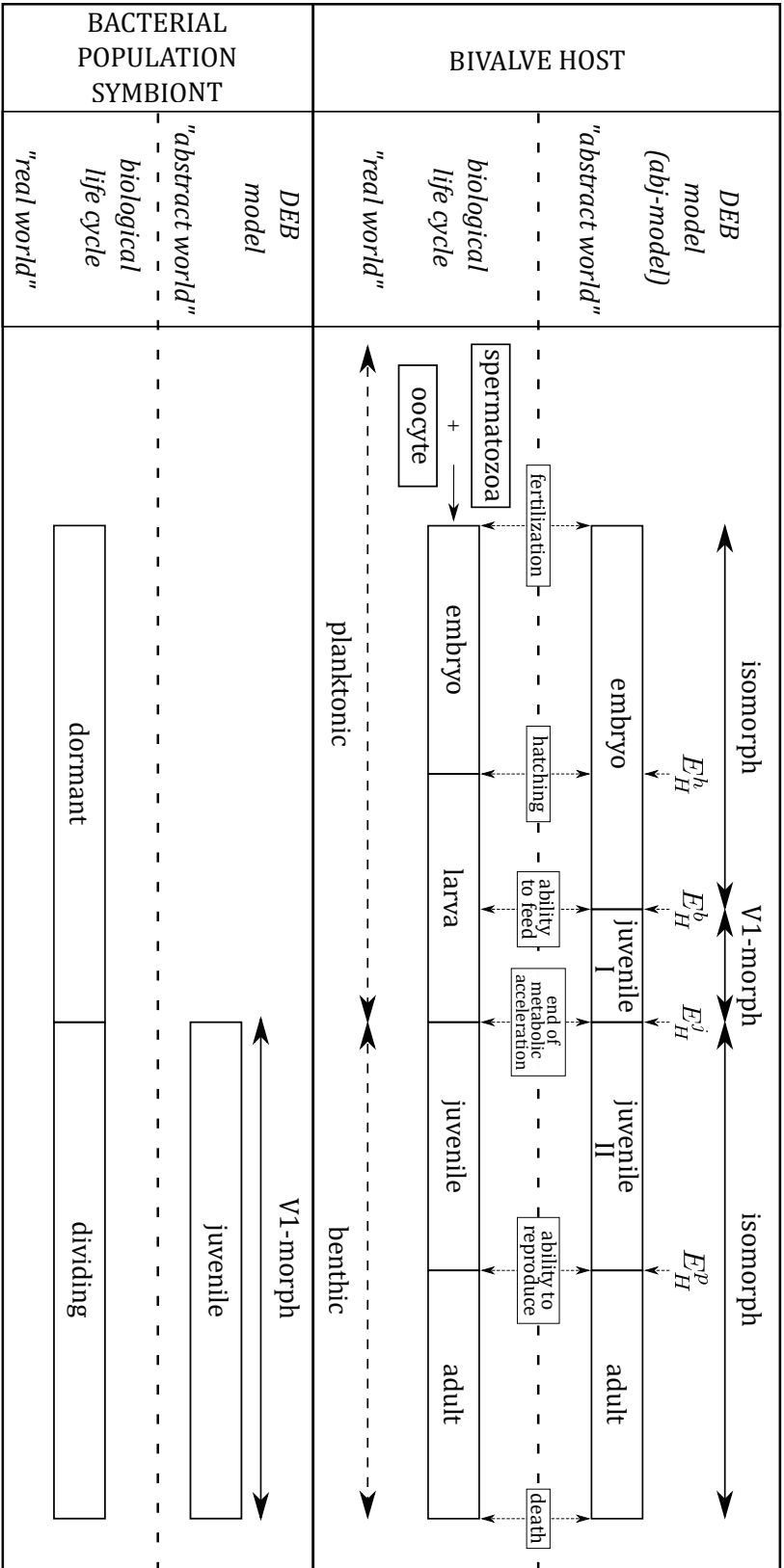


**Figure 2.2:** The "real world" representation of the biological life cycle versus the "abstract world" of the dynamic energy budget (DEB) theory on the different life stages of *Christineconcha regab* and its sulfur-oxidizing symbionts.  $E_H^h$ , host maturity level at birth (J) ;  $E_H^b$ , host maturity level at hatching (J) ;  $E_H^j$ , host maturity level at metamorphosis (J) ;  $E_H^p$ , host maturity level at puberty (J). "juvenile II" stage corresponds to a juvenile in a biological sense whereas "juvenile I" corresponds to a larval stage.

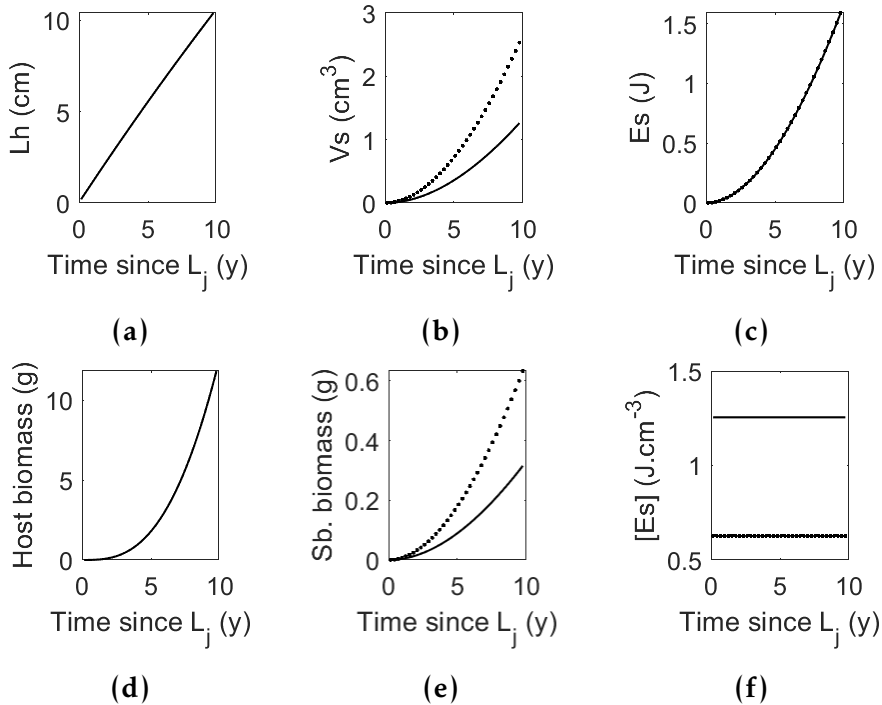


**Figure 2.3:** Modeled *Christineconcha regab* host and sulfur-oxidizing symbionts variables since host metamorphosis ( $L_j$ , predicted at 0.1991 cm) for 10 years using *C. regab* abj-farming model ( $T = 2.55^\circ\text{C}$ ; functional response for host (a, d):  $f_h = 0.18$ ; functional response for symbionts (b, c, e, f): plain line:  $f_s = 1$ , dotted line:  $f_s = 0.5$ ). (a) Host shell length ( $L_h$ , cm); (b) symbionts structure ( $V_s$ ,  $\text{cm}^3$ ); (c) symbionts reserve ( $E_s$ , J); (d) host biomass (structure+reserve) (in dry weight, g); (e) symbionts biomass (structure+reserve) (in dry weight, g); and (f) symbionts reserve density (reserve/structure) ( $[E_s]$ ,  $\text{g}\cdot\text{cm}^{-3}$ ).

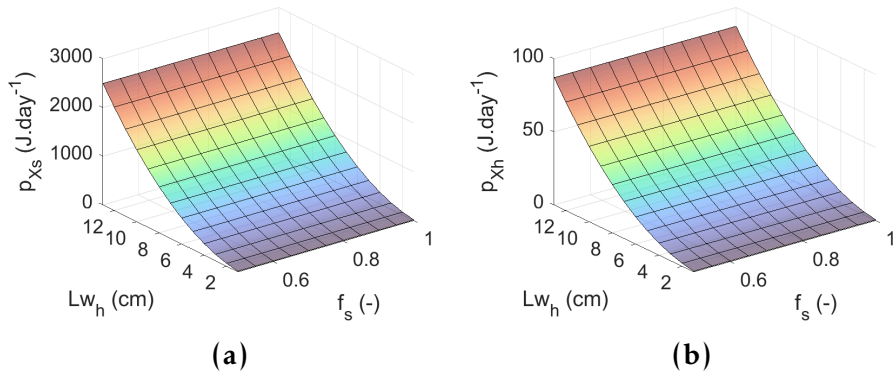


**Figure 2.4:** Modeled ingestion fluxes with *Christineconcha regab* abj-farming model. (a) Symbiont ingestion and (b) host ingestion flux as a function of symbiont functional response ( $f_s$ ) and host shell length ( $Lw_h$ ) modeled with *Christineconcha regab* abj-farming DEB model (host functional response ( $f_h$ ) = 0.18 ; T = 2.55°C). (a) mean Pearson coefficient (a)  $\bar{r}(f_s, p_{X_s}) = -0.9871 (\pm 8.4213e-04)$ ; (b)  $\bar{r}(f_s, p_X) = 1$ .

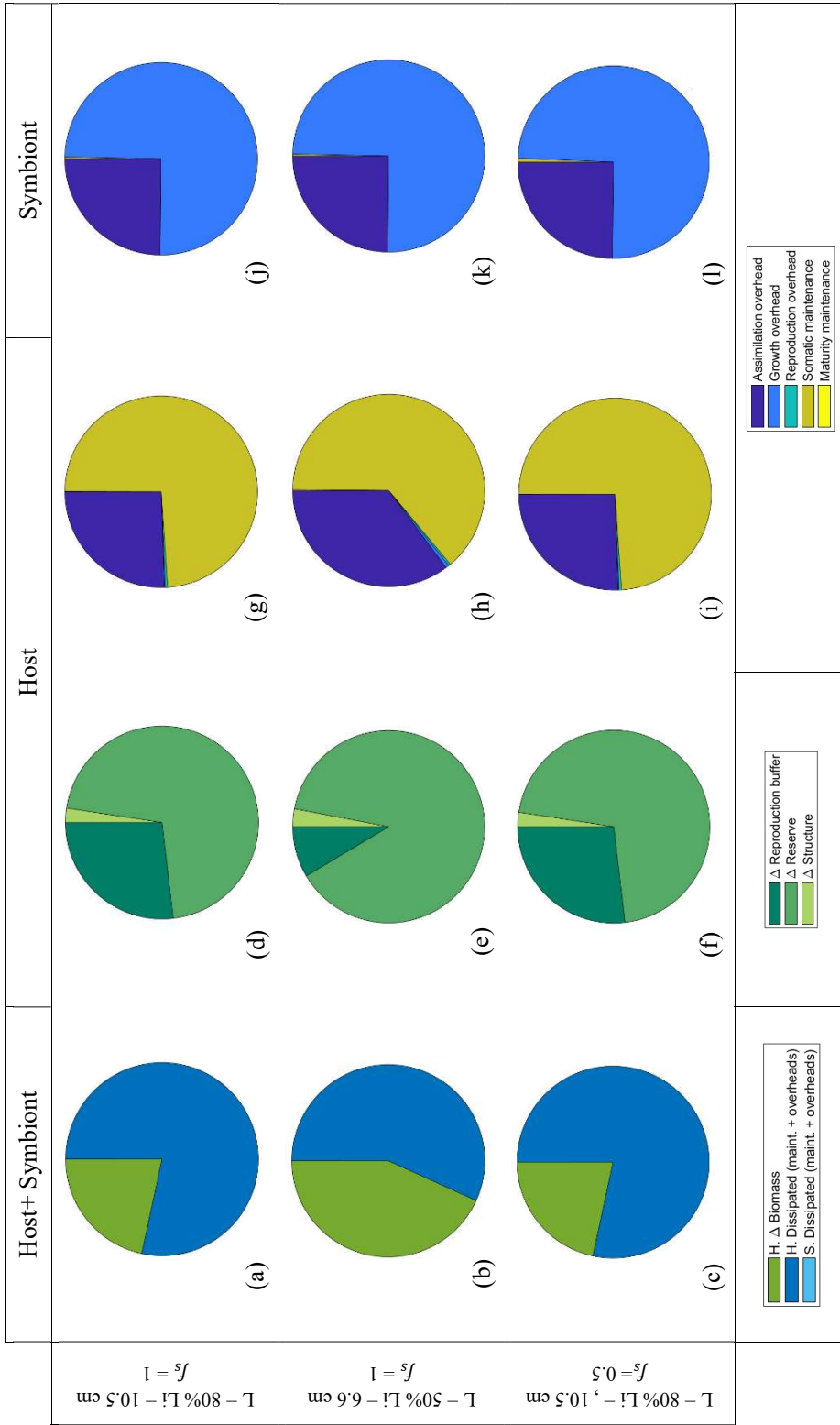


**Figure 2.5:** Pie charts of the energy distribution ( $\text{Jd}^{-1}$ ) within *Christineconcha regab* and its sulfur-oxidizing symbiont population using the abj-farming model (temperature  $T = 2.55^\circ\text{C}$ , host functional response  $f_h = 0.18$ ). L represents the *C. regab* shell length.  $L_i$  represents the maximum shell length estimated by the model ( $L_i = 13.15 \text{ cm}$ ).  $f_s$  represents the symbiont functional response.  $\Delta$  represents the state variation in  $\text{Jd}^{-1}$ .

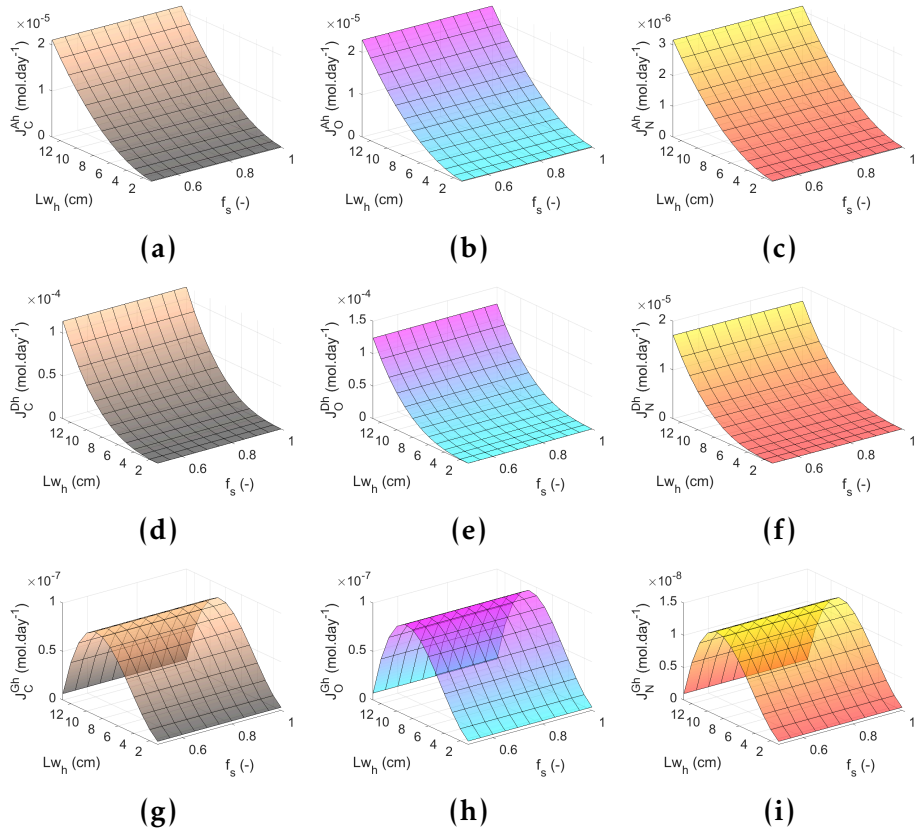


**Figure 2.6:** Host *Christineconcha regab* modeled chemical element (carbon, oxygen and nitrogen) fluxes with the abj-farming dynamic energy budget model of assimilation, dissipation and growth transformations as a function of *C. regab* shell length ( $L$ ) and symbiont functional response ( $f_s$ ).  $J$ , fluxes ( $\text{mol}\cdot\text{d}^{-1}$ ); A, assimilation; D, dissipation; G, growth; C, carbon; O, oxygen; N, nitrogen; and h, host.

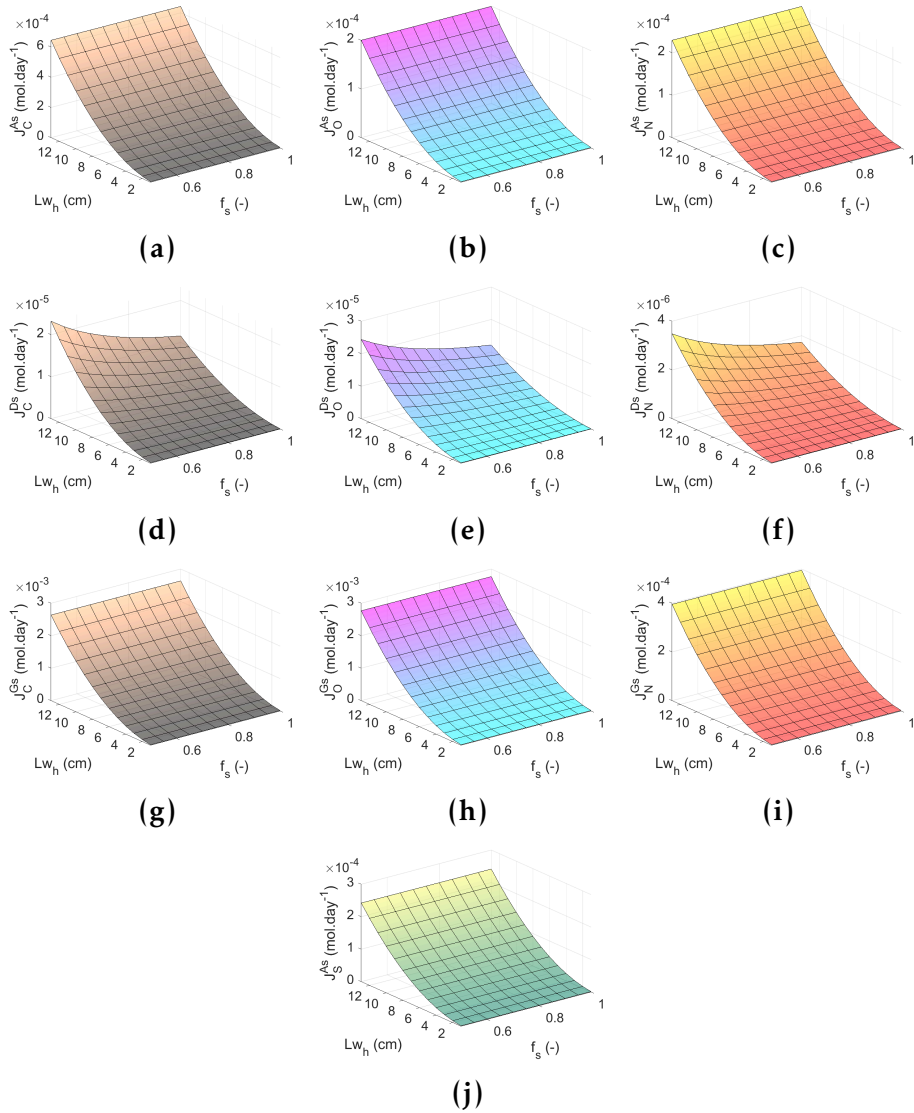


**Figure 2.7:** *Christineconcha regab* symbionts modeled chemical element (carbon, oxygen, nitrogen and sulfur) fluxes with the abj-farming dynamic energy budget model of assimilation, dissipation and growth transformations as a function of *C. regab* shell length ( $L$ ) and symbionts functional response ( $f_s$ ).  $J$ , fluxes (mol.d $^{-1}$ ); A, assimilation; D, dissipation; G, growth; C, carbon; O, oxygen; N, nitrogen; S, sulfur; and s, symbionts.

## 2.6 Supplementary Methods

### 2.6.1 Data collection

**Length at life events** The length at hatching ( $L_h$ , Table 2.4) was estimated as the mean size of the max Feret diameter of mature oocytes (an oocyte was considered mature when its Feret diameter was greater than  $305\ \mu\text{m}$  (From Fig. 9 Jehenne, 2012). Length at metamorphosis ( $L_j$ , Table 2.4) was taken from another vesicomid species (a *Calypptogena* spp. larva, Barry et al., 2007) as no data were available for *C. regab* or closely related species. Maximum length ( $L_i$ , Table 2.4) was taken as the maximum observed shell size in the literature (von Cosel & Olu, 2009). For length at birth ( $L_b$ , Table 2.4) (i.e., the length at which the organism starts feeding on external food and not on maternal reserve), no data were available, and  $L_b$  was added as a size between length at hatching and length at metamorphosis.

**Life span** A minimal lifespan ( $a_m$ , Table 2.4) was estimated from two video surveys carried out by Remoted Operated Vehicle Victor 6000 (Ifremer) in 2001 and 2011 (Marcon et al., 2014; Roy et al., 2007) at the Regab pockmark on a vesicomid clam bed including *C. regab*.

**Fecundity** The maximum reproduction rate ( $R_i$ , Table 2.4) which represented the number of oocytes released in one day, was estimated from image analysis (ImageJ) of histological sections cut of at  $8\ \mu\text{m}$  of gonads and stained in hematoxylin and eosin. For each histological section analyzed, the total number of fully grown oocytes was counted, and fecundity was related to the gonad volume viewed as an ellipsoid, assuming the distribution and proportion of oocytes was the same in the entire gonad (oocyte minimum Ferret diameter of  $305\ \mu\text{m}$ ).

**Fluxes of chemical elements and gill bacterial ratio** Carbon dioxide, oxygen and ammonium fluxes (JC, JO, JN, Table 2.4) were taken from on-site experiments carried out at Regab center and Lobe C using a ben-

thic chamber fitted with a tank encompassing flux measurements on isolated *C. regab* specimens (Khripounoff et al., 2017). Sulfide consumption was measured on individual gills dissected from specimens immediately after recovery (JS, Table 2.4, Supplementary Method 2.6.2). For each specimens, the other gill was fixed to estimate bacterial abundance using symbiont-specific probes and fluorescence *in situ* hybridization (FISH) (vbg, Table 2.4, Supplementary Methods 2.6.3).

**Host-Symbiont biomass ratio** The ratio of host biomass to symbiont biomass in dry weight was also added as data (ratioHSb) (Table 2.4, Supplementary Methods 2.6.3).

**Symbiont macrochemical equation yields** The stoichiometry of the equation of chemosynthesis of sulfur-oxidizing symbionts is not known. Yields of aerobic  $H_2S$  oxidation by the bacteria *Thiobacillus denitrificans*, which is a free-living strict autotroph and facultative anaerobe, were studied in batch reactors (Sublette, 1987).  $SO_4^{2-}$ ,  $O_2$ ,  $NH_4^+$  and biomass stoichiometry of aerobic  $H_2S$  oxidation in mol per mol of  $H_2S$  used were added as zero-variate data (SO4ovH2S, O2ovH2S, NH4ovH2S, BiomovH2S, Table 2.4). *T. denitrificans*' yields of assimilation of mol of  $HS^-$  per C-mol of biomass were also used (YSBs, Table 2.4) (Heijnen & Dijken, 1992). These yields were previously used to model the mussel *Bathymodiolus azoricus* interactions with vent fluid (Husson et al., 2018).

**Clam length, weight and reproduction rate** Relationships between shell length and wet/dry weight (Ww-L and Wd-L respectively, Table 2.4) (Khripounoff et al., 2017) and reproduction rate against shell length and wet weight were also added as univariate data (R-L and R-Ww, Table 2.4) (Jehenne, 2012).

**Clam growth** The mean shell lengths of the major cohorts at the Regab Center and Southwest sites, in August 2008 and February 2011, were added as time-length data related to growth (t-L, Table 2.4) (Decker, 2011; Guillon et al., 2017).

### 2.6.2 Symbiont sulfide consumption

Estimates of sulfide consumption by gill tissue were obtained as described below using a protocol adapted from Goffredi and Barry, 2002a by Carole Decker. Sulfide consumption by intact gills was measured (on the day of collection) by immersing the gill tissue in sulfide-rich filtered seawater solutions. Sulfide solutions were made by dissolving  $\text{Na}_2\text{S}$  in  $\text{N}_2$ -bubbled filtered sea water (FSW) and put into anaerobic Penicillin vials of 25 mL. Gills were rinsed in cold FSW before being added to the vials. After adding the tissue, vials were capped (with septum caps) and final concentration of  $\text{H}_2\text{S}$  was about 0.5 mM. The Vials were rotated at 4°C for up to 36h.

Incubation medium was subsampled using a syringe every 3 to 12h, and  $\text{ZnCl}_2$  was added immediately for sulfide analysis. Vials without tissue were included as controls and showed a loss of only 0.2–0.3  $\mu\text{mol h}^{-1}$  (around 5%). In the laboratory, sulfide concentrations were analyzed using standard photometric procedures (Cline 1969; Fonselius 1983). Rates of sulfide uptake were calculated from the slope of the linear regression obtained with sulfide concentration versus time. Sulfide consumption was expressed in mmol per min and gram gill or tissue dry weight after subtracting the control.

### 2.6.3 Estimation of gill volume occupation by symbionts based on 3D-FISH

Protocol by Sebatién Duperron (Duperron et al., 2016), experiment by Carole Decker. For each specimen (three specimens per species per site, Regab Center and Lobe C), symbiont densities were estimated using 3D FISH (Fluorescence Hybridization In Situ) as the percentage of gill volume occupied by the bacteria (Decker et al., 2013). Numbers of bacteria per unit mass of clam gill were estimated using the percentage of gill volume occupied by bacteria, a bacterial volume of  $4.2 \cdot 10^{-12} \text{ cm}^3$  and a bacterial density of  $1 \text{ g cm}^{-3}$  (Powell and Somero, 1985). Tissues and gills wet/dry mass were determined to the nearest 0.1g for individuals stored in 4% buffered formalin of the same size than those used for this

study. Dry mass was obtained after tissues were dried for 24h at 60°C.

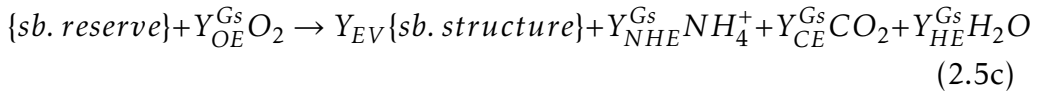
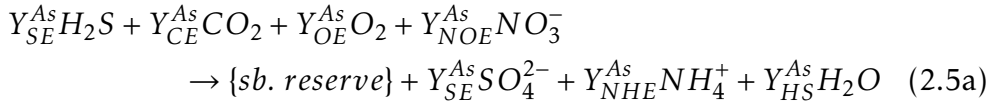
### 2.6.4 Host-Symbiont biomass ratio

The ratio of host biomass to symbiont biomass in dry weight was also added as data (ratioHSb, Table 2.4; Decker unpublished). The biomass ratio (ratioHSb, Table 2.4) was approximated as:

$$\text{ratioHSb} = \frac{\text{tissue dry weight}}{\text{gill dry weight} * \text{gill volume occupation by bacteria}} \quad (2.4)$$

### 2.6.5 Symbiont macrochemical equations for assimilation, dissipation and growth

Assimilation, dissipation and growth transformations of *C. regab* sulfur-oxidizing symbiotic bacteria were defined as:



where Eq. 2.5a is for assimilation, Eq. 2.5b for dissipation and Eq. 2.5c for growth. The symbiont (sb) structure and reserve have the standard DEB macrochemical equation  $CH_{1.8}O_{0.5}N_{0.15}$ .  $Y_{\square E}$ , chemical  $\square$  yield (chemical mol.C-mol of reserve<sup>-1</sup>); As, symbiont assimilation; Ds, symbiont dissipation; Gs, symbionts growth.

### 2.6.6 Temperature correction

Physiological rates of the host and symbiont are corrected to estimate parameters at a reference temperature  $T_{ref} = 293.15$  K (20°C) (Eq. 2.6T is the absolute temperature (K);  $\dot{k}$  is the rate of interest at  $T$ ;  $\dot{k}_1$  is the rate of interest at  $T_{ref}$ ;  $T_A$  is the species-specific Arrhenius temperature

(K) (which is a primary parameter). The Arrhenius temperature is the value of the slope of the linear plot  $\ln(\dot{k})$  against  $T^{-1}$  (Kooijman, 2010).

$$\dot{k}(T) = \dot{k}_1 \exp\left(\frac{T_A}{T_{ref}} - \frac{T_A}{T}\right) \quad (2.6)$$

The temperature ( $T^\circ$ ) at Regab Center and Southwest was  $2.55^\circ\text{C}$  during the WACS cruise (February 2011) and  $2.6^\circ\text{C}$  during the Guineco cruise (August 2008) (Decker et al., 2012; Khripounoff et al., 2017). For Lobes A, B, and C the temperature was  $2.4^\circ\text{C}$  (measured during the Congolobe cruise in December 2011–January 2012, (Khripounoff et al., 2017); this  $T^\circ$  was assumed for WACS Lobes because the WACS sampling was conducted during the same period of the year as the Congolobe sampling. The temperature for the sulfide consumption experiment onboard was  $4^\circ\text{C}$  (Decker unpublished).

### 2.6.7 Symbiont state variables computation

Symbiont state variables were written at steady state, making the assumption that symbiont dynamics were quicker than the host dynamics and come back rapidly to equilibrium (Eq. 2.7).

$$\left\{ \begin{array}{l} \frac{dE_s}{dt} = \dot{p}_{As} - \dot{p}_{Cs} - \dot{p}_{XE} = 0 \\ \frac{dV_s}{dt} = \frac{\dot{p}_{Gs}}{[E_{Gs}]} - \frac{\dot{p}_{XV}}{[E_{Vs}]} = 0 \end{array} \right. \quad (2.7a)$$

$$\left\{ \begin{array}{l} \frac{dE_s}{dt} = \dot{p}_{As} - \dot{p}_{Cs} - \dot{p}_{XE} = 0 \\ \frac{dV_s}{dt} = \frac{\dot{p}_{Gs}}{[E_{Gs}]} - \frac{\dot{p}_{XV}}{[E_{Vs}]} = 0 \end{array} \right. \quad (2.7b)$$

$\gamma$  was defined as the fraction of  $\dot{p}_X$  coming from symbiont reserve  $E_s$  and  $(1 - \gamma)$  defined as the fraction of  $\dot{p}_X$  coming from symbiont structure  $V_s$ .  $\dot{p}_{XE}$  and  $\dot{p}_{XV}$  fluxes were expressed in function of the flux  $\dot{p}_X$  using  $\gamma$  (Eq. 2.9 and Eq. 2.10).

$$\dot{p}_X = \{\dot{p}_{Xm}\} fL^2 = \dot{p}_{XE} + \dot{p}_{XV} \quad (2.8)$$

$$\dot{p}_{XE} = \gamma \{\dot{p}_{Xm}\} fL^2 \quad (2.9)$$

$$\dot{p}_{XV} = (1 - \gamma) \{\dot{p}_{Xm}\} fL^2 \quad (2.10)$$

### 2.6.7.1 Symbiont reserve density $[E_s]$

$\dot{p}_{XE}$  and  $\dot{p}_{XV}$  expressions (Eq. 2.9 and Eq. 2.10) were replaced in state variable dynamic equation (Eq. 2.7a and Eq. 2.7b), giving Eq. 2.11b.

$$\begin{cases} \dot{p}_{As} - \dot{p}_{Cs} - \gamma \{ \dot{p}_{Xm} \} f L^2 = 0 & (2.11a) \\ \frac{\dot{p}_{Gs}}{[E_{Gs}]} - \frac{(1-\gamma) \{ \dot{p}_{Xm} \} f L^2}{[E_{Vs}]} = 0 & (2.11b) \end{cases}$$

To simplify the second equation of the system (eq. 2.11b), the equation was multiplied by  $\frac{[E_{Vs}]\gamma}{1-\gamma}$  giving Eq. 2.12.

$$\begin{aligned} \text{Eq. (2.11b)} * \frac{[E_{Vs}]\gamma}{1-\gamma} &= \left( \frac{\dot{p}_{Gs}}{[E_{Gs}]} - \frac{(1-\gamma) \{ \dot{p}_{Xm} \} f L^2}{[E_{Vs}]} \right) \frac{[E_{Vs}]\gamma}{1-\gamma} \\ &= \frac{\dot{p}_{Gs} [E_{Vs}]\gamma}{[E_{Gs}](1-\gamma)} - \gamma \{ \dot{p}_{Xm} \} f L^2 \end{aligned} \quad (2.12)$$

The system obtained was then Eq. 2.13.

$$\begin{cases} \dot{p}_{As} - \dot{p}_{Cs} - \gamma \{ \dot{p}_{Xm} \} f L^2 = 0 & (2.13a) \\ \frac{\dot{p}_{Gs} [E_{Vs}]\gamma}{[E_{Gs}](1-\gamma)} - \gamma \{ \dot{p}_{Xm} \} f L^2 = 0 & (2.13b) \end{cases}$$

It gave the equality Eq. 2.14.

$$\dot{p}_{As} - \dot{p}_{Cs} - \gamma \{ \dot{p}_{Xm} \} f L^2 = \frac{\dot{p}_{Gs} [E_{Vs}]\gamma}{[E_{Gs}](1-\gamma)} - \gamma \{ \dot{p}_{Xm} \} f L^2 \quad (2.14a)$$

$$\Rightarrow \frac{\dot{p}_{Gs} [E_{Vs}]\gamma}{[E_{Gs}](1-\gamma)} - \dot{p}_{As} + \dot{p}_{Cs} = 0 \quad (2.14b)$$

From Eq. 2.8-2.10, Eq. 2.15 could be written.

$$\{ \dot{p}_{Xm} \} f L^2 = \frac{\dot{p}_{XE}}{\gamma} + \frac{\dot{p}_{XV}}{1-\gamma} \quad (2.15a)$$

$$\Rightarrow \frac{1-\gamma}{\gamma} = \frac{\dot{p}_{XV}}{\dot{p}_{XE}} = \frac{E_{Vs}}{E_s} = \frac{[E_{Vs}]}{[E_s]} \quad (2.15b)$$

$$\Rightarrow \frac{\gamma}{1-\gamma} = \frac{[E_s]}{[E_{Vs}]} \quad (2.15c)$$

$\frac{\gamma}{1-\gamma}$  was replaced by  $\frac{[E_s]}{[E_{Vs}]}$  and  $\dot{p}_{Gs}$  was replaced by  $\dot{p}_{Cs} - \dot{p}_{Ss}$  (see Table 2.1) in Eq. 2.14 giving Eq. 2.16.

$$\frac{(\dot{p}_{Cs} - \dot{p}_{Ss})[E_{Vs}]E_s}{[E_{Gs}][E_{Vs}]} - \dot{p}_{As} + \dot{p}_{Cs} = 0 \quad (2.16a)$$

$$\Leftrightarrow \frac{(\dot{p}_{Cs} - \dot{p}_{Ss})E_s}{[E_{Gs}]} - \dot{p}_{As} + \dot{p}_{Cs} = 0 \quad (2.16b)$$

$\dot{p}_{Cs}$  and  $\dot{p}_{As}$  were replaced in the following development (Eq. 2.17) as they were defined in Table 2.1 in the Methods section.

$$\dot{p}_{Cs} \left( 1 + \frac{[E_s]}{[E_{Gs}]} \right) - \frac{\dot{p}_{Ss}[E_s]}{E_{Gs}} - \dot{p}_{As} = 0 \quad (2.17a)$$

$$\dot{p}_{Cs} \left( 1 + \frac{[E_s]}{[E_{Gs}]} \right) - \frac{[\dot{p}_{Ms}]V_s[E_s]}{E_{Gs}} - \dot{p}_{As} = 0 \quad (2.17b)$$

$$\dot{p}_{Cs}([E_{Gs}] + [E_s]) - [\dot{p}_{Ms}]V_s[E_s] - [\dot{p}_{Ams}]f_sV_s[E_{Gs}] = 0 \quad (2.17c)$$

$$E_s \frac{\dot{k}_{Es}V_s[E_{Gs}] + \dot{p}_{Ss}}{E_s + [E_{Gs}]V_s} ([E_{Gs}] + [E_s]) - [\dot{p}_{Ms}]V_s[E_s] - [\dot{p}_{Ams}]f_sV_s[E_{Gs}] = 0 \quad (2.17d)$$

$$[E_s] \frac{\dot{k}_{Es}V_s[E_{Gs}] + [\dot{p}_{Ms}]V_s}{E_s + [E_{Gs}]V_s} ([E_{Gs}] + [E_s]) - [\dot{p}_{Ms}][E_s] - [\dot{p}_{Ams}]f_s[E_{Gs}] = 0 \quad (2.17e)$$

$$[E_s] \frac{\dot{k}_{Es}[E_{Gs}] + [\dot{p}_{Ms}]}{E_s + [E_{Gs}]} ([E_{Gs}] + [E_s]) - [\dot{p}_{Ms}][E_s] - [\dot{p}_{Ams}]f_s[E_{Gs}] = 0 \quad (2.17f)$$

$$[E_s] (\dot{k}_{Es}[E_{Gs}] + [\dot{p}_{Ms}] - [\dot{p}_{Ms}]) - [\dot{p}_{Ams}]f_s[E_{Gs}] = 0 \quad (2.17g)$$

$$[E_s] \dot{k}_{Es}[E_{Gs}] - [\dot{p}_{Ams}]f_s[E_{Gs}] = 0 \quad (2.17h)$$

$$[E_s] = \frac{[\dot{p}_{Ams}]f_s}{\dot{k}_{Es}} \quad (2.17i)$$

### 2.6.7.2 Symbiont structure $V_s$

$V_s$  was computed from symbiont state variables dynamic equations at the equilibrium (eq. 2.7). Host functional response  $f$  was then defined

by Eq. 2.18.  $v_{K_s}$  was a new symbiont core primary parameter.  $v_{K_s}$  was the half saturation coefficient, with value of food density  $X$  equals to  $V_s + E_s$  (as the host feed by digestion of symbiont reserve  $E_s$  and structure  $V_s$ ) where ingestion  $\dot{p}_{XE} + \dot{p}_{XV}$  is half of its maximum.

$$f = \frac{V_s/V}{V_s/V + v_{K_s}} = \frac{V_s}{V_s + v_{K_s}V} \quad (2.18)$$

Host ingestion flux of symbiont reserve  $\dot{p}_{XE}$  and host ingestion flux of symbiont structure  $\dot{p}_{XV}$  (Eq. 2.9 and Eq. 2.10) were written respectively as in Eq. 2.19 and Eq. 2.20 by replacing  $f$  by host's  $f$  expression (Eq. 2.2).

$$\dot{p}_{XE} = \gamma \{\dot{p}_{Xm}\} \frac{V_s}{V_s + v_{K_s}V} L^2 \quad (2.19)$$

$$\dot{p}_{XV} = (1 - \gamma) \{\dot{p}_{Xm}\} \frac{V_s}{V_s + v_{K_s}V} L^2 \quad (2.20)$$

$V_s$  was computed from symbiont state variables dynamic equations at the equilibrium,  $\frac{dE_s}{dt} = 0$  and  $\frac{dV_s}{dt} = 0$  (Eq. 2.7a). The same expression of  $V_s$  was obtained from the two dynamic equations.

For the computation of  $V_s$  from the state variable  $E_s$  dynamic expression,  $\dot{p}_{XE}$  expression (Eq. 2.19) was replaced in the equation of  $E_s$  dynamic expression at equilibrium (Eq. 2.11a) giving Eq. 2.21.

$$\dot{p}_{As} - \dot{p}_{Cs} - \gamma \{\dot{p}_{Xm}\} \frac{V_s}{V_s + v_{K_s}V} L^2 = 0 \quad (2.21a)$$

$$\dot{p}_{As} - \dot{p}_{Cs} = \gamma \{\dot{p}_{Xm}\} \frac{V_s}{V_s + v_{K_s}V} L^2 \quad (2.21b)$$

$$\frac{\dot{p}_{As} - \dot{p}_{Cs}}{V_s} = \gamma \{\dot{p}_{Xm}\} \frac{1}{V_s + v_{K_s}V} L^2 \quad (2.21c)$$

In Eq. 2.22,  $\frac{\dot{p}_{As} - \dot{p}_{Cs}}{V_s}$  was developed with  $\dot{p}_{As}$  and  $\dot{p}_{Cs}$  expression replaced by their formulation from Table 2.1.  $[E_s]$  was replaced by the formula computed in previous subsection.

$$\frac{\dot{p}_{As} - \dot{p}_{Cs}}{V_s} = \frac{[\dot{p}_{Ams}] f_s V_s - E_s \frac{\dot{k}_{Es} V_s [E_{Gs}] + [\dot{p}_{Ms}] V_s}{E_s + [E_{Gs}] V_s}}{V_s} \quad (2.22a)$$

$$= [\dot{p}_{Ams}] f_s - [E_s] \frac{V_s \dot{k}_{Es} [E_{Gs}] + [\dot{p}_{Ms}]}{[E_s] + [E_{Gs}]} \quad (2.22b)$$

$$= [\dot{p}_{Ams}] f_s - \frac{[\dot{p}_{Ams}] f_s \dot{k}_{Es} [E_{Gs}] + [\dot{p}_{Ms}]}{\dot{k}_{Es} \frac{[\dot{p}_{Ams}] f_s}{\dot{k}_{Es}} + [E_{Gs}]} \quad (2.22c)$$

$$= [\dot{p}_{Ams}] f_s - [\dot{p}_{Ams}] f_s \frac{\dot{k}_{Es} [E_{Gs}] + [\dot{p}_{Ms}]}{[\dot{p}_{Ams}] f_s + [E_{Gs}] \dot{k}_{Es}} \quad (2.22d)$$

$$= [\dot{p}_{Ams}] f_s \left( 1 - \frac{\dot{k}_{Es} [E_{Gs}] + [\dot{p}_{Ms}]}{[\dot{p}_{Ams}] f_s + [E_{Gs}] \dot{k}_{Es}} \right) \quad (2.22e)$$

$$= [\dot{p}_{Ams}] f_s \left( \frac{[\dot{p}_{Ams}] f_s + [E_{Gs}] \dot{k}_{Es}}{[\dot{p}_{Ams}] f_s + [E_{Gs}] \dot{k}_{Es}} - \frac{[E_{Gs}] \dot{k}_{Es} + [\dot{p}_{Ms}]}{[\dot{p}_{Ams}] f_s + [E_{Gs}] \dot{k}_{Es}} \right) \quad (2.22f)$$

$$= [\dot{p}_{Ams}] f_s \left( \frac{[\dot{p}_{Ams}] f_s - [\dot{p}_{Ms}]}{[\dot{p}_{Ams}] f_s + [E_{Gs}] \dot{k}_{Es}} \right) \quad (2.22g)$$

Eq. 2.22 result was replaced in Eq. 2.21 to obtain  $V_s$  expression in Eq. 2.23.

$$[\dot{p}_{Ams}] f_s \left( \frac{[\dot{p}_{Ams}] f_s - [\dot{p}_{Ms}]}{[\dot{p}_{Ams}] f_s + [E_{Gs}] \dot{k}_{Es}} \right) = \gamma \{ \dot{p}_{Xm} \} \frac{1}{V_s + v_{Ks} V} L^2 \quad (2.23a)$$

$$[\dot{p}_{Ams}] f_s \left( \frac{[\dot{p}_{Ams}] f_s - [\dot{p}_{Ms}]}{[\dot{p}_{Ams}] f_s + [E_{Gs}] \dot{k}_{Es}} \right) - \gamma \{ \dot{p}_{Xm} \} \frac{1}{V_s + v_{Ks} V} L^2 = 0 \quad (2.23b)$$

$$(V_s + v_{Ks} V) [\dot{p}_{Ams}] f_s \left( \frac{[\dot{p}_{Ams}] f_s - [\dot{p}_{Ms}]}{[\dot{p}_{Ams}] f_s + [E_{Gs}] \dot{k}_{Es}} \right) - \gamma \{ \dot{p}_{Xm} \} L^2 = 0 \quad (2.23c)$$

$$\frac{\gamma \{ \dot{p}_{Xm} \} L^2}{[\dot{p}_{Ams}] f_s \frac{[\dot{p}_{Ams}] f_s - [\dot{p}_{Ms}]}{[\dot{p}_{Ams}] f_s + [E_{Gs}] \dot{k}_{Es}}} - v_{Ks} V = V_s \quad (2.23d)$$

$V_s$  could also be computed from the state variable  $V_s$  dynamic expression,  $\dot{p}_{XV}$  expression (Eq. 2.20) was replaced in the equation of  $V_s$  dynamic expression at equilibrium (Eq. 2.11b) giving Eq. 2.24.  $\dot{p}_{Gs}$ ,  $\dot{p}_{As}$  and  $\dot{p}_{Cs}$  were replaced by their formulation from Table 2.1 in the development and  $[E_s] = \frac{E_s}{V_s}$ .  $[E_s]$  was replaced by the formula computer in previous subsection.

$$\frac{\dot{p}_{G_s}}{[E_{G_s}]} - \frac{(1-\gamma)\{\dot{p}_{X_m}\} \frac{V_s}{V_s+v_{K_s}V} L^2}{[E_{V_s}]} = 0 \quad (2.24a)$$

$$\frac{\dot{p}_{C_s} - \dot{p}_{S_s}}{[E_{G_s}]} = \frac{(1-\gamma)\{\dot{p}_{X_m}\} \frac{V_s}{V_s+v_{K_s}V} L^2}{[E_{V_s}]} \quad (2.24b)$$

$$\frac{(\dot{p}_{C_s} - \dot{p}_{S_s})[E_{V_s}]}{[E_{G_s}]} = (1-\gamma)\{\dot{p}_{X_m}\} \frac{V_s}{V_s+v_{K_s}V} L^2 \quad (2.24c)$$

$$\left( E_s \frac{\dot{k}_{E_s} V_s [E_{G_s}] + [\dot{p}_{M_s}] V_s}{E_s + [E_{G_s}] V_s} - [\dot{p}_{M_s}] V_s \right) \frac{[E_{V_s}]}{[E_{G_s}]} = (1-\gamma)\{\dot{p}_{X_m}\} \frac{V_s}{V_s+v_{K_s}V} L^2 \quad (2.24d)$$

$$\left( E_s \frac{V_s \dot{k}_{E_s} [E_{G_s}] + [\dot{p}_{M_s}]}{[E_s] + [E_{G_s}]} - [\dot{p}_{M_s}] V_s \right) \frac{[E_{V_s}]}{[E_{G_s}]} = (1-\gamma)\{\dot{p}_{X_m}\} \frac{V_s}{V_s+v_{K_s}V} L^2 \quad (2.24e)$$

$$\left( [E_s] V_s \frac{\dot{k}_{E_s} [E_{G_s}] + [\dot{p}_{M_s}]}{[E_s] + [E_{G_s}]} - [\dot{p}_{M_s}] V_s \right) \frac{[E_{V_s}]}{[E_{G_s}]} = (1-\gamma)\{\dot{p}_{X_m}\} \frac{V_s}{V_s+v_{K_s}V} L^2 \quad (2.24f)$$

$$\left( [E_s] \frac{\dot{k}_{E_s} [E_{G_s}] + [\dot{p}_{M_s}]}{[E_s] + [E_{G_s}]} - [\dot{p}_{M_s}] \right) \frac{[E_{V_s}]}{[E_{G_s}]} - (1-\gamma)\{\dot{p}_{X_m}\} \frac{1}{V_s+v_{K_s}V} L^2 = 0 \quad (2.24g)$$

$$(V_s + v_{K_s}V) \frac{[E_{V_s}]}{[E_{G_s}]} \left( [E_s] \frac{\dot{k}_{E_s} [E_{G_s}] + [\dot{p}_{M_s}]}{[E_s] + [E_{G_s}]} - [\dot{p}_{M_s}] \right) - (1-\gamma)\{\dot{p}_{X_m}\} L^2 = 0 \quad (2.24h)$$

$$(V_s + v_{K_s}V) \frac{[E_{V_s}]}{[E_{G_s}]} \left( \frac{[\dot{p}_{A_m s}] f_s}{\dot{k}_{E_s}} \frac{\dot{k}_{E_s} [E_{G_s}] + [\dot{p}_{M_s}]}{[\dot{p}_{A_m s}] f_s + [E_{G_s}]} - [\dot{p}_{M_s}] \right) - (1-\gamma)\{\dot{p}_{X_m}\} L^2 = 0 \quad (2.24i)$$

$$(V_s + v_{K_s}V) \frac{[E_{V_s}]}{[E_{G_s}]} \frac{[\dot{p}_{A_m s}] f_s \dot{k}_{E_s} [E_{G_s}] - [\dot{p}_{M_s}] \dot{k}_{E_s} [E_{G_s}]}{[\dot{p}_{A_m s}] f_s + \dot{k}_{E_s} [E_{G_s}]} - (1-\gamma)\{\dot{p}_{X_m}\} L^2 = 0 \quad (2.24j)$$

$$(V_s + v_{K_s}V) \frac{[E_{V_s}]}{[E_{G_s}]} \dot{k}_{E_s} [E_{G_s}] \frac{[\dot{p}_{A_m s}] f_s - [\dot{p}_{M_s}]}{[\dot{p}_{A_m s}] f_s + \dot{k}_{E_s} [E_{G_s}]} - (1-\gamma)\{\dot{p}_{X_m}\} L^2 = 0 \quad (2.24k)$$

$$(V_s + v_{K_s}V) [E_{V_s}] \dot{k}_{E_s} \frac{[\dot{p}_{A_m s}] f_s - [\dot{p}_{M_s}]}{[\dot{p}_{A_m s}] f_s + \dot{k}_{E_s} [E_{G_s}]} - (1-\gamma)\{\dot{p}_{X_m}\} L^2 = 0 \quad (2.24l)$$

$$V_s = \frac{(1-\gamma)\{\dot{p}_{X_m}\}}{[E_{V_s}] \dot{k}_{E_s} \frac{[\dot{p}_{A_m s}] f_s - [\dot{p}_{M_s}]}{[\dot{p}_{A_m s}] f_s + \dot{k}_{E_s} [E_{G_s}]} - v_{K_s}V} \quad (2.24m)$$

Then, the equality  $\frac{1-\gamma}{\gamma} = \frac{E_{Vs}}{E_s}$  was used to make  $[E_s]$  appears in the result equation 2.24 and  $[E_s]$  was replaced again by the formula computed in previous subsection.

$$V_s = \frac{\gamma}{\gamma} \frac{(1-\gamma)\{\dot{p}_{Xm}\}L^2}{[E_{Vs}]\dot{k}_{Es} \frac{[\dot{p}_{Ams}]f_s - [\dot{p}_{Ms}]}{[\dot{p}_{Ams}]f_s + \dot{k}_{Es}[E_{Gs}]}} - v_{Ks}V \quad (2.25a)$$

$$V_s = \frac{[E_{Vs}]}{[E_s]} \frac{\gamma\{\dot{p}_{Xm}\}L^2}{[E_{Vs}]\dot{k}_{Es} \frac{[\dot{p}_{Ams}]f_s - [\dot{p}_{Ms}]}{[\dot{p}_{Ams}]f_s + \dot{k}_{Es}[E_{Gs}]}} - v_{Ks}V \quad (2.25b)$$

$$V_s = \frac{1}{\frac{[\dot{p}_{Ams}]f_s}{\dot{k}_{Es}}} \frac{\gamma\{\dot{p}_{Xm}\}L^2}{\dot{k}_{Es} \frac{[\dot{p}_{Ams}]f_s - [\dot{p}_{Ms}]}{[\dot{p}_{Ams}]f_s + \dot{k}_{Es}[E_{Gs}]}} - v_{Ks}V \quad (2.25c)$$

$$V_s = \frac{\gamma\{\dot{p}_{Xm}\}L^2}{[\dot{p}_{Ams}]f_s \frac{[\dot{p}_{Ams}]f_s - [\dot{p}_{Ms}]}{[\dot{p}_{Ams}]f_s + [E_{Gs}]\dot{k}_{Es}}} - v_{Ks}V \quad (2.25d)$$

### 2.6.8 Host and symbiont chemical fluxes prediction

The flux of symbiont biomass was equal to the assimilation flux  $\dot{p}_{As}$  minus the dissipation flux  $\dot{p}_{Ds}$ , minus  $(1 - \kappa_{Gs})$  of the growth flux  $\dot{p}_{Gs}$  (Eq. 2.26).  $\kappa_{Gs}$  was the fraction of symbiont growth energy fixed in symbiont structure (also called growth efficiency).

$$\dot{p}_B = \dot{p}_A - \dot{p}_D - (1 - \kappa_G)\dot{p}_G \quad (2.26)$$

Oxygen, nitrogen and carbon fluxes were measured on both host and symbiont. As both of them contribute to the measured chemical fluxes, predictions were made has the sum of predicted host and symbiont assimilation, dissipation and growth fluxes of carbon, nitrogen and oxygen. Symbiont macrochemical equations for assimilation, dissipation and growth were written for one C-mol of symbiont reserve, using the standard reserve composition  $CH_{1.8}O_{0.5}N_{0.15}$  (Kooijman, 2010). Symbiont yields were predicted by solving macrochemical equations (cf. paper). Two yields  $Y_{SE}^{As}$  ( $H_2S$  yield per C-mol of reserve) and  $Y_{HE}^{As}$  ( $H_2O$  yield per C-mol of reserve) were added as primary parameters to be es-

timated to solve the equations. Sulfide consumption flux  $\dot{J}_{S_{As}}$  ( $\text{mol d}^{-1}$ ) were predicted from symbiont macrochemical equation for assimilation as:

$$\dot{J}_S^{As} = \frac{Y_{SE}^{As} \dot{J}_{As}}{\bar{\mu}_E} \quad (2.27)$$

$Y_{SE}^{As}$  was the yield of mol of sulfide to assimilate a C-mol of reserve ( $H_2S$ -mol/C-mol),  $\bar{\mu}_E$  the chemical potential of reserve ( $\text{J mol}^{-1}$ ),  $[E_s]$  the symbionts reserve density ( $\text{J cm}^{-3}$ ),  $f_s$  the food density (-),  $[E_{ms}]$  the maximum symbiont reserve density ( $\text{J cm}^{-3}$ ).

The yield  $Y_{SBs}$  data (table 2.4) was predicted as:

$$Y_{SBs} = Y_{SE}^{As} * \left( 1 - \frac{[\dot{p}_{Ms}]}{[\dot{p}_{Ams}] f_s} \right) \left( 1 + \kappa_{Gs} \frac{1}{\frac{f_s [E_{ms}]}{[E_{Gs}]} + 1} \right) \quad (2.28)$$

### 2.6.9 Bacterial density in gills (vbg) prediction

The assumption that symbiont metabolism is quicker than host metabolism was made and in consequence, symbiont reserve density  $[E_s]$  goes back quickly to equilibrium when changed. From this assumption, symbiont reserve density  $[E_s]$  and structure  $V_s$  were predicted as in equations below.

$$[E_s] = \frac{[\dot{p}_{Ams}] f_s}{\dot{k}_{Es}} \quad (2.29)$$

$$V_s = \frac{\gamma \{ \dot{p}_{Xm} \} L^2}{[\dot{p}_{Ams}] f_s \frac{[\dot{p}_{Ams}] f_s - [\dot{p}_{Ms}]}{[\dot{p}_{Ams}] f_s + [E_{Gs}] \dot{k}_{Es}}} - v_{Ks} V \quad (2.30)$$

$vbg$  was defined by the physical volume of the symbiont  $V_{Ts}^p$  ( $\text{cm}^3$ ) divided by the physical volume of gills  $V_g^p$  ( $\text{cm}^3$ ).

$$vbg = \frac{V_{Ts}^p}{V_g^p} \quad (2.31)$$

The physical volume of symbiont  $V_{T_s}^p$  was the addition of the physical volume of symbiont structure  $V_{V_s}^p$  ( $\text{cm}^3$ ) and physical volume of symbiont reserve  $V_{E_s}^p$  ( $\text{cm}^3$ ). We made the hypothesis that changes in symbiont reserve do not affect symbiont structure.

$$V_{T_s}^p = V_{V_s}^p + V_{E_s}^p \quad (2.32)$$

The physical length of the symbiont structure  $L_{V_s}^p$  (cm) was linked to its structural length  $L_s$  (cm) by the shape coefficient of symbiont structure  $\delta_{M_{V_s}}$ .

$$L_{V_s}^p = \frac{L_s}{\delta_{M_{V_s}}} \Rightarrow (L_{V_s}^p)^3 = V_{V_s}^p = \frac{V_s}{(\delta_{M_{V_s}})^3} \quad (2.33)$$

The total physical volume of symbiont reserve  $V_{E_s}^p$  was linked to the symbiont reserve  $E_s$  (J) by the compound parameters  $\omega_E$  ( $\text{g mol}^{-1}$ ), which was the reserve molar weight,  $\mu_E$  ( $\text{J mol}^{-1}$ ), which was the chemical potential of reserve and  $d_E$  ( $\text{g cm}^{-3}$ ) which was the specific density of reserve.

$$V_{E_s}^p = E_s \frac{\omega_E}{\mu_E d_E} \text{ with } E_s = [E_s] V_s \quad (2.34)$$

The total physical length of gills  $L_g^p$  (cm) was defined by  $W_{dg}$  (g),  $d_V$  ( $\text{g cm}^{-3}$ ) which was the specific density of structure and  $\delta_{M_g}$  which was host gills shape coefficient.

$$L_g^p = \left( \frac{W_{dg}}{d_V} \right)^{1/3} \frac{1}{\delta_{M_g}} \Rightarrow V_g^p = \frac{W_{dg}}{d_V} \frac{1}{\delta_{M_g}^3} \quad (2.35)$$

Symbiont structure shape coefficient  $\delta_{M_{V_s}}$  was added as a primary parameter to be estimated.

## 2.7 Supplementary Figures and Tables

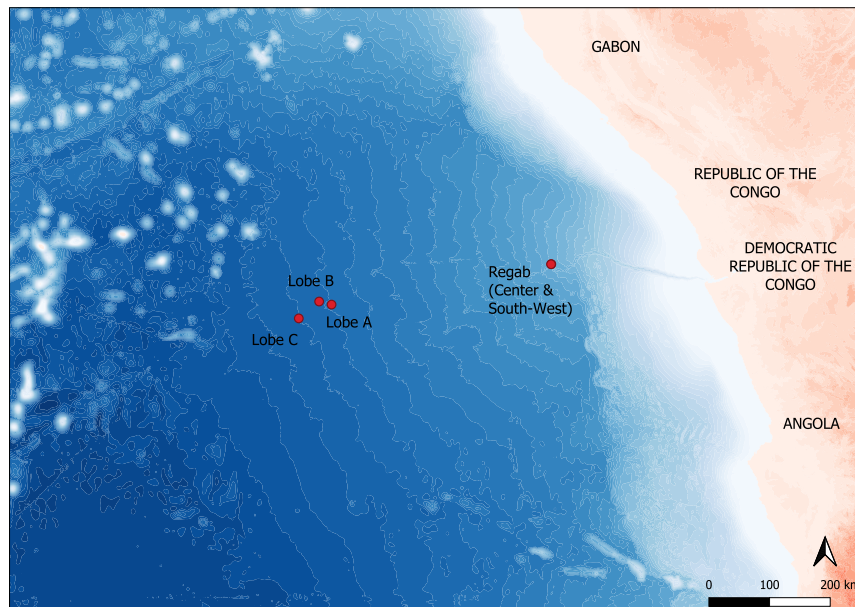


**Figure 2.8:** Map of the Gulf of Guinea (Southeast Atlantic) showing *Christineconcha regab* sampling sites (red dots) of studied specimens from which zero- and univariate data used in this study were obtained during scientific cruises (BIOZAIRE (Vangriesheim, 2001), Guineco (Boetius, 2008), WACS (West Africa Cold Seeps) cruise (Olu, 2011) and Congolobe cruise (Rabouille, 2011)) (Lobe A, S 6°28.281 E 6°02.143, -4751 m ; Lobe B S6°25.229 E5°49.709, -4712 m ; Lobe C, S6°42.068 E5°29.273, -5070 m ; Regab Center S5°47.8674 E9°42.6881, -3072 m ; Regab Southwest S5°47.9761 E9°42.4825, -3170 m (Decker, 2011; Khripounoff et al., 2017)). White isobaths every 250 meters (background bathymetric data from GEBCO Compilation Group (2023) GEBCO 2023 Grid (doi:10.5285/f98b053b-0cbc-6c23-e053-6c86abc0af7b)).

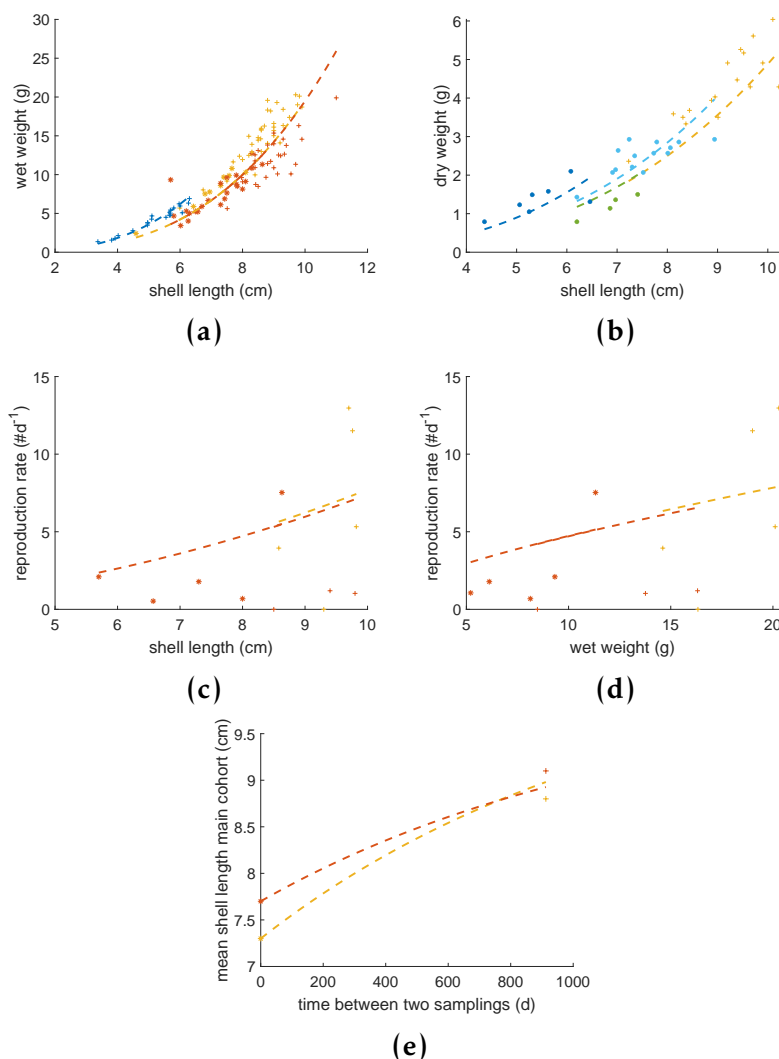


**Figure 2.9:** *Christineconcha regab* univariate data (Table 2.4) (markers) and abj Dynamic Energy Budget model predictions (dashed lines). Relationships between shell length ( $L$ , cm) and (a) wet weight ( $Ww$ , g), (b) dry weight ( $Wd$ , g), and (c) reproduction rate ( $R$ , # number of oocytes produced per day); between (d) wet weight ( $Ww$ , g) and reproduction rate ( $R$ , # number of oocytes produced per day); and between (e) the mean shell length of the main cohorts ( $L$ , cm) and the time elapsed two sampling events ( $t$ , days). Marker types correspond to sampling cruises in the Gulf of Guinea: \*, GUINECO (Aug2008); +, Wacs (Feb2011); ●, Congolobe (Dec2011–Jan2012). Colors of modeled curves correspond to sampling sites: Red, Regab Southwest (3154 m depth); Yellow, Regab Center (3156 m depth) (Khripounoff et al., 2015); Green, Lobes B (4712 m depth); Light Blue, Lobes A (4751 m depth); Dark Blue, Lobes C (5070 m depth) (Khripounoff et al., 2017).

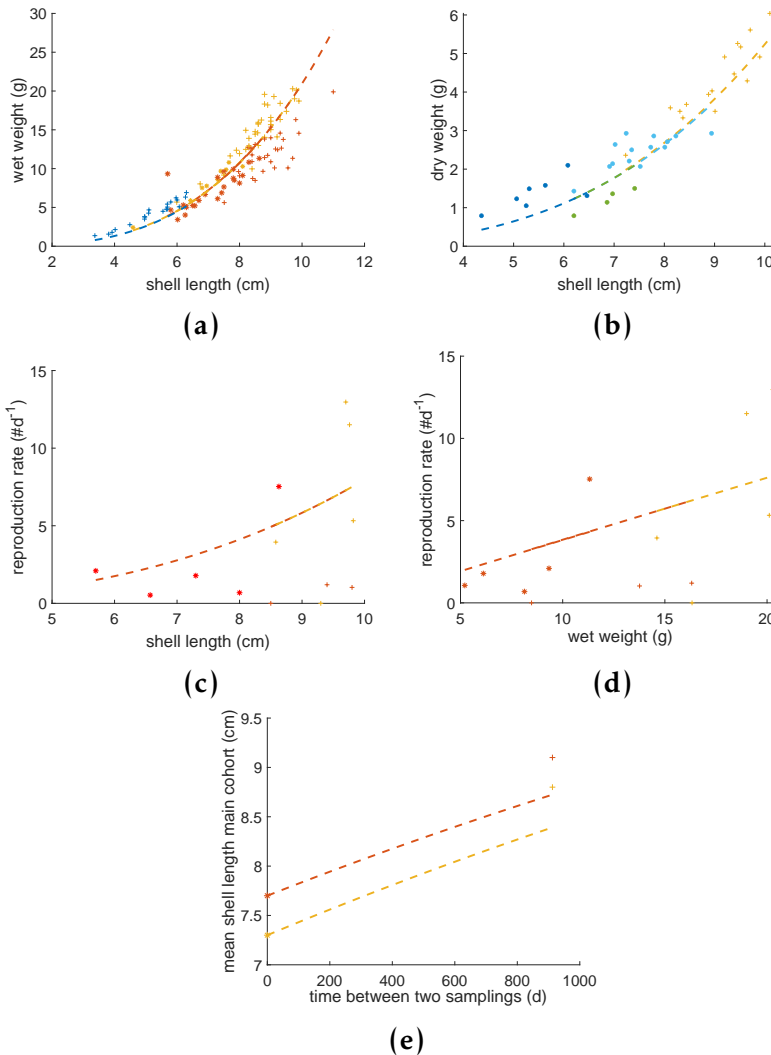


**Figure 2.10:** *Christineconcha regab* univariate data (Table 2.4) (markers) and abj-farming Dynamic Energy Budget model predictions (dashed lines). Relationships between shell length ( $L$ , cm) and (a) wet weight ( $W_w$ , g), (b) dry weight ( $W_d$ , g), and (c) reproduction rate ( $R$ , # number of oocytes produced per day); between (d) wet weight ( $W_w$ , g) and reproduction rate ( $R$ , # number of oocytes produced per day); and between (e) the mean shell length of the main cohorts ( $L$ , cm) and the time elapsed between two sampling events ( $t$ , days). Marker types correspond to sampling cruises in the Gulf of Guinea: \*, GUINECO (Aug2008); +, Wacs (Feb2011); ●, Congolobe (Dec2011–Jan2012). Colors of modeled curves correspond to sampling sites: Red, Regab Southwest (3154 m depth); Yellow, Regab Center (3156 m depth) (Khripounoff et al., 2015); Green, Lobes B (4712 m depth); Light Blue, Lobes A, (4751 m depth); Dark Blue, Lobes C (5070 m depth) (Khripounoff et al., 2017).

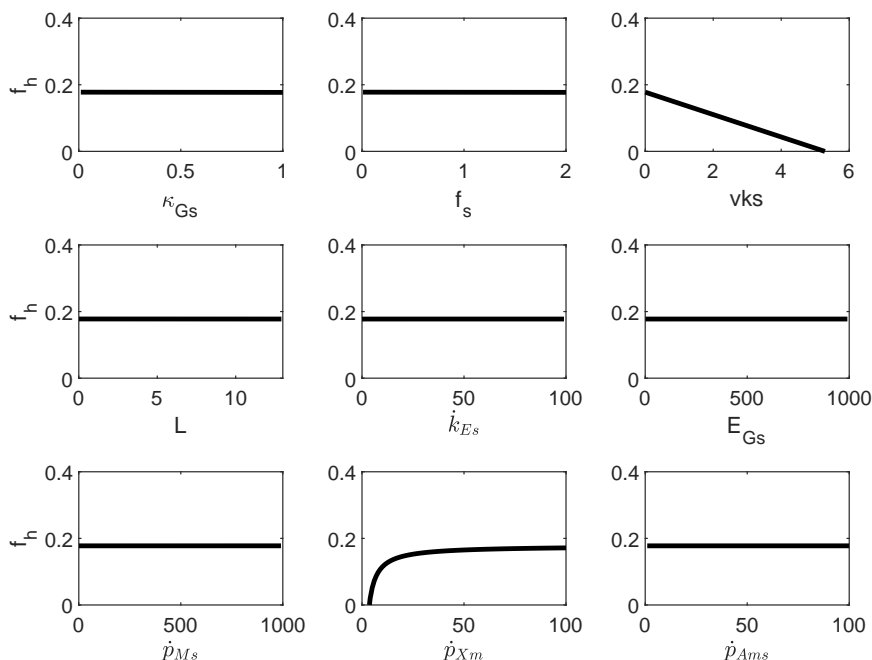


Figure 2.11: Parameter sensitivity to host functional response  $f_h$ .

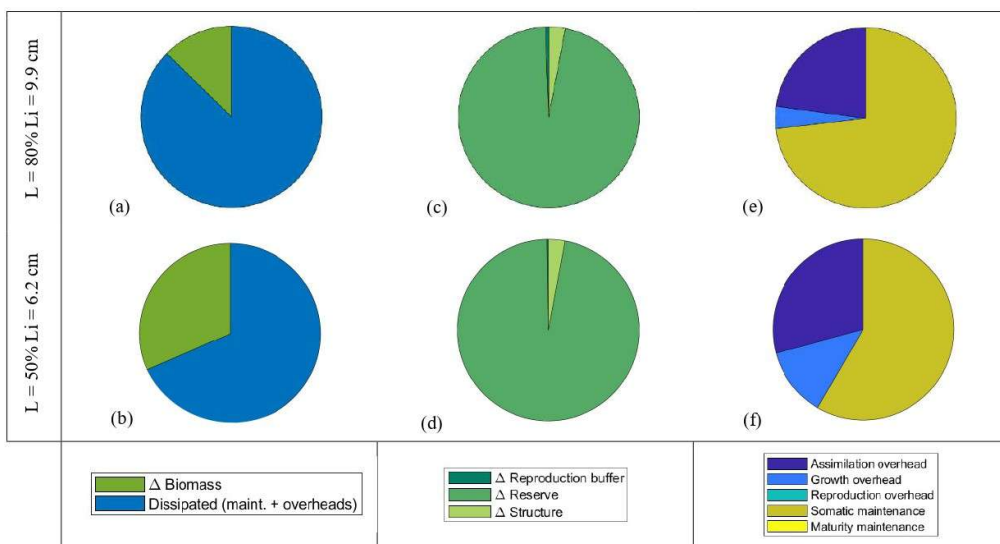
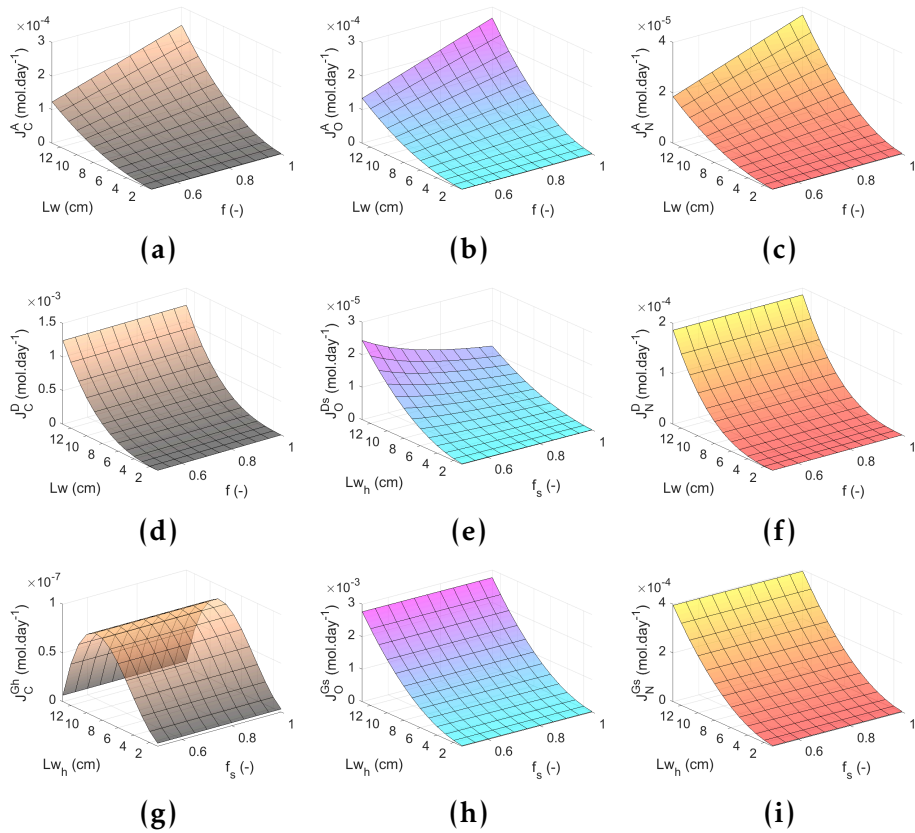
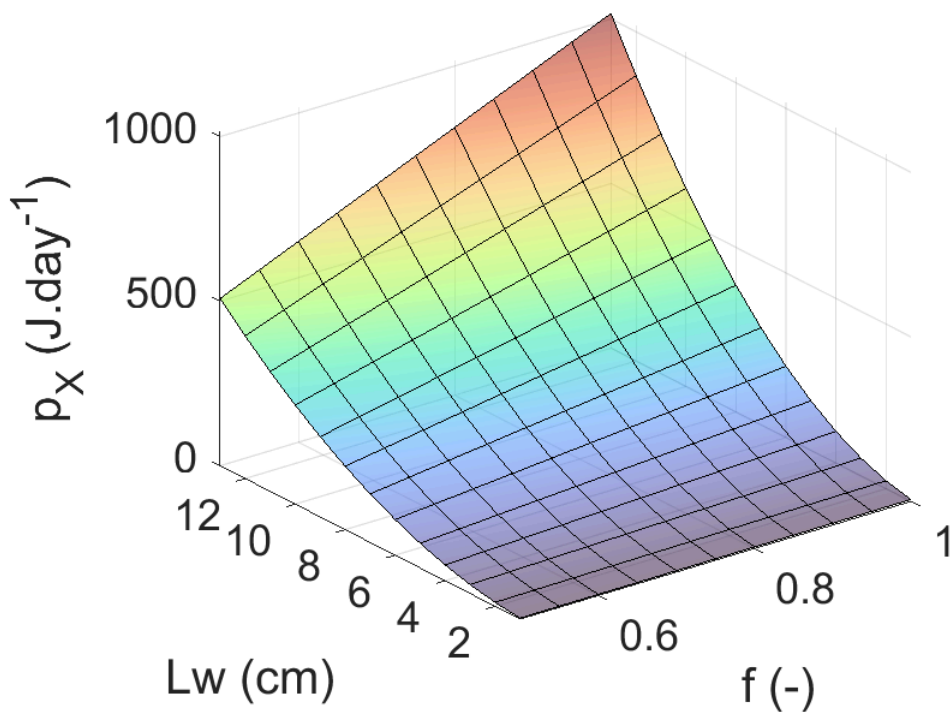


Figure 2.12: Pie charts of the energy distribution ( $Jd^{-1}$ ) within *Christineconcha regab* using abj Dynamic Energy Budget model (temperature  $T = 2.55^{\circ}C$ , functional response  $f = 0.8$ ).  $L$  stands for *C. regab* shell length.  $Li$  stands for the maximum shell length estimated by the model ( $Li = 12.3$  cm).  $\Delta$  stands for the variation in  $Jd^{-1}$ .



**Figure 2.13:** *C. regab* modeled chemical (Carbon, Oxygen and Nitrogen) fluxes with abj Dynamic Energy Budget model of Assimilation, Dissipation and Growth transformations in function of *C. regab* shell length ( $L$ ) and functional response ( $f$ ). Assimilation: 2.13a, 2.13b, 2.13c ; Dissipation: 2.13d, 2.13e, 2.13f ; Growth: 2.13g, 2.13h, 2.13i.



**Figure 2.14:** *Christineconcha regab* ingestion ( $p_X$ ) flux (mol d<sup>-1</sup>) in function of *C. regab* functional response ( $f$ ) and shell length ( $L_w$ ) modeled with *C. regab* abj DEB model ( $T = 2.55^\circ\text{C}$ ).

**Table 2.2:** abj Dynamic Energy Budget model state variables (reserve, structure, maturity and reproduction buffer) and fluxes ( $\dot{p}$ ).

Notation	Unit	Definition	Formula
$E$	J	reserve	$\frac{dE}{dt} = \dot{p}_A - \dot{p}_C$
$V$	cm <sup>3</sup>	structure	$\frac{dV}{dt} = \frac{\dot{p}_G}{[E_G]}$
$E_H$	J	maturity	$\frac{dE_H}{dt} = \dot{p}_R$ if $E_H < E_H^p$ $\frac{dE_H}{dt} = 0$ otherwise
$E_R$	J	reproduction buffer	$\frac{dE_R}{dt} = 0$ if $E_H < E_H^p$ $\frac{dE_R}{dt} = \kappa_R \dot{p}_R$ otherwise
$\dot{p}_X$	Jd <sup>-1</sup>	ingestion	$\{\dot{p}_{Xm}\} f V^{2/3} = \frac{\dot{p}_A}{\kappa_X}$ , when $E_H \geq E_H^b$
$\dot{p}_A$	Jd <sup>-1</sup>	assimilation	$\{\dot{p}_{Am}\} s_M f V^{2/3}$
$\dot{p}_P$	Jd <sup>-1</sup>	ingestion not assimilated	$(1 - \kappa_p) \dot{p}_X$
$\dot{p}_C$	Jd <sup>-1</sup>	reserve mobilization	$E \frac{\dot{v}_{sM} E_G V^{2/3} + \dot{p}_S}{\kappa E + [E_G] V}$
$\dot{p}_S$	Jd <sup>-1</sup>	somatic maintenance	$[\dot{p}_M] V$
$\dot{p}_G$	Jd <sup>-1</sup>	growth	$\kappa \dot{p}_C - \dot{p}_S$
$\dot{p}_J$	Jd <sup>-1</sup>	maturity maintenance	$\dot{k}_j E_H$
$\dot{p}_R$	Jd <sup>-1</sup>	maturation and reproduction	$(1 - \kappa) \dot{p}_C - \dot{p}_J$

**Table 2.3:** Acceleration coefficient ( $s_M$ ) to model metabolic acceleration in the abj model.  $E_H$ , host level of maturity (J);  $E_H^b$ , host level of maturity at birth (J);  $E_H^j$ , host level of maturity at metamorphosis (J);  $E_H^p$ , level of maturity at puberty (J);  $L_b$ , structural length at birth (cm);  $L_j$  structural length at metamorphosis (cm) (Kooijman, 2010).

Host maturity level ( $E_{Hh}$ )	$s_M$
$E_H < E_H^b$ (embryo)	$\frac{L_b}{L_b} = 1$
$E_H^b \leq E_H < E_H^j$ (early juvenile)	$\frac{L}{L_b}$
$E_H^j \leq E_H$ (late juvenile + adult)	$\frac{L_j}{L_b}$

**Table 2.4:** Zero- and univariate data of *Christineconcha regab* abj and abj-farming Dynamic Energy Budget models.

	Model	Data	Notation	Unit	References	
Zero-variate data	abj	length at hatching	$L_h$	cm	Jehenne, 2012	
		length at birth	$L_b$	cm	estimated*	
		length at metamorphosis	$L_j$	cm	Barry et al., 2007	
		length at puberty	$L_p$	cm	Jehenne, 2012	
		ultimate length	$L_i$	cm	von Cosel and Olu, 2009	
		life span	am	d	Marcon et al., 2014; Roy et al., 2007	
		max estimated reproduction rate	$R_i$	#d <sup>-1</sup>	This study	
		oxygen flux - dry weight	JO	mol d <sup>-1</sup>	Khripounoff et al., 2017	
		carbon flux - dry weight	JC	mol d <sup>-1</sup>	Khripounoff et al., 2017	
		nitrogen flux - dry weight	JN	mol d <sup>-1</sup>	Khripounoff et al., 2017	
	X	sulfur flux - gill dry weight	JS	mol d <sup>-1</sup>	Decker unpublished	
		mean gill volume occupation by bacteria	vbg	-	Decker unpublished	
		ratio biomass host / biomass symbionts	ratioHSb	-	Decker unpublished	
		$SO_4/H_2S$	SO4ovH2S	mol mol <sup>-1</sup>	Sublette, 1987	
		$O_2/H_2S$	O2ovH2S	mol mol <sup>-1</sup>	Sublette, 1987	
		$NH_4/H_2S$	NH4ovH2S	mol mol <sup>-1</sup>	Sublette, 1987	
biomass/ $H_2S$	BiomovH2S	g mol <sup>-1</sup>	Sublette, 1987			
		$HS^-$ /biomass	YSBs	mol C-mol <sup>-1</sup>	Heijnen and Dijken, 1992	
Univariate data	abj	abj-farming	dry weight - shell length	Wd-L	g - cm	Khripounoff et al., 2017
			wet weight - shell length	Ww-L	g - cm	Jehenne, 2012
			reproduction rate - shell length	R-L	#d <sup>-1</sup> - cm	This study
			reproduction rate - wet weight	R-Ww	#d <sup>-1</sup> - g	This study
			time between samplings - mean individual shell length	t-L	cm - d	Decker, 2011; Guillon et al., 2017

**Table 2.5:** Functional responses in *Christineconcha regab* abj and abj-farming dynamic energy budget (DEB) models related to the studied sites and data. Data in *italics* are related to *C. regab* sulfur-oxidizing symbionts and were used only in the abj-farming model.  $f$ , *C. regab* functional response in the abj model;  $f_s$ , symbiont functional response in the abj-farming model.

		Cruises			
$f$	$f_s$	Site	Guineco	WACS	Congolobe
abj	abj-farming		(Aug2008)	(Feb2011)	(Dec2011– Jan2012)
$f_C$	$f_{Cs}$	Regab Center	L-Ww, t-L	L-Ww, L-R, Ww-R, L-Wd, t-L, <i>vbg</i> , <i>ratioHSb</i>	JO-Wd, JC-Wd, JN-Wd
$f_{SWs}$	$f_{SWs}$	Regab Southwest	L-Ww, L-R, Ww-R, t-L	L-Ww, L-R, Ww-R, t-L, <i>vbg</i> , <i>ratioHSb</i>	-
$f_{LA}$	$f_{LAS}$	Lobe A	-	L-Wd	-
$f_{LB}$	$f_{LBS}$	Lobe B	-	L-Wd	-
$f_{LC}$	$f_{LCS}$	Lobe C	L-Ww, L-Wd	<i>vbg</i> , <i>ratioHSb</i>	JO-Wd, JC-Wd, JN-Wd, L-Wd
	$f_{Ss}$	on-board experiment from different sites, extreme observed values	-	<i>JS-Wdg</i>	-
$f_i$	$f_{si}$		$L_h, L_b, L_j, L_p, L_i, am, R_i$		

**Table 2.6:** abj Dynamic Energy Budget model estimated parameters

Notation	Unit	Definition
$\{\dot{p}_{Am}\}$	$\text{Jd}^{-1}\text{cm}^{-2}$	maximum assimilation flux
$\{\dot{F}_m\}$	$\text{cm}^2\text{d}^{-1}\text{m}^{-2}$	maximum surface area specific searching rate
$\kappa_X$	-	digestion efficiency of food to reserve
$\kappa_P$	-	faecation efficiency of food to faeces
$\dot{v}$	$\text{cm d}^{-1}$	energy conductance
$\kappa$	-	allocation fraction to soma
$\kappa_R$	-	reproduction efficiency
$[\dot{p}_M]$	$\text{Jd}^{-1}\text{cm}^3$	volume-specific somatic maintenance cost
$\dot{k}_j$	$\text{cm d}^{-1}$	maturity maintenance rate coefficient
$[E_G]$	$\text{Jcm}^{-3}$	specific cost for structure
$E_H^h$	J	maturity at hatching
$E_H^b$	J	maturity at birth
$E_H^j$	J	maturity at metamorphosis
$E_H^p$	J	maturity at puberty
$\dot{h}_a$	$\text{cm d}^{-2}$	Weibull aging acceleration
$s_G$	-	Gonbertz stress coefficient
$\delta_M$	-	shape coefficient
$\delta_{Me}$	-	shape coefficient of larva

## 2.8 Additional work: in research of *C.regab* larval size(s)

### 2.8.1 Preliminary observation

Bivalve larval sizes at birth and metamorphosis are data needed to calibrate an abj DEB model. On a bivalve shell, the sizes of the prodissoconch 1 (P1), the shell when the larva feed on its yolk reserve, and prodissoconch 2 (p2) for planktotrophic larva might be observed. For *C. regab*, at least the prodissoconch 1 was expected, as *C. regab* larva are supposed to be lecithotroph because of the large size of its oocytes (about 200  $\mu\text{m}$ ) (Decker, 2011). If a P2 is visible on the shell, it would mean that *C. regab* larva is a facultative planktotroph. With first binocular observation, the delimitation of P1 and (maybe) P2 was not obvious and the shells were eroded. Nevertheless some shell structures were visible. Other techniques to observe the shells were tested afterward.

**Table 2.7:** Zerovariate data (Table 2.4) predictions by *Christineconcha regab* abj and abj-farming Dynamic Energy Budget models. Prd: model prediction ; RE: relative error. (See Table. 2.4 for data description).

Notation	Description	Unit	Data	abj		abj-farming	
				Prd	RE	Prd	RE
Lh	length at hatching	cm	0.0388	0.0281	0.277	0.0388	<0.001
Lb	length at birth	cm	0.1	0.3286	2.286	0.1001	<0.001
Lj	length at metamorphosis	cm	0.2	0.1718	0.141	0.1991	0.005
Lp	length at puberty	cm	3.43	3.072	0.104	3.423	0.002
Li	ultimate length	cm	12.26	12.35	0.007	13.15	0.073
am	life span	d	3650	4173	0.1433	3643	0.002
Ri	max estimated reproduction rate	#d <sup>-1</sup>	12.97	13.86	0.069	17.72	0.366
JO_C	oxygen flux ; Regab Center	mol d <sup>-1</sup>	0.001662	0.0006	0.610	0.0012	0.284
JO_LC	oxygen flux ; Lobe C	mol d <sup>-1</sup>	0.0005522	0.0006	0.087	0.0007	0.254
JC_C	carbon flux ; Regab Center	mol d <sup>-1</sup>	0.001672	0.0006	0.644	0.0012	0.267
JC_LC	carbon flux ; Lobe C	mol d <sup>-1</sup>	0.0007145	0.0006	0.228	0.0008	0.095
JN_C	nitrogen flux ; Regab Center	mol d <sup>-1</sup>	8.978e-05	7e-05	0.156	7e-05	0.189
JN_LC	nitrogen flux ; Lobe C	mol d <sup>-1</sup>	3.9e-05	4e-05	0.084	3e-05	0.182
JS_LC	sulfur flux ; Lobe C	mol d <sup>-1</sup>	5.69e-05			8e-05	0.516
JS_C	sulfur flux ; Regab Center	mol d <sup>-1</sup>	5.56e-05			0.0001	1.105
JS_SW	sulfur flux ; Regab Southwest	mol d <sup>-1</sup>	7.48e-05			0.0001	0.575
SO4ovH2S	yield SO <sub>4</sub> /H <sub>2</sub> S	mol mol <sup>-1</sup>	0.99			1	0.010
O2ovH2S	yield O <sub>2</sub> /H <sub>2</sub> S	mol mol <sup>-1</sup>	1.81			1.208	0.333
NH4ovH2S	yield NH <sub>4</sub> /H <sub>2</sub> S	mol mol <sup>-1</sup>	0.1			1.808	17.08
BiomovH2S	yield biomass/H <sub>2</sub> S	g mol <sup>-1</sup>	4.5			17.03	2.784
YSBs	yield HS <sup>-</sup> /biomass	mol C-mol <sup>-1</sup>	3.33			0.6768	0.797
Vbg_LC	mean gill volume occupation by bacteria; Lobe C	-	0.575			0.5744	0.001
Vbg_C	mean gill volume occupation by bacteria; Regab center	-	0.522			0.5194	0.005
Vbg_SW	mean gill volume occupation by bacteria; Regab south-west	-	0.548			0.5515	0.006
ratioH_Sb_LC	ratio biomasses host / symbionts; Lobe C	-	8.16			8.150	0.001
ratioH_Sb_C	ratio biomasses host / symbionts; Regab center	-	8.4			8.345	0.007
ratioH_Sb_SW	ratio biomasses host / symbionts; Regab south-west	-	7.92			7.937	0.002

**Table 2.8:** Estimated parameters of *Christineconcha regab* with abj model (MRE = 0.094; SMAE = 0.053; SMSE = 0.029) and abj-farming model (MRE = 0.195; SMAE = 0.088; SMSE = 0.049) at T = 20°C. Estim., estimated parameter; H., host; Sb., symbionts.

abj				abj-farming			
Notation	Description	Unit	Estim.	Notation	Description	Unit	Estim.
$z$	zoom factor	-	1.619	$z_h$	H. zoom factor	-	4.786
$\{F_m\}$	maximum surface area specific searching rate	$d^{-1} cm^2$	6.5	$\{F_{mh}\}$	H. maximum surface area specific searching rate	$d^{-1} cm^2$	6.5
$\kappa_X$	digestion efficiency of food to reserve	-	0.8	$\kappa_{Xh}$	H. digestion efficiency of food to reserve	-	0.8
$\kappa_P$	faecation efficiency of food to faeces	-	0.1	$\kappa_{Ph}$	H. faecation efficiency of food to faeces	-	0.1
$\dot{v}$	energy conductance	$cm d^{-1}$	0.7762	$\dot{v}_h$	H. energy conductance	$cm d^{-1}$	0.003505
$\kappa$	allocation fraction to soma	-	0.999	$\kappa_h$	H. allocation fraction to soma	-	0.9051
$\kappa_R$	reproduction efficiency	-	0.95	$\kappa_{Rh}$	H. reproduction efficiency	-	0.95
$[P_M]$	volume-specific somatic maintenance cost	$J d^{-1} cm^3$	95.59	$[P_{Mh}]$	H. volume-specific somatic maintenance cost	$J d^{-1} cm^3$	568.3
$k_j$	maturity maintenance rate coefficient	$d^{-1}$	0.002	$k_{jh}$	H. maturity maintenance rate coefficient	$d^{-1}$	0.002
$[E_G]$	specific cost for structure	$J cm^{-3}$	6687	$[E_{Gh}]$	H. specific cost for structure	$J cm^{-3}$	6475
$E_H$	maturity at hatching	J	2.439e-08	$E_{Hh}^h$	H. maturity at hatching	J	9.642e-05
$E_H^b$	maturity at birth	J	3.918e-05	$E_{Hh}^b$	H. maturity at birth	J	0.00187
$E_H^j$	maturity at metamorphosis	J	0.0006293	$E_{Hh}^j$	H. maturity at metamorphosis	J	0.001877
$E_H^p$	maturity at puberty	J	4.279	$E_{Hh}^p$	H. maturity at puberty	J	45.6
$\dot{h}_a$	Weibull aging acceleration	$d^{-2}$	2.157e-08	$\dot{h}_{ah}$	H. Weibull aging acceleration	$d^{-2}$	2.134e-05
$s_G$	Gonbertz stress coefficient	-	0.0001	$s_{Gh}$	H. Gonbertz stress coefficient	-	0.0001
$\delta_M$	shape coefficient	-	0.2637	$\delta_{Mh}$	H. shape coefficient	-	0.06551
$\phi_{Me}$	shape coefficient of larva	-	0.05482	$\delta_{Meh}$	H. shape coefficient of larva	-	0.1303
				$vks$	host half saturation coefficient	-	0.005
				$[P_{Ams}]$	Sb. maximum assimilation rate	$J d^{-1} cm^{-2}$	5665
				$\{F_{ms}\}$	Sb. maximum specific searching rate	$d^{-1} cm^2$	6.5
				$\kappa_{Xs}$	Sb. digestion efficiency of food to reserve	-	0.8
				$\kappa_{Ps}$	sb. faecation efficiency of food to faeces	-	0.1
				$k_{Es}$	Sb. specific-energy conductance	$d^{-1}$	4513
				$[P_{Ms}]$	Sb. volume-specific somatic maintenance cost	$J d^{-1} cm^3$	18.12
				$[E_{Gs}]$	Sb. specific cost for structure	$J cm^{-3}$	2.143e+04
				$\delta_{MVs}$		-	1.001
				$Y_{SE}^{As}$	Sb. H2S assimilation yield per C-mol of reserve	$H_2S mol C-mol^{-1}$	0.3756
				$Y_{HE}^{As}$	Sb. H2O assimilation yield per C-mol of reserve	$H_2O mol C-mol^{-1}$	1.718e-11

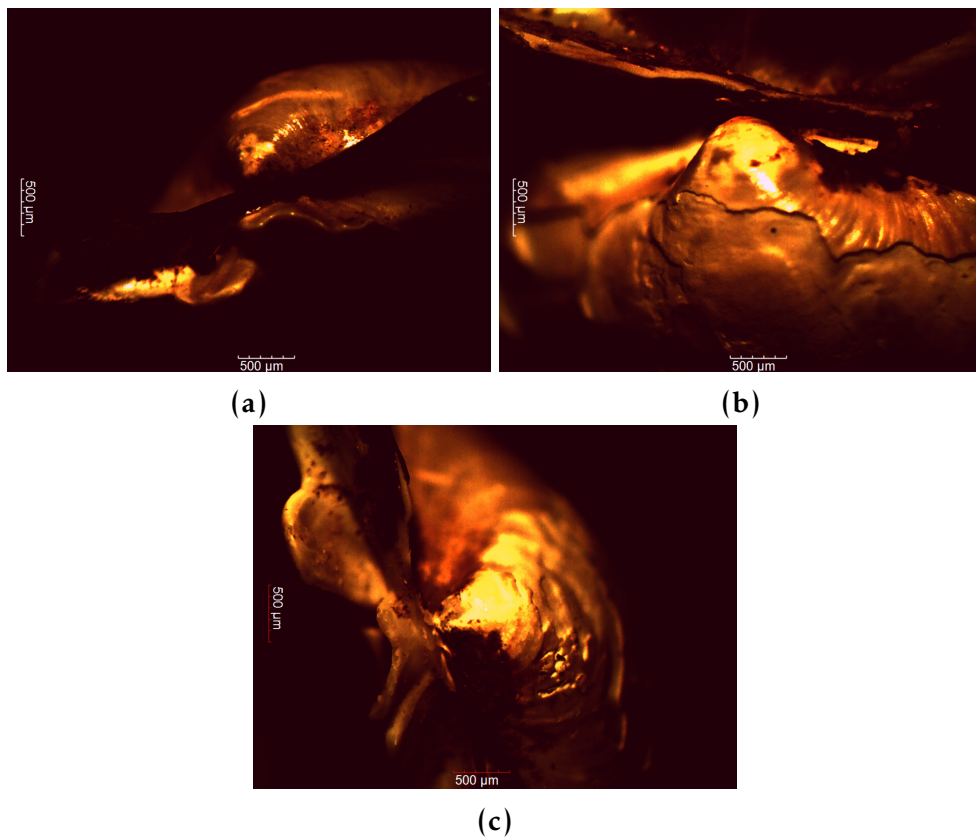


**Figure 2.15:** Images of *Christineconcha regab* shell with binocular magnifier. (a) CrG1BB10 and (b) individuals from the Guineco cruise (august 2008) in the Gulf of Guinea; (c) CrW2CBB1 individual from the WACS cruise in the Gulf of Guinea.

### 2.8.2 Scanning Electron Microscopy (SEM)

SEM was used to look at the surface of the shell, and in particular the hinge part, to try to observe the prodissoconch size(s) as it has been possible for other bivalve species in previous studies (Fig. 2.17) (Gaudron et al., 2012; Gaudron et al., 2016). Five *C. regab* shells were selected for SEM (specimens CRG21BB1, CRG31BB1 and CRG24BB8 from Guineco cruise in the Gulf of Guinea (August 2008); specimens CRW5BB2 and CRW20BB1 from WACS cruise (February 2011). As *C. regab* is a large species, apex part of shell was isolated from the rest of the shell by cutting around with a small hand-held circular saw, slowly to avoid the shell to break. Then the pieces were fixed on SEM stubs, the exterior of the shell against the stub. The surface of apex shell pieces was coated with gold-palladium with a sputter-coater to make it conductive. Argon was used as sputter gas. Samples preparation and micrographs were realized with the help of L. Courcot (UMR8187 LOG, Wimereux). Unfortunately, *C. regab* shells were too old (from WACS cruises in 2011 and Guineco cruises in 2008) and shell surfaces were too damaged to see P1 and maybe P2 delimitations (Fig. 2.18).

### 2.8.3 Sclerochronology

As SEM did not give good results to estimate the size of the larval shell because of the damaged shell surface, sclerochronology used to try to estimate the size of the larval shell looking at inside shell structures. Looking at inside shell increments has been done for cockles (Bellamy et al., 2010) (Fig. 2.19). Preparation of samples and images were done by R. Elleboode, Operational coordinator of the sclerochronology centre, and A. Dussuel at Ifremer, Boulogne-sur-Mer. A valve of two different *C. regab* specimens were fixed in resin to cut them more easily and to avoid breaking them while cutting (Fig. 2.20 a and b). A slice of each shells were cut with a precision saw keeping the hinge, our centre of interest, inside the slice. The slices of resin were then mounted each on a glass slide with a temperature-sensitive glue which is easy to unglue with heat (Fig. 2.20 d). The glass slides were fixed by capillarity on a

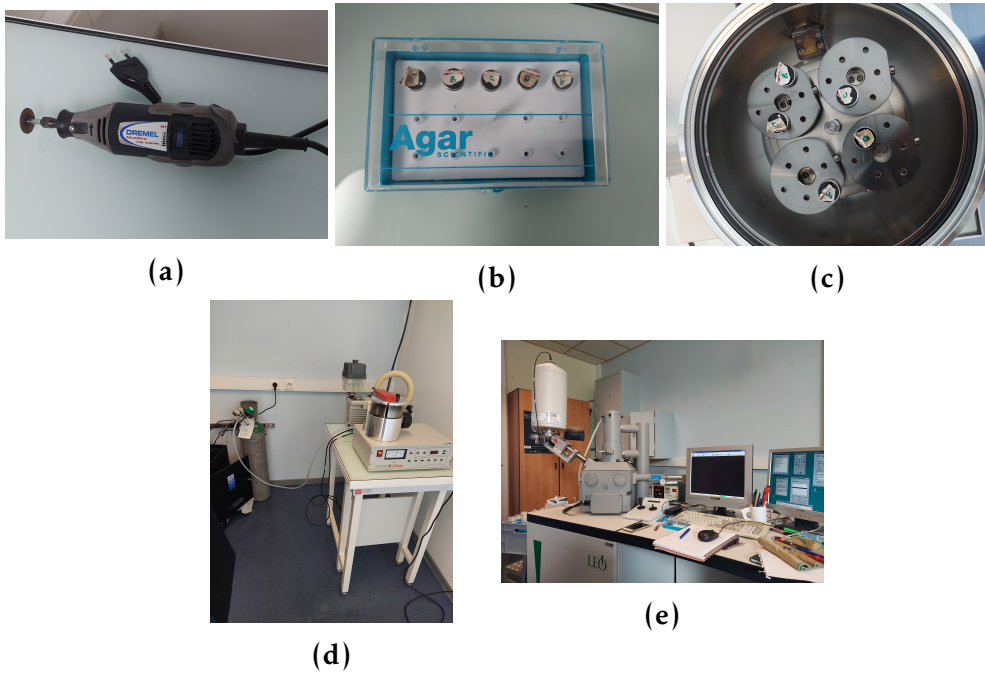


**Figure 2.16:** *Christineconcha regab* shell preparation for scanning electron microscopy. (a) small circular-saw used to cut *C. regab* shells; (b) pieces of *C. regab* shells ready for coating; (c) *C. regab* apex shell parts in the sputter-coater; (d) argon bottle on the left and sputter-coater on the right; (e) scanning electron microscope (UMR8187 LOG, Wimereux).

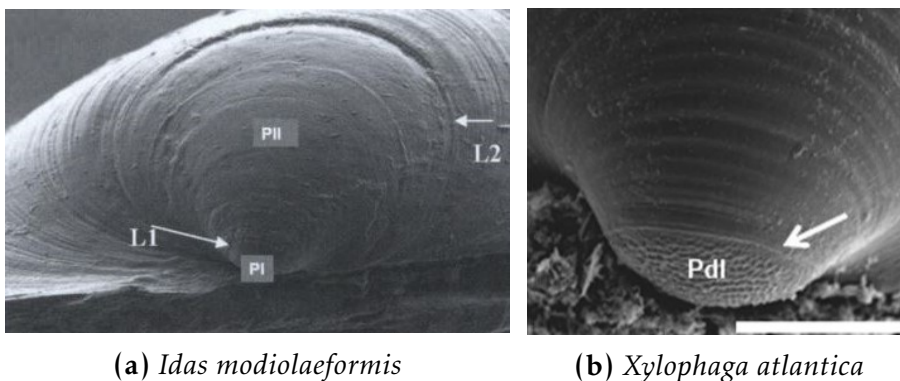


**Figure 2.17:** Scanning Electron Microscopy of the deep sea bivalves species *Idas modiolaeformis* (Gaudron et al., 2012) and *Xylophaga atlantica* (Gaudron et al., 2016). PI or PdI, Prodissoconch 1; PII, prodissoconch 2.

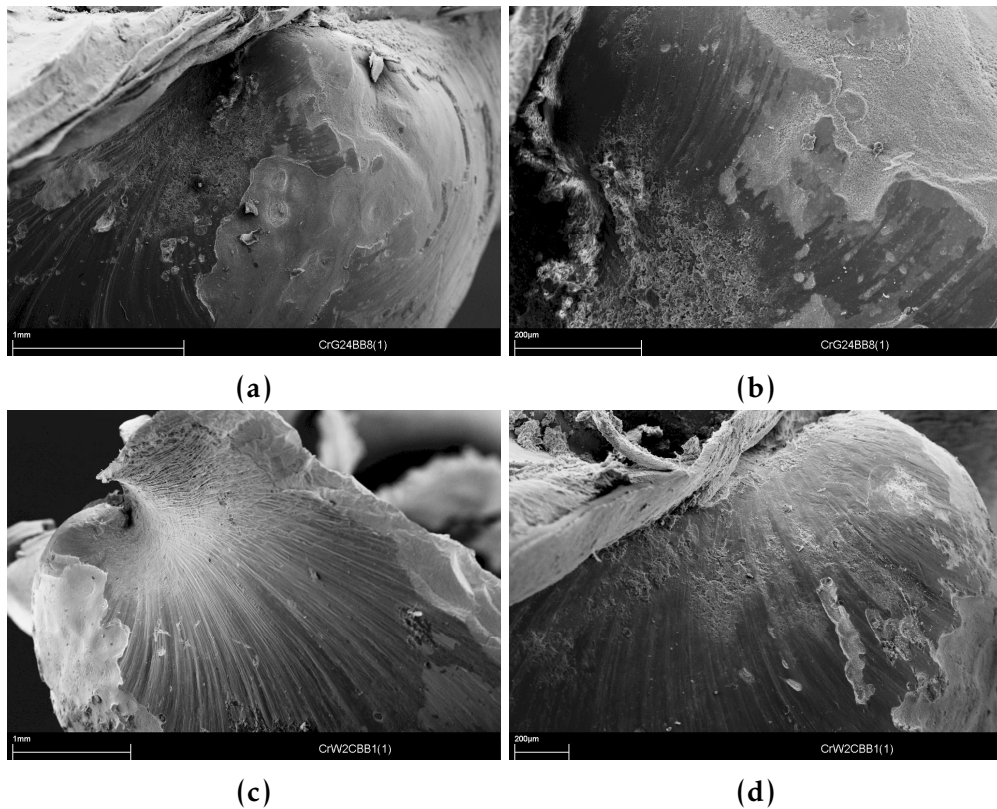


**Figure 2.18:** Scanning Electron Micrographs on *Christineconcha regab* shells. (a, b) CRG24BB8 shell from the Guineco cruise in the Gulf Guinea (August 2008); (c, d) CRG24BB8 shell from the WACS cruise in the Gulf of Guinea (February 2011). Images obtained with the help of L. Courcot (UMR8187 LOG, Wimereux).

block and the slice were grind and polished to obtain a thinner slice (Fig. 2.20e). Images of shell slices (Fig. 2.21) are hard to interpret as the apex of the *C. regab* shells seem eroded or damaged. Nevertheless, structures can be observed and it should be a good alternative to SEM to determined  $L_b$  for deep sea bivalve species and study growth with the observation of growth increments.

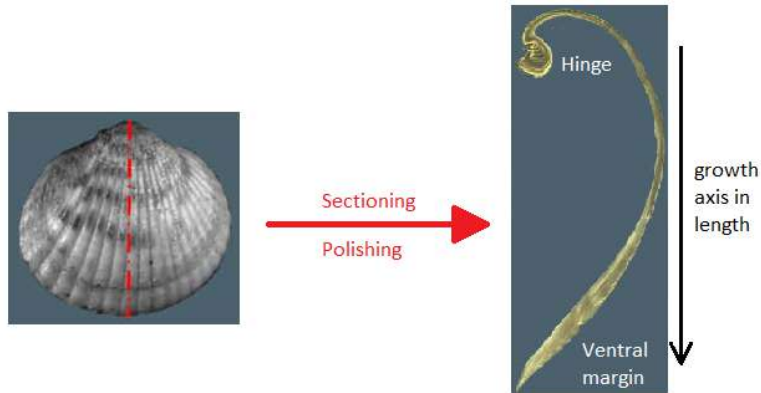


**Figure 2.19:** Slicing scheme of a cockle shell (Figure modified from Bellamy et al., 2010).

#### 2.8.4 Binocular observation on well preserved shell

Well preserved *C. regab* shells from Lobes of the gulf of Guinea could be observed at Roscoff biological station. A change in shell surface texture from rather smooth to less smooth was observed (Fig. 2.22). This is likely marking the end of the prodissoconch 1 (P1) or prodissoconch (P2). This larval shell was estimated around 420  $\mu\text{m}$  from mean measurement on three shells. Further observations (as SEM and sclerochronology done previously) need to be done on these shells to make sure which prodissoconch is present.

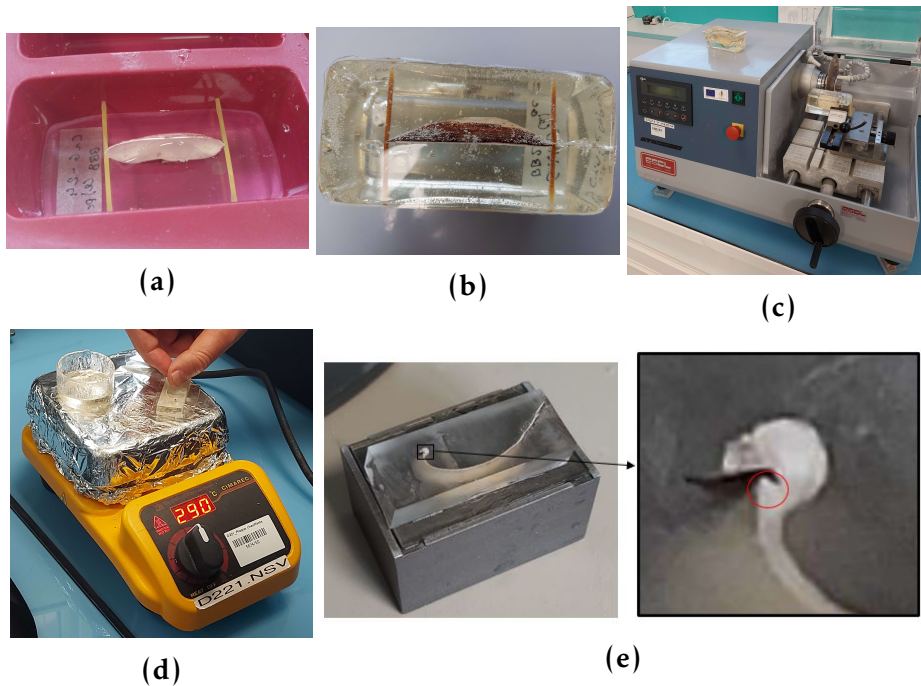


**Figure 2.20:** *Christineconcha regab* shell preparation for sclerochronology. (a) *C. regab* shell being fixed in resin. Two spaghetti were used to maintain the shell straight and resin was firstly poured at mid-height of the mould. Then resin was poured again to fill the mould. (b) *C. regab* shell demoulded, fixed in resin. (c) Precision saw (Ifremer, Boulogne-sur-mer). (d) A slice of *C. regab* shell mounted on a glass slide with thermo-glue. (e) Glass slide was fixed by capillarity on a block to grind and polish the slice (left), a zoom at the shell apex (right), the red circle shows the area of interest. All the preparations were realized by R. Elleboode and A. Dussuel at Ifremer, Boulogne-sur-Mer.

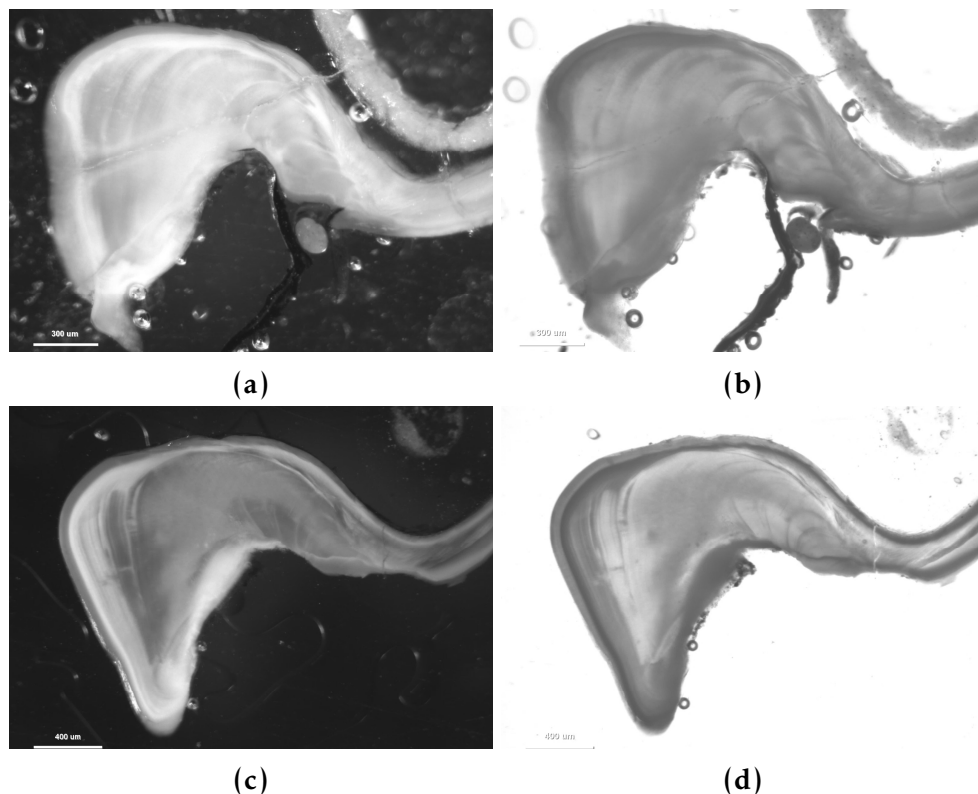


**Figure 2.21:** Images of *Christineconcha regab* shell slices. (a) and (b), shell of CRG24BB8 individual from Guineco Cruise in the Gulf of Guinea in August 2008; (c) and (d), shell of CRW5BB2 individual from WACS cruise in the Gulf of Guinea in February 2011. (a) and (c), reflected light; (b) and (d), transmitted light. Images by R. Elleboode and A. Dussuel, Ifremer, Boulogne-sur-mer.

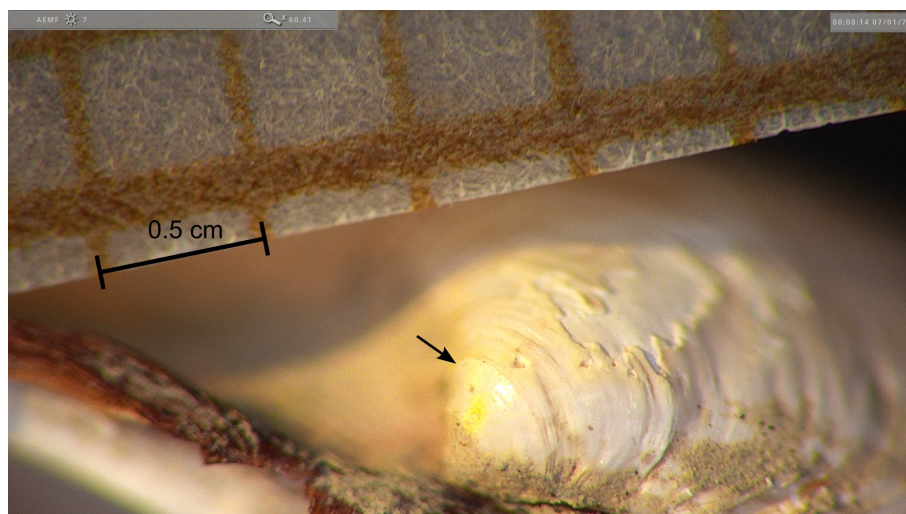


**Figure 2.22:** Binocular magnifier observation of a well preserved *C. regab* shell. Arrow, likely the end of prodissoconch 1 (P1).

## References

- Add-My-Pet Species List*. (2024). [https://www.bio.vu.nl/thb/deb/deblab/add\\_my\\_pet/species\\_list.html](https://www.bio.vu.nl/thb/deb/deblab/add_my_pet/species_list.html)
- Barry, J. P., Whaling, P. J., & Kochevar, R. K. (2007). Growth, production, and mortality of the chemosynthetic vesicomid bivalve, *Calypotogena kilmeri* from cold seeps off central California. *Marine Ecology*, 28(1), 169–182. <https://doi.org/10.1111/j.1439-0485.2007.00119.x>
- Bayer, F. M., Voss, G. L., & Robins, C. R. (1966). The R/V Pillsbury deep-sea biological expedition to the Gulf of Guinea, 1964-1965. *Studies in Tropical Oceanography*, (1). <https://www.vliz.be/en/imis?module=ref&refid=214965&printversion=1&dropIMISitle=1>
- Bellamy, E., Mahe, K., de Rafelis, M., & Lartaud, F. (2010). Growth of the common Cockle *Cerastoderma edule* : Validation of the periodicity of increment deposition by Calcein marker. <https://archimer.ifremer.fr/doc/00011/12268/>
- Bénard, A., Vavre, F., & Kremer, N. (2020). Stress & Symbiosis: Heads or Tails? *Frontiers in Ecology and Evolution*, 8. <https://www.frontiersin.org/articles/10.3389/fevo.2020.00167>
- Bertics, V. J., Treude, T., & Ziebis, W. (2007). Vesicomid Clams Alter Biogeochemical Processes at Pacific Methane Seeps. 2007, B43E–1649. <https://ui.adsabs.harvard.edu/abs/2007AGUFM.B43E1649B>  
ADS Bibcode: 2007AGUFM.B43E1649B
- Boetius, A. (2008). GUINECO (M76-3B) cruise, RV Meteor.
- Boetius, A., Ravensschlag, K., Schubert, C. J., Rickert, D., Widdel, F., Gieseke, A., Amann, R., Jørgensen, B. B., Witte, U., & Pfannkuche, O. (2000). A marine microbial consortium apparently mediating anaerobic oxidation of methane. *Nature*, 407(6804), 623–626. <https://doi.org/10.1038/35036572>
- Boetius, A., & Wenzhöfer, F. (2013). Seafloor oxygen consumption fuelled by methane from cold seeps. *Nature Geoscience*, 6(9), 725–734. <https://doi.org/10.1038/ngeo1926>

- Bridges, A., Howell, K., Amaro, T., Atkinson, L., Barnes, D., Bax, N., Bell, J., Bernardino, A., Beuck, L., Braga-Henriques, A., Brandt, A., Bravo, M., Brix, S., Butt, S., Carranza, A., Doti, B., Elegbede, I., Esquete, P., Freiwald, A., & Wienberg, C. (2023, August 11). Review of the Central and South Atlantic Shelf and Deep-Sea Benthos: Science, Policy, and Management. <https://doi.org/10.1201/9781003363873-5>
- Cardini, U., Bartoli, M., Lücker, S., Mooshammer, M., Polzin, J., Lee, R. W., Micić, V., Hofmann, T., Weber, M., & Petersen, J. M. (2019). Chemosymbiotic bivalves contribute to the nitrogen budget of seagrass ecosystems. *The ISME Journal*, 13(12), 3131–3134. <https://doi.org/10.1038/s41396-019-0486-9>
- Cary, S. C., & Giovannoni, S. J. (1993). Transovarial inheritance of endosymbiotic bacteria in clams inhabiting deep-sea hydrothermal vents and cold seeps. *Proceedings of the National Academy of Sciences*, 90(12), 5695–5699. <https://doi.org/10.1073/pnas.90.12.5695>
- Charlou, J. L., Donval, J. P., Fouquet, Y., Ondreas, H., Knoery, J., Cochonat, P., Levaché, D., Poirier, Y., Jean-Baptiste, P., Fourré, E., & Chazallon, B. (2004). Physical and chemical characterization of gas hydrates and associated methane plumes in the Congo–Angola Basin. *Chemical Geology*, 205(3), 405–425. <https://doi.org/10.1016/j.chemgeo.2003.12.033>
- Childress, J. J., & Girguis, P. R. (2011). The metabolic demands of endosymbiotic chemoautotrophic metabolism on host physiological capacities. *Journal of Experimental Biology*, 214(2), 312–325. <https://doi.org/10.1242/jeb.049023>
- Cruaud, P., Decker, C., Olu, K., Arnaud-Haond, S., Papot, C., Baut, J. L., Vigneron, A., Khripounoff, A., Gayet, N., Cathalot, C., Caprais, J.-C., Pignet, P., Godfroy, A., & Cambon-Bonavita, M.-A. (2019). Ecophysiological differences between vesicomid species and metabolic capabilities of their symbionts influence distribution patterns of the deep-sea clams. *Marine Ecology*, 40(3), e12541. <https://doi.org/10.1111/maec.12541>

- Cunning, R., Muller, E. B., Gates, R. D., & Nisbet, R. M. (2017). A dynamic bioenergetic model for coral-Symbiodinium symbioses and coral bleaching as an alternate stable state. *Journal of Theoretical Biology*, 431, 49–62. <https://doi.org/10.1016/j.jtbi.2017.08.003>
- Decker, C. (2011, January 1). *Diversité, écologie et adaptation des bivalves Vesicomidae associés aux environnements réducteurs profonds des marges continentales* (These de doctorat). Brest. <https://www.theses.fr/2011BRES2054>
- Decker, C., Caprais, J.-C., Khripounoff, A., & Olu, K. (2012). First respiration estimates of cold-seep vesicomid bivalves from in situ total oxygen uptake measurements. *Comptes Rendus Biologies*, 335(4), 261–270. <https://doi.org/10.1016/j.crv.2012.03.002>
- Decker, C., Olu, K., Arnaud-Haond, S., & Duperron, S. (2013). Physical Proximity May Promote Lateral Acquisition of Bacterial Symbionts in Vesicomid Clams. *PLOS ONE*, 8(7), e64830. <https://doi.org/10.1371/journal.pone.0064830>
- de Oliveira, A. L., Mitchell, J., Girguis, P., & Bright, M. (2022). Novel Insights on Obligate Symbiont Lifestyle and Adaptation to Chemosynthetic Environment as Revealed by the Giant Tubeworm Genome. *Molecular Biology and Evolution*, 39(1), msab347. <https://doi.org/10.1093/molbev/msab347>
- Dubilier, N., Bergin, C., & Lott, C. (2008). Dubilier N, Bergin C, Lott C.. Symbiotic diversity in marine animals: The art of harnessing chemosynthesis. *Nat Rev Micro* 6: 725-740. *Nature reviews. Microbiology*, 6(10), 725–40. <https://doi.org/10.1038/nrmicro1992>
- Duperron, S., Quiles, A., Szafranski, K., Léger, N., & Shillito, B. (2016). Estimating symbiont abundances and gill surface areas in specimens of the hydrothermal vent mussel *Bathymodiolus puteoserpentis* maintained in pressure vessels. *Frontiers in Marine Science*, 3. <https://doi.org/10.3389/fmars.2016.00016>
- Fiala-Medioni, A., & Le Pennec, M. (1987). Trophic Structural Adaptations in Relation to the Bacterial Association of Bivalve Molluscs from Hydrothermal Vents and Subduction Zones. <https://>

DalSpace.library.dal.ca//handle/10222/76959

Accepted: 2020-01-07T14:00:19Z

- Gaudron, S. M., Demoyencourt, E., & Duperron, S. (2012). Reproductive Traits of the Cold-Seep Symbiotic Mussel *Idas modiolaeformis*: Gametogenesis and Larval Biology. *The Biological Bulletin*, 222(1), 6–16. <https://doi.org/10.1086/BBLv222n1p6>
- Gaudron, S. M., Haga, T., Wang, H., Laming, S., & Duperron, S. (2016). Plasticity in reproduction and nutrition in wood-boring bivalves (*Xylophaga atlantica*) from the Mid-Atlantic Ridge. *Marine Biology*, 163(10), 213. <https://doi.org/10.1007/s00227-016-2988-6>
- Gaudron, S. M., Lefebvre, S., & Marques, G. M. (2021). Inferring functional traits in a deep-sea wood-boring bivalve using dynamic energy budget theory. *Scientific Reports*, 11(1), 22720. <https://doi.org/10.1038/s41598-021-02243-w>
- Goffredi, S. K., & Barry, J. P. (2002a). Energy acquisition and allocation in vesicomid symbioses. *Cahiers de Biologie Marine*, (3-4). <https://doi.org/10.21411/CBM.A.5ADE9CC5>
- Goffredi, S. K., & Barry, J. P. (2002b). Species-specific variation in sulfide physiology between closely related Vesicomid clams. *Marine Ecology Progress Series*, 225, 227–238. <https://doi.org/10.3354/meps225227>
- Guillon, E., Menot, L., Decker, C., Krylova, E., & Olu, K. (2017). The vesicomid bivalve habitat at cold seeps supports heterogeneous and dynamic macrofaunal assemblages. *Deep Sea Research Part I: Oceanographic Research Papers*, 120, 1–13. <https://doi.org/10.1016/j.dsr.2016.12.008>
- Halary, S., Riou, V., Gaill, F., Boudier, T., & Duperron, S. (2008). 3D FISH for the quantification of methane- and sulphur-oxidizing endosymbionts in bacteriocytes of the hydrothermal vent mussel *Bathymodiolus azoricus*. *The ISME Journal*, 2(3), 284–292. <https://doi.org/10.1038/ismej.2008.3>
- Heijnen, J. J., & Dijken, J. P. V. (1992). In search of a thermodynamic description of biomass yields for the chemotrophic growth of mi-

- croorganisms. *Biotechnology and Bioengineering*, 39(8), 833–858. <https://doi.org/10.1002/bit.260390806>
- Husson, B., Sarrazin, J., van Oevelen, D., Sarradin, P.-M., Soetaert, K., & Menesguen, A. (2018). Modelling the interactions of the hydrothermal mussel *Bathymodiolus azoricus* with vent fluid. *Ecological Modelling*, 377, 35–50. <https://doi.org/10.1016/j.ecolmodel.2018.03.007>
- Ikuta, T., Igawa, K., Tame, A., Kuroiwa, T., Kuroiwa, H., Aoki, Y., Takaki, Y., Nagai, Y., Ozawa, G., Yamamoto, M., Deguchi, R., Fujikura, K., Maruyama, T., & Yoshida, T. (2016). Surfing the vegetal pole in a small population: Extracellular vertical transmission of an 'intracellular' deep-sea clam symbiont. *Royal Society Open Science*, 3(5), 160130. <https://doi.org/10.1098/rsos.160130>
- Ip, J. C.-H., Xu, T., Sun, J., Li, R., Chen, C., Lan, Y., Han, Z., Zhang, H., Wei, J., Wang, H., Tao, J., Cai, Z., Qian, P.-Y., & Qiu, J.-W. (2020). Host–Endosymbiont Genome Integration in a Deep-Sea Chemosymbiotic Clam. *Molecular Biology and Evolution*. <https://doi.org/10.1093/molbev/msaa241>
- Jehenne, F. (2012). *La reproduction des bivalves Vesicomidae des suintements froids profonds du golfe de Guinée*. (Thèse de master). Université d'Aix-Marseille. Station Biologique de Roscoff.
- Johnson, S. B., Krylova, E. M., Audzijonyte, A., Sahling, H., & Vrijenhoek, R. C. (2017). Phylogeny and origins of chemosynthetic vesicomid clams. *Systematics and Biodiversity*, 15(4), 346–360. <https://doi.org/10.1080/14772000.2016.1252438>
- Kaare-Rasmussen, J. O., Moeller, H. V., & Pfab, F. (2023). Modeling food dependent symbiosis in *Exaiptasia pallida*. *Ecological Modelling*, 481, 110325. <https://doi.org/10.1016/j.ecolmodel.2023.110325>
- Khripounoff, A., Caprais, J. C., Decker, C., Essirard, M., Le Bruchec, J., Noel, P., & Olu, K. (2015). Variability in gas and solute fluxes through deep-sea chemosynthetic ecosystems inhabited by vesicomid bivalves in the Gulf of Guinea. *Deep Sea Research Part I: Oceanographic Research Papers*, 95, 122–130. <https://doi.org/10.1016/j.dsr.2014.10.013>

- Khripounoff, A., Caprais, J. C., Decker, C., Le Bruchec, J., Noel, P., & Husson, B. (2017). Respiration of bivalves from three different deep-sea areas: Cold seeps, hydrothermal vents and organic carbon-rich sediments. *Deep Sea Research Part II: Topical Studies in Oceanography*, 142, 233–243. <https://doi.org/10.1016/j.dsr2.2016.05.023>
- König, S., Le Guyader, H., & Gros, O. (2015). Thioautotrophic bacterial endosymbionts are degraded by enzymatic digestion during starvation: Case study of two lucinids *Codakia orbicularis* and *C. orbiculata*. *Microscopy Research and Technique*, 78(2), 173–179. <https://doi.org/10.1002/jemt.22458>
- Kooijman, S. A. L. M. (2010). *Dynamic Energy Budget Theory for Metabolic Organisation*. Cambridge University Press.
- Kooijman, S. A. L. M., Auger, P., Poggiale, J. C., & Kooi, B. W. (2003). Quantitative steps in symbiogenesis and the evolution of homeostasis. *Biological Reviews*, 78(3), 435–463. <https://doi.org/10.1017/S1464793102006127>
- Krylova, E. M., & Sahling, H. (2010). Vesicomidae (Bivalvia): Current Taxonomy and Distribution. *PLOS ONE*, 5(4), e9957. <https://doi.org/10.1371/journal.pone.0009957>
- Krylova, E. M., Sahling, H., & Janssen, R. (2010). Abyssogena: A new genus of the family Vesicomidae (Bivalvia) from deep-water vents and seeps. *Journal of Molluscan Studies*, 76(2), 107–132. <https://doi.org/10.1093/mollus/eyp052>
- Lan, Y., Sun, J., Chen, C., Sun, Y., Zhou, Y., Yang, Y., Zhang, W., Li, R., Zhou, K., Wong, W. C., Kwan, Y. H., Cheng, A., Bougouffa, S., Van Dover, C. L., Qiu, J.-W., & Qian, P.-Y. (2021). Hologenome analysis reveals dual symbiosis in the deep-sea hydrothermal vent snail *Gigantopelta aegis*. *Nature Communications*, 12(1), 1165. <https://doi.org/10.1038/s41467-021-21450-7>
- Lan, Y., Sun, J., Zhang, W., Xu, T., Zhang, Y., Chen, C., Feng, D., Wang, H., Tao, J., Qiu, J.-W., & Qian, P.-Y. (2019). Host–Symbiont Interactions in Deep-Sea Chemosymbiotic Vesicomid Clams: Insights From Transcriptome Sequencing. *Frontiers in Marine Science*, 6, 680. <https://doi.org/10.3389/fmars.2019.00680>

- Li, Y., Tassia, M. G., Waits, D. S., Bogantes, V. E., David, K. T., & Halanych, K. M. (2019). Genomic adaptations to chemosymbiosis in the deep-sea seep-dwelling tubeworm *Lamellibrachia luymesii*. *BMC Biology*, *17*(1), 91. <https://doi.org/10.1186/s12915-019-0713-x>
- Lika, K., Kearney, M. R., & Kooijman, S. A. L. M. (2011). The “covariation method” for estimating the parameters of the standard Dynamic Energy Budget model II: Properties and preliminary patterns. *Journal of Sea Research*, *66*(4), 278–288. <https://doi.org/10.1016/j.seares.2011.09.004>
- Marcon, Y., Sahling, H., Allais, A.-G., Bohrmann, G., & Olu, K. (2014). Distribution and temporal variation of mega-fauna at the Regab pockmark (Northern Congo Fan), based on a comparison of videomosaics and geographic information systems analyses. *Marine Ecology*, *35*(1), 77–95. <https://doi.org/10.1111/maec.12056>
- Mariño, J., Augustine, S., Dufour, S. C., & Hurford, A. (2019). Dynamic Energy Budget theory predicts smaller energy reserves in thyasirid bivalves that harbour symbionts. *Journal of Sea Research*, *143*, 119–127. <https://doi.org/10.1016/j.seares.2018.07.015>
- Marques, G. M., Augustine, S., Lika, K., Pecquerie, L., Domingos, T., & Kooijman, S. A. L. M. (2018). The AmP project: Comparing species on the basis of dynamic energy budget parameters. *PLOS Computational Biology*, *14*(5), e1006100. <https://doi.org/10.1371/journal.pcbi.1006100>
- Marques, G. M., Lika, K., Augustine, S., Pecquerie, L., & Kooijman, S. A. L. M. (2019). Fitting multiple models to multiple data sets. *Journal of Sea Research*, *143*, 48–56. <https://doi.org/10.1016/j.seares.2018.07.004>
- Martins, I., Colaço, A., Dando, P. R., Martins, I., Desbruyères, D., Saradin, P.-M., Marques, J. C., & Serrão-Santos, R. (2008). Size-dependent variations on the nutritional pathway of *Bathymodiolus azoricus* demonstrated by a C-flux model. *Ecological Modelling*, *217*(1), 59–71. <https://doi.org/10.1016/j.ecolmodel.2008.05.008>

- Menot, L., Galéron, J., Olu, K., Caprais, J.-C., Crassous, P., Khripounoff, A., & Sibuet, M. (2010). Spatial heterogeneity of macrofaunal communities in and near a giant pockmark area in the deep Gulf of Guinea. *Marine Ecology*, 31(1), 78–93. <https://doi.org/10.1111/j.1439-0485.2009.00340.x>
- Muller, E. B., Kooijman, S. A. L. M., Edmunds, P. J., Doyle, F. J., & Nisbet, R. M. (2009). Dynamic energy budgets in syntrophic symbiotic relationships between heterotrophic hosts and photoautotrophic symbionts. *Journal of Theoretical Biology*, 259(1), 44–57. <https://doi.org/10.1016/j.jtbi.2009.03.004>
- Newton, I. L. G., Girguis, P. R., & Cavanaugh, C. M. (2008). Comparative genomics of vesicomid clam (Bivalvia: Mollusca) chemosynthetic symbionts. *BMC Genomics*, 9, 585. <https://doi.org/10.1186/1471-2164-9-585>
- Newton, I. L. G., Woyke, T., Auchtung, T. A., Dilly, G. F., Dutton, R. J., Fisher, M. C., Fontanez, K. M., Lau, E., Stewart, F. J., Richardson, P. M., Barry, K. W., Saunders, E., Detter, J. C., Wu, D., Eisen, J. A., & Cavanaugh, C. M. (2007). The Calyptogena magnifica Chemoautotrophic Symbiont Genome. *Science*, 315(5814), 998–1000. <https://doi.org/10.1126/science.1138438>
- Olive, G., Rodrigues, C. F., & Cunha, M. R. (2011). Chemosymbiotic bivalves from the mud volcanoes of the Gulf of Cadiz, NE Atlantic, with descriptions of new species of Solemyidae, Lucinidae and Vesicomidae. *ZooKeys*, (113), 1–38. <https://doi.org/10.3897/zookeys.113.1402>
- Olu, K., Decker, C., Pastor, L., Caprais, J. .-, Khripounoff, A., Morineaux, M., Ain Baziz, M., Menot, L., & Rabouille, C. (2017). Cold-seep-like macrofaunal communities in organic- and sulfide-rich sediments of the Congo deep-sea fan. *Deep Sea Research Part II: Topical Studies in Oceanography*, 142, 180–196. <https://doi.org/10.1016/j.dsr2.2017.05.005>
- Olu, K. (2011). WACS cruise, RV Pourquoi pas ? <https://doi.org/10.17600/11030010>

- Ondréas, H., Olu, K., Fouquet, Y., Charlou, J. L., Gay, A., Dennielou, B., Donval, J. P., Fifis, A., Nadalig, T., Cochonat, P., Cauquil, E., Bourillet, J. F., Moigne, M. L., & Sibuet, M. (2005). ROV study of a giant pockmark on the Gabon continental margin. *Geo-Marine Letters*, 25(5), 281–292. <https://doi.org/10.1007/s00367-005-0213-6>
- Ozawa, G., Shimamura, S., Takaki, Y., Takishita, K., Ikuta, T., Barry, J. P., Maruyama, T., Fujikura, K., & Yoshida, T. (2017). Ancient Occasional Host Switching of Maternally Transmitted Bacterial Symbionts of Chemosynthetic Vesicomyid Clams. *Genome Biology and Evolution*, 9(9), 2226–2236. <https://doi.org/10.1093/gbe/evx166>
- Peek, A. S., Feldman, R. A., Lutz, R. A., & Vrijenhoek, R. C. (1998). Cospeciation of chemoautotrophic bacteria and deep sea clams. *Proceedings of the National Academy of Sciences*, 95(17), 9962–9966. <https://doi.org/10.1073/pnas.95.17.9962>
- Perez, M., Breusing, C., Angers, B., Beinart, R. A., Won, Y.-J., & Young, C. R. (2022). Divergent paths in the evolutionary history of maternally transmitted clam symbionts. *Proceedings of the Royal Society B: Biological Sciences*, 289(1970), 20212137. <https://doi.org/10.1098/rspb.2021.2137>
- Pfab, F., Brown, A. L., Detmer, A. R., Baxter, E. C., Moeller, H. V., Cunningham, R., & Nisbet, R. M. (2022). Timescale separation and models of symbiosis: State space reduction, multiple attractors and initialization. *Conservation Physiology*, 10(1), coac026. <https://doi.org/10.1093/conphys/coac026>
- Pop Ristova, P., Wenzhöfer, F., Ramette, A., Zabel, M., Fischer, D., Kasten, S., & Boetius, A. (2012). Bacterial diversity and biogeochemistry of different chemosynthetic habitats of the REGAB cold seep (West African margin, 3160 m water depth). *Biogeosciences*, 9(12), 5031–5048. <https://doi.org/10.5194/bg-9-5031-2012>
- Powell, M. A., & Somero, G. N. (1986). Adaptations to Sulfide by Hydrothermal Vent Animals: Sites and Mechanisms of Detoxification and Metabolism. *Biological Bulletin*, 171(1), 274–290. <https://doi.org/10.2307/1541923>

- Pruski, A. M., Decker, C., Stetten, E., Vétion, G., Martinez, P., Charlier, K., Senyarich, C., & Olu, K. (2017). Energy transfer in the Congo deep-sea fan: From terrestrially-derived organic matter to chemosynthetic food webs. *Deep Sea Research Part II: Topical Studies in Oceanography*, 142, 197–218. <https://doi.org/10.1016/j.dsr2.2017.05.011>
- Rabouille, C., Baudin, F., Dennielou, B., & Olu, K. (2017a). Organic carbon transfer and ecosystem functioning in the terminal lobes of the Congo deep-sea fan: Outcomes of the Congolobe project. *Deep Sea Research Part II: Topical Studies in Oceanography*, 142, 1–6. <https://doi.org/10.1016/j.dsr2.2017.07.006>
- Rabouille, C., Dennielou, B., Baudin, F., Raimonet, M., Droz, L., Khripounoff, A., Martinez, P., Mejanelle, L., Michalopoulos, P., Pastor, L., Pruski, A., Ragueneau, O., Reyss, J. .-, Ruffine, L., Schnyder, J., Stetten, E., Taillefert, M., Tourolle, J., & Olu, K. (2019). Carbon and silica megasink in deep-sea sediments of the Congo terminal lobes. *Quaternary Science Reviews*, 222, 105854. <https://doi.org/10.1016/j.quascirev.2019.07.036>
- Rabouille, C., Olu, K., Baudin, F., Khripounoff, A., Dennielou, B., Arnaud-Haond, S., Babonneau, N., Bayle, C., Beckler, J., Bessette, S., Bombled, B., Bourgeois, S., Brandily, C., Caprais, J. C., Cathalot, C., Charlier, K., Corvaisier, R., Croguennec, C., Cruaud, P., ... Bez, M. (2017b). The Congolobe project, a multidisciplinary study of Congo deep-sea fan lobe complex: Overview of methods, strategies, observations and sampling. *Deep Sea Research Part II: Topical Studies in Oceanography*, 142, 7–24. <https://doi.org/10.1016/j.dsr2.2016.05.006>
- Rabouille, C. (2011). CONGOLOBE cruise, RV Pourquoi pas ?
- Rodrigues, C. F., Hilário, A., & Cunha, M. R. (2013). Chemosymbiotic species from the Gulf of Cadiz (NE Atlantic): Distribution, life styles and nutritional patterns. *Biogeosciences*, 10(4), 2569–2581. <https://doi.org/10.5194/bg-10-2569-2013>
- Roy, K. O.-L., Caprais, J.-C., Fifis, A., Fabri, M.-C., Galéron, J., Budzinsky, H., Ménach, K. L., Khripounoff, A., Ondréas, H., & Sibuet,

- M. (2007). Cold-seep assemblages on a giant pockmark off West Africa: Spatial patterns and environmental control. *Marine Ecology*, 28(1), 115–130. <https://doi.org/10.1111/j.1439-0485.2006.00145.x>
- Savoye, B., Babonneau, N., Dennielou, B., & Bez, M. (2009). Geological overview of the Angola–Congo margin, the Congo deep-sea fan and its submarine valleys. *Deep Sea Research Part II: Topical Studies in Oceanography*, 56(23), 2169–2182. <https://doi.org/10.1016/j.dsr2.2009.04.001>
- Savoye, B., Cochonat, P., Apprioual, R., Bain, O., Baltzer, A., Bellec, V., Beuzart, P., Bourillet, J.-F., Cagna, R., Cremer, M., Crusson, A., Dennielou, B., Diebler, D., Droz, L., Ennes, J.-C., Floch, G., Guiomar, M., Harmegnies, F., Kerbrat, R., ... Voisset, M. (2000). Structure et évolution récente de l'éventail turbiditique du Zaïre : premiers résultats scientifiques des missions d'exploration Zaiango1 & 2 (marge Congo–Angola). *Comptes Rendus de l'Académie des Sciences - Series IIA - Earth and Planetary Science*, 331(3), 211–220. [https://doi.org/10.1016/S1251-8050\(00\)01385-9](https://doi.org/10.1016/S1251-8050(00)01385-9)
- Savoye, B., Ondréas, H., Sibuet, M., Sibuet, J.-C., Cochonat, P., & Bourillet, J.-F. (1998). ZAIANGO. <https://doi.org/10.18142/267>
- Sen, A., Dennielou, B., Tourolle, J., Arnaubec, A., Rabouille, C., & Olu, K. (2017). Fauna and habitat types driven by turbidity currents in the lobe complex of the Congo deep-sea fan. *Deep Sea Research Part II: Topical Studies in Oceanography*, 142, 167–179. <https://doi.org/10.1016/j.dsr2.2017.05.009>
- Sibuet, M., & Olu, K. (1998). Biogeography, biodiversity and fluid dependence of deep-sea cold-seep communities at active and passive margins. *Deep Sea Research Part II: Topical Studies in Oceanography*, 45(1), 517–567. [https://doi.org/10.1016/S0967-0645\(97\)00074-X](https://doi.org/10.1016/S0967-0645(97)00074-X)
- Sogin, E. M., Kleiner, M., Borowski, C., Gruber-Vodicka, H. R., & Dubilier, N. (2021). Life in the Dark: Phylogenetic and Physiological Diversity of Chemosynthetic Symbioses. *Annual Review of Micro-*

- biology*, 75(1), 695–718. <https://doi.org/10.1146/annurev-micro-051021-123130>
- Sogin, E. M., Leisch, N., & Dubilier, N. (2020). Chemosynthetic symbioses. *Current Biology*, 30(19), R1137–R1142. <https://doi.org/10.1016/j.cub.2020.07.050>
- Stewart, F. J., & Cavanaugh, C. M. (2009). Pyrosequencing analysis of endosymbiont population structure: Co-occurrence of divergent symbiont lineages in a single vesicomid host clam. *Environmental Microbiology*, 11(8), 2136–2147. <https://doi.org/10.1111/j.1462-2920.2009.01933.x>
- Stewart, F. J., Young, C. R., & Cavanaugh, C. M. (2008). Lateral Symbiont Acquisition in a Maternally Transmitted Chemosynthetic Clam Endosymbiosis. *Molecular Biology and Evolution*, 25(4), 673–687. <https://doi.org/10.1093/molbev/msn010>
- Sublette, K. L. (1987). Aerobic oxidation of hydrogen sulfide by *Thiobacillus denitrificans*. *Biotechnology and Bioengineering*, 29(6), 690–695. <https://doi.org/10.1002/bit.260290605>
- Szafranski, K. M., Gaudron, S. M., & Duperron, S. (2014). Direct evidence for maternal inheritance of bacterial symbionts in small deep-sea clams (Bivalvia: Vesicomidae). *Naturwissenschaften*, 101(5), 373–383. <https://doi.org/10.1007/s00114-014-1165-3>
- Tada, Y., Fujikura, K., Oguri, K., Kitazato, H., & Tanabe, K. (2010). In situ fluorochrome calcein marking of deep-sea molluscs using a new growth chamber. *Aquatic Ecology*, 44(1), 217–222. <https://doi.org/10.1007/s10452-009-9290-3>
- Turekian, K. K., & Cochran, J. K. (1981). Growth Rate of a Vesicomid Clam from the Galápagos Spreading Center. *Science*, 214(4523), 909–911. <https://doi.org/10.1126/science.214.4523.909>
- Turekian, K. K., Cochran, J. K., & Bennett, J. T. (1983). Growth rate of a vesicomid clam from the 21° N East Pacific Rise hydrothermal area. *Nature*, 303(5912), 55–56. <https://doi.org/10.1038/303055a0>
- Vangriesheim, A. (2001). BIOZAIRE. <https://doi.org/10.18142/179>

- von Cosel, R., & Olu, K. (2009). Large Vesicomidae (Mollusca: Bivalvia) from cold seeps in the Gulf of Guinea off the coasts of Gabon, Congo and northern Angola. *Deep Sea Research Part II: Topical Studies in Oceanography*, 56(23), 2350–2379. <https://doi.org/10.1016/j.dsr2.2009.04.016>
- Zheng, P., Wang, M., Li, C., Sun, X., Wang, X., Sun, Y., & Sun, S. (2017). Insights into deep-sea adaptations and host–symbiont interactions: A comparative transcriptome study on *Bathymodiolus* mussels and their coastal relatives. *Molecular Ecology*, 26(19), 5133–5148. <https://doi.org/10.1111/mec.14160>



## Chapter 3

# *Loripes orbiculatus*, a mixotroph shallow-water bivalve

### 3.1 About Lucinidae (J. Fleming, 1828)

#### 3.1.1 The diversity of the Lucinidae

The Lucinidae (Mollusca, Bivalvia) are marine mollusc bivalves that appeared in late Silurian time (about 444 m.y. (million years) ago) and stayed at a rather low diversity for approximately 340 m.y. (Stanley, 2014). When seagrasses and mangroves appeared near the end of the Cretaceous time (from 145.5 to 65.5 m.y. ago), an important radiation of the Lucinidae occurred (Stanley, 2014). Lucinid diversity was not much influenced by the terminal Cretaceous mass extinction where most of marine species went extinct. Lucinidae radiation kept on in the warm Paleocene time (from about 66 to 56 m.y. ago) of the Cenozoic Era (Stanley, 2014; Taylor & Glover, 2021). Lucinids may have used their chemosymbionts to survive the late Cretaceous mass extinction, as there were no observed changes in their morphology and lifestyle (Stanley, 2014; Vrijenhoek, 2013). During the Eocene (from about 56 to 34 m.y.) and Oligocene (from 34 m.y. to 23 m.y.) Lucinidae were some of the largest consumer in the marine ecosystems (Vermeij, 2010).

At present time, Lucinidae is the most diverse and abundant bivalve family with more than 400 species (Taylor & Glover, 2021). The Lu-

cinidae family is composed of eleven sub-families, of which three are entirely fossils (Taylor & Glover, 2021). Recent classification identified ninety-six living genera within the Lucinidae family (Taylor et al., 2022). 73% of this classification was based on the molecular sequencing of small subunit (SSU) ribosomal ribonucleic acid (RNA) 18S and 28S, and cytochrome b genes (Taylor et al., 2022).

Lucinid bivalves live from tropical to temperate latitudes, from shallow to deep water, up to a known depth of 2570 m (Taylor & Glover, 2021). They are endobenthic inhabiting various marine habitats such as seagrass bed, mangroves, organic enriched habitats (e.g., sunken vegetation and seawages area), oxygen minimum zones, coral reefs, hydrocarbon seeps (such as mud volcanoes and pockmarks), and hydrothermal vents (“Diversity of Chemosymbiotic Bivalves on Coral Reefs”, 2007; Taylor & Glover, 2021; Taylor et al., 2014). The common feature of these habitats is the existence of a sulfidic layer below an oxic layer of sediments (Taylor & Glover, 2021).

The symbiosis of Lucinidae, their sulfur-oxidizing symbionts and seagrasses were described as the foundation of seagrass ecosystems (van der Heide et al., 2012). Shallow-water lucinid species have been much more studied than deep water ones (> 200 m depth) (Taylor & Glover, 2021; Taylor et al., 2014). Studies in the Philippines’ water showed depth zonation for deep-sea species, and for some species peculiar elongate morphologies not present in shallow-water lucinid, suggesting that deeper water lucinid radiated independently (Taylor et al., 2014).

Lucinid largest specimens are fossils, including *Superlucina magamaris* (Dall, 1901) from Jamaica dated from the Eocene with a size of 30 cm and *Nipponothracia gigantea* (Shikama, 1964) from Japan dated from the Miocene (from 23 to 5 m.y. ago) with a size of 22 cm (Taylor & Glover, 2021). From that time on, the maximum body size of Lucinidae decreased significantly until at least the early Miocene where sizes were still substantially higher than recent sizes (Vermeij, 2010).

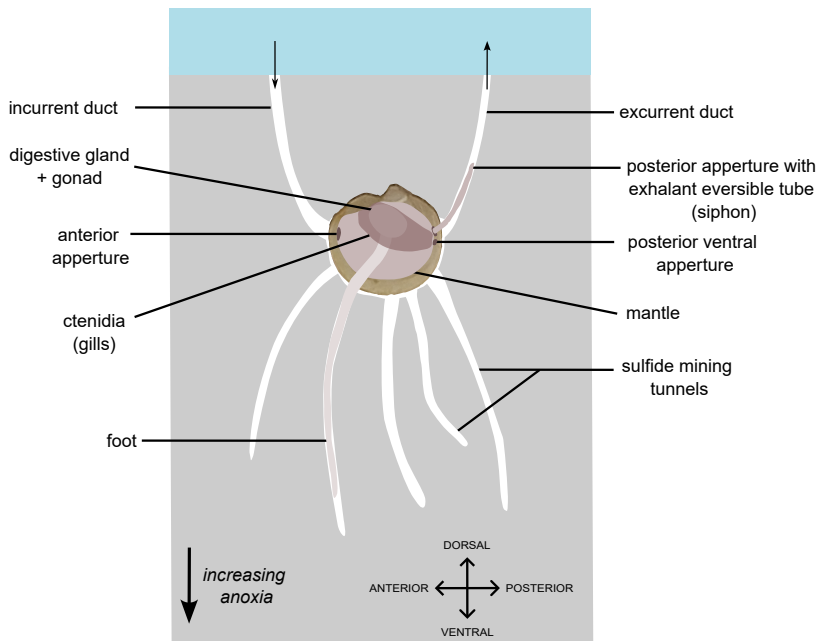


**Figure 3.1:** Lucine in its environment (adapted from Taylor and Glover, 2000, Lamers et al., 2013 and Taylor and Glover, 2021).

### 3.1.2 Notheworthy features of the Lucinidae

Lucinidae have specific and distinct morphological characteristics, including an extensible vermiform foot, an anterior aperture and two posterior apertures, the dorsal one being an excurrent eversible tube and the ventral one may be only for pseudofaeces (Figs. 3.1 and 3.2) (Taylor & Glover, 2000, 2021). A flow of water passes through the mantle cavity from the anterior to the posterior (Fig. 3.1). Lucinids present large and thick ctenidia (gills) in demibranchs (Fig. 3.2), housing sulfur-oxidizing bacteria contained in specialized gill cells (bacteriocytes) (Fig. 3.3) (Taylor & Glover, 2021).

Symbionts of lucinids belong to the Proteobacteria phylum (Taylor & Glover, 2021). Lysozymes and digested bacteria were observed at the base of the bacteriocytes (Taylor & Glover, 2021). Their highly extensible foot is used for burrowing and mining for sulfide for their symbionts, forming tunnels ventrally (Fig. 3.1) (Taylor & Glover, 2021). Their foot possesses an array of chemosensory receptors for sulfide (Yuen et

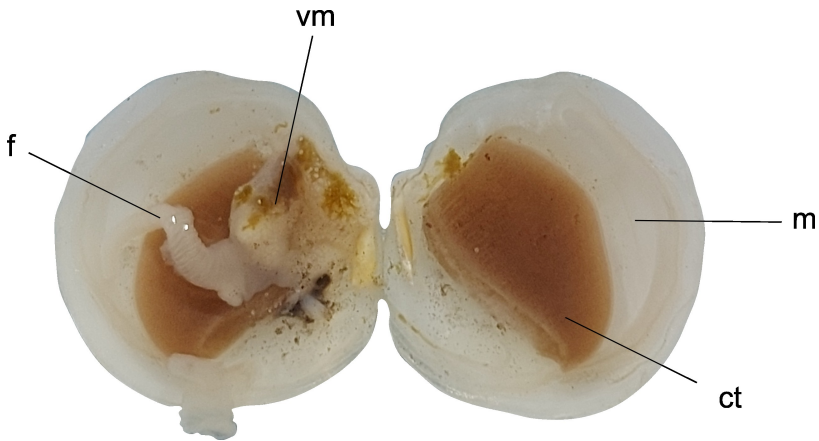


**Figure 3.2:** *Loripes orbiculatus* general anatomy. ct, ctenidia (gills); m, mantle; f, foot; vm, visceral mass (gonad + digestive gland).

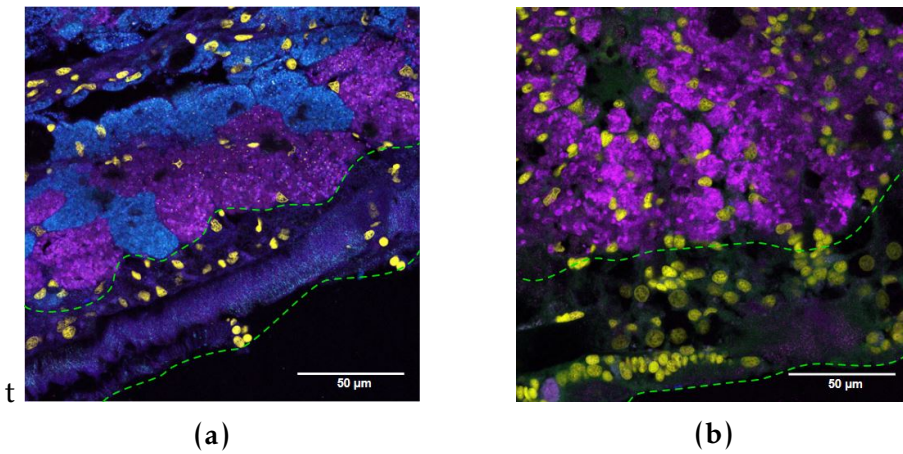


**Figure 3.3:** Fluorescence in situ hybridization of sulfur-oxidizing symbionts in two lucinid gill species. (a) Spatial distribution of *Candidatus Thiodiazotropha taylori* in the gills of *C. costata* and (b) *L. orbiculatus*. Magenta, *Ca. T. taylori*; cyan, *Ca. T. endolucinida*; yellow, DAPI labeled nuclei; green dashed lines, zone of ciliated epithelial cells (Images from Osvatic et al., 2021)

al., 2019). Genomic analysis suggested that the lucinid host may regulate symbionts access to nutrients with metabolite transporters (Yuen et al., 2019). Granules near bacteriocytes, found to be rich in sulfur, were observed to accumulate with age in some lucinid species (Taylor & Glover, 2021).

Lucinid symbionts of the genus *Candidatus* Thiodiazotropha have been found to be associated with seagrass roots (Martin et al., 2020; Zauner et al., 2022). Different lucinid species have the same symbiont species (Fig. 3.4 and Table 3.1) (Osvatic et al., 2021). Also, different symbiont species were observed to coexist in gill epithelial cells; but not inside the same bacteriocytes (Fig. 3.3) (Osvatic et al., 2021). Lucinid symbionts species share metabolic pathways for sulfur-oxidation, nitrogen and inorganic carbon fixation. But there are differences between them such as their Rubisco forms (I or II), the abilities to fix C-1 organic compounds (e.g., methanol with methanol dehydrogenase), to use nitrate as an electron acceptor instead of oxygen for respiration and to hydrolyze urea to ammonia (Table. 3.1) (Osvatic et al., 2021; Osvatic et al., 2023). Symbionts of the genus *Ca.* Thiodiazotropha from clams below 50 m depth did not have the core functional genes for nitrogen fixation therefore this capability seems to be restricted to shallow-water lucinid (Osvatic et al., 2023). Deep-sea lucinid species hosted sulfur-oxidizing bacteria from the order Thiohalomonadales which were close phylogenetically to symbionts of hydrothermal vent gastropods (Osvatic et al., 2023).

Larvae of Lucinidae are aposymbiotics (i.e., acquire symbionts from their environment) (Fig. 3.5) (Gros et al., 2012; Zauner et al., 2022).

## 3.2 About *Loripes orbiculatus* (Poli, 1795)

### 3.2.1 Description of *Loripes orbiculatus*

*Loripes* (Poli, 1791) genus is composed of small white-shelled species, with an obliquely inserted internal ligament (externally visible) and external growth increments. *L. orbiculatus* is the accepted name for *Loripes*

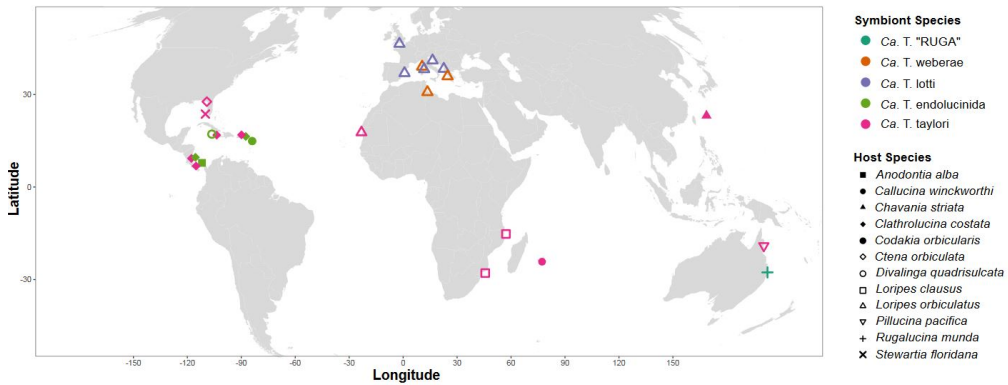


**Figure 3.4:** Geographic of lucinid symbiont species. The genus *Ca.* Thiodiazotropha reveals both localized (Mediterranean and Caribbean) and globally distributed symbiont groups. Shapes represent host species and colors represent symbiont species. *Ca. T. taylori* (pink) was found in association with eight lucinid species across the globe. *Ca. T. sp. 'RUGA'* (teal) is the endosymbiont of a *R. munda* specimen from Tin Can Bay, Queensland, Australia. *Ca. T. endolucinida* (green) is distributed throughout the Caribbean and also associates with multiple host species. *Ca. T. endoloripes*, previously described as a single species by Petersen et al. (15), is in fact two closely related species (*Ca. T. weberae* in orange and *Ca. T. lotti* in purple), so far found exclusively within *L. orbiculatus* in the Mediterranean. (Figure from Osvatic et al., 2021).

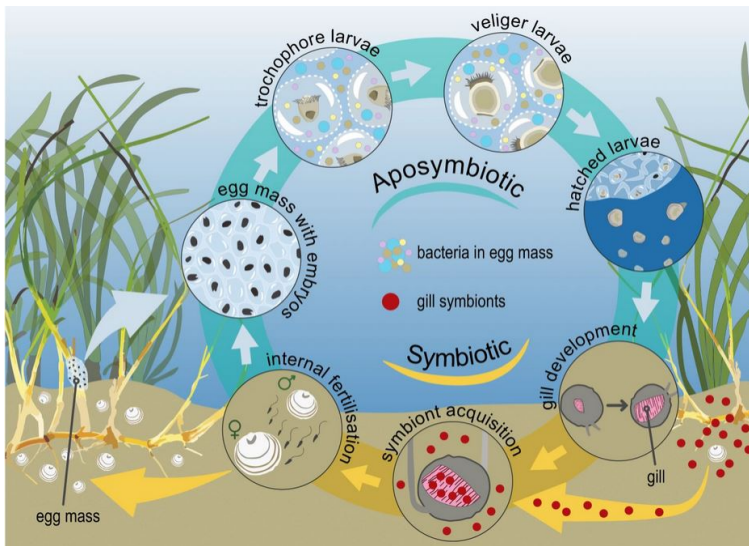


**Figure 3.5:** Lucinid *Loripes orbiculatus* life cycle. (Figure from Zauner et al., 2022).

**Table 3.1:** Predicted major metabolic functions annotated in the metagenome assembled genomes (MAGs, i.e. microbial genomes reconstructed from metagenome data) of *Loripes orbiculatus* symbionts *Ca. T. taylori*, *Ca. T. weberae*, *Ca. T. lotti*. (Table from Osvatic et al., 2021).

Feature	<i>Ca. T. taylori</i>	<i>Ca. T. weberae</i>	<i>Ca. T. lotti</i>
<b>Carbon metabolism</b>			
CBB cycle, form I (RuBisCO)	+	+	+
CBB cycle, form II (RuBisCO)	-	-	-
Methylotrophy pathway*	+	-	-
<b>Nitrogen metabolism</b>			
Diazotrophy, nitrogenase	+	+	+
Respiratory nitrate reductase	-	-	-
Copper-containing nitrite reductase (NO-forming)	-	-	+
Nitric-oxide reductase	+	+	+
Nitrous-oxide reductase	+	+	+
Periplasmic nitrate reductase	+	+	+
Nitrite reductase NADPH subunit	+	+	+
Urease	+	+	-
Ammonia assimilation	+	+	+
<b>Sulfur metabolism</b>			
Sqr	+	+	+
Truncated SOX	+	+	+
DSR	+	+	+
DsrMKJOP complex	+	+	+
APR	+	+	+
FCC	+	+	+

*lacteus* (Linnaeus, 1758 sensu Poli, 1791) and *Loripes lucinalis* (Lamarck, 1818) (junior name) found in the literature which are no longer considered as valid names (“WoRMS - World Register of Marine Species - *Loripes Lacteus* (Linnaeus, 1758) Sensu Poli, 1791”, 2024; “WoRMS - World Register of Marine Species - *Loripes Lucinalis* (Lamarck, 1818)”, 2024). *L. orbiculatus* length is up to 30 mm, with thin and almost circular shell (Cosel & Gofas, 2019; Taylor & Glover, 2021).

### 3.2.2 Distribution and ecology of *Loripes orbiculatus*

*L. orbiculatus* is a common shallow-water species in the temperate area in Europe. The species lives in the Irish Sea, in the Southwest coast of Ireland and England, western part of the Channel, southward to Mauritania, in Madeira, Canary Islands, in the Mediterranean Sea and in the Black Sea (Cosel & Gofas, 2019; Taylor & Glover, 2021). *L. orbiculatus* can be found in muddy and fine sand, also in muddy gravel, from the infralittoral zone to about 150 m depth in sub-tidal area, and in/near seagrass meadows (Cosel & Gofas, 2019; Taylor & Glover, 2021). *L. orbiculatus* usually burrows within 3 to 4 cm below the surface (max 10 cm) in Banc d’Arguin, Mauritania (Gils et al., 2016; van Gils et al., 2012).

*L. orbiculatus* associates with various seagrasses, at their roots or close to them, such as *Zostera marina* and *Z. noltii* (in the Thau Lagoon, Mediterranean, France), *Posidonia oceanica* (Elba Island, Italy) and *Cymodocea nodosa* (Alfacs bay, Mediterranean, Spain and Upper Corsica lagoon) (Cardini et al., 2019; de Fouw et al., 2023; Johnson et al., 2002; Roques et al., 2020; Sanmartí Boixeda, 2020) (non exhaustiv list). The sulfur-oxidizing symbionts of lucinids detoxify the sediments and this creates a mutualistic relationship between the lucinid, its symbionts and seagrasses. This mutualism helps the seagrasses to mitigate sediment sulfide stress and favor their growth (de Fouw et al., 2023; Sanmartí et al., 2018; van der Geest et al., 2020). In the Thau lagoon in France, a positive correlation between *Z. noltii* seagrass biomass and *L. orbiculatus* density has been observed. *Z. noltii* leaves sulfide concentration was significantly reduced with higher densities of *L. orbiculatus*, thus reduc-

ing *Z. noltii* sulfide stress (van der Geest et al., 2020).

A model was developed to predict *L. orbiculatus* distribution based on seagrass biomass of *Z. noltii* and *Z. marina*, temperature and mud content. This model was quite accurate as 86% of predictions were aligned with data. *L. orbiculatus* presence was indeed found significantly correlated with low mud content, presence of *Zostera* meadows and an annual temperature above 1°C (no *L. orbiculatus* were found in seagrass meadows with temperature below 1°C) (de Fouw et al., 2023).

In the Banc d'Arguin, Mauritania, interactions between *L. orbiculatus*, seagrasses of *Z. noltii* and the molluscivore shorebird *Calidris canutus canutus* (red knot), have been studied for more than ten years. Red knots feed on two bivalve species, *L. orbiculatus* which is abundant and *Dosinia isocardia* which is less abundant, with a preference for *D. isocardia* (van Gils et al., 2012; van Gils et al., 2013). Sulfur content in *L. orbiculatus* specimens was believed to limit the predation of *C. c. canutus* on them (Oortwijn et al., 2022). *L. orbiculatus* was observed to be a toxic prey for red knots, provoking diarrhea because of the presence of the sulfide-oxidizing bacteria within its gills (Gils et al., 2016). However *L. orbiculatus* was still observed to constitute an important part of red knots diet, as they rely on *L. orbiculatus* as food source when other preys are not abundant enough (van Gils et al., 2013). *C. c. canutus* specimens were exposed to three diets: *L. orbiculatus* from a seagrass bed, *L. orbiculatus* from a mud flat, and sulfide-starved *L. orbiculatus* that had the lowest sulfur content (Oortwijn et al., 2022). *L. orbiculatus* from the seagrass bed had a higher sulfur content than the ones from mud flat. Intake rate was observed higher for birds fed on *L. orbiculatus* with the lowest sulfide content (Oortwijn et al., 2022).

In Roscoff, France, *L. orbiculatus* lives in sympatry with two other lucinid species, *Lucinoma borealis* and *Lucinella divaricata*, near *Z. marina* seagrass bed (Ann Andersen personal communication). *L. divaricata* is present in a relative low density compared to the two other species (Ann Andersen personal communication). *L. orbiculatus* and *L. divaricata* belong both to the *Lucininae* sub-family, while *L. borealis* belongs to the *Codakiinae* sub-family (Taylor & Glover, 2021). *L. borealis* and *L. divar-*

*icata* are close phylogenetically based on the 18S ribosomal RNA, 28S ribosomal RNA and cytochrome b sequences (Taylor & Glover, 2021).

*L. orbiculatus* density in Roscoff around the seagrass beds was observed to be lower than in Banc d'Arguin, Mauritania (i.e., 340–780 individuals  $m^{-2}$ ) (Ann Andersen personal communication). *Zostera* seagrass beds in Roscoff are protected and it is forbidden to dig inside, where density of lucinid species might be higher. In the Thau Lagoon, larger *L. orbiculatus* were located inside the seagrass beds while smaller specimens were found at the edge (Rossi et al., 2013). There, *L. orbiculatus* density of about  $3395 \pm 195$  individuals  $m^{-2}$  was stable from May to October in *Z. noltii* meadow, even with important temperature changes (4 °C to 26 °C). In the Mediterranean Alfacos bay, Spain, *L. orbiculatus* density in *Cymodocea nodosa* meadows was  $889 \pm 225$  specimens  $m^{-2}$  in seagrasses while in bare sediments it was  $172 \pm 80$  specimens  $m^{-2}$  (Sanmartí Boixeda, 2020). In Corsica, mean density of *L. orbiculatus* was 775 individuals  $m^{-2}$ , ranging from 242 to 2666 individuals  $m^{-2}$  (Johnson et al., 2002).

### 3.2.3 *Loripes orbiculatus* symbionts

*L. orbiculatus* gills weight represented about 32.5–35% of the total body wet weight (Johnson et al., 1994; Johnson et al., 2002). Gill bacterial density was estimated to  $2 \times 10^{10}$  bacteria per gram of gill tissue (Johnson et al., 1994). Bacteriocytes containing gamma - Proteobacteria, mucocytes and intercalary cells were observed in *L. orbiculatus* gills (Herry et al., 1989; Pales Espinosa et al., 2013; Roques et al., 2020). *L. orbiculatus* gill tissues were composed mainly of bacteriocytes, from 40 to 70%, 56.4% in average in *L. orbiculatus* from the Thau Lagoon (Mediterranean Sea) (Roques et al., 2020). At the apical part of the bacteriocytes, symbiont size varied from 0.5 to 3  $\mu m$  were observed whereas larger bacteria, size up to 5  $\mu m$ , were more electron-dense and situated at the basal part of bacteriocytes (Johnson & Fernandez, 2001). Symbionts are about 55% of the gill cross-sectional surface area in *L. orbiculatus* from Brittany (West of France, Atlantic Ocean) (Johnson & Fernandez, 2001). A single bac-

terioocyte was observed to contain many vacuoles with one symbiont per vacuole (Pales Espinosa et al., 2013). Initially, the presence of the Ru-bisco in bacteriocytes with Rubisco antibodies was an evidence demonstrating that *L. orbiculatus* symbionts were able to fix carbon through the Calvin-Benson cycle (Dreier et al., 2012; Herry et al., 1989). The presence of APS-reductase enzyme only in gills highlighted the sulfur-oxidation metabolism of symbionts (Dreier et al., 2012; Herry et al., 1989). Glutamine synthetase enzyme of nitrogen assimilation pathway was also detected (Dreier et al., 2012).

*L. orbiculatus* symbiont species belong to the genera *Candidatus* Thiodiazotropha (C. T.). *Candidatus* Thiodiazotropha nomenclature is not validly published and is taxonomically preferred genera name. In “Thiodiazotropha”, “thio” and “diazotroph” are references to *L. orbiculatus* symbionts’ metabolism (sulfur-oxidizing and nitrogen-fixing) (Oren et al., 2020; Petersen et al., 2016). In Elba island, Italy, *L. orbiculatus* symbiont carbon fixation varied seasonally; it was observed roughly 10-fold higher in October than in April, increasing its C:N ratio (Cardini et al., 2019).

Phylogenomics, fluorescence hybridization *in-situ* and q-PCR identified two symbiont phylotypes, named Clone 1 - Roscoff and Clone 2 - Roscoff, inside *L. orbiculatus* gills from Roscoff, France (Pales Espinosa et al., 2013). Clone-1 density was significantly higher than Clone-2 density and both phylotypes were found significantly in higher density in gills compared to the mantle and the gonad (Pales Espinosa et al., 2013). Clone-1 density in gills and Clone-2 density in the mantle were closed (Pales Espinosa et al., 2013). Clone 1-Roscoff matched with 91% of already sequenced *L. orbiculatus*’ symbiont genomes from Croatia and other lucinid species, while the second phylotype matched with free living-bacteria found also in marine sediments (Pales Espinosa et al., 2013). Recently, two symbiont species *Candidatus* Thiodiazotropha weberae and C. T. lotti were identified in *L. orbiculatus*, and were both previously confounded as a single species C. T. endoloripes (Osvatic et al., 2021; Petersen et al., 2016). The symbiont species C. T. taylori was found in seven lucinid species other than *L. orbiculatus* from different lucinid

sub-family (Lucininae, Leucosphaerinae, and Codakiinae) (Fig. 3.4) (Osvatic et al., 2021). *C. T. lotti* and *C. T. weberae* were found in *L. orbiculatus* specimens from Atlantic and mediterranean European coasts while *C. T. taylora* in specimens from Mauritania (Fig. 3.4) (Osvatic et al., 2021; Zauner et al., 2022). The advanced explanations that was put forward was that *C. T. taylora* was not adapted to European coast temperate temperature compared to *C. T. lotti* and *C. T. weberae* (Osvatic et al., 2021). In the Banc d'Arguin, Mauritania, *Ca. Thiadiazotropha* was detected in the sediment and in the seagrass roots (Zauner et al., 2022).

It has recently been shown through molecular biology that *L. orbiculatus* symbionts were capable of fixing nitrogen in addition to oxidizing sulfide (Petersen et al., 2016). Based on genomics, *L. orbiculatus* symbionts of the genus *Ca. Thiadiazotropha* were found to be able to use oxygen, oxidized nitrogenous compounds (nitrate and nitrite) and hydrogen as terminal electron acceptors (metabolic pathway Chapter 1, Fig. 1.8), and to oxidize reduced sulfur compounds to sulfate through various pathways to fix inorganic carbon via the Calvin–Benson–Bassham (CBB) cycle with RuBisCO form I to generate organic carbon (metabolic pathway in Chapter 1, Figs. 1.6a and 1.7) (Table. 3.1) (Osvatic et al., 2021; Petersen et al., 2016). *Ca. T. taylora* is also able to use methanol as a source of energy with an xox-type methanol dehydrogenase and fix organic C1-carbon via the serine pathway (metabolic pathway in Chapter 1, Fig. 1.6b) (Osvatic et al., 2021; Petersen et al., 2016). All *L. orbiculatus* symbionts were also capable of assimilating nitrogen gas and ammonia (Osvatic et al., 2021). Urea produced by the host may be used by symbionts which genome encoded urease that uptake and convert urea to ammonia (Table. 3.1) (Osvatic et al., 2021; Petersen et al., 2016). Although N-waste form(s) of *L. orbiculatus* are not known, it has been suggested that *L. orbiculatus* might use DUR-3 urea transporter, found expressed in its gills, to provide its symbionts with urea (Osvatic et al., 2021; Yuen et al., 2019). Elemental sulfur ( $S^0$ ) granules were observed inside host cells, produced by the symbionts. (Johnson & Fernandez, 2001; Pales Espinosa et al., 2013).

Both the feeding of *L. orbiculatus* with microalgae and the starvation

of *L. orbiculatus* in the laboratory caused a loss of symbionts, observed by fluorescence *in-situ* hybridization (FISH) and quantitative Real-Time polymerase chain reaction (qPCR) analyses. The decrease stabilized after five weeks of experiment (Pales Espinosa et al., 2013). An attempt of re-aquisition of symbionts after a symbiont loss of starved *L. orbiculatus* was attempted but unsuccessful (Pales Espinosa et al., 2013).

Symbionts were absent from *L. orbiculatus* male gametes (Johnson et al., 1996b) and also *Ca. Thiodiazotropha* was not detected in reproductive gelatinous egg masses (Fig. 3.5) (Zauner et al., 2022). As in other lucinid species, symbionts are acquired from lateral transmission (from the environment) (Fig. 3.5) (Zauner et al., 2022).

### 3.2.4 *Loripes orbiculatus* mixotrophy

Labial palps (thought to be use for suspension-feeding in mollusk) and digestive gland are reduced in *L. orbiculatus* (Le Pennec et al., 1995). Nevertheless, particulate organic matter was found in its intestine indicating that *L. orbiculatus* feed on it (Le Pennec et al., 1995).

The  $\delta^{13}\text{C}$  (‰) signature of a sample is the variation of the stable isotopes ratio  $^{13}\text{C}/^{12}\text{C}$  of a sample relatively to the  $^{13}\text{C}/^{12}\text{C}$  ratio of a reference (Eq. 3.1). Isotopes have the same number of protons, but a different number of neutrons. For example,  $\delta^{13}\text{C}$  has one more neutron than  $^{12}\text{C}$  and because of that it is heavier. A “stable” isotope means non-radioactive. The  $\delta^{15}\text{N}$  (‰) signature is determined similarly as the  $\delta^{13}\text{C}$  (Eq. 3.2).

$$\delta^{13}\text{C} = 1000 \left[ \frac{^{13}\text{C}/^{12}\text{C}_{\text{sample}}}{^{13}\text{C}/^{12}\text{C}_{\text{reference}}} \right] \quad (3.1)$$

$$\delta^{15}\text{N} = 1000 \left[ \frac{^{15}\text{N}/^{14}\text{N}_{\text{sample}}}{^{15}\text{N}/^{14}\text{N}_{\text{reference}}} \right] \quad (3.2)$$

The standard reference for  $\delta^{13}\text{C}$  is the signature of a Cretaceous belemnite sample from the PeeDee (PDB) rock formation in South Carolina, USA ( $^{13}\text{C}/^{12}\text{C}_{\text{PDB}} = 0.0112372$ ). For  $\delta^{15}\text{N}$ , the standard reference is atmosphere (atm) signature ( $^{15}\text{N}/^{14}\text{N}_{\text{atm}} = 0.0036765$ ) (He et al., 2009;

Mariotti, 1983).

Consumers (i.e., not primary producers) fix heavier isotopes and release lighter ones resulting in an enrichment of  $\delta^{13}\text{C}$  and  $\delta^{15}\text{N}$  (‰) (Cabrera & Rasmussen, 1996). This shift of signatures between food source and consumers is called fractionation ( $\Delta\delta^{13}\text{C}$  for carbon and  $\Delta\delta^{15}\text{N}$  for nitrogen) (Zanden & Rasmussen, 2001). As an example,  $\Delta\delta^{15}\text{N}$  between a consumer and its organic carbon food source is assumed to be about 3.4‰ (Aberle & Malzahn, 2007; Zanden & Rasmussen, 2001). Trophic interactions between organisms can thus be inferred from their respective isotopic signatures. A rather close isotopic signature to a certain food source indicates the importance of this food source in the consumer diet (Zanden & Rasmussen, 2001). Primary producers usually have varying isotopic signatures and lighter compared to their inorganic carbon and nitrogen source because of their enzymes (e.g., ribulose-1,5-bisphosphate carboxylase/oxygenase (RuBisCO) I and II, nitrogenase) preference for the lighter isotope (Petersen et al., 2016; Robinson & Cavanaugh, 1995). Nitrogen-fixing bacteria have a  $\delta^{15}\text{N}$  between -2 and 0‰ (Petersen et al., 2016). Organic carbon generated by chemosynthesis have lower  $\delta^{13}\text{C}$  and  $\delta^{15}\text{N}$  signatures than carbon generated by photosynthesis. Therefore, symbiotic bivalves have also lower signatures.

*L. orbiculatus* from many locations presented a depleted  $\delta^{13}\text{C}$  signature compared to symbionts-free bivalves, corresponding to a carbon source of chemoautotrophic origin (Table. 3.2). Isotopic  $\delta^{13}\text{C}$  signature of planktotrophic bivalves in Brest, France, ranged from -18.1 to -20.1‰ (Johnson et al., 1994). Suspended particulate organic matter from the water column in the Banc d'Arguin, Mauritania, had a  $\delta^{13}\text{C}$  signature of  $-18.7 \pm 1.2\text{‰}$ , which is of the same order that planktotrophic bivalves (Geest et al., 2014). In the Banc d'Arguin, bacterial pellets were made from *L. orbiculatus* gills by centrifuging the gills to remove animal cells. They had a mean signature of  $-27.2 \pm 0.2\text{‰}$ , which is more depleted than the signature of suspended particulate organic matter (Geest et al., 2014). In another study in the Banc D'Arguin, *L. orbiculatus* individuals presented a mean  $\delta^{13}\text{C}$  values of  $-23.4 \pm 1.8\text{‰}$ , significantly lower than

other co-occurring symbiont-free bivalve species (Petersen et al., 2016). In Elba, Italy, *L. orbiculatus* had a  $\delta^{13}\text{C}$  signature of  $-25.9 \pm 1.6\text{‰}$  (Petersen et al., 2016). In Brest, France, mean  $\delta^{13}\text{C}$  was  $-29.7 \pm 0.5\text{‰}$  for *L. orbiculatus* gills and  $-27.1 \pm 0.5\text{‰}$  for its foot (Johnson et al., 1994).  $\delta^{13}\text{C}$  and  $\delta^{15}\text{N}$  values were also found to be similar to those of *L. orbiculatus* symbiotic bacteria in *L. orbiculatus* from the Thau lagoon (between  $-30$  and  $-28\text{‰}$  for  $\delta^{13}\text{C}$  and between  $-4$  and  $2\text{‰}$  for  $\delta^{15}\text{N}$ .) (Rossi et al., 2013). *L. orbiculatus* specimens from Mediterranean (Italia)  $\delta^{13}\text{C}$  signatures were also depleted, from  $-27.8$  et  $-24.4\text{‰}$ . (Dreier et al., 2012).  $\delta^{15}\text{N}$  signature of *L. orbiculatus* in the Banc d'Arguin was about  $-0.5\text{‰}$  and about  $-1.1\text{‰}$  in Elba which correspond to signatures of nitrogen fixing bacteria (Petersen et al., 2016).

*L. orbiculatus* isotopic signatures differ at a large scale (regional) but also at a smaller scale. *L. orbiculatus* from the edge of seagrass beds and from the middle of seagrass beds had different nutritional behaviour, as shown by isotopic signatures ( $\delta^{13}\text{C}$  and  $\delta^{15}\text{N}$ ) (Table. 3.2) (Rossi et al., 2013). Small lucines at the edge of seagrass beds assimilated less bacterial carbon and nitrogen than in the inner part of the seagrass beds (Rossi et al., 2013).

*L. orbiculatus*  $\delta^{13}\text{C}$  signature varied greatly seasonally (Table 3.2). In Roscoff (western english channel), *L. orbiculatus* had depleted  $\delta^{15}\text{N}$  and  $\delta^{13}\text{C}$  isotopic signatures:  $-1.6 \pm 0.1\text{‰}$  and  $-26.8 \pm 0.2\text{‰}$  in February, respectively, and  $0.8 \pm 0.1\text{‰}$  and  $-26.0 \pm 0.1\text{‰}$  in August, respectively.

To summarize,  $\delta^{13}\text{C}$  signatures of *L. orbiculatus* fluctuated in function of *L. orbiculatus* locations, of seasons and of *L. orbiculatus* shell sizes (i.e., age) (Table. 3.2).

Endosymbiont lysis was observed as the degeneration and fusion of vacuoles containing symbionts, resulting in electron-dense inclusions and large granular bodies in basal part of *L. orbiculatus* gills (Johnson & Fernandez, 2001; Pales Espinosa et al., 2013). In Brest, France, digestion of endosymbionts varied seasonally, with lower gill weight observed in March compared to September, October and January, corresponding to the period of gamete development in *L. orbiculatus* (Johnson & Fernandez, 2001). Heterotrophic contribution from filter-feeding in *L. orbicu-*



*latus* was also estimated to vary seasonally, being about estimated 21% in March to 39% in September in Banc d'Arguin (Mauritania) (Geest et al., 2014). *L. orbiculatus* mixotrophy fluctuated seasonally (Cardini et al., 2019; Geest et al., 2014). About 63% of *L. orbiculatus* carbon was estimated to come from its sulfur-oxidizing symbionts in Brest, France (Johnson et al., 1994).

Transcriptomic analysis of *L. orbiculatus* organs suggested that *L. orbiculatus* “farming” may not play a big role in its nutrition, and that “milking” could be its main source of symbiotic nutrients (Yuen et al., 2019). *L. orbiculatus* may digest symbionts in the case of sulfide shortage (Yuen et al., 2019). Tissues autoradiography of *L. orbiculatus* specimens exposed to labeled carbon ( $^{14}\text{C}$ ) revealed that carbon was fixed mainly in the bacteriocytes near the ciliary zones within the gills (Herry et al., 1989). A low concentration was detected in gill filament central part (Herry et al., 1989). Intermediate cells within gill filaments were also highly marked even if there were no symbionts in these cells. Labelled carbon was also detected in the host mantle and foot (Herry et al., 1989).

### 3.2.5 Reproduction of *Loripes*

*L. orbiculatus* is a gonochoric species, each individual being either male or female (Johnson & Pennec, 1994; Johnson et al., 1996b). *L. orbiculatus* in the Banc d'Arguin, Mauritania (East-Atlantic) and in the Bay of Brest, France (East-Atlantic) presented a semi-annual gametogenic cycle. In Brest, *L. orbiculatus* spawned from May to June, and are thought to also spawn between November and December. In Mauritania, there was a spawning event between January and February, and between July and August (Geest et al., 2014). Only one reproductive period during late spring/early summer was observed in the Thau Lagoon, France (Mediterranean Sea) (Roques et al., 2020). In Roscoff (France, Western english channel) May was a breeding period for *L. orbiculatus* specimens. Collected specimens during this thesis spawned spontaneously in the laboratory overnight. *L. orbiculatus* was observed to release gelatinous egg masses of about 3 to 4 cm in diameter in Mauritania (Zauner et al.,

2022). The gelatinous mass contained individuals in early larval development stage of *L. orbiculatus*, such as trochophore and veliger larvae (Fig. 3.5) (Zauner et al., 2022). Gelatinous masses that may be from *L. orbiculatus*, were also observed in the Roscoff seagrass beds (Ann Andersen personal communication).

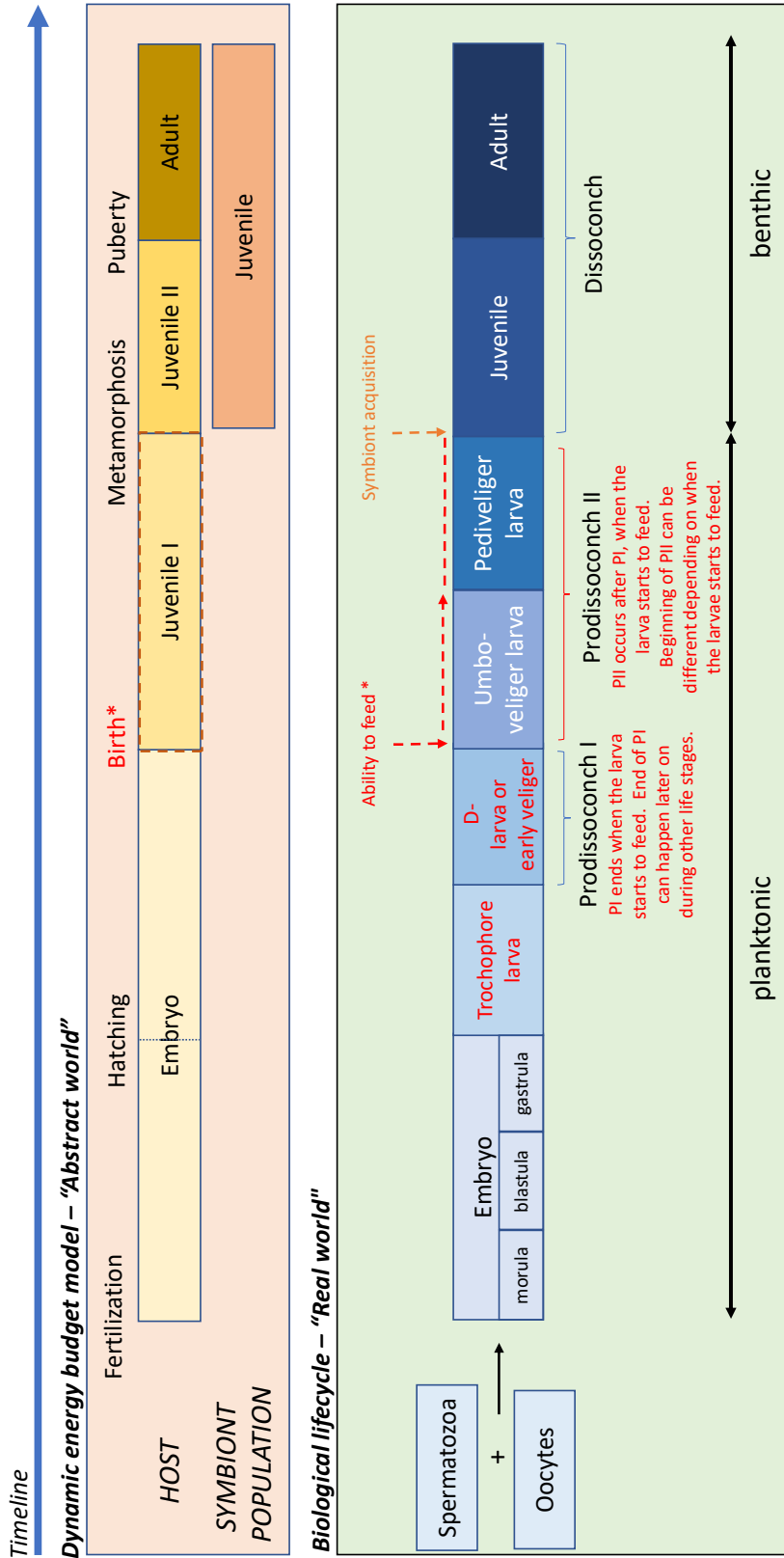
Along a year, the wet weight of the visceral mass (complex formed by the gonad and the digestive gland) varied between 12 and 61.2 mg (Johnson et al., 1996a). The highest wet weight of the visceral mass was measured the months before the spawning event, in October, November and April (Johnson et al., 1996a). After the spawning event, *L. orbiculatus* total wet weight was approximately 50% lower than before (Johnson et al., 1996a).

Gill mucocytes (i.e., cells that secrete mucus) were found in low but highly variable proportions between individuals (7.6% in average) (Roques et al., 2020). A negative correlation between gill bacteriocytes and mucocytes was observed (Roques et al., 2020). Mucocytes present inside gill cells may help the host to increase heterotrophic nutrition during the reproductive period or/and may be related to host immunity (Roques et al., 2020).

### 3.3 A DEB model for *Loripes orbiculatus*

#### 3.3.1 Biological cycle vs. DEB cycle

The life cycle of *L. orbiculatus* is similar to other bivalve life cycle (Fig. 3.6). The main differences between the deep-sea species *Christineconcha regab* and *L. orbiculatus* are in their way to feed and the way they acquire their symbionts (see Chapter 2). *L. orbiculatus* is mixotroph, feeding on both its symbionts and particulate organic matter (POM). The start of feeding, called the birth event in DEB, is not related explicitly to an event or stage of the biological cycle (Fig. 3.6). *L. orbiculatus* facultative planktotroph larva obtain the ability to feed at the umbo-veliger larva stage but might start to feed later. The larva relies first on its maternal reserve (lecithotroph) and start feeding when needed (planktotroph) (Fig. 3.6).



\* Ability to feed (birth in DEB) can happen during different larva stages depending on the food need and emptiness of the vitellin reserve of the mother oocyte. Birth can be close to metamorphosis.

**Figure 3.6:** abj model versus bivalve biological cycle: case of planktotroph facultative larvae. Known approximative development time from Zauner et al., 2022: trochophore larvae, 8 days after egg mass release; veliger larval stage, 12 days.

Lucinid acquire their symbionts from their environment once they settled (Fig. 3.6) (Zauner et al., 2022).

### 3.3.2 DEB modeling scheme of *Loripes orbiculatus*

For the host bivalve, the standard macrochemical equation have to be modified by adding an additional food source. *L. orbiculatus* is a mixotrophic bivalve and two food sources should be modeled, particulate organic mater and symbiotic food sources.

Main metabolic pathways encoded in *L. orbiculatus* symbiont *Ca. Thio-diazotropha* were described previously in this Chapter 3. Nitrogen fixation by the symbionts have to be implemented in the symbiont macrochemical equation. An additional symbiont reserve for sulfur composed of elemental sulfur ( $S^0$ ) should be added to model granules stored as elemental sulfur in *L. orbiculatus* by its symbionts. Symbionts may produced their granules when they have enough sulfur and may use them in case of sulfide shortage. Chemical molecules input and output are represented in Fig. 3.7a. A prelliminary modeling scheme for lucines has been thought out taking into account the use of a sulfur reserve (Fig. 3.7b).

## 3.4 Zero and univariate data for *Loripes orbiculatus* DEB model

### 3.4.1 List of required data

Data (zerovariate and univariate) are needed to calibrate *L. orbiculatus* DEB model. In order to acquire the necessary data, sampling and experiments have to be carried out. Non exhaustive classical data of DEB models are listed in Tables 3.4 and 3.3 for zerovariate data and univariate respectively. Additional data necessary to model the additional sulfur reserve, farming and milking strategy and mixotrophy of *L. orbiculatus* are listed in Tables 3.5 and 3.6.

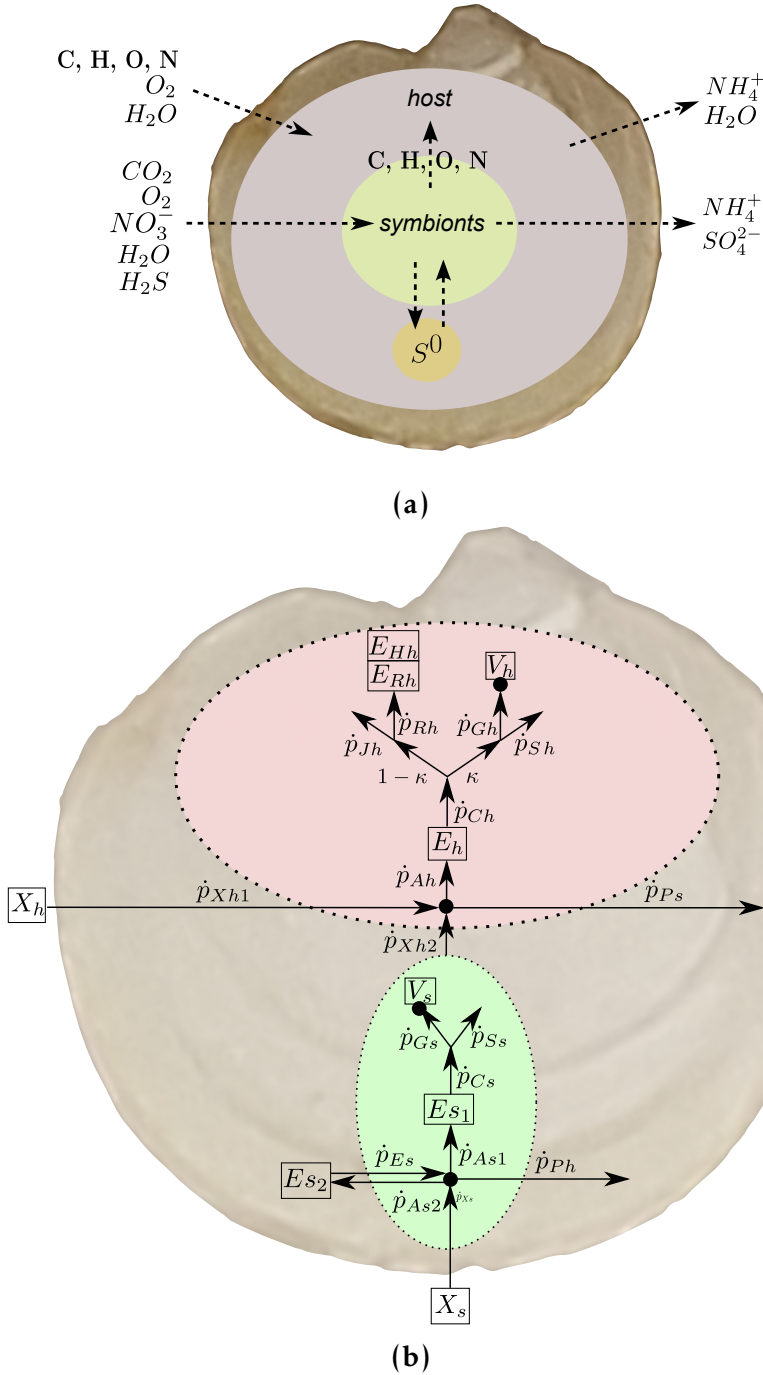


**Figure 3.7:** (a), *Loripes orbiculatus* and its thiotrophic symbionts chemical element fluxes for dynamic energy budget model; (b), Conceptual modeling scheme of *Loripes orbiculatus* dynamic energy budget model. Compared to *Christinaconcha regab* abj-farming modeling scheme in Chapter 2 (Fig. 2.1), another food source for particulate organic matter ( $X_h$ ) and an additional ingestion flux ( $\dot{p}_{Xh1}$ ) have been added for the host; a sulfur reserve ( $Es_2$ ) with corresponding storing and mobilizing fluxes ( $\dot{p}_{Es}$  and  $\dot{p}_{As}$  respectively) have been added for the symbionts. Arrow, energy flux; Square, state variable. For details on state variables and fluxes units and notations, refer to Chapter 2.

**Table 3.3:** Classic univariate data for an abj Dynamic Energy Budget (DEB) model, intended for *Loripes orbiculatus* DEB model. For *L. orbiculatus*, shell height is preferred to shell length as its valves are almost circular.

Notation	Description	Unit
H-dH	Height, Change in height	cm, cm
t-H	Time, Height	d, cm
Height-Ww	Height, Wet weight	cm, g
Height-Wd	Height, Dry weight	cm, g
Height-WwR	Height, Gonad wet weight	l, g
Height-R	Height, Reproduction rate	l, g
Height-GSI	Height, Gonado somatic index	l, %
Ww-R	Wet weight, Reproduction rate	g, #/d
Ww-JO	Wet weight, O <sub>2</sub> consumption	g, mol/d
Ww-JC	Wet weight, CO <sub>2</sub> production	g, mol/d
Ww-JN	Wet weight, NH <sub>4</sub> <sup>+</sup> production	g, mol/d
Wd-Ww	Dry weight, wet weight	g, g
Wd-Wa	Dry weight, ash free dry weight	g, g
Wd-JO	Dry weight, O <sub>2</sub> consumption	mol/d
Wd-JC	Dry weight, CO <sub>2</sub> production	g, mol/d
Wd-JN	Dry weight, NH <sub>4</sub> <sup>+</sup> production	g, mol/d

### 3.4.2 Acquisition methods of required data

#### *Biometry*

Univariate data (Table. 3.3) such as H-Ww (height - wet weight), H-Wd (height - dry weight), Wd-Ww (dry weight - wet weight), Wd-Wa (dry weight - ash-free dry weight) are determined by measuring shell height, with a caliper, and by weighing wet, dry, and ash-free bivalve soft body (removed from its shell). For H-R (height - reproduction rate) and Ww-R (wet weight - reproduction rate) (Fig. 3.3), the weight of the fresh gonad have to be weighted. The wet weight is the fresh, non-dried weight of the total biomass. Dry weight is the dry weight of the total biomass. Ash free dry weight is the dry weight minus the weight of ashes. The t-H (time - height) (Fig. 3.3) growth can be determined by measurements of cohort shell lengths at given sites at different times of the year or by laboratory experiments.

**Table 3.4:** Classic zerovariate data for an abj Dynamic Energy Budget (DEB) model, intended for *Loripes orbiculatus* DEB model.

Notation	Description	Unit
$a_b$	Age at birth	d
$a_j$	Age at metamorphosis	d
$a_p$	Age at puberty	d
$a_m$	Age at death (life span)	d
$H_h$	Height at hatching	cm
$H_b$	Height at birth	cm
$H_j$	Height at metamorphosis	cm
$H_p$	Height at puberty	cm
$H_i$	Ultimate height	cm
$Ww_h$	Wet weight at hatching	g
$Ww_b$	Wet weight at birth	g
$Ww_j$	Wet weight at metamorphosis	g
$Ww_p$	Wet weight at puberty	g
$Ww_i$	Ultimate wet weight	g
$Wd_h$	Dry weight at hatching	g
$Wd_b$	Dry weight at birth	g
$Wd_j$	Dry weight at metamorphosis	g
$Wd_p$	Dry weight at puberty	g
$Wd_i$	Ultimate dry weight	g
$R_i$	Maximum reproduction rate	#d <sup>-1</sup>
$Fm$	Maximum filtering rate	cm <sup>2</sup> s <sup>-1</sup>

**Table 3.5:** Novel intended zerovariate data for *Loripes orbiculatus* Dynamic Energy Budget (DEB) model.

Notation	Description	Unit
SO4ovH2S	Yield SO4/H2S	mol/mol
O2ovH2S	Yield O2/H2S	mol/mol
NH4ovH2S	Yield NH4/H2S	mol/mol
BiomovH2S	Yield Biomass/H2S	mol/mol
YSBs	molH2S/C-mol biomass	mol/C-mol
Symbf-Wd	Symbiont contribution to host diet	%
CFarm or Cmilk	Host C from farming or milking	%

**Table 3.6:** Additional univariate data for *Loripes orbiculatus* Dynamic Energy Budget model.

Data Label	Description	Data Unit
vbg-Wdg	Volume bacteria in gills, dry weight gills	-, g
JS-Wd	Sulfur consumption, tissues dry weight	mol/day, g
S-Wd	Gill sulfur content, tissues dry weight	%S, g

### ***Scanning Electron Microscopy (SEM)***

Using SEM on the shell, Prodissoconch I (P1) and Prodissoconch II (P2) can be observed. P1 is the shell secreted by the shell gland of the bivalve larva using its yolk reserve and P2 is the shell secreted by the mantle of the larva feeding from plankton in the water column before its settlement (Taylor & Glover, 2021). P1 and P2 have already been observed for various lucinid species, showing a wide spectrum of P1 and P2 sizes in lucinid, with deeper lucinid generally without visible P2 (Taylor & Glover, 2021). The DEB birth event  $L_b$  (size of the organism when it starts feeding in its environment; i.e. planktotrophy) and  $L_j$  (size of the organism at metamorphosis when the larva settle) can be estimated as the size of P1) and as the size of P1 plus the size of P2 respectively (Table. 3.4).

### ***Histology***

Length at hatching  $L_h$  (Table. 3.4) can be estimated by the maximum size of the oocytes observed by histology of the female gonad coupled with microscopic observation. The maximum reproduction rate  $R_i$  (Table. 3.4) is estimated from the number of oocytes in the gonads of the largest mature individuals, of the maximum size  $L_i$ . The size, wet weight and dry weight of the smallest observed mature individual (i.e., with gametes) gives the size  $L_p$ , wet weight  $Ww_p$  and dry weight  $Wd_p$  of first sexual maturity. Length-reproduction rate L-R and wet/dry weights-reproduction rate can also be determined for sets of organisms, and also Length-Gonadosomatic index (GSI, Eq. 3.3) (Table. 3.4).

$$GSI = \frac{\text{gonadweight}}{\text{totaltissueweight}} 100 \quad (3.3)$$

### ***Spawning induction, reproduction and rearing experiments***

In the laboratory, gamete release (oocytes and spermatozoa) can be induced by triggering mature specimens with a thermal shock (e.g., using ice), osmotic shock (e.g., with potassium chloride KCl), using neurotransmitters (e.g., serotonin) or by mechanical shock (e.g., shaken).

Spawning induction experiments, followed by fertilization and rearing experiments, of tropical symbiotic lucines *Codakia orbicularis* and *Lucinoma aequizonata* have been done to study their embryonic, larval and post-larval development; but also to study the way they acquire their symbionts (Gros et al., 1996; Gros et al., 1999; Gros et al., 1997). The injection of 0.3 ml of 4 mM serotonin into the visceral mass of *Codakia orbicularis*, and of 0.2 ml of 4 mM serotonin into the posterior adductor muscle of *Lucinoma aequizonata* induced spawning. Similar spawning experiments have also been done on species from other bivalve families such as Mytilidae (symbiotic deep-sea mussel *Bathymodiolus childressi* and Veneridae (non-symbiotic tropical *Anomalocardia brasiliiana*) (Arel-lano & Young, 2009; Mouëza et al., 1999). Various stimuli were tested on *Anomalocardia brasiliiana* (temperature fluctuations, osmotic stress and serotonin). For this species, gametes were most often obtained through spontaneous spawning after an intensive diet up to 3,000 algal cells L<sup>-1</sup>. Injection of 0.4-0.5 mL of 2 mmol l<sup>-1</sup> serotonin in the anterior abductor of the deep-sea mussel *Bathymodiolus childressi* successfully induced spawning. Serotonin injection seems to be the most suitable way to induce spawning in *L. orbiculatus*. However, it is possible that the two species do not release gametes when exposed to serotonin as for *Linga pensylvanica* and *Lucina pectinata* during their entire breeding period (Gros et al., 1999). Spawning is induced before removing the tissues from the shell. Data on age at birth ( $a_b$ ), age at metamorphosis ( $a_j$ ) and age at puberty ( $a_p$ ) can be estimated from reproduction and rearing experiments. Reproduction rate can be estimated by counting the number of spawned oocytes, for a range of individual sizes and weights to obtain H-R (height - reproduction rate) and Ww-R (wet weight - reproduction rate).  $R_i$  can also be estimated by the maximum number of oocytes of the largest mature individuals of maximum size ( $L_i$ ), instead of counting oocytes with gonad histology.

#### ***FISH (Fluorescence In Situ Hybridization)***

RNA-probes bind with a fluorochrome targeting specific RNA sequences of sulfur-oxidizing symbionts in gills can be used to quantify the volume

of these bacteria present in the gills (Duperron, 2015). FISH was used in the literature on *L. orbiculatus* gills to study the different symbionts spatial distribution (Osvatic et al., 2021). One of the gill is dried and weighed to obtain its dry weight and the other one is processed for FISH to determine the volume of symbionts within the gill. The volume of bacteria within the gill related to the dry weight of the other gill will be used in the parametrization the DEB model as vbg-Wdg data, as in *C. regab* abj-farming model in Chapter 2 (Table. 3.6).

### ***Chemical element fluxes measurements***

The fluxes of  $O_2$ ,  $CO_2$  and  $H_2S$  can be measured in small individual and hermetic aquaria using suitable probes such as microsensors (Unisense, ltd).  $NH_4^+$  can be measured by titration and using fluorimetry (SOM-LIT protocol). These measurements can be done at the same time as the growth experiment in order to have a variation in food level and temperature. Sufficient specimens should be provided as weighing of the specimens (and therefore dissection) is required here in order to obtain the Ww-JO, Ww-JC, Ww-JN, Wd-JO, Wd-JC and Wd-JN data as a function of food (f) and temperature (T).

### ***Calcein staining***

Calcein is a fluorochrom marker used to stain calcified structures. This stain is notably used to study growth. In bivalves, calcein fluorochroms are incorporated into the new calcifying shell, letting a visible green fluorescent mark by fluorochroms light excitation (excitation peak wavelength at 494 nm). The suitability of calcein staining for bivalves in-situ, in terms of marking success and possible effects on growth performance, has been studied for *L. orbiculatus* (Geest et al., 2019; van der Geest et al., 2011; van Gils et al., 2012). In this study, staining was carried in the field on seagrass directly. Seagrass patches delimited with PVC rings pushed 10 cm into the sediment were immersed with calcein solutions from 100 to 800 mgL<sup>-1</sup> for about 2 hours (time allowed by the tidal cycle). The results of the study suggested an age-dependent effect on

the success of calcein marking because small (i.e., young) lucinids were significantly better marked than larger ones meaning that 2 hours immersion with calcein was insufficient to produce an internal fluorescent mark in the larger lucinids in the field (van der Geest et al., 2011). A minimum growth rate about  $8 \mu\text{m d}^{-1}$  was estimated to obtain a marked in the study conditions cited previously (van der Geest et al., 2011). The t-L growth data can be obtained by using calcein staining and sampling individuals randomly about every three months to observe with a binocular fluorescence magnifier the growth streaks. Growth rate is estimated from the time between the date of staining and date of sampling, and the length between the calcein mark and the shell edge.

#### ***Growth experiment***

L-dL data (i.e., shell size and shell size change (growth)) or t-L (i.e., time and shell length) data as a function of food level (f) and temperature (T), can be measured by varying the food level of several groups of organisms in aquarium at a certain time interval. The temperature could also be varied.

#### ***Sulfur content analysis***

The measurement of the sulfur content of the gills (%S) can be measured with a Carbon/Sulfur analyzer (Cruaud et al., 2019) or mass spectrometry. Mass spectrometry analysis could estimate the nitrogen (%N) and carbon (%C) gill contents at the same time as sulfur to obtain C/N, C/S and N/S ratio of gills.

#### ***Stable isotopes***

Stable isotopes analyses ( $\delta^{13}\text{C}$ ,  $\delta^{15}\text{N}$ ,  $\delta^{34}\text{S}$ ) could also be done as an indicators of nutrient sources (symbiont or/and particulate organic matter (POM)) (Conway et al., 1989; Johnson et al., 1994; Petersen et al., 2016). The percentages of symbiosis (Symbf-Wd) contribution (compared to particulate organic matter) can be obtained by using Bayesian stable isotopes mixing models such as MixSIAR (Stock et al., 2018) on

data of isotopic values of both the possible food sources and the lucinid bivalves.

***“Milked” or “farmed” carbon?: Isotopically marked carbon and TUNEL method***

In chemosymbioses, how much carbon comes from “milking” and from “farming” is not well known, as this is challenging to trace (Sogin et al., 2021; Sogin et al., 2020). As milked carbon has been suggested to be important in *L. orbiculatus* (Yuen et al., 2019), it cannot be bypassed in the model. Some lead to try to quantify, even approximatively, assimilated carbon from farming would be to study the rate of apoptosis of *L. orbiculatus* gill cells as it has been done for mytilid species, deep sea symbiotic ones (*Bathymodiolus azoricus*, *Bathymodiolus puteoserpentis* and *B. aff. boomerang*) and a shallow-water one *Mytilus edulis* using TUNEL method (Transferase dUTP Nick-End Labeling) (Piquet et al., 2019). The deep species mussels showed an higher and highly variable gill cells apoptosis compared to *M. edulis* which is not symbiotic (Piquet et al., 2019). Tracking carbon translocation from the symbionts to the host using labeled  $^{14}\text{C}$  could help to quantify milking (Herry et al., 1989). With autoradiography of organs of *L. orbiculatus* exposed to labeled  $^{14}\text{C}$ , differences in coloration was observed between gills and other organs such as the mantle (Herry et al., 1989). Seasonal analyses of carbon translocation by tissue autoradiography and gill cell apoptosis using TUNEL method, both linked to isotopic analyses of tissues could give new insights into carbon host assimilation of symbiotic carbon. However this would require a consequent amount of work with actual knowledge. Modeling hypotheses could be made on the quantity of milked carbon, and on the preferential use of milked or farmed carbon by setting priority of use, for example. *L. orbiculatus* could use available milked carbon first and farmed carbon as a last resort. Available milked carbon for host could be modeled by setting priority on carbon used; firstly used by symbionts and carbon remains would be available to the host.

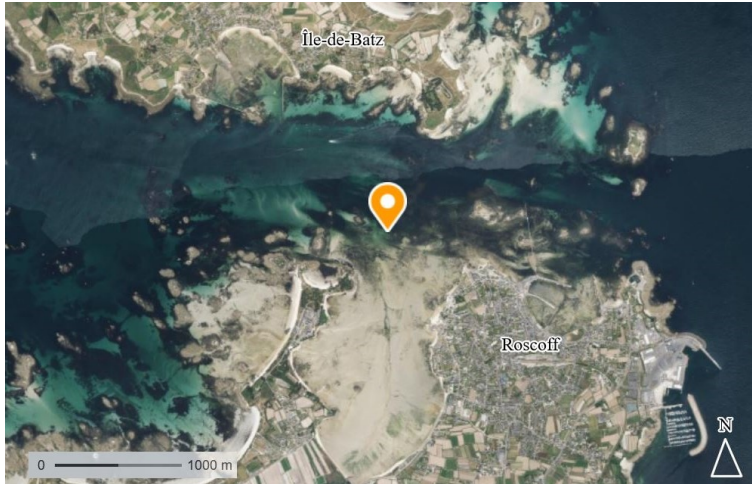


**Figure 3.8:** Lucines sampling site (N 48°43'47.5" W 3°59'50.2"), Roscoff, France (aerial view from 2021; Generated and modified from [geoportail.gouv.fr](http://geoportail.gouv.fr)).

## 3.5 Experiments carried on *L. orbiculatus*

### 3.5.1 Sampling and identification of the collected specimens

Study site (N 48°43'47.5" W 3°59'50.2") is situated on Roscoff foreshore (Western English channel, France) (Fig. 3.9). Lucinid species were sampled near *Z. marina* seagrass beds during high coefficient tide (> 95) in May 2022, between the 15<sup>th</sup> and 20<sup>th</sup>, and in March 2023 between the 20<sup>th</sup> and 25<sup>th</sup> (Table. 3.7). Outside the period of high tide coefficient, it is not possible to access some areas of the seagrass meadows. Sediments near seagrasses where lucines were collected smelt strongly hydrogen sulfide and were black, which is a characteristics of anoxic reduced sediments.

Collected specimens were identified on the day of collection. The three lucinid species, *Loripes orbiculatus*, *Lucinoma borealis* and *Lucinella divaricata* are known to live in sympatry in Roscoff seagrass beds. Collected specimens were observed under a binocular microscope and were morphologically identified and sorted. Inserted ligament of *L. orbiculatus* is internal and not visible from the exterior, whereas it is external

**Table 3.7:** Roscoff tides table on lucinid species sampling days (from mar-ree.info).

Date of sampling	Tide	Coef.	Time	Duration	Height	Tidal range
16/05/2022	Low water		00h59		1.30m	
				05h53		7.61m
	High water	97	06h52		8.91m	
				06h29		7.73m
	Low water		13h21		1.18m	
				05h54		7.84m
High water	99	19h15		9.02m		
18/05/2022	Low water		02h27		1.02m	
				05h54		7.92m
	High water	98	08h21		8.94m	
				06h27		7.66m
	Low water		14h48		1.28m	
				05h53		7.70m
High water	95	20h41		8.98m		
21/03/2023	High water	102	05h52		9.19m	
				06h26		8.42m
	Low water		12h18		0.77m	
				06h02		8.33m
High water	106	18h20		9.10m		

for *L. borealis* and visible from the exterior, as for all the species of the genus *Lucinoma* (Taylor & Glover, 2021). *L. borealis* shell is more sub-circular than *L. orbiculatus* shell, which is more circular. *L. divaricata*, as all the species of the genus *Lucinella*, possesses an internal ligament as *L. orbiculatus*. *L. divaricata* shell presents oblique sculpture (i.e., oblique ornamentation on the outer surface of the shell) in addition to growth increments that distinguishes it to *L. orbiculatus*. No *L. divaricata* specimens were identified, which is not too surprising as their density in Roscoff is very low compared to the two other lucinid species (Ann Andersen personal communication).

**Table 3.8:** Planned analyses on lucinid specimens sampled in Roscoff (Western English channel, France).

Sampling date	Body part	Planned analyses	Variable measured
16 & 18 May 2022	Shell	Biometry	Height (cm)
		SEM	P1 and P2 heights (cm)
	Wet and dry tissues	Biometry	Wet and dry weight (g)
	Gills	Mass spectroscopy	%C, %N, %S
		Biometry	Gills dry weight (g)
FISH		% bacterial volume in gills	
Gonad	Histology	Number of oocyte, size at first maturity	
21 March 2023	Gills	Mass spectroscopy	%C, %N, %S
	Shell	Calcein staining	Growth in height (cm)

### 3.5.2 First sampling period - May 2022 Roscoff

A summary of planned analysis of collected specimens are presented in Table 3.8.

### 3.5.2.1 Biometry, dissection and fixation

29 *L. orbiculatus* and 14 *L. borealis* shell heights were measured using a digital caliper. The shell was opened by sliding inside shell between the 2 valves the tip of a scalpel and cutting the anterior and posterior adductor muscles. The wet body was removed from the shell and weighed to determine the fresh weight. The wet body was then dried in an oven at 60°C for 24 hours and weighted to determine the dry weight. Shells were rinsed with tap water and air dried for SEM analysis.

### 3.5.2.2 Gonad fixation

A range of specimens from different sizes (from 4.5 mm to 13 mm) were selected. The gonad/visceral mass was removed from the body previously weighted and weighted to obtain gonad wet weight. Then, the gonad- visceral mass was fixed and stored in formaldehyde 10% at 4°C.

### 3.5.2.3 Gill fixation, for C/N/S and FISH analyses

Gills of collected specimens were dissected using sterile scalpels immediately on a cold ice plate. For each specimen the first gill was fixed with ethanol 100% for sulfur analysis and the second one was fixed using the protocol from Duperron, 2015. Gills were fixed in 4% formaldehyde in twice filtered (0.22 µm) autoclaved seawater and stored in the fridge at 4 °C for 4 hours. Then, fixative was removed by rinsing twice with twice-filtered seawater and mix by inversion. Tissue were dehydrated in the increasing ethanol series (50%, 70%, 80%, 20 min each). Tissue samples were stored in 80% ethanol at 4°C until FISH analysis.

## 3.5.3 Second sampling period - March 2023 Roscoff

### 3.5.3.1 Biometry, dissection and fixation

Shell sizes and wet weights of collected specimens were measured as during the first period of sampling in May 2022.

### 3.5.3.2 Gills fixation, for C/S

Gills were dissected and freeze-dried for storage. The gills were transported by car with ice packs from Roscoff to the Wimereux marine station.

### 3.5.3.3 Growth experiment

Sediments were collected at the study site for growth experiment, to a maximum depth of 10 cm. Specimens were collected and taken to the laboratory alive. These specimens were transported by car with ice packs and oxygenated with an  $O_2$  pump, from Roscoff to Wimereux marine station.

## 3.5.4 Experimental settling and sample analysis protocols

### 3.5.4.1 Growth experiment with different food levels

**Aquaria settings** 58 specimens of *L. orbiculatus* were acclimated for five days prior the start of the growth experiment. These specimens were transported by car with ice packs to Wimereux marine station. The growth experiment was conducted at Wimereux marine station for 92 days (three months) from March to June 2023. The capacity of each aquarium was of 3 liters (30 cm x 10 cm x 10 cm). Two *L. orbiculatus* aquaria were supplied with an  $Na_2S$  solution, two with a micro-algal solution, two with the  $Na_2S$  solution plus the microalgal solution and one was “starved”. Sediments collected in Roscoff were put in the oven at 121°C for 24h and then sieved (mesh 2 mm diameter) and homogenized by mixing it before distributing about one liter of sediment per aquarium. Sediment was sampled in each aquarium for sulfur analysis to measure the concentration of sulfur in the sediments at the beginning of the experiment. The aquaria were filled with 1.5 liter of twice filtered seawater (filtered once at 0.45  $\mu\text{m}$  then at 0.22  $\mu\text{m}$ ). “ $Na_2S$ ” aquaria were initially seeded with  $Na_2S$  in the sediments (Fig. 3.9).

***Lucines density per aquarium*** Number of lucines per aquarium was determined as a function of the density and biomass observed in the field to avoid being above the carrying capacity which would result in a negative impact on the growth. Density of lucines in each aquarium were chosen not to exceed ten individuals per aquarium with a sediment surface of  $0.03 \text{ m}^2$ , which corresponds to  $300 \text{ individuals m}^{-2}$ , and was below observed density of biomass in the field: mean density of *L. orbiculatus* in Banc d'Arguin, Mauritania was  $16 \text{ individuals m}^{-2}$  in bare sediments and  $339 \text{ individuals m}^{-2}$  in seagrass-covered sediments (Geest et al., 2019). Also *L. orbiculatus* biomass in 1986, 1988 & 2007 was constant, ranging from  $1.1$  to  $2.6 \text{ g ash-free dry weight m}^{-2}$  (Geest et al., 2019). Lucinid biomass was chosen to not exceed the value of  $2.6 \text{ g dry weight gm}^{-2}$  which corresponds to a weight of  $0.078$  for  $0.03 \text{ m}^2$  surface sediment of the aquarium, giving  $0.009 \text{ g}$  as the mean individual dry weight. As dry weight cannot be obtained for living organism, the dry-weight against shell sizes curve obtained with specimens from may 2022 was used (Fig. 3.12b) to determine the mean size of individuals that should not be exceeded which was  $8.5 \text{ mm}$ . The average size of the 58 collected specimens was  $5.8 \text{ mm}$ . Specimens were distributed in each aquarium so that there was a similar size distribution of specimens in each aquarium.

***Preparation of microalgae solution*** To have a concentration similar to the concentration of algae that is in the field, chlorophyll profiles of Roscoff SOMLIT stations ([www.somlit.fr](http://www.somlit.fr)) were used as reference. A peak about  $4 \mu\text{gL}^{-1}$  of chlorophyll a (chl<sub>a</sub>) was observed in may 2022 in Roscoff. An algal mix (Shellfish Diet 1800 Reed Mariculture) of five marine microalgae (*Isochrysis*, *Pavlova*, *Tetraselmis*, *Thalassiosira weissflogii* and *Thalassiosira pseudonana*) of about  $2 \times 10^9$  cells per ml was used to prepare a stock solution of feed the lucines of  $5 \times 10^7$  cells per ml. The feeding consisted in  $5 \text{ mL}$  of the stock solution pipetted into each algae-treated aquaria. As the volume of water in each aquaria was  $2.5 \text{ liter}$ , one feeding resulted in an approximated concentration of  $1 \times 10^5$  cells per mL. *Isochrysis galbana* chlorophyll a is about  $0.4 \text{ pg}$  per cell (Fabregas

et al., 1985; Valenzuela-Espinoza et al., 2002). A concentration equivalent to  $6.66 \mu\text{gL}^{-1}$  was given to feed the lucines *ad libitum*.

**Preparation of  $\text{Na}_2\text{S}$  solution** In long term experiments (> 1 month) in the literature, sulfur was supplied to chemosymbiotic species through different means. Organic matter was added into the sediments with dog food to stimulate sulfide production for the farming of the deep sea vesicomyid clam *Calyptogena okutanii* (Ohishi et al., 2016) and for the rearing of vesicomyid of the genus *Phreagena* (Ikuta et al., 2016). Organic matter sticks input into the sediments were also used in the field to enrich sediment in sulfide, near *L. orbiculatus* specimens (van der Geest et al., 2020). Also direct aqueous  $\text{Na}_2\text{S}$  supply was done, either into the water column for an artificial cold seep systems with vesicomyid *Calyptogena okutanii* specimens (Miyake et al., 2012) or directly into the sediments for the rearing of the polychaete *Capitella* sp. (Tsutsumi et al., 2001). Enriched agar in  $\text{Na}_2\text{S}$  were also added directly into the sediments in tanks in a study on *Z. marina* seagrass (Goodman et al., 1995).

In the Thau Lagoon where organic matter sticks have been used to enrich sediment in sulfide, after 50 days, pore water sulfide have been measured with the addition of organic matter (OM treatment) about  $1170 \mu\text{molL}^{-1}$  and with the addition of organic matter and *L. orbiculatus* at  $716 \mu\text{molL}^{-1}$  (L + OM treatment) for similar densities of lucines ( $3694 \pm 542$  and  $3609 \pm 377$  *L. orbiculatus*  $\text{m}^{-1}$  for OM and L + OM treatments respectively) (van der Geest et al., 2020). To avoid the input of a lethal concentration into the sediments, it was hypothesis that acceptable concentration for the lucines was about  $1170\text{--}716 \mu\text{molL}^{-1}$  for about  $3609$  *L. orbiculatus*, giving  $0.2563 \mu\text{mol}$  per *L. orbiculatus* for 50 days (van der Geest et al., 2020). The number of *L. orbiculatus* per aquarium varied from  $n = 7$  for the control to  $n = 8$  for the other aquaria. The concentration of the solution given to the lucines was set for 7 lucines at  $0.036 \mu\text{mol/L}$  /day.  $0.072 \mu\text{mol}$  was given to lucines about three times a week per aquarium as 5 mL in 5 different points of a prepared solution of  $14.4 \mu\text{M}$  per liter. Sediments for aquaria with sulfur treatments were initially seeded with  $\text{Na}_2\text{S}$  solution before starting the growth ex-

periments. Preparation of the solution, and seeding of sediments was performed under a hood in an inflated-saturated nitrogen box. As  $Na_2S$  is hygroscopic, prepared solution was re-saturated in nitrogen after each feeding.

**Calcein staining** 58 *L. orbiculatus* specimens were exposed overnight for 14h to a calcein (Sigma, CAS 1461-15-0) concentration of  $200 \text{ mg L}^{-1}$  of unfiltered seawater, protected from light with an opaque black sheet around the aquarium. 3 small individuals ( $< 0.5 \text{ cm}$ ) died.

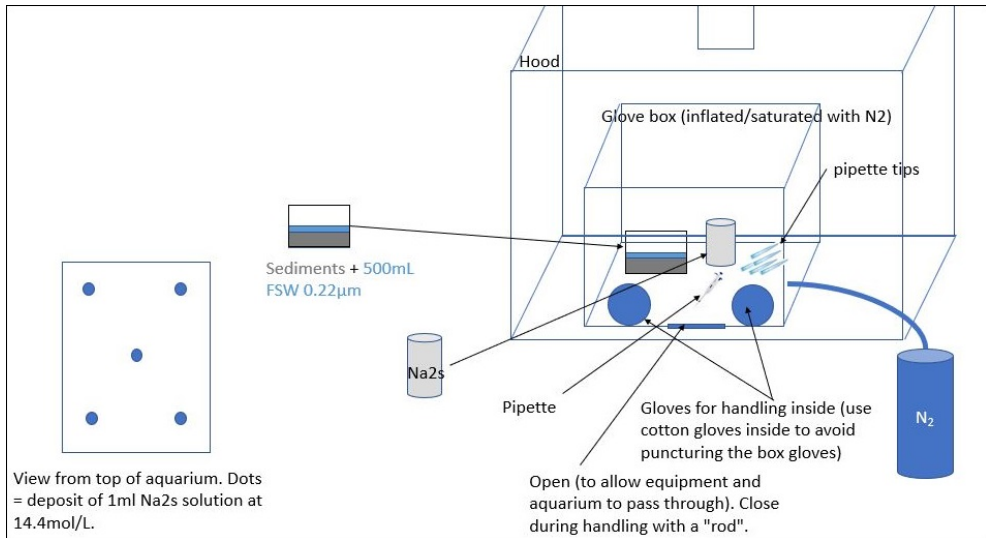


**Figure 3.9:** First input of  $Na_2S$  into the sediments in *L. orbiculatus* growth experiment.

### 3.5.4.2 Fluorescence observation

Calcein marks on shells of the growth experiment were observed with the ZEISS Axio Zoom fluorescence microscope and Zen software (Zeiss) with the help of A. Delagrangé (UMR8187, Wimereux). Calcein excitation peak at 494 nm is at the limit of the 38 HE GFP filter of the Axio Zoom excitation wavelength range (450–490 nm) that was used. Nevertheless, excitation ranges overlapped. Calcein emission peak (517 nm) is included within 38 HE GFP filter emission range (500–550 nm).

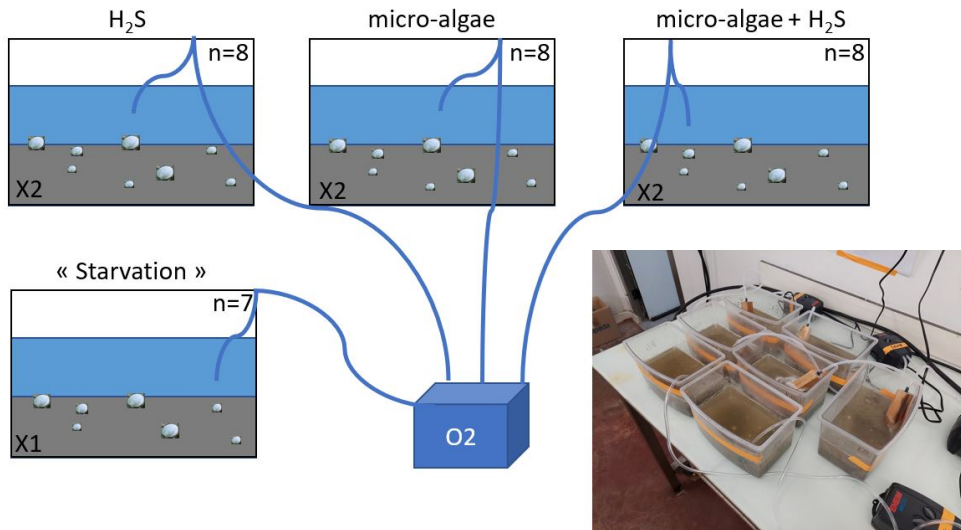


**Figure 3.10:** *Loripes orbiculatus* growth experiment set-up.

### 3.5.4.3 %C, %N and %S determination

Gill content was determined for *L. orbiculatus* and *L. borealis* sampled in May 2022, *L. orbiculatus* and *L. borealis* sampled in March 2023, and *L. orbiculatus* from the growth experiment. Sediment content was also determined for sediment from the growth experiments, at the beginning and at the end of the experiments. Ethanol was removed from May 2022 samples using a pasteur pipette and a 100  $\mu$ l micropipette and frozen samples from March 2023 and June 2023 were thawed. All the samples were dehydrated in the oven for at least 48h at 60°C. Dried gills were weighed on a precision balance on aluminium foils. Grinding to ensure homogenized samples was then carried out with a mortar and pestle to obtain powder. Material was cleaned with ethanol between each samples. Samples were put back into the oven until C/S analysis and at room temperature in a desiccator during samples processing. The Thermo Scientific Flash Smart 2000 analyzer was calibrated with the analytical standard BBOT (2,5-Bis (5-tert-butyl-2-benzo-oxazol-2-yl)), which was closest the closest standard for elemental analysis in content to the gill samples. Two mass standards of 2 and 3 mg were prepared with vanadium pentoxide (O5V2) at 8–10 mg in two pewter

Pods using the method of Krotz and Giazzi (2018). Vanadium pentoxide (CAS: 1314-62-1) was used to detect sulfur present in gills by catalyzing its combustion. 10 mg of Vanadium pentoxide was used as blank in a pewter pod. To determine the optimum amount of gill powder to prepare for chromatography peaks, two *L. orbiculatus* gills from 16/05/22, with a dry weight of 14 mg, were used. A signal was obtained with a weight of 3–4 mg for these 2 samples. The remaining samples were subsequently prepared using the same protocol.

#### 3.5.4.4 Shell observation with SEM

Similar protocol as for the observation of the shell of the deep-sea species *Christineconcha regab* in Chapter 2 was applied. As lucines are small in sizes, shells were fixed directly on SEM stubs, the exterior of the shell against the stub. The surface of shells was coated with gold-palladium with a sputter-coater to make it conductive. Argon was used as sputter gas. Samples preparation and micrographs were realized with the help of L. Courcot (UMR8187 LOG, Wimereux).

#### 3.5.4.5 Histology of the female gonads

Gonads of *Loripes orbiculatus* (n = 12) and of *Lucinoma borealis* (n = 5) were dehydrated in an ethanol series (70–100%), cleared in Diasolv and impregnated in paraffin. Each sample was then embedded in paraffin, sectioned at 7 µm using a microtome (Leica Ltd.), and stained with Hematoxylin and Eosin (Mammone et al., 2020) using the Leica Biosystems – HistoCore SPECTRA ST. Histological sections were examined under a microscope (Axioscope 5, Zeiss Ltd.) equipped with the Zen software (Zeiss Ltd.).

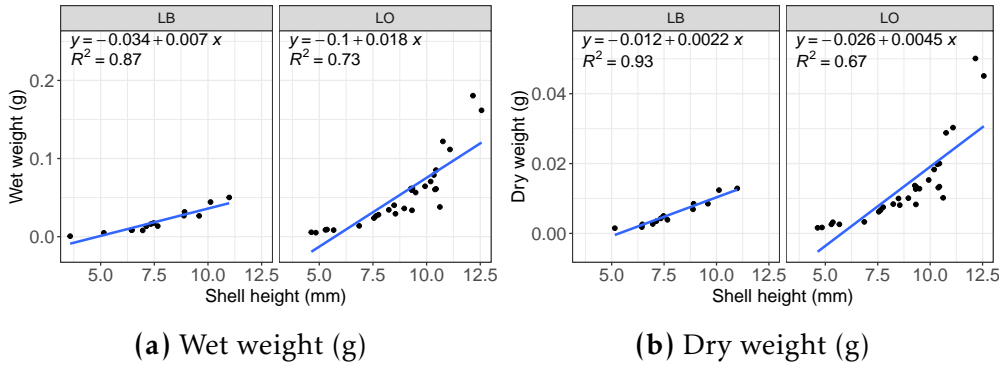


**Figure 3.11:** Weights and shell heights of lucines sampled in May 2022 in Roscoff, France. LO, *Loripes orbiculatus*; LB, *Lucinoma borealis*.

## 3.6 Results and discussion

### 3.6.1 Length-weight data

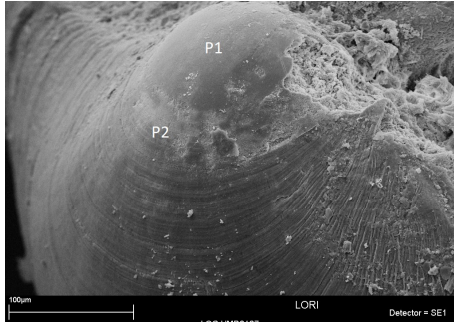
Length-weight data (Fig. 3.12) are useful to parameterize the shape coefficient ( $\delta_M$ ) which is a parameter of DEB models.  $\delta_M$  is used to predict the weight in function of the length or height (Eqs. 3.4 and 3.5). The shape coefficient converts the measured length ( $L_{physical}$ ), or height in the case of lucinid bivalves ( $H_{physical}$ ), to the DEB concept of structural length (L):  $L = \delta_M L_{physical}$  (Kooijman, 2010).

$$Ww_{physical} = (H_{physical}\delta_M)^3(1 + f\omega) \quad (3.4)$$

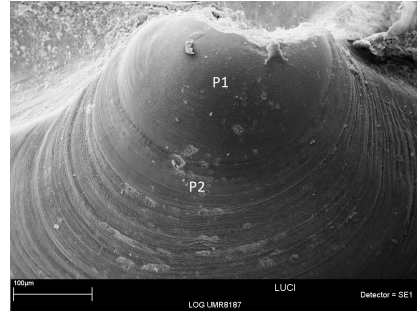
**Equation 3.4:** Lucines wet weight prediction with DEB theory.  $Ww_{physical}$ , measured wet weight;  $H_{physical}$ , measured shell height;  $\delta_M$ , shape factor (-);  $f$ , functional response (-);  $\omega$ , contribution of dry mass of reserve to total dry biomass (i.e., total = reserve + structure) (-);  $d_V$ , specific density of dry mass ( $\text{g cm}^{-3}$ ).

$$Wd_{physical} = (H_{physical}\delta_M)^3(1 + f\omega)d_V \quad (3.5)$$

**Equation 3.5:** Lucines dry weight prediction with DEB theory.  $Wd_{physical}$ , measured dry weight;  $H_{physical}$ , measured shell height;  $\delta_M$ , shape factor (-);  $f$ , functional response (-);  $\omega$ , contribution of dry mass of reserve to total dry biomass (i.e., total = reserve + structure) (-); dry mass ( $\text{g cm}^{-3}$ ).



(a) *Loripes orbiculatus*



(b) *Lucinoma borealis*

**Figure 3.12:** Scanning electron microscopy micrograph of two lucinid species, *Loripes orbiculatus* and *Lucinoma borealis*, from Roscoff, France.. P1, Prodissoconch I; P2, prodissoconch II. Images obtained with the help of Lucie Courcot (UMR8187 LOG).

In Chapter 2,  $\delta_M$  for *C. regab* deep-sea vesicomyid species was estimated to 0.2637 and to 0.0651 with abj and abj-farming model, respectively.

### 3.6.2 Length at birth and length at metamorphosis

*L. orbiculatus* and *L. borealis* shells were observed using a scanning electron microscope (SEM) (Fig. 3.12).  $L_b$ , estimated at mean measured P1, was 152  $\mu\text{m}$  for *L. orbiculatus* ( $n = 10$ ) and 167  $\mu\text{m}$  for *L. borealis* ( $n = 7$ ).  $L_j$ , estimated with mean measured P1+P2, was 212  $\mu\text{m}$  for *L. borealis* and 231  $\mu\text{m}$  for *L. orbiculatus*. Lucines shells are fragile and were damaged during the manipulations (Fig. 3.12).

### 3.6.3 Length at puberty and reproduction rate

Out of the 12 specimens of *L. orbiculatus* observed on histological sections, most of the female gonads observed had oocytes in an advanced stage of gametogenesis where oocytes diameters were  $122.4 \pm 7.8 \mu\text{m}$  ( $n = 5$ ) (Fig. 3.13). Some females spawned spontaneously overnight in the laboratory after the day of collection. Specimens of shell height below 5 mm had undifferentiated germinal cells or gonidia under division in the gonad. Only the smallest female of a

size of 6.75 mm was carrying visible acinus with oogonia in division and could be considered as the length at puberty for females *L. orbiculatus*. Females *L. orbiculatus* from 8.4 mm to 13.1 mm in shell height ( $n = 7$ ) had oocytes in the gonad. The number of oocytes following the size (R – L) could be estimated in these specimens by using the same method used for *Christineconcha regab* in Chapter 2. This work was planned but not conducted unfortunately.

In Brest (Brittany, France), oocyte sizes were observed throughout one year, from September 1991 to September 1992 (Johnson & Pennec, 1994). In June all *L. orbiculatus* had spawned as no oocytes were observed in the gonad anymore (Johnson & Pennec, 1994). Oocyte sizes ranged from 14 to 95  $\mu\text{m}$  in diameter (Johnson & Pennec, 1994). Average oocyte sizes increased from September October, was lower in December, and increased again until May where larger oocyte sizes were observed (Johnson & Pennec, 1994). Rather large oocyte (about 120  $\mu\text{m}$ ) were observed in *L. orbiculatus* from Roscoff suggesting a lecithotrophic larval development (Fig. 3.13).

*L. orbiculatus* oocytes were surrounded by a protective “jelly” (Fig. 3.13). This “jelly” has been observed in other lucinid species, surrounding mature oocyte and spawned eggs (Bigatti et al., 2004; Gros et al., 1997).

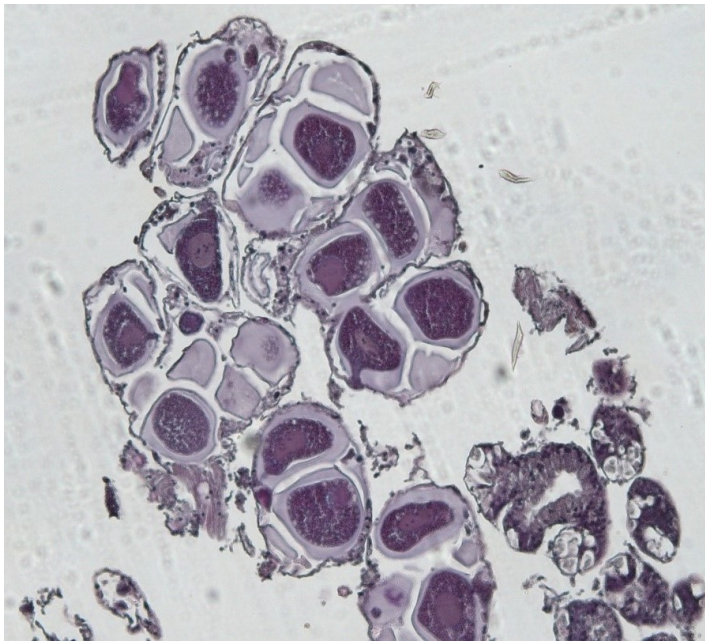


**Figure 3.13:** *Loripes orbiculatus* oocytes (Roscoff, France).

### 3.6.4 Growth of *Loripes orbiculatus*

The exposition of calcein concentration of  $800 \text{ mgL}^{-1}$  for 14 hours might have been lethal for small lucinid specimens as only small ones died overnight ( $n = 3$ ). Calcein marks were observed on shells (Fig. 3.15) but not as a clear marked as in image from the literature in (van der Geest et al., 2011; van Gils et al., 2012). Here the shells were not clean using  $\text{H}_2\text{O}_2$  to remove the periostracum (most external shell organic coating). Therefore some autofluorescence of chlorophyll pigments of microalgae deposited on shells might have hidden the signal. Even if excitation wavelength covered the range of excitation of calcein, the excitation not at the excitation peak of calcein could have resulted in a lower fluorescent mark.

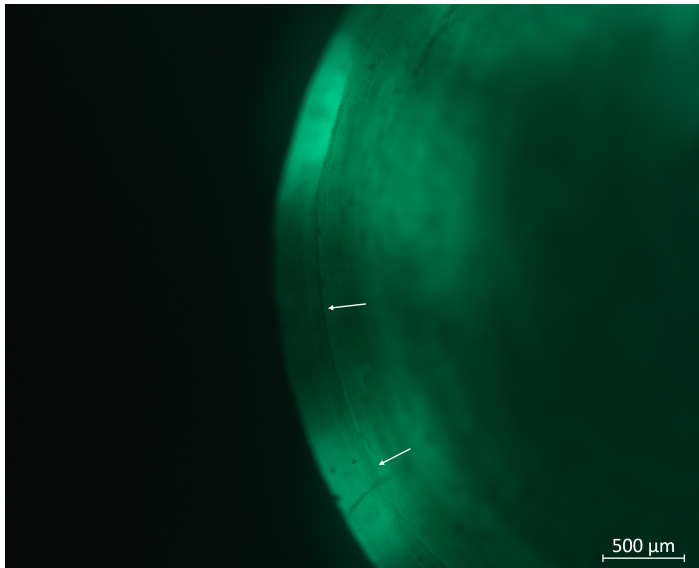


**Figure 3.14:** Calcein mark on *Loripes orbiculatus* shell observed by fluorescence. Arrows show calcein mark.

Growth of *L. orbiculatus* specimens per treatment were compared by fitting a von Bertalanffy growth curve to each treatment to estimate the growth rate coefficient  $k$  ( $\text{d}^{-1}$ ) and the maximum size  $J_\infty$  (cm) using matlab function *fminsearch*. von Bertalanffy Growth function was defined as in tag-recapture studies (Eq. 3.6) (Geest et al., 2019).

$$\Delta H = H_2 - H_1 = (H_\infty - H_1)(1 - \exp(-k\Delta t)) \quad (3.6)$$

**Equation 3.6:** Growth in shell height expressed with von Bertalanffy Growth

function for tag-recapture method.  $\Delta H =$  , growth in shell height;  $H_1$ , initial the shell height;  $H_2$ , shell height at recapture;  $H_\infty$ , maximum height reachable in given conditions;  $\Delta t$ , the duration between the measures  $H_1$  and  $H_2$  which is 92 days in *Loripes orbiculatus* growth experiment.

Fits to experimental data per treatment are represented in Fig. 3.15. Growth was observed to be lower for larger specimens compared to smaller ones as expected (Fig. 3.15, Tables 3.12 and 3.13).  $H_\infty$  was estimated in the highest for  $Na_2S$  treatment and microalgae treatment and the lowest for starvation treatment (Table 3.9).  $k$  growth coefficient was estimated to be the lowest for  $Na_2S$  treatment and the highest for starvation treatment. Growth curves for each treatment were modeled using estimated parameters  $H_\infty$  and  $k$  growth coefficient per treatment, and estimated in *L. orbiculatus* capture-recapture experiment in the field in Banc d'Arguin, Mauritania (Geest et al., 2019) for 10.000 days (27 years), until the estimated ultimate height was reached in each treatment. Growth from the field in Mauritania was quicker, than *L. orbiculatus* from the growth experiment and this might be due to the stressful condition of being in the laboratory and not in the field. 27 years is a bit of a long time for them to reach their maximum height compared to estimate life span of bivalves, and they might die before. Mauritania's is situated in tropical latitude while France in temperate latitude, temperature is higher in Mauritania and thus we could expect a higher growth rate of *L. orbiculatus* in Mauritania.

**Table 3.9:** Estimated  $H_\infty$  (cm) and  $k$  coefficient of von Bertalanffy growth function per *Loripes orbiculatus* treatment.  $n$ , number of *L. orbiculatus* per treatments.

treatment	$H_\infty$ ( $\mu\text{m}$ )	$k$ ( $\text{d}^{-1}$ )	$n$
microalgae	1.4328e+04	3.4655e-04	16
$Na_2S$	1.4904e+04	2.4755e-04	15
microalgae- $Na_2S$	1.2575e+04	3.2379e-04	13
starvation	1.0506e+04	3.8993e-04	5

### 3.6.5 Elemental contents analyses from field sampling

#### 3.6.5.1 Gill elemental content

Normality and homoscedasticity were tested using Shapiro-Wilk and Leven tests, respectively. As samples did not follow a normal distribution, Kruskal-Wallis non-parametric test was applied, and in cases of significant difference,

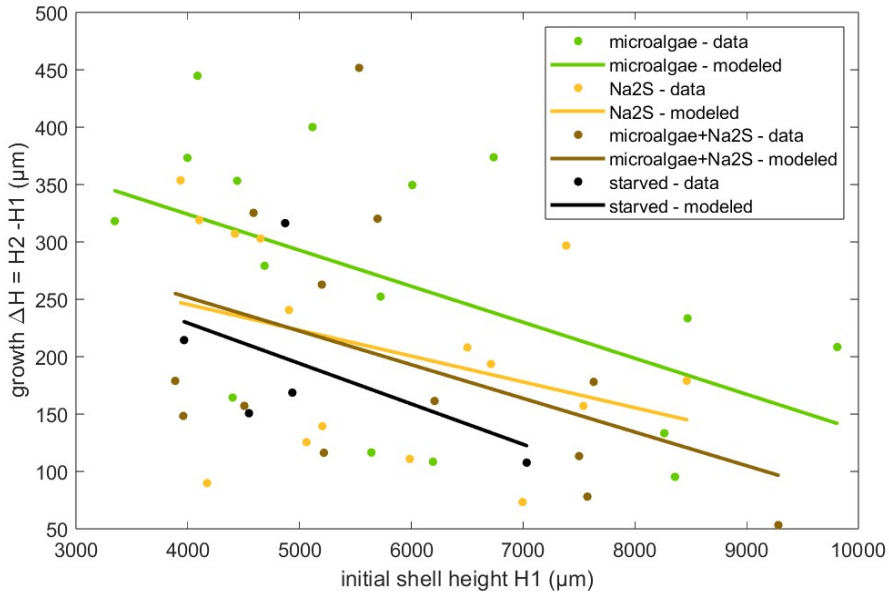


**Figure 3.15:** Measured and modeled growth with von Bertalanffy growth function of *Loripes orbiculatus* for each treatments.

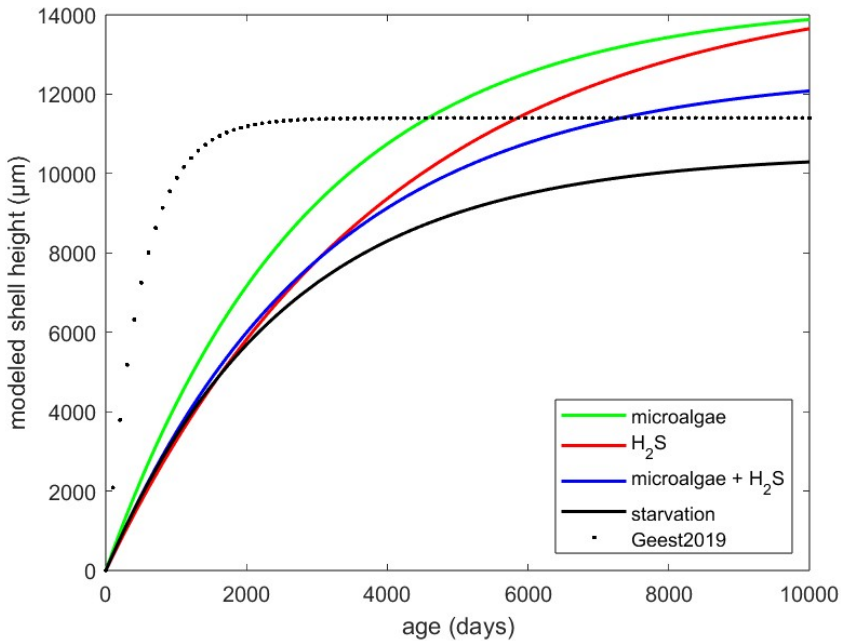


**Figure 3.16:** Modeled growth of *Loripes orbiculatus* with von Bertalanffy growth function in each treatment condition and in Banc d'Arguin, Mauritania ( $k = 0.002$  and  $H_{\infty} = 11.4$  cm (Geest et al., 2019)).

post-hoc pairwise Dunn test, with Bonferroni correction was used. Statistical tests were run using R using R-Studio interface.

**Table 3.10:** Biometry and gill chemical elements composition of *Loripes orbiculatus* lucines from Roscoff (France). H, shell height (mm); DW, dry weight (g); N, nitrogen; C, carbon; S, sulfur.

	H (mm)	gill DW (g)	% N	% C	% S	C/N	C/S	N/S
LO23	14.09	0.038	8.46	41.87	2.92	4.95	14.36	2.90
n=12	13.94	0.021	8.30	41.87	2.72	5.05	15.37	3.05
	13.65	0.039	6.23	38.43	4.16	6.17	9.23	1.50
	12.14	0.023	6.92	41.90	4.19	6.05	10.01	1.65
	12.05	0.021	7.27	45.69	4.90	6.28	9.33	1.49
	13.62	0.021	7.91	40.11	3.33	5.07	12.04	2.37
	12.43	0.012	8.60	40.92	2.48	4.76	16.48	3.46
	12.04	0.017	7.49	40.10	3.66	5.35	10.95	2.05
	10.76	0.010	8.77	40.91	2.69	4.66	15.20	3.26
	12.42	0.014	9.11	41.69	2.44	4.58	17.08	3.73
	11.11	0.026	5.95	38.19	4.62	6.42	8.27	1.29
	12.41	0.019	8.90	47.03	2.32	5.29	20.23	3.83
LO22	13.09	0.014	6.31	36.11	4.52	5.72	7.99	1.40
n=17	11.33	0.004	6.60	38.63	4.23	5.85	9.12	1.56
	11.5	0.005	9.33	39.48	2.28	4.23	17.32	4.09
	12.34	0.010	10.90	43.14	2.07	3.96	20.87	5.27
	10.59	0.010	7.13	39.25	3.69	5.50	10.63	1.93
	11.11	0.010	6.57	37.86	4.00	5.76	9.46	1.64
	11.61	0.003	7.09	38.72	3.94	5.46	9.82	1.80
	11.93	0.015	10.64	41.78	1.93	3.93	21.60	5.50
	5.07	0.002				not measured		
	4.54	0.001				not measured		
	5.34	0.001				not measured		
	8.77	0.002	8.54	39.57	1.99	4.63	19.89	4.29
	8.39	0.002	8.77	41.13	1.50	4.69	27.35	5.83
	8.45	0.002	9.67	40.62	1.77	4.20	22.97	5.47
	9.91	0.010	6.31	37.67	4.50	5.97	8.36	1.40
	6.75	0.001	8.70	40.86	1.61	4.69	25.32	5.39
	10.74	0.004	9.70	41.51	1.80	4.28	23.04	5.39

**Gill carbon content (%C)** *Lucinoma borealis* gills content %C was significantly lower in March 2023 compared to May 2022 (p-value adjusted < 0.01) (Fig. 3.17a, statistics Table 3.14, individual details Table 3.10). *Loripes orbiculatus* gills %C was not significantly different between May 2022 and March 2023, but was significantly lower than %C of *L. borealis* from March 2023 (p-value

**Table 3.11:** Biometry and gill chemical elements composition of *Lucinoma borealis* lucines from Roscoff (France). H, shell height (mm); DW, dry weight (g); N, nitrogen; C, carbon; S, sulfur. LB23, *L. borealis* collected in March 2023; LO22 *L. borealis* collected in May 2022; n, number of specimens.

	H (mm)	gill DW (g)	% N	% C	% S	C/N	C/S	N/S
LB23	8.9	0.004	7.24	38.72	1.24	5.35	31.13	5.82
n=10	7.92	0.004	8.28	37.41	1.25	4.52	30.02	6.64
	7.31	0.004	6.65	35.38	1.03	5.32	34.32	6.45
	8.24	0.005	6.72	35.72	1.61	5.32	22.13	4.16
	7.41	0.002			not measured			
	6.7	0.002			not measured			
	7.92	0.003	6.36	32.52	2.26	5.11	14.38	2.81
	7.39	0.003			not measured			
	6.32	0.001			not measured			
	6.72	0.003	7.07	35.95	1.59	5.09	22.60	4.44
LB22	10.29	0.009	7.79	40.81	3.20	5.24	12.74	2.43
n=7	10.13	0.003	8.18	41.27	1.46	5.05	28.25	5.60
	9.23	0.002	8.26	39.57	1.59	4.79	24.87	5.19
	6.81	0.001			not measured			
	4.93	0.000	7.92	39.01	1.23	4.92	31.59	6.42
	26.39	0.029	12.49	61.34	1.02	4.91	60.35	12.28
	26.39	0.051	10.16	43.65	2.15	4.30	20.30	4.72

**Table 3.12:** Measured growths and chemical elements composition of *Loripes orbiculatus*' gills from growth experiment (1/2). Trt., treatment;  $H_2$ , shell height at the end of the growth experiment ( $\mu\text{m}$ );  $\Delta H$ ,  $H_1 - H_2$  where  $H_2$  is the shell height ( $\mu\text{m}$ ) at the beginning of the growth experiment marked by calcein staining; N, nitrogen; C, Carbon; S, Sulfur.

Trt.	$H_2$ ( $\mu\text{m}$ )	$\Delta H$ ( $\mu\text{m}$ )	% N	% C	% S	C/N	C/S	N/S
starv. n=7	7140	108	9.15	37.62	2.43	4.11	15.51	3.77
	5104	169	7.52	34.57	2.81	4.60	12.31	2.68
	5188	316	9.91	45.28	3.53	4.57	12.82	2.81
	4698	151				not measured		
	4181	214	7.42	30.51	3.74	4.11	8.16	1.98
2 deaths during the experiment								
$\mu\text{A}$ 1 n=8	8454	95	9.68	46.93	4.68	4.85	10.04	2.07
	7110	374	7.81	33.82	2.31	4.33	14.64	3.38
	5759	116	6.86	35.26	3.75	5.14	9.40	1.83
	5977	252	7.32	32.32	2.46	4.41	13.16	2.98
	4532	445	10.11	43.69	5.09	4.32	8.59	1.99
	4966	279	4.88	22.31	2.11	4.57	10.56	2.31
	3665	318				not measured		
	10019	208				not measured		
$\mu\text{A}$ 2 n=8	8396	133	9.27	39.70	2.67	4.28	14.85	3.47
	8705	233	8.66	38.15	2.36	4.40	16.14	3.67
	6302	108	8.61	36.41	2.72	4.23	13.41	3.17
	5516	400	10.88	48.18	2.90	4.43	16.64	3.76
	6358	349	7.61	32.66	2.25	4.29	14.53	3.38
	4795	353	2.08	8.79	0.67	4.23	13.18	3.12
	4565	164	8.32	36.84	2.95	4.42	12.48	2.82
	4370	373	7.49	33.53	2.26	4.48	14.86	3.32
$H_2S$ 1 n=8	8643	179	9.29	49.48	4.95	5.32	9.99	1.88
	7068	73	8.22	36.06	2.32	4.39	15.55	3.54
	6710	208	8.96	37.96	14.00	4.24	2.71	0.64
	6906	194	8.87	36.80	2.66	4.15	13.83	3.33
	4953	303	7.63	33.63	2.68	4.40	12.53	2.84
	4729	307	7.25	32.71	2.62	4.51	12.49	2.77
	4422	319				not measured		
	4262	90				not measured		
$H_2S$ 2 n=8	7682	297	8.35	37.10	2.33	4.44	15.93	3.58
	7697	157	7.68	35.46	2.68	4.62	13.24	2.87
	6097	111	11.78	50.42	3.29	4.28	15.33	3.58
	5188	125	7.82	34.79	2.29	4.45	15.17	3.41
	5344	139	8.37	34.76	2.43	4.15	14.29	3.44
	4289	354	8.59	32.85	2.90	3.82	11.34	2.97
	5146	241	8.61	31.44	6.86	3.65	4.59	1.26
a death during the experiment								

**Table 3.13:** Measured growths and chemical elements composition of *Loripes orbiculatus*'gills from growth experiment (2/2). Trt., treatment; H2, shell height at the end of the growth experiment ( $\mu\text{m}$ );  $\Delta\text{H}$ , H1-H2 where H2 is the shell height ( $\mu\text{m}$ ) at the beginning of the growth experiment marked by calcein staining; N, nitrogen; C, Carbon; S, Sulfur.

Trt.	H2 ( $\mu\text{m}$ )	$\Delta\text{H}$ ( $\mu\text{m}$ )	% N	% C	% S	C/N	C/S	N/S
$\mu\text{A-H}_2\text{S 1}$	9337	53	9,36	40,14	2,51	4,29	15,98	3,73
n=8	7653	78	8.61	36.84	1.01	4.28	36.59	8.55
	6369	161	8.02	33.18	2.12	4.14	15.69	3.79
	5462	263	7.58	33.61	2.30	4.43	14.63	3.30
	6018	320	8.34	34.49	2.30	4.14	15.01	3.63
	4663	157				not measured		
	4913	325	3.18	19.57	1.14	6.15	17.11	2.78
	4108	148	8.52	32,55	3.32	3.82	9.79	2.56
$\mu\text{A-H}_2\text{S 2}$	7809	178	8.59	36.11	2.40	4.20	15.01	3.57
n=8	7614	113	7.70	35.59	3.38	4.62	10.53	2.28
	5985	452	10.81	48.93	3.02	4.53	16.21	3.58
	5334	116				not measured		
	4066	179	9.36	36.24	6.12	3.87	5.92	1.53
3 deaths during the experiment								

adjusted  $< 0.05$ ) (Fig. 3.17a, statistics Table 3.14, specimen individual details Tables 3.10 and 3.11 for *L. orbiculatus* and *L. borealis*, respectively).

**Gill nitrogen content (%N)** Nitrogen content (%N) seemed to be lower in March 2024 compared to May 2022, however there were no significant differences between the two months of sampling, and between species (p-values adjusted  $> 0.05$ ) (Fig. 3.17b, statistics Table 3.14, specimen individual details Tables 3.10 and 3.11 for *L. orbiculatus* and *L. borealis*, respectively).

**Gill C/N** Gill C/N seemed to be higher in March 2024 compared to May 2022, however there were no significant differences between the two months of sampling, and between species (p-values adjusted  $> 0.05$ ) (Fig. 3.18a, statistics Table 3.14, specimen individual details Tables 3.10 and 3.11 for *L. orbiculatus* and *L. borealis*, respectively).

*L. orbiculatus* C/N ratio of live specimens from Italia (Mediterranea Sea) were about 3.2 in June 2010 Sicily and 3.1 in Venice in April 2011 (Dreier et al., 2012). Mean C/N ratio of *L. orbiculatus* from both May and March 2023 are observed higher than those from Italia (4.92 and 5.39, mean C/N ratios from *L. orbiculatus* gill collected in May 2022 and March 2023, respectively).

**Gill S (%S), C/S and N/S** 2022 and 2023 *Loripes orbiculatus* gill sulfur content (%S) were significantly higher than *Lucinoma borealis* gills from May 2022 (p-values adjusted <0.05) (Fig. 3.17c, statistics Table 3.14, specimen individual details Tables 3.10). Consequently, C/S and N/S from 2022 and 2023 *Loripes orbiculatus* gill were significantly lower than *Lucinoma borealis* gills from May 2022 (p-values adjusted < 0.05) (Fig. 3.18b and c, statistics Table 3.14, specimen individual details Tables 3.10 and 3.11 for *L. orbiculatus* and *L. borealis*, respectively). There were no intraspecies significant differences between months (p-values adjusted > 0.05).

Sulfur percentages of *L. orbiculatus* specimens from two mauritanian sites were in between 2 and 3.2% which is similar to *L. orbiculatus* gill sulfur percentage from Roscoff (France) in our study (Oortwijn et al., 2022).

*Loripes orbiculatus* and *Lucinoma borealis* were collected at the same location, and thus are exposed to the same abiotic conditions, these results might highlight interspecies differences in terms of sulfur processing. These interspecies differences could be due to their symbiont populations, in terms of symbiont metabolism or/and symbiont quantity. *L. borealis* was found in lower quantity at the sampling sites compared to *L. orbiculatus* and might not be as well adapted as *L. orbiculatus* to the seagrass sulfidic conditions. Sulfide in the sediment on the field is not distributed homogeneously and *L. borealis* could be living in area with less concentrated in sulfide while *L. orbiculatus* in area more concentrated sulfide, accumulating more sulfur.

In Mauritania, *L. orbiculatus* from two different locations presented variation in percentage of total sulfur (Oortwijn et al., 2022). In our study, *L. orbiculatus* gills also presented variations of S percentage, although not significant, with a mean concentration higher in March 2023 than May 2022.

In Mill Bay, England, elemental gill sulfur contents of *L. borealis* from near *Zostera marina* beds varied greatly seasonally, unlike what is observed in our study (Dando et al., 1986). The lowest *L. borealis* gill sulfur concentrations were measured in February and April ( $9.4 \pm 3.2$  and  $12.1 \pm 1.4$  g atoms of S  $\text{g}^{-1}$  of gill fresh mass), when the sediment concentration were lower than in October ( $0.2$  mg atoms  $\text{dm}^{-3}$  in February) (Dando et al., 1986). The highest concentrations were measured in October ( $68.1 \pm 23.7$  g atom of S  $\text{g}^{-1}$  of gill fresh mass), which coincided with a peak of sulfur concentration in sediment in October ( $4$  mg of S atom  $\text{dm}^{-3}$  of sediment) (Dando et al., 1986). Degradation of the seagrasses is known to increase sulfide production in the sediments (Dando et al., 1986). Fluctuation of environmental sulfide concentration and consequently, a lower concentration in the environment was suggested to con-

trol sulfide intrusion in *L. orbiculatus* (Dando et al., 1986).

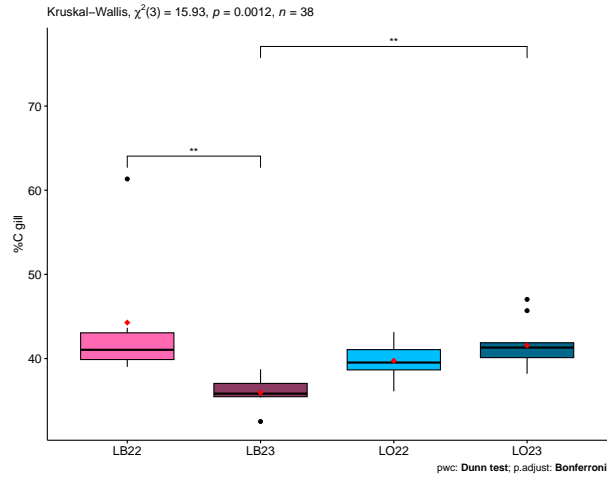
In Roscoff, a chlorophyll peak happens in May ([www.somlit.fr/](http://www.somlit.fr/)). Mean gill sulfur percentage of *L. orbiculatus* is observed higher in March 2023 than in May 2022 where chlorophyll is at its peak (SOMLIT Roscoff: chlo a between 1.5 and 4  $\mu\text{g/L}$  in May 2022; between 0.60 and 0.70  $\mu\text{g/L}$  in March 2023). If internal lucines gill sulfur concentration was only reflecting external sulfide concentration, the gill sulfur concentration should be higher in May than in March because of higher organic matter deposition and decay which causes an increase of sediment sulfide, or it is not what was observed.

*L. orbiculatus* reproduction period occurs in May in Roscoff (personal observation). During *L. orbiculatus* reproduction period, it was observed that gill lysis was increased together with gamete development, suggesting the lysis provides energy for *L. orbiculatus* gametogenesis (Johnson & Fernandez, 2001).

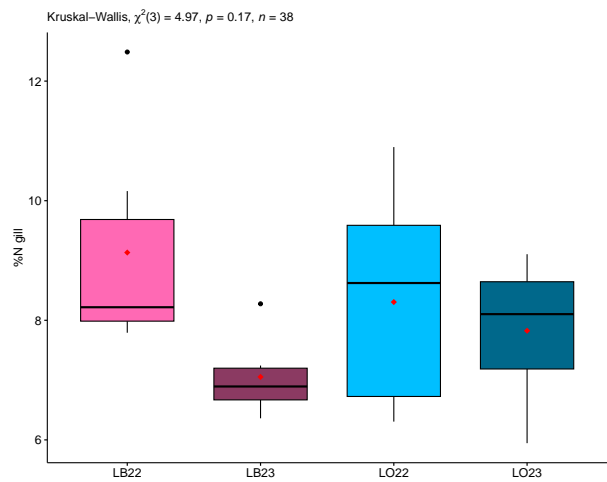
The abj-farming model of the deep-sea species *Christineconcha regab* in Chapter 2 suggested that symbiont consumed more sulfide when the host feed more. Under host predation pressure, symbionts might consume more sulfide, that could result in a lower sulfide concentration within its host, as it is observed for *L. orbiculatus* gills May 2022 and March 2023. Still, more observations are needed to validate this hypothesis as observations were done on small sample populations and the differences were not statistically different.

Sulfur gill percentage quantified by mass spectrometry may include different-sulfur forms, available for the symbionts, such as free circulating ionic forms (e.g., thiosulfate, an intermediate of symbiont sulfide oxydation pathways) and elemental forms (e.g., elemental S observed as granules). This available sulfide can be used to approximate a sulfur reserve for the symbiont in the dynamic energy model. Sulfur is also known to play an essential role in amino acid metabolism (e.g., cystein) (Allen, 1961) and DNA repair (Lukianova & David, 2005). This sulfur is also measured by the mass spectrometer but not available for the symbiont. This sulfur “background” concentration could be determined with sulfide starved specimens.

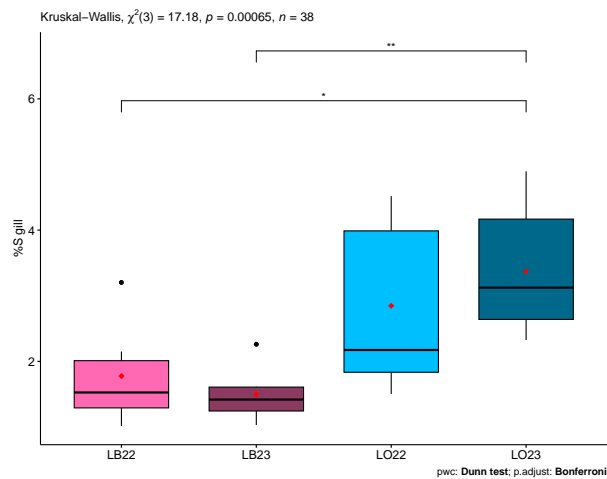
Sampling monthly and comparing the density of sulfur granules formed along the year, using Scanning Electron Microscopy, and to relate it to symbiont density, determined using fluorescence hybridization *in-situ*, and surveying at the same time dissolved organic matter in sea-water would give insight into *L. orbiculatus* and *L. borealis* strategies to deal with seagrasses toxic sulfidic conditions and their shift in food source, from symbiotic to organic matter filterfeeding, along the year.



(a)

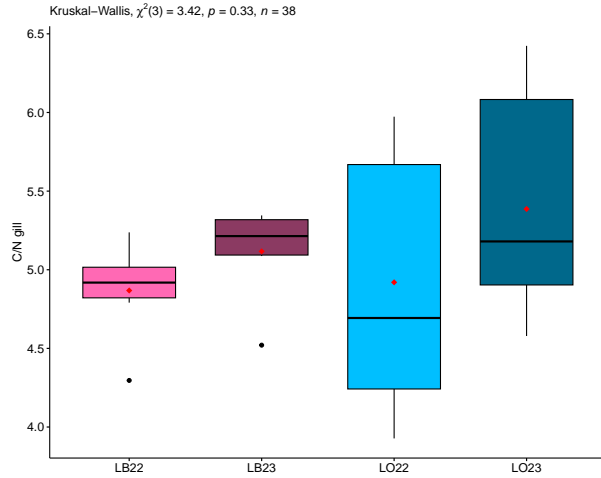


(b)

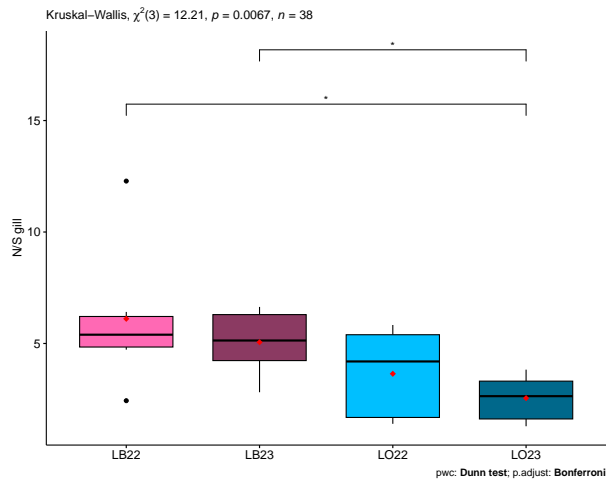


(c)

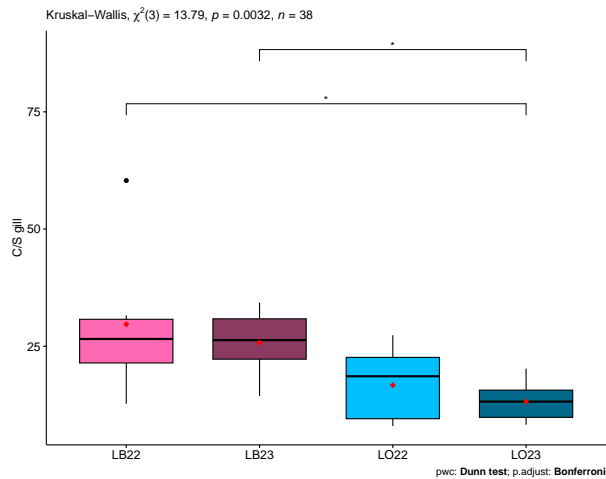
**Figure 3.17:** Carbon, nitrogen and sulfide content of Roscoff lucines gills from the field. LB, *Lucinoma borealis*; LO, *Loripes orbiculatus*; 22, sampled in May 2022; 23, sampled in March 2023.



(a)



(b)



(c)

**Figure 3.18:** C/N, N/S and C/S ratio of Roscoff lucines' gills from the field. LO, *Loripes orbiculatus*; 22, sampled in May 2022; 23, sampled in March 2023.

**Table 3.14:** Statistics on *Loripes orbiculatus* gill elemental composition (carbon, nitrogen and sulfide) from Roscoff. p-value: \*, < 0.05; \*\*, < 0.01.

	%S	%C	%N	C/S	C/N	N/S
<b>Test of normality: Shapiro-Wilk</b>						
LB22	0.278	0.00269**	0.0341*	0.203	0.422	0.174
LB23	0.379	0.773	0.335	0.646	0.0306*	0.537
LO22	0.00868**	0.998	0.146	0.0403*	0.0652	0.00407**
LO23	0.169	0.103	0.328	0.509	0.108	0.203
<b>Test of homoscedasticity: Levene</b>						
All	0.1492	0.2816	0.2231	0.08783	0.03787*	0.1903
<b>Test of comparison: Kruskal-Wallis</b>						
All	0.000649***	0.00117**	0.174	0.00321**	0.331	0.00669**
<b>Tests post-hoc: Dunn, Bonferroni p-values adjusted</b>						
LB22 LB23	1	0.00700**		1		1
LB22 LO22	0.237	0.968		0.206		0.461
LB22 LO23	0.0120*	1		0.0207*		0.0239*
LB23 LO22	0.0767	0.0878		0.191		0.561
LB23 LO23	0.00269**	0.00127**		0.0188*		0.0317*
LO22 LO23	1	0.558		1		0.858

### 3.6.6 Gill and sediment elemental content from growth experiment

#### 3.6.6.1 Sediment elemental content

After 92 days, an overall enrichment of sediment content in carbon, nitrogen and sulfur was observed within all treatments (Figs. 3.19a, b, d). The enrichment in carbon was higher at the sediment surface than at the bottom- in all treatments (Fig. 3.19a). Nitrogen enrichment was more important at the sediment surface in all treatments except treatments with micro-algae only (Fig. 3.19b) than at the bottom. C/N ratio of sediments decreased compared to initial values (Fig. 3.19c). C/N ratio was the highest at the surface of sediment from lucines aquaria fed with microalgae (Fig. 3.19c). At the beginning of the growth experiment, sulfur content of sediment was very low and/or not detected in aquarium sediments, even in the sediment initially seeded with  $Na_2S$  for  $Na_2S$  and microalgae- $Na_2S$  feeding treatments (aquaria  $S_1$ ,  $S_2$ ,  $\mu AS_1$  and  $\mu AS_2$ ) (Fig. 3.19d). Sediments were also enriched in sulfur in each treatment, more heavily at the surface for treatments where addition of sulfur was carried out (Fig. 3.19d). In microalgae-only treatments, sulfur content in % was higher in bottom sediment than at the surface (Fig. 3.19d). There were no

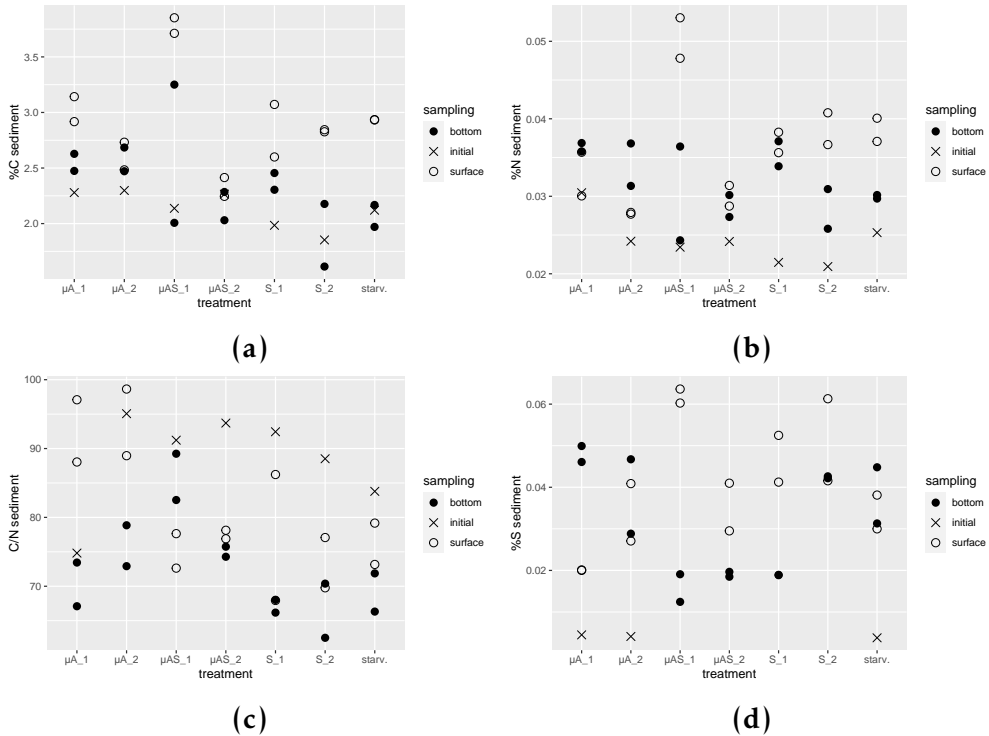


**Figure 3.19:** Carbon, nitrogen and sulfur content of sediments from *Loripes orbiculatus* growth experiment per feeding treatments. Sediments: Bottom, sediment sampled at the bottom of the aquarium at the end of the growth experiment (after 92 days); Initial, sediment sampled at the beginning of the growth experiment ; Surface sampling, sediment sampled at the bottom of the aquarium at the end of the growth experiment (after 92 days). Feeding treatments:  $\mu A$ , microalgae;  $S$ ,  $Na_2S$ ; starv., starvation; 1 & 2, treatment replicates. Note: In (d), sulfur content was below limit of detection in initial sediments for four treatments ( $\mu AS_1$ ,  $\mu AS_2$ ,  $S_1$ ,  $S_2$ ).

visible sulfur content differences between surface and bottom sediment in the starvation treatment (Fig. 3.19d).

### 3.6.6.2 Gill elemental content

At the end of *L. orbiculatus* growth experiment, there were no significant differences in gills %C, %N and %S and as a consequences in C/N, C/S and N/S ratio between each treatment of the growth experiment (Fig. 3.20a, b, c and Table. 3.15). In a previous study, both feeding of *L. orbiculatus* with microalgae and starvation of *L. orbiculatus* in laboratory caused a loss of symbionts, which was observed to stabilize after five weeks (Pales Espinosa et al., 2013). Lower total sulfur percentage also resulted from starved *L. orbiculatus* (Oortwijn et

al., 2022).

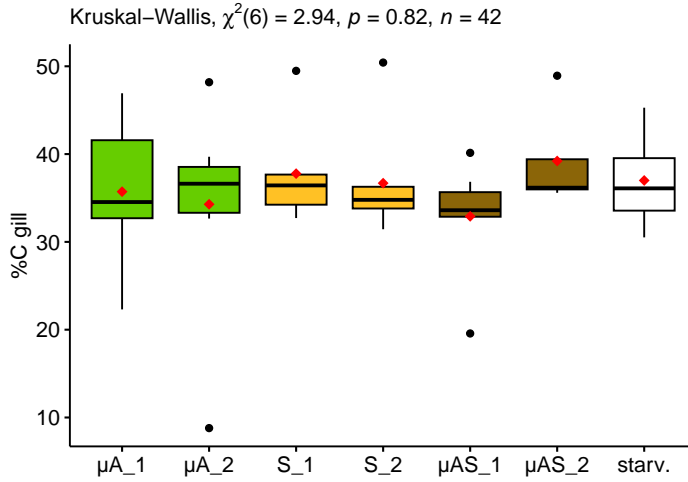
**Table 3.15:** Statistics on *Loripes orbiculatus* gill carbon, nitrogen and sulfur content from the growth experiment. Feeding treatments:  $\mu$ A, microalgae; S,  $\text{Na}_2\text{S}$ ; starv., starvation; 1 & 2, treatment replicates. p-value: \*, < 0.05; \*\*, < 0.01; \*\*\*, < 0.001.

	%S	%C	%N	C/S	C/N	N/S
<b>Test of normality: Shapiro-Wilk</b>						
S_1	0.00128**	0.0494*	0.580	0.152	0.100	0.344
S_2	0.000888***	0.00738**	0.0255*	0.00833**	0.365	0.00307**
starv.	0.565	0.849	0.284	0.738	0.0424*	0.791
$\mu$ AS_1	0.476	0.0671	0.00478**	0.00351**	0.0301*	0.00183**
$\mu$ AS_2	0.206	0.00489**	0.931	0.579	0.550	0.254
$\mu$ A_1	0.221	0.772	0.757	0.438	0.299	0.279
$\mu$ A_2	0.00977**	0.0302*	0.0313*	0.757	0.187	0.961
<b>Test of homoscedasticity: Levene</b>						
All	0.6296	0.9361	0.9136	0.7635	0.7648	0.6707
<b>Test of comparison: Kruskal-Wallis</b>						
All	0.12	0.817	0.873	0.108	0.604	0.136

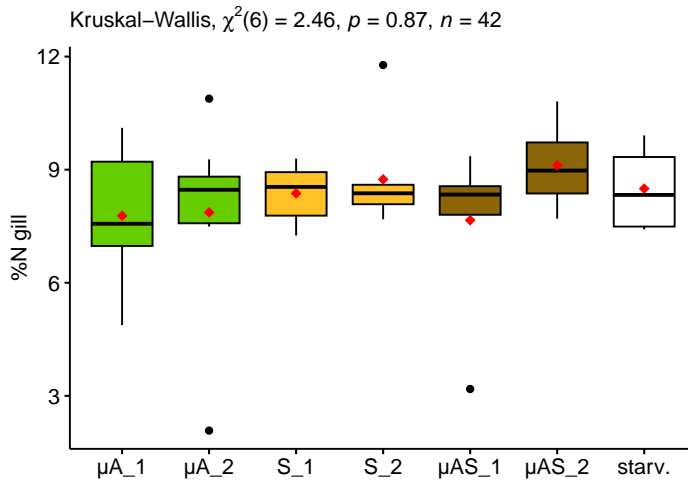
*L. orbiculatus* and *L. borealis* gill sulfur content was not well correlated to gill dry weight, nor with the sizes of specimens (Fig. 3.22). Also difference in content in gills between the species, for similar sizes is observed (Fig. 3.22). *L. orbiculatus* seems to have a higher capacity for sulfur accumulation.

### 3.6.7 Fluorescence *in-situ* hybridization on gill

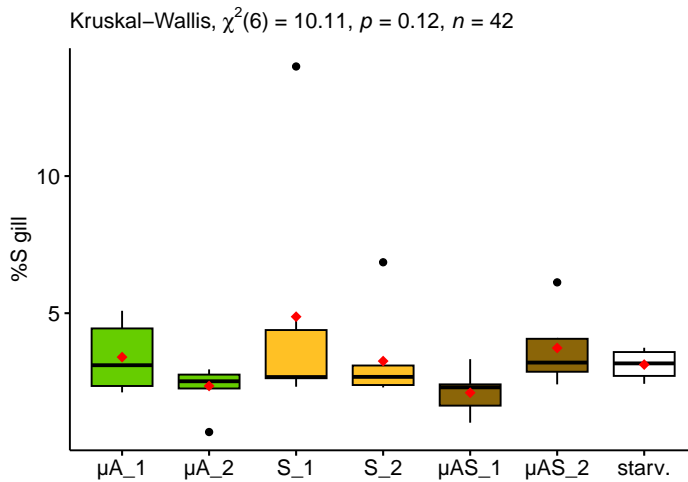
Fixed gill samples for fluorescence *in-situ* hybridization (FISH) to estimate the volume of bacteria within the gills could not be processed during the time of the thesis unfortunately.



(a)

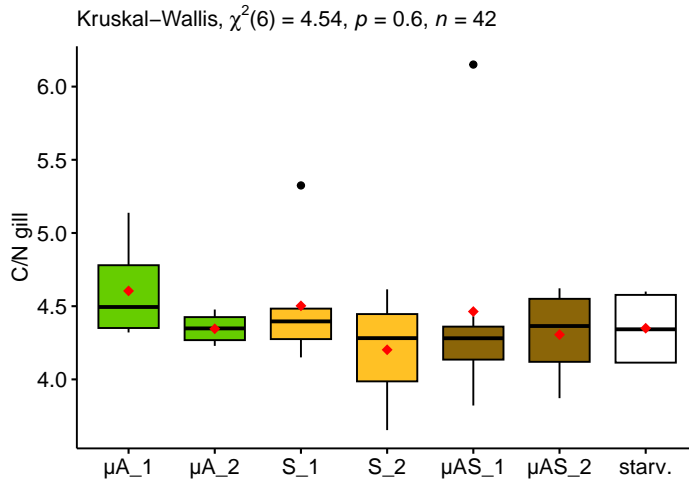


(b)

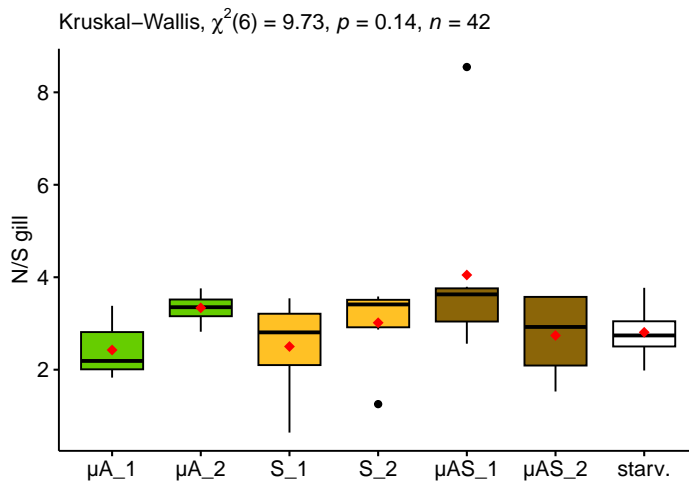


(c)

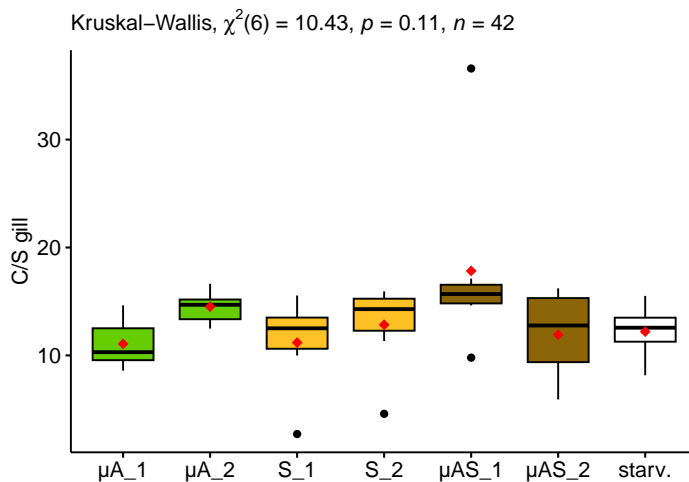
**Figure 3.20:** Carbon, nitrogen and sulfide content of gills per treatment at the end *Loripes orbiculatus* growth experiment.  $\mu$ A, microalgae; S,  $Na_2S$ ; 1 & 2, treatment replicates.



(a)



(b)



(c)

**Figure 3.21:** C/N, N/S and C/S ratio of gills per treatment at the end of *Loripes orbiculatus* growth experiment.  $\mu$ A, microalgae; S,  $Na_2S$ ; 1 & 2, treatment replicates.

**Table 3.16:** Comparison of gills elemental composition of *Loripes orbiculatus* collected in March 2023 and *L. orbiculatus* at the end of the growth experiment of *L. orbiculatus* specimens which were collected the same day at the same location. LO23, *L. orbiculatus* from the field collected in March 2023; Feeding treatments:  $\mu$ A, microalgae; S,  $Na_2S$ ; starv., starvation; 1 & 2, treatment replicates.

	S	C	N	C/S	C/N	N/S
<b>Test of normality: Shapiro-Wilk</b>						
See Tables 3.14 and 3.15						
<b>Test of homoscedasticity: Levene</b>						
All	0.9007	0.7058	0.5751	0.716	0.2535	0.5738
<b>Test of comparison: Kruskal-Wallis</b>						
All	0.786	0.0429*	0.0679	0.22	0.000781***	0.174
<b>Tests post-hoc: Dunn, Bonferroni p-values adjusted</b>						
LO23 S_1		1			0.187	
LO23 S_2		0.312			0.005 **	
LO23 starv.		1			0.187	
LO23 $\mu$ AS_1		0.001*			0.006**	
LO23 $\mu$ AS_2		0.240			0.201	
LO23 $\mu$ A_1		1			1	
LO23 $\mu$ A_2		0.494			0.012*	

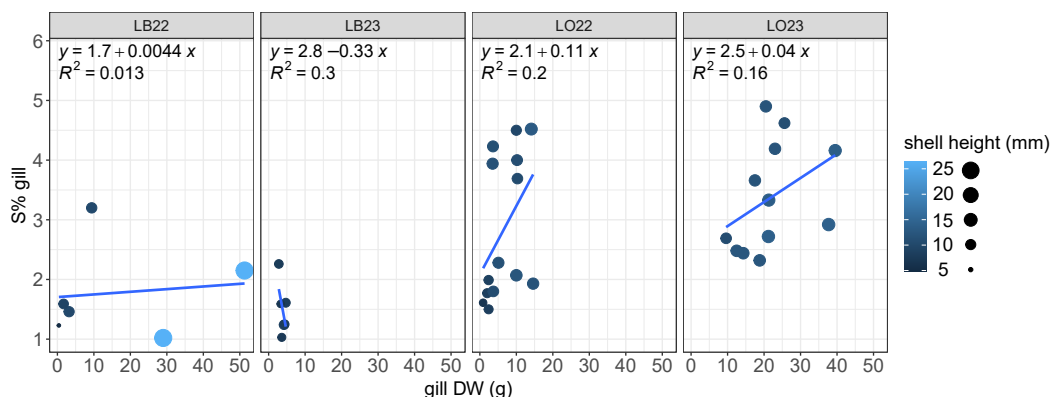


**Figure 3.22:** Gill sulfur content in function of gill dry weight and shell height of lucines *Loripes orbiculatus* and *Lucinoma borealis* sampled in May 2022 and March 2023 in Roscoff (France).

## References

- Aberle, N., & Malzahn, A. M. (2007). Interspecific and nutrient-dependent variations in stable isotope fractionation: Experimental studies simulating pelagic multitrophic systems. *Oecologia*, 154(2), 291–303. <https://doi.org/10.1007/s00442-007-0829-5>
- Allen, K. (1961). Amino Acids in the Mollusca. *American Zoologist*, 1(2), 253–261. <https://www.jstor.org/stable/3881256>
- Arellano, S. M., & Young, C. M. (2009). Spawning, Development, and the Duration of Larval Life in a Deep-Sea Cold-Seep Mussel. *Biological Bulletin*, 216(2), 149–162. <https://doi.org/10.2307/25470737>
- Bigatti, G., Peharda, M., & Taylor, J. (2004). Size at first maturity, oocyte envelopes and external morphology of sperm in three species of lucinidae (Mollusca: Bivalvia) from Florida Keys, U.S.A. *Malacologia*, 46(2), 417–426. [https://bibliotecadigital.exactas.uba.ar/collection/paper/document/paper\\_00762997\\_v46\\_n2\\_p417\\_Bigatti](https://bibliotecadigital.exactas.uba.ar/collection/paper/document/paper_00762997_v46_n2_p417_Bigatti)
- Cabana, G., & Rasmussen, J. B. (1996). Comparison of Aquatic Food Chains Using Nitrogen Isotopes. *Proceedings of the National Academy of Sciences of the United States of America*, 93(20), 10844–10847. <https://www.jstor.org/stable/40242>
- Cardini, U., Bartoli, M., Lückner, S., Mooshammer, M., Polzin, J., Lee, R. W., Micić, V., Hofmann, T., Weber, M., & Petersen, J. M. (2019). Chemosymbiotic bivalves contribute to the nitrogen budget of seagrass ecosystems. *The ISME Journal*, 13(12), 3131–3134. <https://doi.org/10.1038/s41396-019-0486-9>
- Carlier, A., Riera, P., Amouroux, J.-M., Bodiou, J.-Y., Desmalades, M., & Grémare, A. (2009). Spatial heterogeneity in the food web of a heavily modified Mediterranean coastal lagoon: Stable isotope evidence. *Aquatic Biology*, 5(2), 167–179. <https://doi.org/10.3354/ab00147>
- Conway, N., Capuzzo, J. M., & Fry, B. (1989). The role of endosymbiotic bacteria in the nutrition of *Solemya velum*: Evidence from a stable isotope analysis of endosymbionts and host. *Limnology and*

- Oceanography*, 34(1), 249–255. <https://doi.org/10.4319/lo.1989.34.1.0249>
- Cosel, R. von, & Gofas, S. (2019, October 23). *Marine Bivalves of Tropical West Africa* (1st ed.). Muséum national d'Histoire naturelle. <https://doi.org/10.5852/fft48>
- Cruaud, P., Decker, C., Olu, K., Arnaud-Haond, S., Papot, C., Baut, J. L., Vigneron, A., Khripounoff, A., Gayet, N., Cathalot, C., Caprais, J.-C., Pignet, P., Godfroy, A., & Cambon-Bonavita, M.-A. (2019). Ecophysiological differences between vesicomid species and metabolic capabilities of their symbionts influence distribution patterns of the deep-sea clams. *Marine Ecology*, 40(3), e12541. <https://doi.org/10.1111/maec.12541>
- Dando, P. R., Southward, A. J., Southward, E. C., & Bone, Q. (1986). Chemoautotrophic symbionts in the gills of the bivalve mollusc *Lucinoma borealis* and the sediment chemistry of its habitat. *Proceedings of the Royal Society of London. Series B. Biological Sciences*, 227(1247), 227–247. <https://doi.org/10.1098/rspb.1986.0021>
- de Fouw, J., Holmer, M., Beca-Carretero, P., Boström, C., Brice, J., Brun, F. G., Cruijisen, P. M. J. M., Govers, L. L., Garmendia, J. M., Meysick, L., Pajusalu, L., Richir, J., Robroek, B., Valle, M., van der Ven, P., Eklöf, J. S., & van der Heide, T. (2023). A facultative mutualism facilitates European seagrass meadows. *Ecography*, 2023(5), e06636. <https://doi.org/10.1111/ecog.06636>
- Diversity of chemosymbiotic bivalves on coral reefs: Lucinidae (Mollusca, Bivalvia) of New Caledonia and Lifou. (2007). *Zoosystema*, 29(1), 109–181. <https://sciencepress.mnhn.fr/en/periodiques/zoosystema/29/1/diversite-des-bivalves-chemosymbiotiques-des-recifs-coralliens-lucinidae-mollusca-bivalvia-de-nouvelle-caledonie-et-de-lifou>
- Dreier, A., Stannek, L., Blumenberg, M., Taviani, M., Sigovini, M., Wrede, C., Thiel, V., & Hoppert, M. (2012). The fingerprint of chemosymbiosis: Origin and preservation of isotopic biosignatures in the nonseep bivalve *Loripes lacteus* compared with *Venerupis aurea*.

- FEMS microbiology ecology*, 81(2), 480–493. <https://doi.org/10.1111/j.1574-6941.2012.01374.x>
- Duperron, S. (2015). Characterization of Bacterial Symbionts in Deep-Sea Fauna: Protocols for Sample Conditioning, Fluorescence In Situ Hybridization, and Image Analysis. [https://doi.org/10.1007/8623\\_2015\\_73](https://doi.org/10.1007/8623_2015_73)
- Fabregas, J., Herrero, C., Abalde, J., & Cabezas, B. (1985). Growth, chlorophyll a and protein of the marine microalga *Isochrysis galbana* in batch cultures with different salinities and high nutrient concentrations. *Aquaculture*, 50(1), 1–11. [https://doi.org/10.1016/0044-8486\(85\)90147-4](https://doi.org/10.1016/0044-8486(85)90147-4)
- Geest, M. van der, Lely, J. A. C. van der, Gils, J. A. van, Piersma, T., & Lok, T. (2019). Density-dependent growth of bivalves dominating the intertidal zone of Banc d'Arguin, Mauritania: Importance of feeding mode, habitat and season. *Marine Ecology Progress Series*, 610, 51–63. <https://doi.org/10.3354/meps12851>
- Geest, M. van der, Sall, A. A., Ely, S. O., Nauta, R. W., Gils, J. A. van, & Piersma, T. (2014). Nutritional and reproductive strategies in a chemosymbiotic bivalve living in a tropical intertidal seagrass bed. *Marine Ecology Progress Series*, 501, 113–126. <https://doi.org/10.3354/meps10702>
- Gils, J. A. van, Lisovski, S., Lok, T., Meissner, W., Ożarowska, A., Fouw, J. de, Rakhimberdiev, E., Soloviev, M. Y., Piersma, T., & Klaassen, M. (2016). Body shrinkage due to Arctic warming reduces red knot fitness in tropical wintering range. *Science*. <https://doi.org/10.1126/science.aad6351>
- Goodman, J. L., Moore, K. A., & Dennison, W. C. (1995). Photosynthetic responses of eelgrass (*Zostera marina* L.) to light and sediment sulfide in a shallow barrier island lagoon. *Aquatic Botany*, 50(1), 37–47. [https://doi.org/10.1016/0304-3770\(94\)00444-Q](https://doi.org/10.1016/0304-3770(94)00444-Q)
- Gros, O., Darrasse, A., Durand, P., Frenkiel, L., & Mouëza, M. (1996). Environmental transmission of a sulfur-oxidizing bacterial gill endosymbiont in the tropical lucinid bivalve *Codakia orbicularis*.

- Applied and Environmental Microbiology*, 62(7), 2324–2330. <https://doi.org/10.1128/aem.62.7.2324-2330.1996>
- Gros, O., DUPLESSIS, M. R., & FELBECK, H. O. R. S. T. (1999). Embryonic development and endosymbiont transmission mode in the symbiotic clam *Lucinoma aequizonata* (Bivalvia: Lucinidae). *Invertebrate Reproduction & Development*, 36(1-3), 93–103. <https://doi.org/10.1080/07924259.1999.9652683>
- Gros, O., Elisabeth, N. H., Gustave, S. D. D., Caro, A., & Dubilier, N. (2012). Plasticity of symbiont acquisition throughout the life cycle of the shallow-water tropical lucinid *Codakia orbiculata* (Mollusca: Bivalvia). *Environmental Microbiology*, 14(6), 1584–1595. <https://doi.org/10.1111/j.1462-2920.2012.02748.x>
- Gros, O., Frenkiel, L., & Mouëza, M. (1997). Embryonic, Larval, and Post-Larval Development in the Symbiotic Clam *Codakia orbicularis* (Bivalvia: Lucinidae). *Invertebrate Biology*, 116(2), 86–101. <https://doi.org/10.2307/3226973>
- He, X., Xu, M., Qiu, G. Y., & Zhou, J. (2009). Use of <sup>15</sup>N stable isotope to quantify nitrogen transfer between mycorrhizal plants. *Journal of Plant Ecology*, 2(3), 107–118. <https://doi.org/10.1093/jpe/rtp015>
- Herry, A., Diouris, M., & Le Pennec, M. (1989). Chemoautotrophic symbionts and translocation of fixed carbon from bacteria to host tissues in the littoral bivalve *Loripes lucinalis* (Lucinidae). *Marine Biology*, 101(3), 305–312. <https://doi.org/10.1007/BF00428126>
- Ikuta, T., Igawa, K., Tame, A., Kuroiwa, T., Kuroiwa, H., Aoki, Y., Takaki, Y., Nagai, Y., Ozawa, G., Yamamoto, M., Deguchi, R., Fujikura, K., Maruyama, T., & Yoshida, T. (2016). Surfing the vegetal pole in a small population: Extracellular vertical transmission of an 'intracellular' deep-sea clam symbiont. *Royal Society Open Science*, 3(5), 160130. <https://doi.org/10.1098/rsos.160130>
- Johnson, M. A., Diouris, M., & Pennec, M. L. (1994). Endosymbiotic Bacterial Contribution in the Carbon Nutrition of *Loripes lucinalis* (Mollusca: Bivalvia), 13.
- Johnson, M. A., & Fernandez, C. (2001). Bacterial symbiosis in *Loripes lucinalis* (Mollusca: Bivalvia) with comments on reproductive strat-

- egy. *Journal of the Marine Biological Association of the United Kingdom*, 81(2), 251–257. <https://doi.org/10.1017/S002531540100371X>
- Johnson, M. A., Fernandez, C., & Pergent, G. (2002). The ecological importance of an invertebrate chemoautotrophic symbiosis to phanerogam seagrass beds. *Bulletin of Marine Science*, 71(3), 1343–1351.
- Johnson, M. A., Paulet, Y. M., Donval, A., & Le Pennec, M. (1996a). Histology, histochemistry and enzyme biochemistry in the digestive system of the endosymbiont-bearing bivalve *Loripes lucinalis* (Lamarck). *Journal of Experimental Marine Biology and Ecology*, 197(1), 15–38. [https://doi.org/10.1016/0022-0981\(95\)00142-5](https://doi.org/10.1016/0022-0981(95)00142-5)
- Johnson, M. A., & Pennec, M. (1994). The development of the female gamete in the endosymbiont-bearing bivalve *Loripes lucinalis*. *Journal of the Marine Biological Association of the United Kingdom*, 74(1), 233–242. <https://doi.org/10.1017/S0025315400035797>
- Johnson, M. J., Casse, N., & Le Pennec, M. (1996b). Spermatogenesis in the endosymbiont-bearing bivalve *Loripes lucinalis* (Veneroida: Lucinidae). *Molecular Reproduction and Development*, 45(4), 476–484. [https://doi.org/10.1002/\(SICI\)1098-2795\(199612\)45:4<476::AID-MRD10>3.0.CO;2-V](https://doi.org/10.1002/(SICI)1098-2795(199612)45:4<476::AID-MRD10>3.0.CO;2-V)
- Kooijman, S. A. L. M. (2010). *Dynamic Energy Budget Theory for Metabolic Organisation*. Cambridge University Press.
- Lamers, L., Govers, L., Janssen, I., Geurts, J., Van der Welle, M., Van Katwijk, M., Van der Heide, T., Roelofs, J., & Smolders, A. (2013). Sulfide as a soil phytotoxin—a review. *Frontiers in Plant Science*, 4. <https://www.frontiersin.org/articles/10.3389/fpls.2013.00268>
- Le Pennec, M., Beninger, P. G., & Herry, A. (1995). Feeding and digestive adaptations of bivalve molluscs to sulphide-rich habitats. *Comparative Biochemistry and Physiology Part A: Physiology*, 111(2), 183–189. [https://doi.org/10.1016/0300-9629\(94\)00211-B](https://doi.org/10.1016/0300-9629(94)00211-B)
- Lukianova, O. A., & David, S. S. (2005). A role for iron–sulfur clusters in DNA repair. *Current Opinion in Chemical Biology*, 9(2), 145–151. <https://doi.org/10.1016/j.cbpa.2005.02.006>

- Mariotti, A. (1983). Atmospheric nitrogen is a reliable standard for natural  $^{15}\text{N}$  abundance measurements. *Nature*, 303(5919), 685–687. <https://doi.org/10.1038/303685a0>
- Martin, B. C., Middleton, J. A., Fraser, M. W., Marshall, I. P. G., Scholz, V. V., Hausl, B., & Schmidt, H. (2020). Cutting out the middle clam: Lucinid endosymbiotic bacteria are also associated with seagrass roots worldwide. *The ISME Journal*, 14(11), 2901–2905. <https://doi.org/10.1038/s41396-020-00771-3>
- Miyake, H., Kitada, M., Lindsay, D., Itoh, T., Nemoto, S., & Miwa, T. (2012). How to Keep Deep-Sea Animals. <https://doi.org/10.5772/35690>
- Mouëza, M., Gros, O., & Frenkiel, L. (1999). Embryonic, Larval and Post-larval Development of the Tropical Clam, *Anomalocardia brasiliensis* (Bivalvia, Veneridae). *Journal of Molluscan Studies*, 65(1), 73–88. <https://doi.org/10.1093/mollus/65.1.73>
- Ohishi, K., Yamamoto, M., Tame, A., Kusaka, C., Nagai, Y., Sugimura, M., Inoue, K., Uematsu, K., Yoshida, T., Ikuta, T., Toyofuku, T., & Maruyama, T. (2016). Long-term Cultivation of the Deep-Sea Clam *Calyptogena okutanii*: Changes in the Abundance of Chemoautotrophic Symbiont, Elemental Sulfur, and Mucus. *The Biological Bulletin*. <https://doi.org/10.1086/BBLv230n3p257>
- Oortwijn, T., de Fouw, J., Petersen, J. M., & van Gils, J. A. (2022). Sulfur in lucinid bivalves inhibits intake rates of a molluscivore shorebird. *Oecologia*, 199(1), 69–78. <https://doi.org/10.1007/s00442-022-05170-3>
- Oren, A., Garrity, G. M., Parker, C. T., Chuvochina, M., & Trujillo, M. E. (2020). Lists of names of prokaryotic Candidatus taxa. *International Journal of Systematic and Evolutionary Microbiology*, 70(7), 3956–4042. <https://doi.org/10.1099/ijsem.0.003789>
- Osvatic, J. T., Wilkins, L. G. E., Leibrecht, L., Leray, M., Zauner, S., Polzin, J., Camacho, Y., Gros, O., van Gils, J. A., Eisen, J. A., Petersen, J. M., & Yuen, B. (2021). Global biogeography of chemosynthetic symbionts reveals both localized and globally distributed sym-

- biont groups. *Proceedings of the National Academy of Sciences*, 118(29), e2104378118. <https://doi.org/10.1073/pnas.2104378118>
- Osvatic, J. T., Yuen, B., Kunert, M., Wilkins, L., Hausmann, B., Girguis, P., Lundin, K., Taylor, J. D., Jospin, G., & Petersen, J. M. (2023). Gene loss and symbiont switching during adaptation to the deep sea in a globally distributed symbiosis. *The ISME Journal*, 17(3), 453–466. <https://doi.org/10.1038/s41396-022-01355-z>
- Pales Espinosa, E., Tanguy, A., Le Panse, S., Lallier, F., Allam, B., & Boutet, I. (2013). Endosymbiotic bacteria in the bivalve *Loripes lacteus*: Localization, characterization and aspects of symbiont regulation. *Journal of Experimental Marine Biology and Ecology*, 448, 327–336. <https://doi.org/10.1016/j.jembe.2013.07.015>
- Petersen, J. M., Kemper, A., Gruber-Vodicka, H., Cardini, U., van der Geest, M., Kleiner, M., Bulgheresi, S., Mußmann, M., Herbold, C., Seah, B. K. B., Antony, C. P., Liu, D., Belitz, A., & Weber, M. (2016). Chemosynthetic symbionts of marine invertebrate animals are capable of nitrogen fixation. *Nature Microbiology*, 2(1), 1–11. <https://doi.org/10.1038/nmicrobiol.2016.195>
- Bandiera\_abtest: a  
Cc\_license\_type: cc\_by  
Cg\_type: Nature Research Journals  
Primary\_atype: Research  
Subject\_term: Biogeochemistry;Microbial ecology;Symbiosis;Water microbiology  
Subject\_term\_id: biogeochemistry;microbial-ecology;symbiosis;water-microbiology
- Piquet, B., Shillito, B., Lallier, F. H., Duperron, S., & Andersen, A. C. (2019). High rates of apoptosis visualized in the symbiont-bearing gills of deep-sea *Bathymodiolus* mussels. *PLOS ONE*, 14(2), e0211499. <https://doi.org/10.1371/journal.pone.0211499>
- Robinson, J. J., & Cavanaugh, C. M. (1995). Expression of form I and form II Rubisco in chemoautotrophic symbioses: Implications for the interpretation of stable carbon isotope values. *Limnology and*

- Oceanography*, 40(8), 1496–1502. <https://doi.org/10.4319/lo.1995.40.8.1496>
- Roques, C., Grousset, E., Troussellier, M., Hermet, S., Le Carrer, J., Sar, C., & Caro, A. (2020). A trade-off between mucocytes and bacteriocytes in *Loripes orbiculatus* gills (Bivalvia, Lucinidae): A mixotrophic adaptation to seasonality and reproductive status in a symbiotic species? *Marine Biology*, 167(10), 154. <https://doi.org/10.1007/s00227-020-03768-w>
- Rossi, F., Colao, E., Martinez, M. J., Klein, J. C., Carcaillet, F., Callier, M. D., Wit, R. de, & Caro, A. (2013). Spatial distribution and nutritional requirements of the endosymbiont-bearing bivalve *Loripes lacteus* (sensu Poli, 1791) in a Mediterranean *Nanozostera noltii* (Hornemann) meadow. *Journal of Experimental Marine Biology and Ecology*, 440, 108–115. <https://doi.org/10.1016/j.jembe.2012.12.010>
- Sanmartí, N., Solé, L., Romero, J., & Pérez, M. (2018). Seagrass-bivalve facilitative interactions: Trait-mediated effects along an environmental gradient. *Marine Environmental Research*, 133, 99–104. <https://doi.org/10.1016/j.marenvres.2017.12.002>
- Sanmartí Boixeda, N. (2020). Biological interactions and resilience of seagrass ecosystems. <http://diposit.ub.edu/dspace/handle/2445/179407>
- Accepted: 2021-07-28T07:47:37Z
- Sogin, E. M., Kleiner, M., Borowski, C., Gruber-Vodicka, H. R., & Dübilier, N. (2021). Life in the Dark: Phylogenetic and Physiological Diversity of Chemosynthetic Symbioses. *Annual Review of Microbiology*, 75(1), 695–718. <https://doi.org/10.1146/annurev-micro-051021-123130>
- Sogin, E. M., Leisch, N., & Dübilier, N. (2020). Chemosynthetic symbioses. *Current Biology*, 30(19), R1137–R1142. <https://doi.org/10.1016/j.cub.2020.07.050>
- Stanley, S. M. (2014). Evolutionary radiation of shallow-water Lucinidae (Bivalvia with endosymbionts) as a result of the rise of seagrasses

- and mangroves. *Geology*, 42(9), 803–806. <https://doi.org/10.1130/G35942.1>
- Stock, B. C., Jackson, A. L., Ward, E. J., Parnell, A. C., Phillips, D. L., & Semmens, B. X. (2018). Analyzing mixing systems using a new generation of Bayesian tracer mixing models. *PeerJ*, 6, e5096. <https://doi.org/10.7717/peerj.5096>
- Taylor, J. D., & Glover, E. (2000). Functional anatomy, chemosymbiosis and evolution of the Lucinidae. *Geological Society, London, Special Publications*, 177(1), 207–225. <https://doi.org/10.1144/GSL.SP.2000.177.01.12>
- Taylor, J. D., & Glover, E. (2021, January 14). *Biology, evolution and generic review of the chemosymbiotic bivalve family Lucinidae*.
- Taylor, J. D., Glover, E., Yuen, B., & Williams, S. T. (2022). Closing the gap: A new phylogeny and classification of the chemosymbiotic bivalve family Lucinidae with molecular evidence for 73% of living genera. *Journal of Molluscan Studies*, 88(4), eyac025. <https://doi.org/10.1093/mollus/eyac025>
- Taylor, J. D., Glover, E. A., & Williams, S. T. (2014). Diversification of chemosymbiotic bivalves: Origins and relationships of deeper water Lucinidae. *Biological Journal of the Linnean Society*, 111(2), 401–420. <https://doi.org/10.1111/bij.12208>
- Tsutsumi, H., Wainright, S., Montani, S., Saga, M., Ichihara, S., & Kogure, K. (2001). Exploitation of a chemosynthetic food resource by the polychaete *Capitella* sp. I. *Marine Ecology Progress Series*, 216, 119–127. <https://doi.org/10.3354/meps216119>
- Valenzuela-Espinoza, E., Millán-Núñez, R., & Núñez-Cebrero, F. (2002). Protein, carbohydrate, lipid and chlorophyll a content in *Isochrysis* aff. *galbana* (clone T-Iso) cultured with a low cost alternative to the f/2 medium. *Aquacultural Engineering*, 25(4), 207–216. [https://doi.org/10.1016/S0144-8609\(01\)00084-X](https://doi.org/10.1016/S0144-8609(01)00084-X)
- van der Geest, M., van der Heide, T., Holmer, M., & de Wit, R. (2020). First Field-Based Evidence That the Seagrass-Lucinid Mutualism Can Mitigate Sulfide Stress in Seagrasses. *Frontiers in Marine Sci-*

- ence, 7. <https://www.frontiersin.org/articles/10.3389/fmars.2020.00011>
- van der Geest, M., van Gils, J. A., van der Meer, J., Olff, H., & Piersma, T. (2011). Suitability of calcein as an in situ growth marker in burrowing bivalves. *Journal of Experimental Marine Biology and Ecology*, 399(1), 1–7. <https://doi.org/10.1016/j.jembe.2011.01.003>
- van der Heide, T., Govers, L. L., de Fouw, J., Olff, H., van der Geest, M., van Katwijk, M. M., Piersma, T., van de Koppel, J., Silliman, B. R., Smolders, A. J. P., & van Gils, J. A. (2012). A Three-Stage Symbiosis Forms the Foundation of Seagrass Ecosystems. *Science*, 336(6087), 1432–1434. <https://doi.org/10.1126/science.1219973>
- van Gils, J. A., van der Geest, M., Jansen, E. J., Govers, L. L., de Fouw, J., & Piersma, T. (2012). Trophic cascade induced by molluscivore predator alters pore-water biogeochemistry via competitive release of prey. *Ecology*, 93(5), 1143–1152. <https://doi.org/10.1890/11-1282.1>
- van Gils, J. A., van der Geest, M., Leyrer, J., Oudman, T., Lok, T., Onrust, J., de Fouw, J., van der Heide, T., van den Hout, P. J., Spaans, B., Dekinga, A., Brugge, M., & Piersma, T. (2013). Toxin constraint explains diet choice, survival and population dynamics in a molluscivore shorebird. *Proceedings of the Royal Society B: Biological Sciences*, 280(1763), 20130861. <https://doi.org/10.1098/rspb.2013.0861>
- Vermeij, G. J. (2010). Shifting sources of productivity in the coastal marine tropics during the Cenozoic era. *Proceedings of the Royal Society B: Biological Sciences*, 278(1716), 2362–2368. <https://doi.org/10.1098/rspb.2010.2362>
- Vrijenhoek, R. C. (2013). On the instability and evolutionary age of deep-sea chemosynthetic communities. *Deep Sea Research Part II: Topical Studies in Oceanography*, 92, 189–200. <https://doi.org/10.1016/j.dsr2.2012.12.004>

- WoRMS - World Register of Marine Species - *Loripes lacteus* (Linnaeus, 1758) *sensu* Poli, 1791. (2024). <https://www.marinespecies.org/aphia.php?p=taxdetails&id=140281>
- WoRMS - World Register of Marine Species - *Loripes lucinalis* (Lamarck, 1818). (2024). <https://www.marinespecies.org/aphia.php?p=taxdetails&id=152887>
- Yuen, B., Polzin, J., & Petersen, J. M. (2019). Organ transcriptomes of the lucinid clam *Loripes orbiculatus* (Poli, 1791) provide insights into their specialised roles in the biology of a chemosymbiotic bivalve. *BMC Genomics*, 20(1), 820. <https://doi.org/10.1186/s12864-019-6177-0>
- Zanden, M. J. V., & Rasmussen, J. B. (2001). Variation in  $\delta^{15}\text{N}$  and  $\delta^{13}\text{C}$  trophic fractionation: Implications for aquatic food web studies. *Limnology and Oceanography*, 46(8), 2061–2066. <https://doi.org/10.4319/lo.2001.46.8.2061>
- Zauner, S., Vogel, M., Polzin, J., Yuen, B., Mußmann, M., El-Hacen, E.-H. M., & Petersen, J. M. (2022). Microbial communities in developmental stages of lucinid bivalves. *ISME Communications*, 2, 56. <https://doi.org/10.1038/s43705-022-00133-4>



# Chapter 4

## General discussion and perspectives

### 4.1 *Christineconcha regab* abj-farming model

#### 4.1.1 Parameter estimation

Both *Christineconcha regab* abj and abj-farming dynamic energetic models in Chapter 2 successfully estimated a consistent parameter set using the add-my-pet procedure (Marques et al., 2018). Thank to previous studies on this species many data were available on both the host and its symbionts compared to other deep-sea species; that made it possible to build such models. *C. regab* sulfur-oxidizing symbionts were well integrated into initially developed abj model, giving the abj-farming model. Symbionts related data (i.e., sulfur consumption, fraction of bacteria in the the host gill and host/symbiont biomass ratio) were well predicted from estimated DEB parameters of the abj-farming model.

Some uncertainties in the results remain in the life-span and the growth-rate of *C. regab*: abj and abj-farming models predicted different growth rate from the same input of growth-rate from a cohort analysis. DEB is a powerful tool, if well calibrated: efforts to obtain additional data on growth rate are necessary for *C. regab*, and globally for all deep-sea species.

A downside of the abj-farming model is its complexity in terms of number of parameters. Increasing the model complexity increases the chances to obtain different minimum of the loss function during the estimation (i.e, different solutions). Hence, filters were added to keep the parameters inside a “reasonable” parameter space, defined by educated/smart guess mixed by pre-

conceived ideas led by our current knowledge (Augustine & Kooijman, 2019). With the addition of filters, the final estimated parameter set dependency on initial parameter set is increasing. Filters restrain the estimation. Therefore better solutions (i.e., with a lower minimum) could exist in a parameter space that is not reachable during the estimation procedure given initial parameter set and given filters.

The number of steps chosen for the Nelder-Mead simplex estimation procedure also impacts the final estimated parameters. From the return of experiences of DEB parameter estimations, it was suggested that using “first 200 and then later 500, turned out to be much more robust than a single long series of steps”, but this is a bit hazy (Augustine & Kooijman, 2019). The estimation of abj-farming model parameters required the trial of different initial parameter values, and to “play” with the step number to obtain a satisfactory parameter set.

Some estimated parameter values had the tendency to be pull to unrealistic values, too high (e.g., symbionts food level  $> 10$ ) or too low (e.g., vks  $< 0.00001$ ) and were fixed to reasonable values. Some data might be “conflictual” because of the assumption to keep one food level per site and not for each sampling cruises. abj-farming model would require more application to understand the behavior of new symbiont parameters (e.g., vks). Manual testing by trial and errors of some parameter values were required. Having more data type per site at a given times, given temperatures and most importantly given food levels would improve greatly the abj-farming model parameter estimation.

### 4.1.2 abj-farming model hypotheses and assumptions

The assumption that the vesicomid host feed mainly by digestion of its symbionts was made to build the abj-farming model. However, there might be some additional exchanges occurring between both partners as it was described in the literature in other bivalve species (Ponnudurai et al., 2017; Sogin et al., 2020). Omic studies (proteomics and genomics) of the hydrothermal vent mussel *Bathymodiolus azoricus* and its symbionts suggested that sulfur-oxidizing symbionts may provide its host with amino acid and cofactor (Ponnudurai et al., 2017). If it was possible to maintain vesicomid specimens alive, it would be interesting to follow the carbon assimilation using marked carbon and to highlight cell apoptosis rate as it was done in deep-sea vent mytilid *Bathy-*

*modiolus azoricus* (Piquet et al., 2022).

Beside a good correlation between collected data and predictions made by the abj-farming model in Chapter 2, assumptions and hypotheses of the abj-farming model could be validated by model predictions followed by field observations. Consumption of sulfur and density of bacteria within host gills could be predicted with the abj-farming model for a given host size. Then field observations, if they are congruent with initial predictions, could validate the abj-farming model, to some extent. Environmental sulfide and total sulfur inside hosts from different sites in the field could be measured to compare with predicted symbiont food level by the model.

The abj-farming model was based on the hypothesis that the dynamics of the symbionts were quicker than the host's dynamics (e.g., growth rate). A downside of symbiont fast dynamic assumption is that the variation of symbiont state variables (reserve and structure) cannot be dynamically studied. The variations of reserve and structure were considered to go back quickly to equilibrium (i.e.,  $\frac{dE}{dt} = 0$  and  $\frac{dV}{dt} = 0$ ).

Host and symbionts reserve and structure composition were considered as having the same composition for the sake of simplicity and because they were unknown for *C. regab* symbiont. Or in reality they should not. For the host, the assumption that its structure and reserve are of the same composition is what is usually done in DEB models ("Add-My-Pet Species List", 2024; Kooijman, 2010). However, bacteria's composition of reserve and structure composition should be different (Kooijman, 2010). High concentration of sulfur have been found in vesicomid species, including in *C. regab* (12.7% to 17.2% of tissues dry weight, (Khripounoff et al., 2017)). Sulfur reserve was not included into abj-farming model as there was a lack of data (i.e., unknown host size and weight for a given percentage of sulfur of host tissues in the paper (Khripounoff et al., 2017)). In future scientific campaign, sulfur concentration in *C. regab* specimens should be quantified precisely using mass spectrometry, for example as it has been done for lucines in Chapter 3 and a sulfur reserve should be definitively added in *C. regab* abj-farming model.

The host is the one digging for sulfide in the sediment with its foot and might control this way symbionts access to sulfide. This cannot be explicitly defined in the DEB model because of a lack of data and knowledge on this process. Omics studies showed the presence of transporters on the host foot and it is believed that hypotaurine and thiotaurine play a key role in sulfide transport via hemolymph in deep-sea symbiotic mytilid of the *Bathymodiolus* genus (e.g., *Bathymodiolus azoricus*, *B. boomerang*, *B. septemdiarum* and *B. plat-*

*ifrons*) and vesicomid bivalves species (e.g., *Calyptogena magnifica*) (Koito et al., 2016; Kuroda et al., 2021; Pruski et al., 2000).

Homeostasis can be defined as the “maintenance of nearly constant conditions in the internal environment” (Guyton & Hall, 2011). In nature there are a lot of example of homeostasis to maintain one’s living organism consistency (e.g., thermoregulation, osmotic regulation). The idea that a deep-sea symbiotic species could use some kind of homeostatic processes to keep food available for itself in an harsh environment such as deep sea would make sense. Omics studies could help identify *C. regab* and its symbiont genes that could be link to host farming and homeostatic strategies (e.g., genes involves in bacteriocytes cell apoptosis control, sulfide transport regulation).

### 4.1.3 Perspectives on *Christineconcha regab* traits

Functional traits of *C. regab* and its symbionts could be unraveled with the abj-farming model developed in Chapter 2. However the Chapter 2 of this thesis focused only on the dynamic relationship between the host and its symbionts. The abj-farming DEB model could be used also to study additional host bivalve traits. Deep-sea species functional traits are highly valuables as there are difficult to study.

A low level of genetic diversity between Regab and Lobes sites in the Gulf of Guinea suggested a high connectivity between the sites (Hassan et al., 2023). The pelagic larval duration (PLD) is the amount of time larvae stay in the water column. PLD is used to approximate dispersal distance and population connectivity (Cowen et al., 2007; Gaudron et al., 2021; McVeigh et al., 2017; Young et al., 2012). With *C. regab* DEB model, the PLD could be estimated by the time predicted between birth and end of metamorphosis (i.e., settlement time, end of dispersal) (Gaudron et al., 2021). Knowing this estimation, it would be interesting to see, for example, if a larva could reach a given site, using hydrodynamic models and scenario of dispersal strategies (McVeigh et al., 2017). The hypotheses of dispersal strategy (e.g., demersal drift and/or dispersal near the surface (McVeigh et al., 2017)) could be verified by predicting the location where the species could settle, followed by field verification. Additionally, DEB provides useful tool to estimate food level at a site only from specimens collection at a given temperature. This information could also help unraveling settlement strategies of deep-sea larvae.

Total Reproductive Output (TRO) is “the total number of oocytes accumulated during the lifespan of the species” (Gaudron et al., 2021). TRO could also

be estimated under different scenarios of temperature and food level, giving an estimation of the number of offsprings of a given population (Gaudron et al., 2021).

## 4.2 Perspectives of the abj-farming model

### 4.2.1 Lead for *Loripes orbiculatus* DEB model development

A conceptual model for mixotroph lucinid species *Loripes orbiculatus* has been thought out in Chapter 3. Accordingly, lab experiments were carried out to collect data on *L. orbiculatus* such as weight, length, gill sulfur content and growth. *L. orbiculatus* gonad samples were fixed and sliced to estimate the total reproductive output and lowest observed size and weight at first maturity. Gills were also fixed to estimate symbiont density to be analyzed by FISH. These samples have not been fully processed yet. Fluxes of oxygen, nitrogen, carbon and sulfur content also remained to be measured.

Two food sources have to be modeled because of *L. orbiculatus* photosynthetic and chemosynthetic based nutrition. The proportion between both food sources could be modeled using isotopes stable data from the literature (see Chapter 3). Host macrochemical equations have to be reviewed accordingly. The sulfur-oxidizing symbiont macrochemical equations should also be reviewed with the add of an additional reserve for sulfur, as a state variable, and symbiont fixation of nitrogen (Petersen & Yuen, 2020).

To summarize, remaining work consist of (1) collecting the missing data, (2) defining state variables of the model (i.e., with differential equations) and (3) conceptualizing and code in Matlab predictions for each data, (4) estimating parameters following the AmP procedure (Marques et al., 2018).

### 4.2.2 Bivalve functional traits, from shallow to deep sea

At present, a popular hypothesis is that shallow-water bivalves colonized deep-sea hydrothermal vent and seeps through the intermediary of organic falls (Distel et al., 2000). This hypothesis has been first advanced and supported by phylogenetic studies on mytilid mussels (Distel et al., 2000). Organic fall mussel diversity is higher than hydrothermal vents mussel diversity, based on the current knowledge (Thubaut et al., 2013). Multiple habitat shifts from organic

fall to cold-seeps and hydrothermal vent may have happened through evolution (Thubaut et al., 2013). Highly specialized adaptation of mussels to hydrothermal vents, the harshest deep-sea habitat, were suggested to be a “kind of evolutionary dead end” of their lineage (Thubaut et al., 2013). For now, the inverse radiation, from hydrothermal vent to organic falls, is not supported by species samplings (Thubaut et al., 2013). Some species were found to live at both hydrothermal vents and cold seeps, or cold seeps and organic falls but not at vents and organic falls (Thubaut et al., 2013).

Once DEB models are applied to different symbiotic bivalve species, it could be interesting to seek for patterns in parameters and life/functional traits (e.g. sizes, growth-rates, reproduction rates, survival) of symbiotic species compared to non-symbiotic species. Similarly, the different symbiotic bivalve families could be compared and also their habitats (e.g., deep versus shallow sea, cold seeps versus hydrothermal vent versus organic fall). These could help increasing our understanding on how bivalve species adapted themselves to the different chemosynthetic environments, and why some bivalve species are symbiotic while others are not in the same environment.

### 4.2.3 **abj-farming model applicability to other chemosymbiotic species**

The abj-farming model could be applied to other symbiotrophic species from the deep-sea such as Siboglinidae, Bathymodiolinae and chemosymbiotic snails that have similar feeding strategies: intracellular symbionts digestion in specialized organ which is thought to be their main source of food (Dubilier et al., 2008; Sogin et al., 2020). The abj-farming model could be applied directly to snails as there are no need for core modification of the abj-farming model. Deep-sea symbiotic snails like *Alviniconcha* have a reduced digestive system and house sulfur-oxidizing symbionts within their gills (Dubilier et al., 2008; Laming et al., 2020). There are some evidence lysosomal digestion (Laming et al., 2020). In the case of symbiotic bathymodiolin mussels, symbionts are contained inside their gills and are digested, as vesicomyid clams (Dubilier et al., 2008; Piquet et al., 2019; Sogin et al., 2020). The difference with vesicomyid clam is that they possess two types of symbiont, sulfur and methane oxidizers (MOX and SOX, respectively) (Duperron et al., 2016; Szafranski et al., 2015). Methane should be included into symbiont macrochemical equations. MOX and SOX can be modeled as a single entity, that would be the simplest way, or they can be modeled separately. In symbiotic siboglinid tubeworms, that don't

have digestive system, sulfur-oxidizing symbionts are housed in their trophosome (Dubilier et al., 2008; Sogin et al., 2020). Using the abj-farming model, bacterial density in siboglinid trophosome could be modeled as for the bivalve gill bacterial density.

## 4.3 DEB and chemosynthetic environment challenges

### 4.3.1 Coastal challenges

Seagrasses and mangroves are threaten in some areas, mainly because of climate change, coastal development, pollution causing poor water quality. The lucinid, as they were observed to facilitate seagrass growth and are key species in mangroves ecosystems (see Chapter 3), can be used as a “tool” of restoration of these fragile ecosystems. With DEB, the contribution of lucines in term of sulfidic soil detoxification and nutrients supply could be estimated using DEB. The population dynamic of lucines could be studied with DEB-IBM (individual based model) and scenarios of climate change and anthropogenic disturbance could be made (De Cubber et al., 2023; Martin et al., 2012; Yang et al., 2022). Scenarios could help to determine temperature and nutrient thresholds of lucine populations, and thus their resiliency. The results of such studies could help designing restoration and/or managing these ecosystems.

### 4.3.2 Deep-sea chemosynthetic ecosystems challenges

There is still an important knowledge gap about deep-sea ecosystems functioning and resiliency. As most of deep-sea chemosynthetic ecosystems are located beyond states jurisdiction (>200 miles from the territorial sea baseline defined as the low-water line) and as the interest for deep-sea resources is skyrocketing (such as for polymetallic nodules (Fig. 4.1), polymetallic sulfides and cobalt-rich ferromanganese crusts), protection of the biodiversity while exploiting deep-sea resources are nowadays one of the top priority (“International Seabed Authority”, 2024). Since nearly one century, an effort has been made by the United Nations to codify the law of the sea, including sea beyond states jurisdiction. However deep-sea biodiversity concern in United Nations treaties is something very recent.

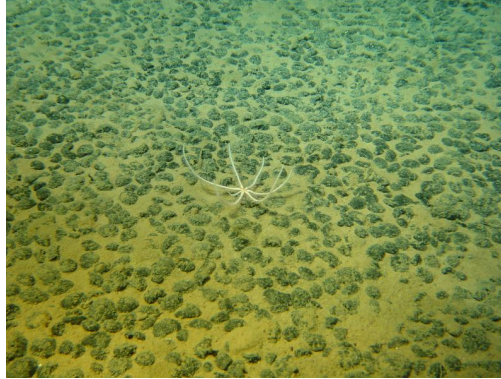
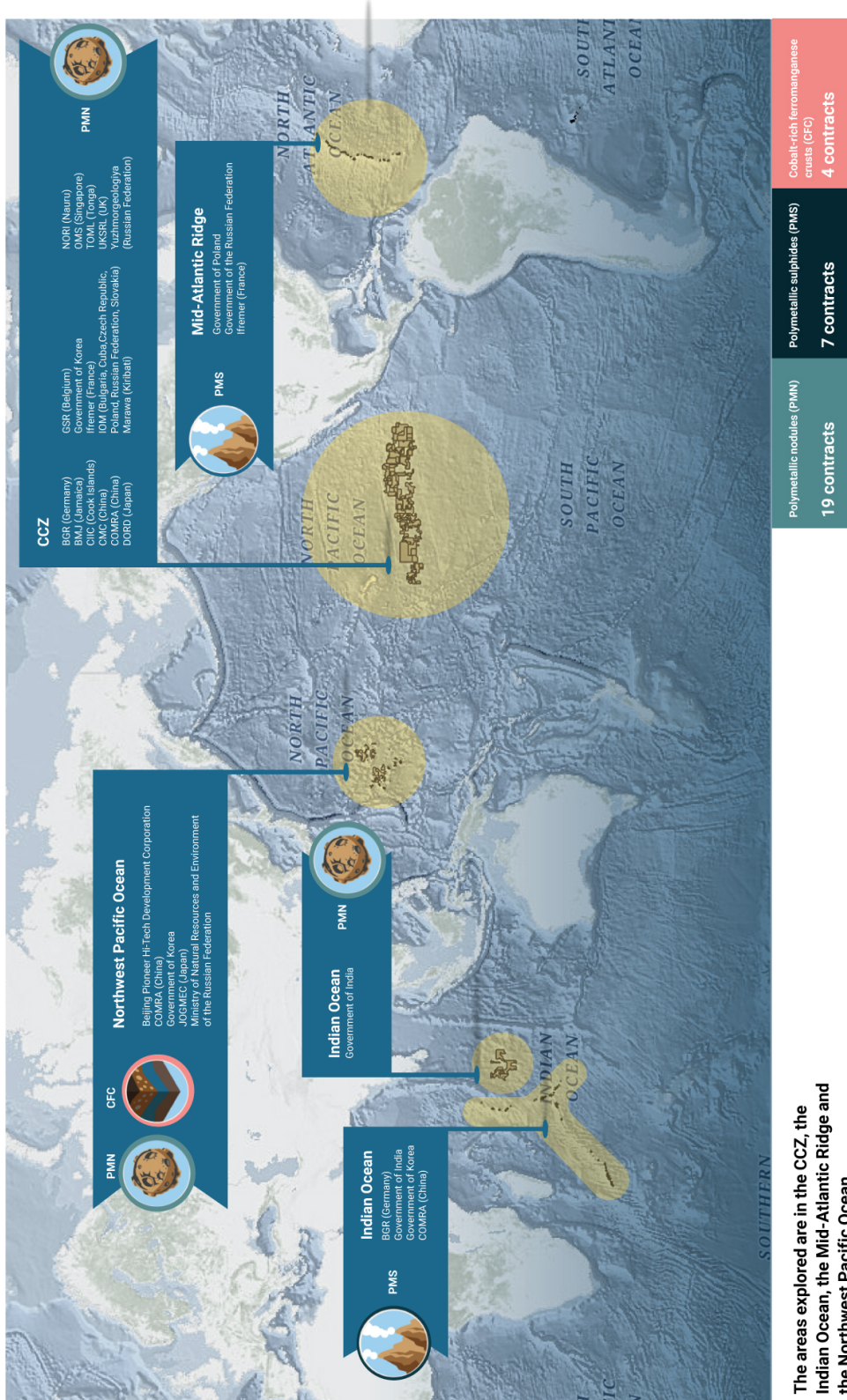


**Figure 4.1:** Deep-sea polymetallic nodules. (Ifremer (2004) <https://image.ifremer.fr/data/00424/53575/>).

In 1958 in Geneva was held the first United Nations Conference on the Law of the Sea I (UNCLOS I) that led to four treaties, including the Convention on the Territorial Sea and Contiguous Zone, The Convention on the Continental Shelf, the Convention on the High Seas, and the Convention on Fishing and Conservation of Living Resources of the High Seas. However there was nothing yet about deep-sea resources exploitation and conservation (Site national de la Convention sur la diversité biologique, 2024; United Nations Treaty, 1958). In 1960, the UNCLOS II in Geneva was a failure as no new agreements were reached. The 10<sup>th</sup> of December 1982, the UNCLOS III in Montego Bay led to the Convention on the Law of the Sea that came into force the 16<sup>th</sup> of November 1994 (United Nations Treaty, 1994). In the part V of this convention were notably defined the ZEEs (Zone Economic Exclusives). Articles 61 to 68 are dedicated to state resource management and conservation. Section 2 of part VII is dedicated to the “conservation and management of living resources” of the High Seas, however not sufficiently. Another important advancement was that for the first time, something was written about the deep-sea seabed and ocean floor beyond national jurisdiction, named the Area, in The part XI of Convention on the Law of the Sea. The Area and its resources (i.e., “solid, liquid, gaseous mineral resources in situ in the Area at or beneath the seabed, including polymetallic nodules”) are defined as the “common heritage of human kind”. The ISA (international seabed authority) is the authority in charge of delivering contract to explore the Area for polymetallic nodules, polymetallic sulfides and cobalt-rich ferromanganese crusts (Fig. 4.2) (“International Seabed Authority”, 2024). At this time, only 13 areas of particular interest (APEIS) were created by the ISA, all in the Clarion-Clipperton Zone (CCZ) in the Pacific Ocean (“International Seabed Authority”, 2024).



The areas explored are in the CCZ, the Indian Ocean, the Mid-Atlantic Ridge and the Northwest Pacific Ocean.

Figure 4-2: Exploration contracts in the Area in 2023. CCZ, Clarion-Clipperton Zone (Figure taken from [www.isa.org.jm](http://www.isa.org.jm)).

Last year, as a result of international negotiations of the Biodiversity Beyond National Jurisdiction (BBNJ) process, the Agreement under the United Nations Convention on the Law of the Sea on the Conservation and Sustainable Use of Marine Biological Diversity of Areas beyond National Jurisdiction was adopted in New York on the 19th of June 2023, which was an historic breakthrough (United Nations Treaty, -). The agreement is yet to be ratified by the parties and will be implemented 120 days after the 60 ratifications. The agreement stipulates the creation of network of protected areas. Scientific tools to estimate the connectivity between the protected areas and to determine functional traits are needed to create such network (Hilário et al., 2015; Howell et al., 2020). DEB models could be useful tools to reach those goals, estimating functional and life traits, and the pelagic larval duration (i.e., the time the larva stay in the water column before settling to the seafloor). These informations, coupled with hydrodynamic models on the sea-floor and in water column and DEB-IBM models, could help estimating the larval dispersal and the connectivity between different populations more or less close/patchy and help designing protected areas. The impact on food and temperature disturbances on the connectivity could be studied through the impact of food and temperature on the estimated pelagic larval duration with DEB. That could also be studied at the population level using DEB-individual population models (DEB-IBMs) (De Cubber et al., 2023; Martin et al., 2012). Working first on coastal species could help validate the dynamic of the symbiotic models.

## 4.4 Conclusions on scientific contribution

This work studied the dynamic relationships between a bivalve host and its chemosynthetic symbionts in function of two environmental forcing variables (food level and temperature) using a bioenergetic model which is a great great step forward in the field as only a few paper have been published: a conceptual vesicomid model based on energy fluxes (Goffredi & Barry, 2002) and a fully developed model based on chemical elements fluxes on the deep-sea mytilid *Bathymodiolus azoricus* (Husson et al., 2018; Martins et al., 2008). Compared to these models, DEB modeling bring another dimension into the modeling of host-symbiont relationships as it takes into account the whole life cycle of the host. This model unravels life traits of such hard to study species and has lots of possible uses and applications to help increasing the knowledge and could help in designing protected areas. The results of the developed abj-farming

DEB model support that, in the case that the vesicomid *Christineconcha regab* is indeed mainly feeding by the digestion of its symbionts, its nutritional relationship with its symbiont might be based on a kind of homeostasis. Symbionts might be farmed by the host in order to meet its needs. Data necessary to integrate sulfur-oxidizing symbionts within a DEB model for lucinid bivalve *Loripes orbiculatus* have been collected and a conceptual model for the species was described.

This thesis illustrated the wide range of applications and potential of using DEB theory to investigate symbiotic relationships and presents guidances for future work.

## References

- Add-My-Pet Species List*. (2024). [https://www.bio.vu.nl/thb/deb/deblab/add\\_my\\_pet/species\\_list.html](https://www.bio.vu.nl/thb/deb/deblab/add_my_pet/species_list.html)
- Augustine, S., & Kooijman, S. A. L. M. (2019). A new phase in DEB research. *Journal of Sea Research*, 143, 1–7. <https://doi.org/10.1016/j.seares.2018.06.003>
- Cowen, R. K., Gawarkiewicz, G., Pineda, J., Thorrold, S. R., & Werner, F. E. (2007). Population Connectivity in Marine Systems An Overview. *Oceanography*, 20(3), 14–21. <https://www.jstor.org/stable/24860093>
- De Cubber, L., Lefebvre, S., Lancelot, T., Jorge, D. S. F., & Gaudron, S. M. (2023). Unravelling mechanisms behind population dynamics, biological traits and latitudinal distribution in two benthic ecosystem engineers: A modelling approach. *Progress in Oceanography*, 219, 103154. <https://doi.org/10.1016/j.pocean.2023.103154>
- Distel, D. L., Baco, A. R., Chuang, E., Morrill, W., Cavanaugh, C., & Smith, C. R. (2000). Do mussels take wooden steps to deep-sea vents? *Nature*, 403(6771), 725–726. <https://doi.org/10.1038/35001667>
- Dubilier, N., Bergin, C., & Lott, C. (2008). Dubilier N, Bergin C, Lott C.. Symbiotic diversity in marine animals: The art of harnessing chemosynthesis. *Nat Rev Micro* 6: 725-740. *Nature reviews. Microbiology*, 6(10), 725–40. <https://doi.org/10.1038/nrmicro1992>
- Duperron, S., Quiles, A., Szafranski, K., Léger, N., & Shillito, B. (2016). Estimating symbiont abundances and gill surface areas in specimens of the hydrothermal vent mussel *bathymodiolus puteoserpentis* maintained in pressure vessels. *Frontiers in Marine Science*, 3. <https://doi.org/10.3389/fmars.2016.00016>
- Gaudron, S. M., Lefebvre, S., & Marques, G. M. (2021). Inferring functional traits in a deep-sea wood-boring bivalve using dynamic energy budget theory. *Scientific Reports*, 11(1), 22720. <https://doi.org/10.1038/s41598-021-02243-w>

- Goffredi, S. K., & Barry, J. P. (2002). Energy acquisition and allocation in vesicomylid symbioses. *Cahiers de Biologie Marine*, (3-4). <https://doi.org/10.21411/CBM.A.5ADE9CC5>
- Guyton, A., & Hall, J. (2011). *Guyton and Hall Textbook of Medical Physiology*. Saunders/Elsevier. <https://books.google.fr/books?id=di5PtQAACAAJ>
- Hassan, M., Teixeira, S., Decker, C., Fuchs, S., Mouchel, O., Olu, K., & Arnaud-Haond, S. (2023). High connectivity among Vesicomylid bivalves from cold seeps and deep-sea fans of Congo. *Deep Sea Research Part I: Oceanographic Research Papers*, 201, 104174. <https://doi.org/10.1016/j.dsr.2023.104174>
- Hilário, A., Metaxas, A., Gaudron, S. M., Howell, K. L., Mercier, A., Mestre, N. C., Ross, R. E., Thurnherr, A. M., & Young, C. (2015). Estimating dispersal distance in the deep sea: Challenges and applications to marine reserves. *Frontiers in Marine Science*, 2. <https://www.frontiersin.org/article/10.3389/fmars.2015.00006>
- Howell, K. L., Hilário, A., Allcock, A. L., Bailey, D. M., Baker, M., Clark, M. R., Colaço, A., Copley, J., Cordes, E. E., Danovaro, R., Dissanayake, A., Escobar, E., Esquete, P., Gallagher, A. J., Gates, A. R., Gaudron, S. M., German, C. R., Gjerde, K. M., Higgs, N. D., ... Xavier, J. R. (2020). A Blueprint for an Inclusive, Global Deep-Sea Ocean Decade Field Program. *Frontiers in Marine Science*, 7. <https://doi.org/10.3389/fmars.2020.584861>
- Husson, B., Sarrazin, J., van Oevelen, D., Sarradin, P.-M., Soetaert, K., & Menesguen, A. (2018). Modelling the interactions of the hydrothermal mussel *Bathymodiolus azoricus* with vent fluid. *Ecological Modelling*, 377, 35–50. <https://doi.org/10.1016/j.ecolmodel.2018.03.007>
- International Seabed Authority*. (2024). <https://www.isa.org.jm/>
- Khripounoff, A., Caprais, J. C., Decker, C., Le Bruchec, J., Noel, P., & Husson, B. (2017). Respiration of bivalves from three different deep-sea areas: Cold seeps, hydrothermal vents and organic carbon-rich sediments. *Deep Sea Research Part II: Topical Studies in Oceanography*, 142, 233–243. <https://doi.org/10.1016/j.dsr2.2016.05.023>

- Koito, T., Liu, W., Morimoto, S., Inoue, K., & Toyohara, H. (2016). Comparison of taurine related compounds in deep- and shallow-water mussel species. *Plankton and Benthos Research*, 11(3), 81–86. <https://doi.org/10.3800/pbr.11.81>
- Kooijman, S. A. L. M. (2010). *Dynamic Energy Budget Theory for Metabolic Organisation*. Cambridge University Press.
- Kuroda, M., Nagasaki, T., Koito, T., Hongo, Y., Yoshida, T., Maruyama, T., Tsuchida, S., Nemoto, S., & Inoue, K. (2021). Possible Roles of Hypotaurine and Thiotaurine in the Vesicomid Clam *Phreagena okutanii*. *The Biological Bulletin*, 240(1), 34–40. <https://doi.org/10.1086/712396>
- Laming, S. R., Hourdez, S., Cambon-Bonavita, M.-A., & Pradillon, F. (2020). Classical and computed tomographic anatomical analyses in a not-so-cryptic Alviniconcha species complex from hydrothermal vents in the SW Pacific. *Frontiers in Zoology*, 17(1), 12. <https://doi.org/10.1186/s12983-020-00357-x>
- Marques, G. M., Augustine, S., Lika, K., Pecquerie, L., Domingos, T., & Kooijman, S. A. L. M. (2018). The AmP project: Comparing species on the basis of dynamic energy budget parameters. *PLOS Computational Biology*, 14(5), e1006100. <https://doi.org/10.1371/journal.pcbi.1006100>
- Martin, B. T., Zimmer, E. I., Grimm, V., & Jager, T. (2012). Dynamic Energy Budget theory meets individual-based modelling: A generic and accessible implementation. *Methods in Ecology and Evolution*, 3(2), 445–449. <https://doi.org/10.1111/j.2041-210X.2011.00168.x>
- Martins, I., Colaço, A., Dando, P. R., Martins, I., Desbruyères, D., Sarradin, P.-M., Marques, J. C., & Serrão-Santos, R. (2008). Size-dependent variations on the nutritional pathway of *Bathymodiolus azoricus* demonstrated by a C-flux model. *Ecological Modelling*, 217(1), 59–71. <https://doi.org/10.1016/j.ecolmodel.2008.05.008>
- McVeigh, D. M., Eggleston, D. B., Todd, A. C., Young, C. M., & He, R. (2017). The influence of larval migration and dispersal depth on potential larval trajectories of a deep-sea bivalve. *Deep Sea Re-*

- search Part I: Oceanographic Research Papers*, 127, 57–64. <https://doi.org/10.1016/j.dsr.2017.08.002>
- Petersen, J. M., & Yuen, B. (2020). The symbiotic ‘all-rounders’: Partnerships between marine animals and chemosynthetic nitrogen-fixing bacteria. *Applied and Environmental Microbiology*. <https://doi.org/10.1128/AEM.02129-20>
- Piquet, B., Le Panse, S., Lallier, F. H., Duperron, S., & Andersen, A. C. (2022). “There and back again” - Ultrastructural changes in the gills of *Bathymodiolus vent*-mussels during symbiont loss: Back to a regular filter-feeding epidermis. *Frontiers in Marine Science*, 9. <https://www.frontiersin.org/articles/10.3389/fmars.2022.968331>
- Piquet, B., Shillito, B., Lallier, F. H., Duperron, S., & Andersen, A. C. (2019). High rates of apoptosis visualized in the symbiont-bearing gills of deep-sea *Bathymodiolus* mussels. *PLOS ONE*, 14(2), e0211499. <https://doi.org/10.1371/journal.pone.0211499>
- Ponnudurai, R., Kleiner, M., Sayavedra, L., Petersen, J. M., Moche, M., Otto, A., Becher, D., Takeuchi, T., Satoh, N., Dubilier, N., Schweder, T., & Markert, S. (2017). Metabolic and physiological interdependencies in the *Bathymodiolus azoricus* symbiosis. *The ISME Journal*, 11(2), 463–477. <https://doi.org/10.1038/ismej.2016.124>
- Pruski, A. M., Médioni, A. F., Prodon, R., & Colomines, J. C. (2000). Thiotaaurine is a biomarker of sulfide-based symbiosis in deep-sea bivalves. *Limnology and Oceanography*, 45(8), 1860–1867. <https://doi.org/10.4319/lo.2000.45.8.1860>
- Site national de la Convention sur la diversité biologique. (2024). *Les négociations intergouvernementales sur la conservation et l'utilisation durable de la biodiversité marine des zones ne relevant pas de la juridiction nationale*. <https://biodiv.mnhn.fr/fr/les-negociations-intergouvernementales-sur-la-conservation-et-lutilisation-durable-de-la>
- Sogin, E. M., Leisch, N., & Dubilier, N. (2020). Chemosynthetic symbioses. *Current Biology*, 30(19), R1137–R1142. <https://doi.org/10.1016/j.cub.2020.07.050>

- Szafranski, K. M., Piquet, B., Shillito, B., Lallier, F. H., & Duperron, S. (2015). Relative abundances of methane- and sulfur-oxidizing symbionts in gills of the deep-sea hydrothermal vent mussel *Bathymodiolus azoricus* under pressure. *Deep Sea Research Part I: Oceanographic Research Papers*, 101, 7–13. <https://doi.org/10.1016/j.dsr.2015.03.003>
- Thubaut, J., Puillandre, N., Faure, B., Cruaud, C., & Samadi, S. (2013). The contrasted evolutionary fates of deep-sea chemosynthetic mussels (*Bivalvia*, *Bathymodiolinae*). *Ecology and Evolution*, 3(14), 4748–4766. <https://doi.org/10.1002/ece3.749>
- Convention Sur La Mer Territoriale et La Zone Contiguë Geneve1958 (1958). [https://treaties.un.org/Pages/ViewDetails.aspx?src=IND&mtdsg\\_no=XXI-1&chapter=21&clang=\\_fr](https://treaties.un.org/Pages/ViewDetails.aspx?src=IND&mtdsg_no=XXI-1&chapter=21&clang=_fr)
- Convention on the Law of the Sea (1994). [https://treaties.un.org/Pages/ViewDetailsIII.aspx?src=TREATY&mtdsg\\_no=XXI-6&chapter=21&Temp=mtdsg3&clang=\\_en](https://treaties.un.org/Pages/ViewDetailsIII.aspx?src=TREATY&mtdsg_no=XXI-6&chapter=21&Temp=mtdsg3&clang=_en)
- BBNJ (-). [https://treaties.un.org/Pages/ViewDetails.aspx?src=TREATY&mtdsg\\_no=XXI-10&chapter=21&clang=\\_fr](https://treaties.un.org/Pages/ViewDetails.aspx?src=TREATY&mtdsg_no=XXI-10&chapter=21&clang=_fr)
- Yang, T., Han, Q., Gorfine, H., Shan, X., & Ren, J. S. (2022). DEB-IBM for predicting climate change and anthropogenic impacts on population dynamics of hairtail *Trichiurus lepturus* in the East China Sea. *Conservation Physiology*, 10(1), coac044. <https://doi.org/10.1093/conphys/coac044>
- Young, C. M., He, R., Emlet, R. B., Li, Y., Qian, H., Arellano, S. M., Van Gaest, A., Bennett, K. C., Wolf, M., Smart, T. I., & Rice, M. E. (2012). Dispersal of Deep-Sea Larvae from the Intra-American Seas: Simulations of Trajectories using Ocean Models. *Integrative and Comparative Biology*, 52(4), 483–496. <https://doi.org/10.1093/icb/ics090>